INFORMATION TO USERS

This manuscript has been reproduced from the microfilm master. UMI films the text directly from the original or copy submitted. Thus, some thesis and dissertation copies are in typewriter face, while others may be from any type of computer printer.

The quality of this reproduction is dependent upon the quality of the copy submitted. Broken or indistinct print, colored or poor quality illustrations and photographs, print bleedthrough, substandard margins, and improper alignment can adversely affect reproduction.

In the unlikely event that the author did not send UMI a complete manuscript and there are missing pages, these will be noted. Also, if unauthorized copyright material had to be removed, a note will indicate the deletion.

Oversize materials (e.g., maps, drawings, charts) are reproduced by sectioning the original, beginning at the upper left-hand corner and continuing from left to right in equal sections with small overlaps.

Photographs included in the original manuscript have been reproduced xerographically in this copy. Higher quality 6" x 9" black and white photographic prints are available for any photographs or illustrations appearing in this copy for an additional charge. Contact UMI directly to order.

Bell & Howell Information and Learning
300 North Zeeb Road, Ann Arbor, MI 48106-1346 USA
800-521-0600

Inhibition and inactivation of Prostaglandin synthase-2 and Horseradish peroxidase

Susan-Marie Aitken

A Thesis

in

The Department

of

Chemistry and Biochemistry

Presented in Partial Fulfillment of the Requirements

For the Degree of Doctor of Philosophy at

Concordia University

Montreal, Quebec, Canada

February, 2000

ABSTRACT

Inhibition and inactivation of Prostaglandin synthase-2
and Horseradish peroxidase

Susan-Marie Aitken, Ph.D.

Concordia University, 2000

Prostaglandin synthase (PGHS) is a bifunctional enzyme of particular pharmaceutical interest, containing both cyclooxygenase (COX) and peroxidase (POX) active sites. Development of PGHS-2-selective POX inhibitors may reduce the toxic and carcinogenic effects of PGHS-2 xenobiotic activation, as well as further define the role of this activity *in vivo*. Knowledge of the contribution of specific contacts to binding will be crucial to drug design. The results of an investigation of the thermodynamics of binding of a series of aromatic hydroxamic acid analogues to the archetypical peroxidase horseradish peroxidase (HRP) revealed the importance of hydrogen bonds to the distal catalytic residues, in particular the distal arginine of HRP.

The ability of peroxidases, including PGHS-2, to oxidize a wide variety of compounds makes the design of selective, reversible inhibitors very challenging. Therefore, the potential of aromatic hydrazides as mechanism-based peroxidase inhibitors was investigated here, again using HRP as a model peroxidase. The results suggest that benzhydrazide is a mechanism-based inhibitor of HRP. In general hydrazides were observed to be good inhibitors of PGHS-2 POX activity with IC_{50} values in the 1-800 μM range and with 2-naphthoichydrazide (2-NZH) being the most potent (IC_{50} = 1.6 μM).

Comparison of the IC_{50} values for PGHS-2 and HRP support the potential development of peroxidase-selective hydrazides.

The COX activity of PGHS-2 is the target of nonsteroidal antiinflammatory drugs (NSAIDs). The effects of NSAID binding on the structure and conformational stability of PGHS-2 were investigated here. Diclofenac was observed to cause the greatest reduction in the conformational flexibility of PGHS-2, possibly due to its strained (entropically unfavorable) but very enthalpically favorable binding conformation, in comparison with the other compounds of the fenamate family investigated.

Both the COX and POX activities of PGHS-2 isozymes undergo rapid suicide inactivation. The mechanism of inactivation is not known, although it is likely radical-based. Stoichiometric incorporation of ^{14}C-AA was observed here on the time scale of inactivation, suggesting that the incorporation of activated substrate intermediates may be involved in COX inactivation. The negligible degree of H_2O_2-dependent intermolecular crosslinking observed here indicates that this is not a major mechanism of PGHS-2 inactivation.

ACKNOWLEDGEMENTS

First and foremost, I would like to thank my co-supervisors Dave Percival and Ann English for creating the unique opportunity for me to experience research both at Merck Frosst and at Concordia and for their supervision, advice, enthusiasm, and tireless proof-reading. Thanks also to Mike Gresser whose support was instrumental in making my experience at Merck Frosst possible. I am greatly indebted to Joanne Turnbull for being a mentor to me throughout the course of my M.Sc. and Ph.D. Her friendship, support and advice have been valuable beyond measure. I am also very grateful to Marc Ouellet and Jean-Pierre Falgueyret, who enriched my experience with their warmth, companionship and patient assistance. Marc's enthusiasm for all things scientific and for helping others has been an inspiration. Thanks also to everyone at Merck Frosst and Concordia who made my stay enjoyable: Lucile Serfass, Angelo Filosa, David Claveau, Craig Fenwick, George Tsaprailis, Elisabeth Cadieux, Carole Coutts, Kathy Usas, Dinesh Christendat, Vivian Saridakis, and many others. Last but not least, my great appreciation for the friendship and understanding of Lena, my parents and my friends outside of Merck and Concordia. My heart-felt thanks to each of you.

I am also indebted to the many colleagues from whose experience I have benefited in the course of this study. The collaborative research environment encouraged at Merck Frosst has allowed me to work closely with other researchers and their contributions to the work described in this thesis is acknowledged here. PGHS-2 was purified with the guidance and assistance of Marc Ouellet. The investigation of the ability of tepoxalin to act as a PGHS-2 reducing substrate was carried out by Marc

Ouellet. Dr. Brian McKeever assisted with structural interpretation of the thermodynamic data for PGHS-2. Dr. Ashraf Ismail instructed me on the use and interpretation of FTIR. Angelo Filosa and Craig Fenwick instructed me in the operation of ESI-MS. Sameer Massis provided assistance with the operation of the MCS-ITC. MCS-ITC experiments were conducted at the Biotechnology Research Institute and VP-ITC experiments were conducted in the Structural Genomics facility at Concordia. Finally, this work would not have been possible without the intellectual contributions and supervision of Dr. David Percival and Dr. Ann English.

DEDICATION

To my parents,

Joan and Clarence Aitken

Two roads diverged in a yellow wood,

And sorry I could not travel both

And be one traveler, long I stood

And looked down one as far as I could

To where it bent in the undergrowth;

Then took the other, as just as fair,

And having perhaps the better claim,

Because it was grassy and wanted wear;

Though as for that the passing there

Had worn them really about the same,

And both that morning equally lay

In leaves no step had trodden black.

Oh, I kept the first for another day!

Yet knowing how way leads on to way

I doubted if I should ever come back.

—Robert Frost

TABLE OF CONTENTS

LIST OF FIGURES

LIST OF TABLES

LIST OF ABBREVIATIONS

AA	arachidonic acid
ARP	*Arthromyces ramosus* peroxidase
ASA	acetylsalicylic acid (aspirin)
BHA	benzhydroxamic acid
BZA	benzamide
BZH	benzhydrazide
CAPS	3-[cyclohexylamino]-1-propanesulfonic acid
CCP	cytochrome *c* peroxidase
CD	circular dichroism
Compound I	two-electron oxidized species formed when stoichiometric (2 redox equivalents) H_2O_2 reacts with HRP
Compound II	species formed on one-electron reduction of Compound I
Compound III	oxyperoxidase, the O_2 adduct of HRP(Fe^{II})
COX	cyclooxygenase
DMSO	dimethylsulfoxide
DSC	differential scanning calorimetry
DTGS	deuterated triglycine sulfate
EPR	electron paramagnetic resonance spectroscopy
FTIR	Fourier transform infrared spectroscopy
13-HODE	13(S)-hydroxyoctadeca-9Z,11E-dienoic acid
15-HPETE	15-(R)-hydroperoxy-eicosatetraenoic acid

HRP	horseradish peroxidase
HRP(Fe^{III})	native ferric form of HRP
HRP(Fe^{II})	one-electron reduced ferrous form of HRP
HRP(Fe^{II})-CO	CO adduct of ferrous HRP
IC_{50}	inhibitor concentration causing 50% inhibition
INH	isonicotinic hydrazide
IPO	intestinal peroxidase
ITC	isothermal titration calorimetry
K_d	dissociation constant
LPO	lactoperoxidase
Mb	myoglobin
MCD	magnetic circular dichroism spectroscopy
MPO	myeloperoxidase
NATA	N-acetyltyrosinamide
1-NHA	1-naphthoichydroxamic acid
2-NHA	2-naphthoichydroxamic acid
NICH	nicotinic hydrazide
NMBZA	N-methylbenzamide
NMR	nuclear magnetic resonance spectroscopy
NSAIDs	nonsteroidal antiinflammatory drugs
1-NZH	naphthoichydrazide
2-NZH	naphthoichydrazide
3-OH-2-NZH	3-hydroxy-2-naphthoichydrazide

PGHS	prostaglandin synthase (h, human; m, murine; o, ovine)
PGHS(Fe^{III})	native ferric form of PGHS
PGG_2	prostaglandin G_2
PGH_2	prostaglandin H_2
Phe	phenylalanine
13-H-PODE	13(S)-hydroperoxyoctadeca-9X,11E-dienoic acid
POX	peroxidase
RR	resonance Raman spectroscopy
S.D.	standard deviation
SHA	salicylhydroxamic acid
TAPS	N-tris[hydroxymethyl]methyl-3-aminopropanesulfonic acid
T_m	midpoint of thermal denaturation
TMPD	N,N,N'N'-tetramethyl-p-phenyldiamine dihydrochloride
Trp	tryptophan
Tyr	tyrosine

1 INTRODUCTION

1.1 HEME PEROXIDASES

Heme peroxidases catalyze the oxidation of a wide variety of organic and inorganic substrates at the expense of hydrogen peroxide or lipid hydroperoxides (*1, 2*). Peroxidases are involved in an extensive range of biological functions including defense against stress and environmental changes, metabolism of macromolecules (*e.g.*, lignin), developmental processes, and biosynthesis (*3*). Due to their spectroscopic properties, which result from the heme prosthetic group, and their diagnostic, bioindustrial, and molecular biology applications, heme peroxidases comprise one of the most highly studied enzyme families (*3*).

1.1.1 Peroxidase superfamilies

Sequence alignments and comparison of the crystal structures of heme peroxidases show many common features in overall structure, as well as conservation of amino acid residues involved in catalysis (*3, 4*). There are two major groups of heme peroxidases: the plant and the mammalian superfamilies.

1.1.1.1 Plant peroxidase superfamily

An extensive phylogenetic analysis has shown that the heme peroxidases from plants, fungi, and bacteria are evolutionarily related. These enzymes comprise the plant peroxidase superfamily (*4-6*). Although there is less than 20% amino acid sequence identity between most of the plant peroxidases, all contain some catalytic residues in the heme cavity that are highly conserved. Three of the most highly conserved residues are the proximal His (the axial iron ligand) and the distal His and Arg, which are involved in catalysis (*7*).

Comparison of the crystal structures available for enzymes of the plant peroxidase superfamily [cytochrome *c* peroxidase (CCP), lignin peroxidase (LiP), *Arthromyces ramosus* peroxidase (ARP), *Coprinus cinereus* peroxidase (CiP), manganese peroxidase (MnP), pea ascorbate peroxidase (APX), barley peroxidase (BP), peanut peroxidase (PNP) and horseradish peroxidase (HRP)] has shown that although sequence similarity is not high, the overall folding and organization of secondary-structure elements is conserved among the plant peroxidases (*4, 8-12*). They are largely α-helical with little or no β-sheet (*13*) and are divided into two structural domains, which enfold the heme prosthetic group.

Phylogenetic analysis has also revealed the existence of three well-separated classes within this superfamily. Class I includes the intracellular peroxidases of prokaryotic origin (*e.g.*, CCP); class II, the secretory fungal peroxidases (*e.g.*, LiP and MnP); and class III, the secretory plant peroxidases (*e.g.*, HRP) (*7*).

1.1.1.2 Mammalian peroxidase superfamily

The mammalian peroxidase superfamily comprises a group of homologous mammalian peroxidases including prostaglandin synthase (PGHS), myeloperoxidase (MPO), lactoperoxidase (LPO), thyroid peroxidase (TPO), intestinal peroxidase (IPO), and eosinophil peroxidase (EPO). The sequence identity between most of the enzymes of this family is approximately 70%. PGHS, however, is an exception as it has only 20% sequence identity on average to the other mammalian peroxidases (*14*).

The only two mammalian peroxidases for which crystal structures have been solved are MPO and PGHS (*14, 15*). Comparison of the crystal structures has shown that despite the low level of sequence homology between PGHS and the other mammalian

peroxidases, it is structurally similar to MPO. PGHS and MPO share a common topological organization of the helices that form the peroxidase fold and a common heme environment (*15*).

1.1.2 Peroxidase catalysis

1.1.2.1 Catalytic mechanism

Much of the current understanding of the mechanism and catalysis of classical peroxidases (*e.g.*, heme peroxidases with an imidazole as the fifth iron ligand) derives from work on HRP and CCP. These two enzymes have been extensively characterized kinetically and spectroscopically due to the accessibility of HRP (*16*) and because for many years CCP was the only peroxidase of known crystal structure (*17, 18*). The peroxidase mechanism, originally proposed for CCP (*19*), and the characteristics deduced from the analysis of both CCP and HRP are broadly applicable to other plant and mammalian peroxidases (*2, 20-26*). The general sequence of events catalyzed by peroxidases is:

$$POX^{III} + H_2O_2 \rightarrow \text{Compound I} + H_2O \qquad \text{(reaction 1.1)}$$

$$\text{Compound I} + AH_2 \rightarrow \text{Compound II} + \bullet AH \qquad \text{(reaction 1.2)}$$

$$\text{Compound II} + AH_2 \rightarrow POX^{III} + \bullet AH + H_2O \qquad \text{(reaction 1.3)}$$

where POX^{III} represents the ferric (Fe^{III}) resting form of the enzyme, and Compounds I and II are two- and one- oxidizing equivalents above ground state, respectively.

The first step in peroxidase catalysis (reaction 1.1) involves the oxidation of the resting-state ferric enzyme (POX^{III}) (Figure 1.1) to Compound I by hydrogen peroxide. The distal His and Arg play a major role in the formation and stabilization of Compound I (*19, 27, 28*). According to the mechanism for Compound I formation proposed by

Miller et al. (*29*), the distal His abstracts the proton from the α-oxygen of H_2O_2 (Figure 1.1B) and donates it to the β-oxygen (Figure 1.1C), giving rise to a water molecule as the leaving group. As the O-O bond is cleaved, the distal Arg moves toward the iron and H-bonds to the oxene atom, displacing the distal water molecule (Figure 1.1D).

Heterolytic cleavage of the dioxygen bond to give Compound I requires two electrons, one of which comes from the iron atom while the second comes from either the porphyrin or the protein. Therefore, Compound I contains an oxyferryl (Fe^{IV}=O) center and an organic cation radical which can be located either on the heme or on a protein residue, depending on the peroxidase. Extensive spectroscopic and kinetic evidence (*16, 30*), including Mössbaeur (*31-33*), EXAFS (*34*), MCD (*35, 36*), and a crystal structure of CCP Compound I (*37*), support the existence of the Fe^{IV}=O species in Compound I of CCP and HRP (Figure 1.1D). The presence of the Fe^{IV}=O heme in Compound I of the mammalian peroxidases is supported by spectroscopic evidence on those enzymes (*20-24, 26*).

In the second step in peroxidase catalysis (reaction 1.2), the organic cation radical of Compound I is reduced by a substrate molecule (AH_2) to produce Compound II, which also contains an oxyferryl heme. In the last step (reaction 1.3), a second substrate molecule is oxidized and a molecule of water is released to return the peroxidase to the resting POX^{III} state (Figure 1.1A) (*1*).

1.1.2.2 Location of the Compound I radical

The organic cation radical of Compound I can be stored either as a porphyrin radical or as a protein radical (*2*). Amongst the plant peroxidases, this radical generally exists as a porphyrin π-cation radical ($P^{\bullet}$) (*38-43*). However, in class I plant peroxidases

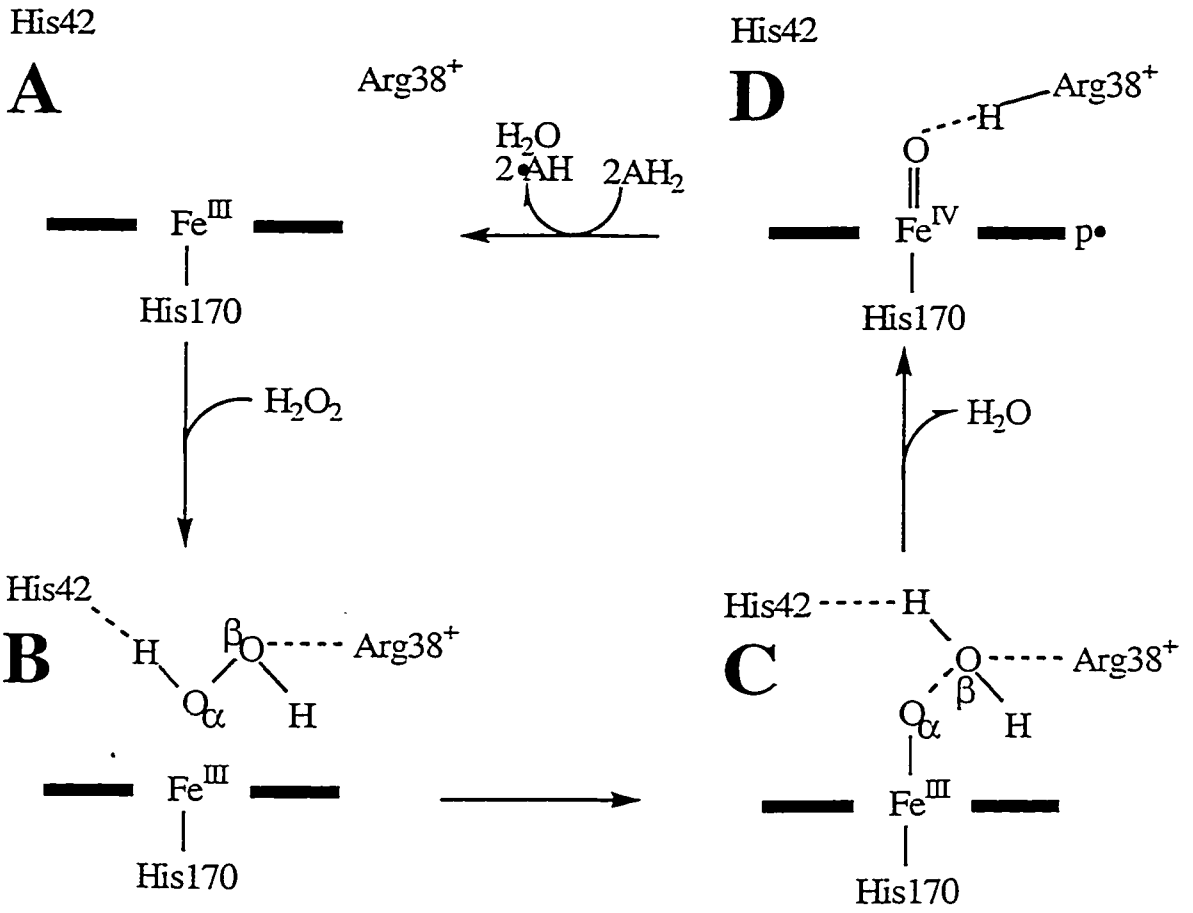

Figure 1.1. Role of the distal catalytic residues (His52 and Arg48 in CCP) in HRP catalysis.

there is a Trp residue present on the proximal side of the heme (Trp191 of CCP) that is the site of the Compound I cation radical (*3, 44*). In class II and III peroxidases this Trp is replaced by a Phe residue, which is not oxidized due to its high reduction potential. Therefore, in class II and III plant peroxidases the cation radical is located on the heme moiety (*13*).

Among the mammalian peroxidases it is more common for an amino acid residue to be the site of the radical. Two examples are LPO and TPO, for which it has been shown that the porphyrin radical oxidizes the protein to give a protein radical (*45-50*). Another example is PGHS, which is discussed in Section 1.3.3 (PGHS catalysis).

The location of the organic cation radical (*i.e.*, porphyrin versus amino acid residue) of Compound I may have physiological relevance, and evidence of this is provided by CCP, LPO and PGHS. CCP has the ability to form numerous protein radicals when exposed to H_2O_2 in the absence of its reducing substrate, cytochrome *c* (*51*). The ability of CCP to turn over H_2O_2 in the presence or absence of a reducing substrate has been suggested to be linked to its proposed role in signaling via control of H_2O_2 concentration (*52*). LPO has recently been observed to undergo H_2O_2-dependent oligomerization via dityrosine crosslinks formed by the reaction of surface tyrosyl radicals. The oligomerization of LPO does not alter the catalytic activity of the enzyme but does change its physical properties and may affect its ability to interact with other proteins (*50*). PGHS is a particularly interesting example of the physiological relevance of the location of the Compound I organic cation radical. As discussed in Section 1.3.3.2, the protein radical produced during peroxidase turnover is the catalytic residue involved in cyclooxygenase catalysis (*53-56*). Additionally, the irreversible loss of PGHS activity

(Sections 1.6 and 7) likely occurs as the result of an activated and unstable protein radical intermediate generated during POX or COX catalysis (*57, 58*). However, the role of radicals in PGHS inactivation has not been fully investigated.

1.2 HORSERADISH PEROXIDASE

1.2.1 Use as an archetypical peroxidase

HRP, a class III peroxidase, from the plant species *Armoracia rusticana*, is one of the most widely studied peroxidases, due in part to its commercial availability, stability, and industrial and biotechnological applications (*59*). HRP comprises a family of isozymes, the most common and well known being the neutral isozyme HRPC (referred to from this point forward as HRP) (*60*). Due to the extensive investigations on the mechanism of HRP and the general applicability of these findings to other classical peroxidases (Section 1.1.), HRP is considered archetypical of this family of enzymes (2). Therefore, it is an attractive model for other less readily available peroxidases.

Figure 1.2 shows the location of the HRP active-site residues involved in binding and catalysis. Phe68, Phe179, and Pro139 are involved in the binding of reducing substrates (*61*). The distal catalytic residues are His42 and Arg38, and these residues are also involved in the binding of reducing substrates (*61*). The proximal iron ligand is His170 (*11*).

1.2.2 Aromatic substrate binding to HRP

Despite the absence of a crystal structure for HRP until recently (*11*), numerous studies have probed the binding of aromatic donor molecules to HRP (*62*). Analysis of these results reveal that, as is typical of peroxidases, the majority of compounds bind weakly, with dissociation constants (K_d) in the millimolar range. However, the binding

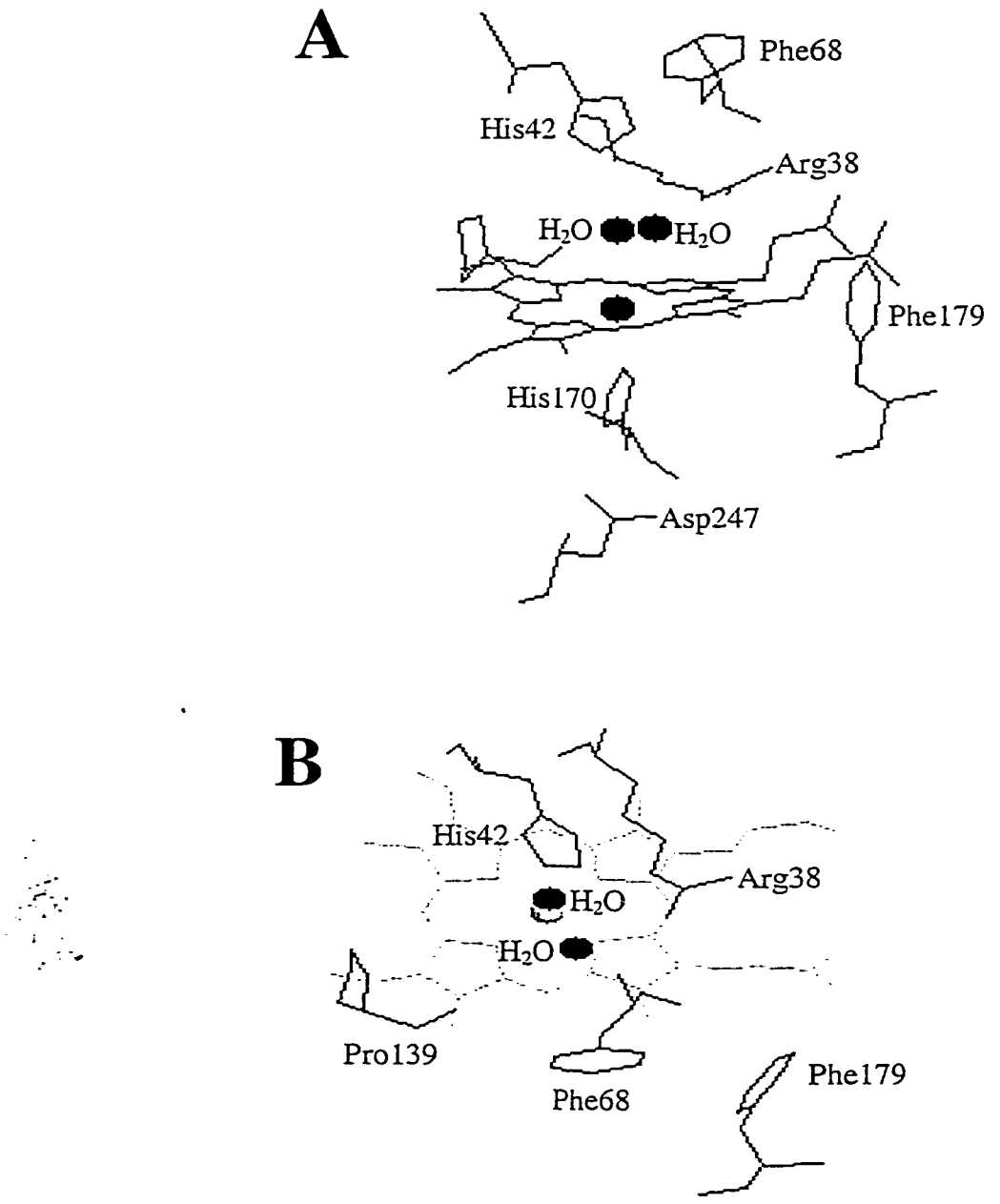

Figure 1.2. Peroxidase site of HRP. (**A**) view along the heme plane and (**B**) perpendicular to the heme plane showing active site amino acids and water molecules. Crystalographic coordinates from Henriksen et al. (*12*).

of benzhydroxamic acid (BHA) to HRP [K_d = 2.4 μM, (*63*)] is a notable exception (*62*) and has provided a useful tool for probing the local environment of the aromatic donor binding site. Schonbaum (*63*) originally proposed that the tight binding of BHA was due to polyfunctional H-bonding within the distal cavity. Subsequently, numerous studies have investigated the H-bonding of BHA, implicating either His42 (*64-69*) or Arg38 (*70-72*), or both of these residues (*73*). The recent crystal structure of the HRP-BHA complex (*61*) provided confirmation that both of these residues, in addition to Pro139, are involved in H-bonding to BHA (Figure 1.3). Since the distal catalytic residues are highly conserved (*4*), BHA can be expected to bind in a similar fashion to other peroxidases. An example is the X-ray structure of the ARP-BHA complex (*74*), which shows the same binding interactions as HRP-BHA. The related compound, salicylhydroxamic acid (SHA) is also observed to bind to ARP and MPO in a similar fashion as BHA to HRP (*75, 76*).

The contribution of H-bonds to protein-ligand interactions is highly unpredictable (*79*). Although the three H-bonds formed by BHA in the distal cavity of HRP (*61*) have been suggested to be responsible for the tight binding of BHA to HRP (*63*), their contribution to the energy of binding is unknown. Knowledge of the thermodynamic driving forces underlying binding is key to understanding the roles of the various H-bonding and hydrophobic interactions in binding of BHA to HRP. Despite the great number of investigations on peroxidase substrate binding, little information is currently available on the thermodynamics of binding. The change in enthalpy ($\Delta H°$) on ligand binding to HRP has been estimated for hydroquinone [$\Delta H°$ = -9.7 kcal/mol, (*80*)] and resorcinol ($\Delta H°$ = -7.6 kcal/mol, (*80*); $\Delta H°$ = -5.9 kcal/mol, (*81*)] at pH 6.0. These $\Delta H°$

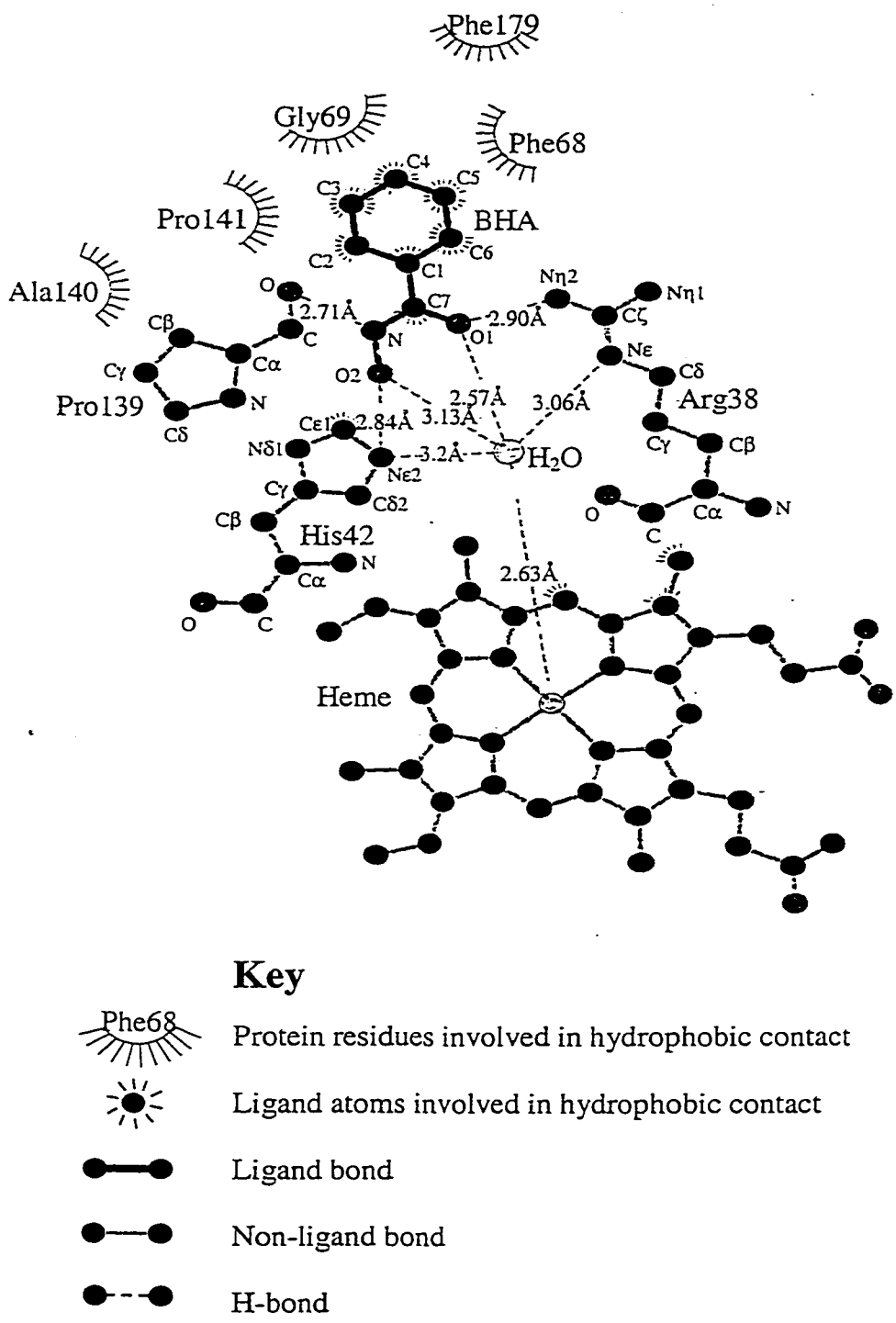

Figure 1.3. LIGPLOT (*77*) diagram of the interactions between BHA and HRP. H-bonds and hydrophobic contacts were calculated with HBPLUS (*78*).

values were estimated from the slope of the Arrhenius plot of 1/T versus -logK_d, assuming that ΔC_p is constant. Results of only one calorimetric study are available, in which the binding of BHA ($\Delta H°$ = -13.9 kcal/mol) and benzhydrazide (BZH, $\Delta H°$ = -10.1 kcal/mol) to HRP at pH 7.0 were investigated using a stopped-flow calorimeter (*82*).

Isothermal titration calorimetry (ITC) is a more accurate method than use of Arrhenius plots for the determination of $\Delta H°$ because it measures the heat of binding directly and does not require the assumption that ΔC_p is constant (*83*). However, ITC has yet to be used to investigate the binding of aromatic compounds to HRP. An ITC investigation of the contribution to binding of each of the H-bonding and hydrophobic interactions observed in the HRP-BHA complex is required to understand the factors controlling the binding of BHA and other aromatic compounds to HRP.

1.3 PROSTAGLANDIN SYNTHASE

1.3.1 Prostaglandin biosynthesis

Prostaglandin synthase (PGHS) is a bifunctional enzyme that catalyzes the first two steps in the biosynthesis of prostaglandins (PG) from arachidonic acid (AA). The first step, catalyzed by the cyclooxygenase (COX) site, is the oxidation of AA to the hydroperoxy endoperoxide prostaglandin G_2 (PGG_2). This is followed by the reduction of PGG_2 to the hydroxy endoperoxide prostaglandin H_2 (PGH_2) by the peroxidase (POX) activity (Figure 1.4). PGH_2 is then transformed by other enzymes into the primary prostanoids (prostaglandins and thromboxanes) (Figure 1.4).

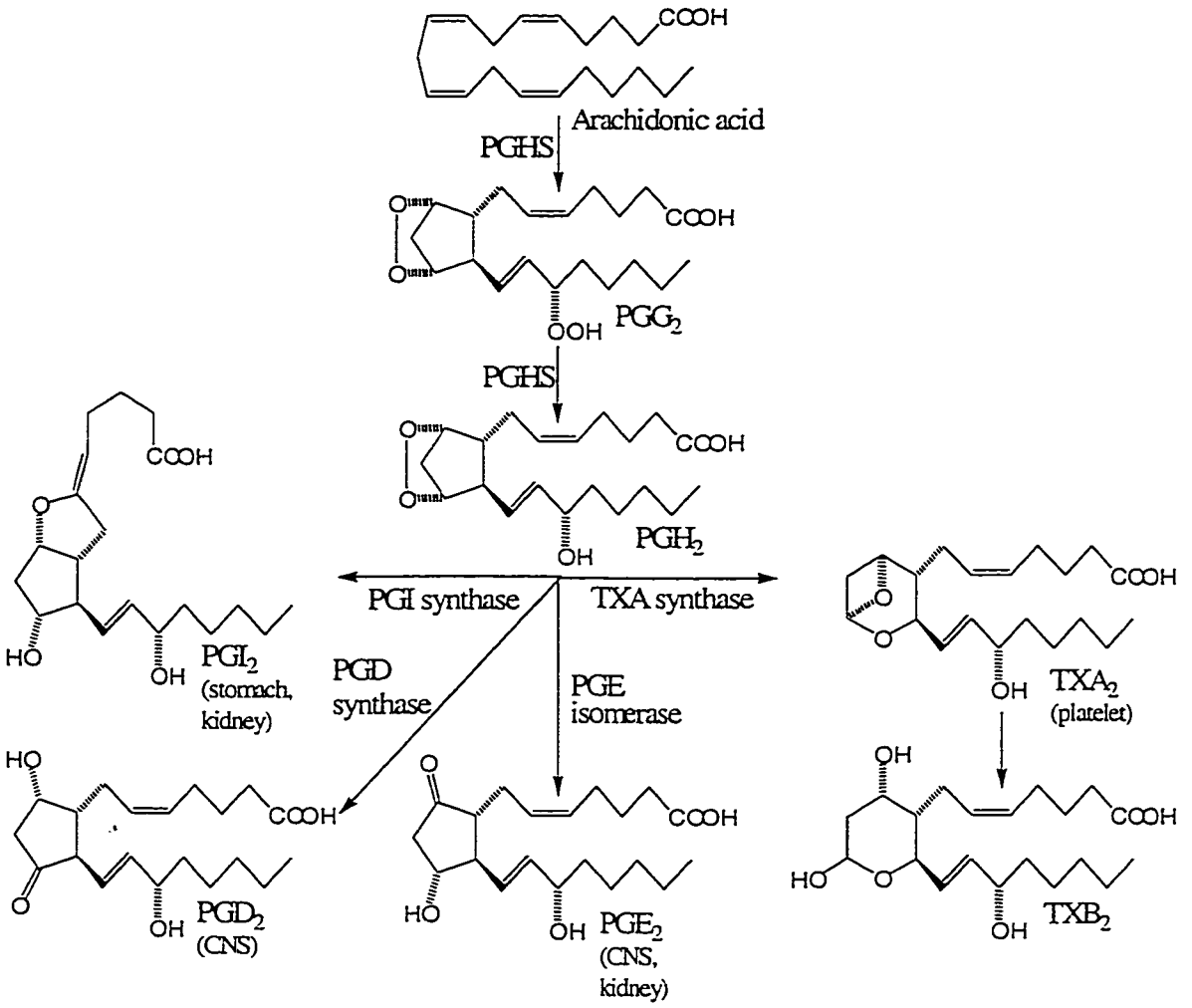

Figure 1.4. Prostaglandin biosynthesis.

In humans, prostaglandins and thromboxanes are involved in diverse functions, including blood clotting, ovulation, initiation of labor, bone metabolism, nerve growth and development, wound healing, kidney function, blood vessel tone, and immune responses. Prostaglandins are also involved in inflammation, and both local tissue injury and inflammatory diseases like osteoarthritis are associated with increased levels of prostaglandins (*84*). In contrast to hormones such as cortisone or thyroxin, which are released from a single site in the body yet have systemic effects, prostaglandins are synthesized in a variety of tissue types and generally function within the immediate environment as autocrine or paracrine mediators (*85*).

1.3.2 PGHS-1 and PGHS-2 isoforms

PGHS (PGHS-1) was first purified in 1976 (*86, 87*) and its gene cloned in 1988 (*88-90*). Shortly thereafter, a second PGHS gene (PGHS-2) was identified (*91-94*). The PGHS-1 and PGHS-2 proteins share ~ 60% sequence identity (*95*) and are derived from distinct genes that diverged well before the divergence of birds and mammals (*96*).

The two isoforms of PGHS are almost identical in structure and the residues involved in catalysis are conserved. However, there are some changes among residues involved in binding; *e.g.*, within the COX channel His513 and Ile523 [all numbering is that of oPGHS-1 (ovine) unless otherwise indicated] of PGHS-1 are replaced with Arg and Val, respectively, in PGHS-2, resulting in the accessibility of a hydrophobic side pocket, which is present but inaccessible in PGHS-1 (*15, 97-99*).

PGHS-1 and PGHS-2 have similar turnover numbers [~3500 mol of AA/min/mol of dimer (*100, 101*)], and K_m values for AA [~5 μM (*101, 102*)] and O_2 [~5 μM (*103, 104*)].

PGHS-1 is detectable in most tissues (*105, 106*), and in cultured cells it is typically expressed at constant levels throughout the cell cycle (*107*). This type of expression pattern suggests the major function of PGHS-1 is to provide prostaglandin precursors for homeostatic regulation. As a result of these findings, PGHS-1 has become known as the *constitutive* isozyme. In contrast, PGHS-2 is undetectable in most mammalian tissues, but its expression can be induced rapidly (2 - 6 h) in fibroblasts (*107-110*), endothelial cells (*111*), monocytes (*112*), and certain other cell types in response to growth factors, tumor promotors, hormones, bacterial endotoxin and cytokines. Therefore, PGHS-2 has been identified as the *inducible* isoform. PGHS-2 induction has also been observed in both human osteoarthritis-affected cartilage (*113*) and in synovial tissue taken from patients afflicted with rheumatoid arthritis (*114*). These observations strongly suggest that PGHS-2 is responsible for the increased prostaglandin production seen in inflamed joint tissues (*115*). Therefore, the development of PGHS-2-selective inhibitors have been the focus of much interest in the pharmaceutical community (*116, 117*).

1.3.3 Structure of PGHS

PGHS is a homodimer with a predominantly α-helical (~42%) structure that is divided into three domains. The EGF-like domain, which forms part of the dimer interface, comprises only residues 34-72. The overall conformation of this domain is very similar to epidermal growth factor (EGF) (*15*). Residues 73-116 are arranged in a spiral of four amphipathic helices which form the mouth of the COX active site. This domain is thought to be inserted monotopically into the membrane bilayer and is therefore referred to as the membrane-binding domain (Figure 1.5). The catalytic domain

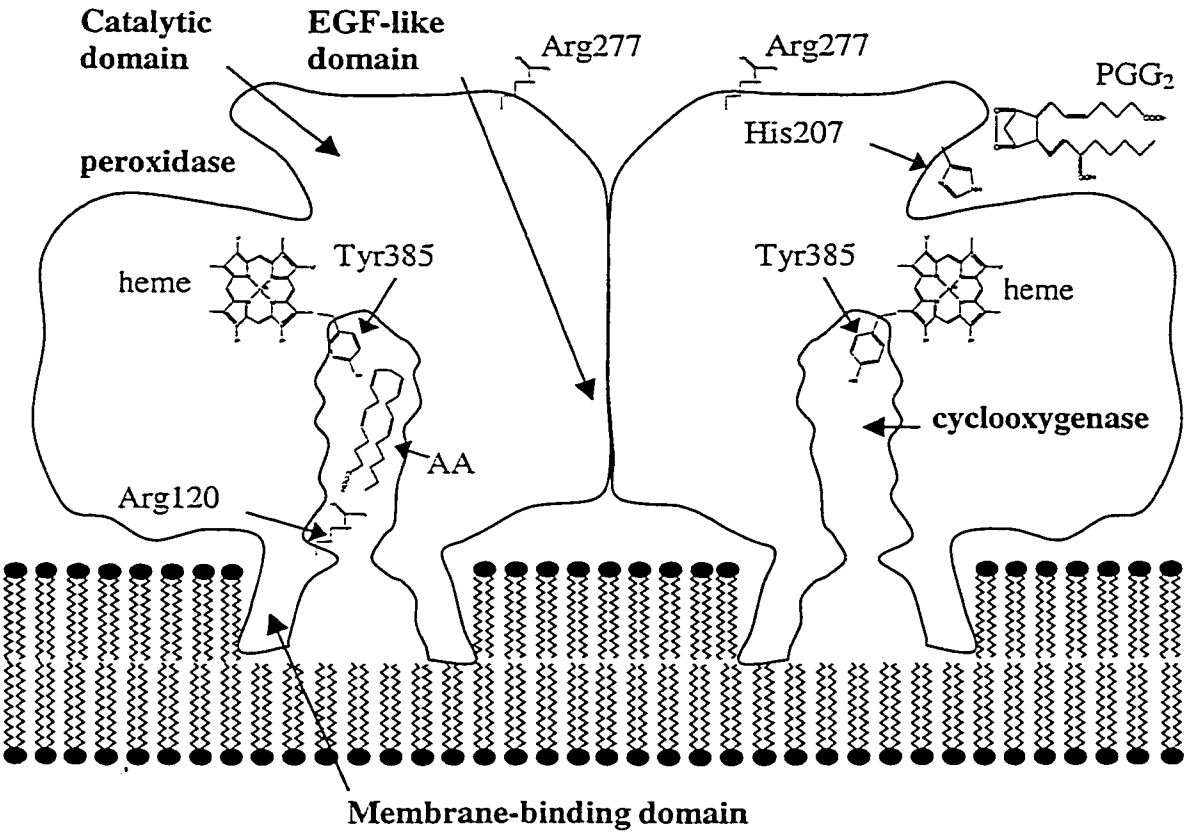

Figure 1.5. Cartoon figure of PGHS structure.

is the largest, comprising residues 117-587, and contains both the COX and POX active sites. The two active sites are physically separated. The COX site is a narrow channel (~8 x 25 Å) that extends through the membrane-binding domain to the center of each monomer, where the key catalytic residue, Tyr385, is located. The peroxidase site is located on the cytosolic surface of the enzyme (Figure 1.5) (*15, 97-99*).

1.3.4 PGHS catalysis

1.3.4.1 Peroxidase activity

The proximal and distal histidines of PGHS are His388 and His 207, respectively. The distal Arg of the plant peroxidase superfamily is replaced by a glutamine (Gln) in PGHS (Gln203). Site-directed mutagenesis has demonstrated that the distal His207 and Gln203 play the same roles as the corresponding residues in HRP (*118, 119*). The POX activity of PGHS preferentially reduces fatty acid hydroperoxides including PGG_2 (*120*). H_2O_2 is also accepted as a substrate, but the rate of oPGHS-1 Compound I formation with PGG_2 as the peroxide substrate is ~1400-fold the rate when H_2O_2 is used (*121, 122*).

Examination of the electronic spectra of the higher oxidation states of PGHS reveals considerable similarity to the higher oxidation states of HRP, CCP and other classical peroxidases (*25*). Addition of hydroperoxide to PGHS in the absence of an electron donor results in production of Compound I (complete within 10 ms) (*121*). The spectrum of Compound I is analogous to Compound I of HRP (*123*). Within 170 ms Compound I is converted to Compound II, indicating that the porphyrin radical cation of Compound I has been reduced (*121*). The spectrum of PGHS Compound II is virtually superimposable on that of HRP (*123-125*). Compound II slowly reverts to the resting enzyme (1-2 min at 5°C) (*121*).

PGHS is typical of many peroxidases in that it can accept a wide variety of compounds as reducing substrates and in general, electron-rich molecules are the best reductants (*126, 127*). Among a series of naturally-occurring compounds, the best substrates are epinephrine and uric acid (*126*). The physiological reducing substrate may vary among tissues but speculation has centered on uric acid (*128, 129*) because, although it is only a fair reducing substrate, it is present in high concentrations (~300 μM) in human plasma (*130, 131*).

While several PGHS-inhibitor crystal structures are available, the emphasis has been on binding interactions in the COX site to the exclusion of the POX site (*15, 97-99*). Therefore, little is known about the interactions involved in the binding of substrates to the POX site of PGHS. The similarity observed in the POX active sites of PGHS and MPO (*15*) suggests that the H-bonding interactions observed in the MPO-SHA structure (*76*) may be conserved in PGHS. An investigation of the binding of SHA, BHA and related compounds to PGHS is required to determine whether the MPO-SHA complex is an appropriate model for substrate binding to the POX site of PGHS.

1.3.4.2 Cyclooxygenase activity

The overall role of the COX activity is to stereospecifically remove the 13-pro-S-hydrogen of AA and control the stereochemistry of oxygenation (*132*). Computer modeling of AA in the COX site shows that the carboxylate group of AA is positioned adjacent to Arg120 (Figure 1.5) (*132*). This is in agreement with site-directed mutagenesis results which suggesting that Arg120 binds the carboxylate group of AA (*133*). Arg120 H-bonds to Glu524 and Tyr355, forming a network which stabilizes PGHS-substrate/inhibitor interactions and closes off the upper part of the COX active site

from the larger opening at the base of the channel (*15*). Disruption of this H-bonding network opens the constriction and enables substrate/inhibitor binding and release to occur (*132*).

The oxygenation reaction catalyzed by the COX site is distinct from many other oxygenases as it activates AA rather than oxygen (*25*). Isotope labeling and spin trapping experiments have shown that the removal of the pro-S hydrogen from C-13, is the rate-limiting step and that AA activation and O_2 attack are not concerted (*134, 135*). Figure 1.6 shows that COX catalysis involves the double dioxygenation of activated AA (*134, 136-139*).

The oxidizing agent that initiates AA oxygenation is a protein tyrosyl radical (Figure 1.6) (*53*) which has been located on Tyr385 by trapping of the radical. Incubation of wild-type enzyme with AA in the presence of nitric oxide quenches the EPR signal of the tyrosyl radical and leads to the formation of nitrotyrosine at position 385 in the protein (*55, 56*). In support of these spin-trapping results, the Y385F mutant is not catalytically active and does not oxidize AA when it is treated with peroxide (*54*). The crystal structures of both PGHS-1 and PGHS-2 reveal that Tyr385 is positioned perfectly to react with AA (*15, 97-99*).

1.3.4.3 Interaction between peroxidase and cyclooxygenase activities

Protein radicals require an oxidant for their formation, which in most cases is a metal-containing prosthetic group (*140*). The ferric resting state of the heme iron of PGHS is thermodynamically incapable of oxidizing Tyr385 because $E_{1/2} = 0.94$ V for free $Tyr^{\bullet} \rightarrow Tyr$ at pH 7.0 and $E_{1/2} = -0.2$ to +0.2V for $Fe^{III} \rightarrow Fe^{II}$ for most heme proteins

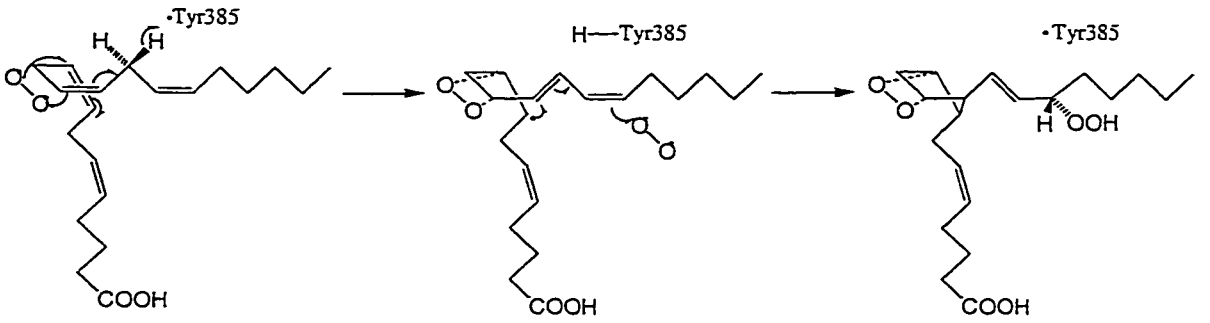

Figure 1.6. Cyclooxygenase catalysis.

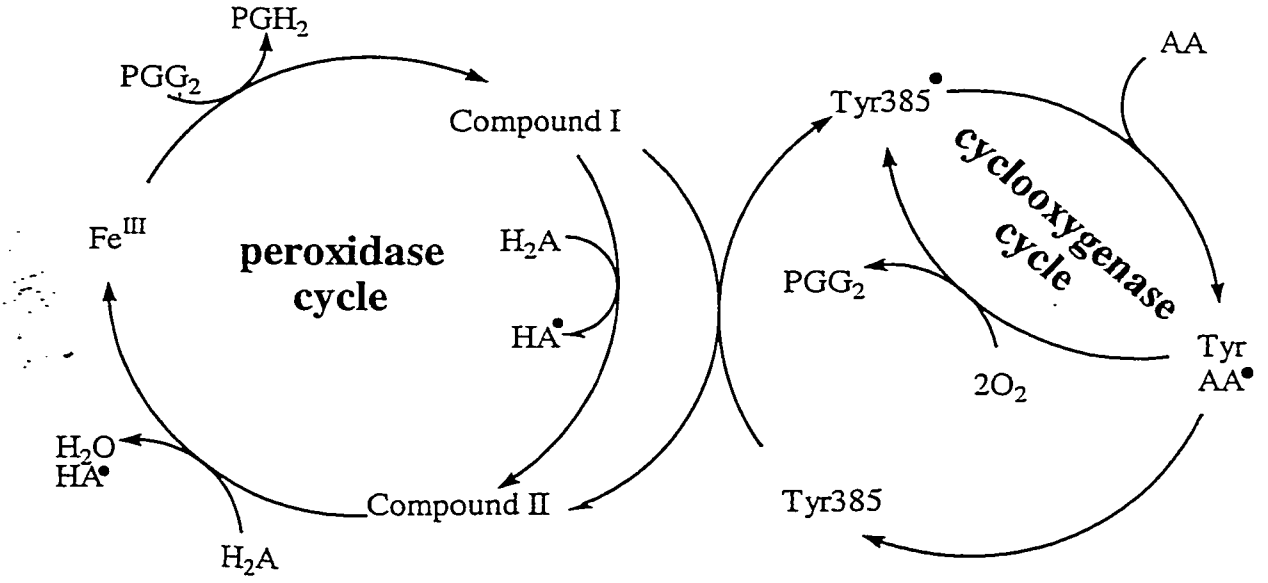

Figure 1.7. Interaction between the cyclooxygenase and peroxidase cycles of PGHS. In the branched-chain mechanism for PGHS the POX and COX cycles function independently following generation of a radical on Tyr385 (*122, 145*).

(*140, 141*). This suggests the involvement of peroxidase intermediates (*e.g.*, Compound I or II) since $E_{1/2} \sim 1$ V for $Fe^{IV} \rightarrow Fe^{III}$ (*132*). This is supported by the observation that a spectroscopically detectable tyrosyl radical is generated on the oxidation of PGHS(Fe^{III}) by organic or fatty acid hydroperoxides (*122, 142-144*). Figure 1.7 shows the branched chain mechanism proposed by Dietz et al. (*122*), in which the tyrosyl radical is generated by an internal electron transfer in POX Compound I.

1.4 PEROXIDASE INHIBITION

1.4.1 Peroxidases as inhibitor or drug targets

Peroxidases generate free radicals and other oxidants (*e.g.*, hypochlorous acid generation by MPO), which are capable of attacking lipids, nucleic acids, and other proteins *in vivo*, thereby resulting in their potential toxicity. The effects of the reactive species produced by PGHS and MPO have been investigated in relation to toxicity and tissue damage *in vivo*. PGHS-POX-dependent bioactivation of xenobiotics has been implicated in carcinogenesis, pulmonary- and nephrotoxicity, and teratogenicity (*146-148*). The hypochlorous acid produced by MPO has been implicated in tissue damage in diseases associated with neutrophil infiltration (*149, 150*). Specific POX inhibitors would be useful in further defining the roles of PGHS-2 and MPO in xenobiotic activation and oxidant-dependent injury in inflammatory diseases.

1.4.2 Reversible versus mechanism-based peroxidase inhibitors

The ability of peroxidases to utilize a variety of reducing substrates has created some confusion in the literature over the classification of compounds as peroxidase inhibitors. An example of this is the report of SHA as an inhibitor of MPO (*151*). SHA is an alternative substrate to the natural substrate, chloride ion, and decreases the

production of hypochlorous acid by MPO. MPO activity is unaffected by SHA; thus, while SHA does inhibit hypochlorous acid production, it is not a MPO inhibitor (*152, 153*).

The design of specific, reversible peroxidase inhibitors is challenging due to the low specificity demonstrated by most peroxidases for reducing substrates. This is compounded by the difficulty of designing an inhibitor that will not be oxidized by the peroxidase, as in the case of SHA and MPO. Another option in peroxidase inhibition is the development of mechanism-based inhibitors. From a pharmaceutical standpoint, mechanism-based inhibitors are not favored due to the risk of an immunogenic response associated with covalent modification of proteins (M.D. Percival, personal communication). However, while drugs are currently not intentionally designed as mechanism-based inhibitors, there are several examples of therapeutics that have been subsequently determined to be mechanism-based inhibitors (*154*). Particularly relevant examples are the inhibition of TPO by the antithyroid drugs methimazole, methylthiouracil and propylthiouracil (*154-156*). In addition, preliminary reports have proposed that 4-aminobenzhydrazide (4-NH_2-BZH) is a specific, mechanism-based inhibitor of MPO (*157, 158*), suggesting that hydrazides may be a promising class of compounds for the development of specific, mechanism-based POX inhibitors. Isoniazid (INH) is an example of a hydrazide that is currently in widespread use for the treatment of tuberculosis (*159*). However, while INH is activated by the Mycobacterial peroxidase/catalase, KatG, the target of activated INH is thought to be enoyl reductase, InhA (*160*), indicating that INH is not acting as a mechanism-based inhibitor. Therefore,

the mechanism of peroxidase inhibition by hydrazides must be thoroughly investigated prior to their development as POX inhibitors.

1.5 Cyclooxygenase inhibition

1.5.1 NSAIDs consumption

Nonsteroidal anti-inflammatory drugs (NSAIDs) inhibit the COX activity of PGHS and generally do not affect the POX activity (*161, 162*). Despite the widespread use of NSAIDs over the last century, their mechanism of action was not fully appreciated until relatively recently. In 1971 Vane reported (*163*) that NSAIDs inhibit prostaglandin formation and demonstrated that their relative PGHS inhibitory potency *in vitro* correlates to their anti-inflammatory activity *in vivo*. Today the market for NSAIDs is huge; *e.g.*, in one year in the US alone, ~50 million people spend 5-10 billion dollars to consume NSAIDs for the treatment of a wide spectrum of pathophysiological conditions, including prophylaxis against cardiovascular disease, relief of the discomfort associated with minor injuries and headaches, and alleviation of the severe pain caused by a variety of inflammatory and degenerative joint diseases (*85*). NSAIDs have also been reported to reduce the risk of Alzheimer's disease by as much as 50% (*164-166*).

1.5.2 NSAID classification

With the exception of acetylsalicylic acid (ASA), NSAIDs can be divided into 2 groups: the reversible inhibitors such as ibuprofen, and the time-dependent inhibitors such as indomethacin, flurbiprofen, and diclofenac (*162, 167, 168*).

Time-dependent inhibition is a two-step process (reaction 1.4) in which rapid equilibrium binding is followed by a slower isomerization to a non-covalent, but tightly-bound complex (*169-171*). Values of k_2 for PGHS-2 were estimated to be 0.0031 s^{-1} and

0.0082 s^{-1} for indomethacin and flurbiprofen, respectively, demonstrating that the conversion of the E•I* complex to E•I is slowly reversible (*171*). Therefore, reaction 1.4 is generally simplified to reaction 1.5.

$$E + I \underset{k_{-1}}{\overset{k_1}{\rightleftharpoons}} E\bullet I \underset{k_{-2}}{\overset{k_2}{\rightleftharpoons}} E\bullet I^* \qquad \text{(reaction 1.4)}$$

$$E + I \overset{K_I}{\rightleftharpoons} E\bullet I \xrightarrow{k_{inact}} E\bullet I^* \qquad \text{(reaction 1.5)}$$

The isomerization of E•I to E•I* is not associated with covalent modification for most inhibitors, with the exception of ASA and its derivatives (*132*). Formation of the E•I* complex occurs in seconds to minutes and may reflect the induction of a subtle protein conformational change, such as the breaking and reforming of the Arg120-Glu524-Tyr355 H-bonding network or binding to the hydrophobic COX side pocket (Section 1.3.4.1.) of PGHS-2 (*132*). The results of investigations of NSAID binding using fluorescence and circular dichroism (CD) spectroscopy agree with crystal structure findings, indicating that NSAID binding does not result in a global change in the conformation of PGHS (*98, 172, 173*). However, limited proteolysis has revealed that oPGHS-1 is protected from attack by trypsin in the presence of heme or time-dependent NSAIDs (indomethacin, flurbiprofen, meclofenamic acid) and to a slightly lesser degree by reversible NSAIDs (flufenamic acid and ibuprofen) (*173*). This suggests that the conformational stability of PGHS is altered by NSAID binding and is related to time-dependency. Fourier transform infrared (FTIR) spectroscopy is a useful technique for probing both conformational stability, via thermal denaturation, and secondary structure.

Therefore, an FTIR investigation of the effect of NSAID binding to PGHS may detect dynamic differences not apparent by crystallography.

1.6 PGHS INACTIVATION

Both the COX and POX activities of PGHS have been reported to undergo inactivation. There appear to be two different inactivation processes: (1) peroxide-dependent inactivation of COX and POX activities, and (2) autoinactivation of COX (the "suicide" reaction) (*57, 174-176*). An understanding of these inactivation processes may provide information on the regulation of PGHS activity and prostaglandin biosynthesis *in vivo*.

1.6.1 Peroxidase inactivation

When PGHS is incubated with peroxides in the absence of a reducing substrate, both the COX and POX activities are inactivated. For this reason a reducing substrate is added as a protective agent in buffers during PGHS purification (*126, 174, 176*). Peroxide-dependent inactivation causes changes in the heme spectrum of the enzyme and may involve modification of the heme group. Furthermore, peroxide-inactivated enzyme does not bind freshly added heme suggesting that the apoprotein is modified (*177*). Recently the kinetics of POX inactivation were investigated in the absence of a reducing substrate, and the rate (~ 0.4 s^{-1} at 24 °C) of inactivation was found to be independent of both the peroxide used and its concentration suggesting that inactivation originates from an activated peroxidase species, such as Compound I (*58*).

1.6.2 Cyclooxygenase inactivation

When PGHS is incubated with AA, the COX activity is inactivated before the AA is completely consumed (*120, 178, 179*). Each mole of purified enzyme can form

between 10 and 1300 mol of PGG_2 before the COX activity disappears (depending on the PGHS, AA, and reductant concentrations) while most of the POX activity still remains (*126, 180*). Kulmacz (*181*) investigated the incorporation of activated enzyme-bound intermediates into oPGHS-1 as a possible mechanism of COX inactivation. Although incorporation of AA into oPGHS-1 was observed, stoichiometric incorporation required ~1 h, while inactivation was complete within ~2 min, indicating that incorporation of an activated intermediate is not a major mechanism of COX inactivation in oPGHS-1 (*181*). Another potential mechanism of inactivation is the rearrangement of an activated and unstable protein radical intermediate to an inactivated enzyme (*57*). However, this possibility has not yet been investigated. Support for a radical-based mechanism of COX inactivation comes from the protective effect of POX reducing substrates against suicide inactivation (*126, 182-185*). Additionally, Tsai et al. (*144*) suggested that NSAID treatment of PGHS-2 changes the pathway of intramolecular electron transfer in Compound I, resulting in the oxidation of a Tyr residue other than Tyr385. Although the identity of this residue is unknown, this finding supports the possibility of inactivation due to unstable protein radical intermediates.

1.7 An Approach to the Study of POX and COX Inhibition and Inactivation

The preceding review highlights some of the key questions which remain unanswered in peroxidase inhibition and PGHS inhibition and inactivation:

1. How do the individual H-bonding and hydrophobic interactions observed in the HRP-BHA X-ray structure contribute to the tight binding of BHA?
2. What is the mechanism of peroxidase inhibition by hydrazides?

3. What are the key interactions involved in ligand binding to the POX site of PGHS-2?
4. Is it feasible to develop reversible inhibitors for the POX activity of PGHS-2?
5. Is the development of specific, mechanism-based inhibitors of the POX activity of PGHS-2 possible?
6. What effect does NSAID binding have on the conformational flexibility of PGHS-2 and what are the thermodynamic parameters of NSAID binding to the COX site of PGHS-2?
7. What are the mechanisms of inactivation of the POX and COX activities of PGHS-2?

Each of these questions was investigated and the results are presented and discussed in the following chapters:

3. Binding of aromatic hydroxamic acid analogues to the peroxidase site of HRP.
4. Inactivation of HRP by hydrazides.
5. Inhibition of the POX activity of PGHS-2
6. NSAID binding to the COX site of PGHS-2
7. Inactivation of PGHS-2

2. MATERIALS AND METHODS

2.1. MATERIALS

Recombinant hPGHS-2 was purified from baculovirus-infected Sf9 cells as previously reported (*186*). Lyophilized grade I horseradish peroxidase and sequencing grade trypsin were obtained from Boehringer Mannheim and PNGase F from New England Biolabs. All hydrazides, hydroxamic acids, and hydroxamic acid analogues were purchased from Lancaster with the exception of 3-hydroxybenzhydrazide (3-OH-BZH) and 4-hydroxybenzhydrazide (4-OH-BZH) which were from Aldrich. 2-naphthohydroxamic acid (2-NHA, Ar = naphth, X = OH) was a provided by Dr. G.R. Schonbaum. Phenylhydrazine was purchased from Sigma, 13-HPODE (13(S)-hydroperoxyoctadeca-9Z,11E-dienoic acid) and 13-HODE (13(S)-hydroxyoctadeca-9Z,11E-dienoic acid) from Biomol, and AA and ^{14}C-AA from Cayman. Diclofenac, meclofenamic acid, and flufenamic acid were purchased from Sigma, and ibuprofen, flurbiprofen, and indomethacin from Cayman. DFU, NS-398, L-761,164 and tepoxalin were synthesized in the Department of Medicinal Chemistry, Merck Frosst Centre for Therapeutic Research. Precast SDS-PAGE gels were purchased from Helix Technologies. All other reagents were of the highest quality available and used without further purification, as were all hydrazides.

2.2. METHODS

2.2.1. ITC of HRP

The ITC experiments on BHA and 2-naphthoichydroxamic acid (2-NHA) at pH 4.0 and on BHA, 2-NHA and SHA at pH 7.0 were performed using a MCS instrument from MicroCal at the Biotechnology Research Institute. All other ITC experiments for

HRP, were performed using a VP instrument from MicroCal at the Structural Genomics Center at Concordia. HRP samples for ITC were prepared by 24-h dialysis in 100 mM buffer at pH 4 (acetate, citrate, or tartarate), pH 6 (sodium phosphate) or pH 7 (sodium phosphate, Tris, imidazole, HEPES, PIPES, or MOPS). Ligand solutions were prepared in dialysis buffer immediately before use to ensure minimal background from buffer mismatch. The dialyzed HRP samples (ranging from 0.0026 - 1.14 mM, Table 3A.1) were added to the 1.4-mL sample cell. The NSAIDs were added to the sample cell in 10-μL injections from a 250-μL syringe rotating at 300 rpm. Typically, 29 injections were made at 4 - 8 min intervals, and the heat of reaction per injection (μcal/s) was determined by integration of the peak area using Origin software (MicroCal). For BZA, 2'HA, N-BH, INH and NICH the contribution of the heat of dilution to the observed heat of binding were determined by injection of ligand into the buffer only and the heat of dilution was subtracted from the observed heat of binding prior to data analysis. For all other experiments the heat of ligand dilution was determined from the baseline following completion of the titration and was subtracted from the observed heat of binding prior to data analysis.

The heat evolved per mole of ligand injected (kcal/mol) was plotted against the ligand/HRP molar ratio and the data were fitted to a single-binding-site model with the Origin software using equation 2.1:

$$1/V_0(dQ/dX_{tot}) = \Delta H^o\left(\frac{1}{2} + \frac{1-(1+r)/2-X_r/2}{X_r^2 - 2X_r(1-r)+(1+r)^2)^{1/2}}\right) \qquad \text{(eq. 2.1)}$$

where X_{tot} is the total ligand concentration in the reaction cell of volume V_0, Q is the heat absorbed or evolved, and $\Delta H°$ is the molar heat of binding. Equation 2.1 also contains two unitless parameters, X_r (eq. 2.2) and r (eq. 2.3), which depend on X_{tot}, the total macromolecule concentration (M_{tot}) and the dissociation constant (K_d):

$$1/r = c = \frac{M_{tot}}{K_d} \qquad \text{(eq. 2.2)}$$

$$X_r = \frac{X_{tot}}{M_{tot}} \qquad \text{(eq. 2.3)}$$

The Gibbs free energy of binding (ΔG°) and the entropy of binding (ΔS°) were calculated from the experimental values with equations 2.4 and 2.5:

$$\Delta G° = -RT\ln(1/K_d) \qquad \text{(eq. 2.4)}$$

$$\Delta G° = \Delta H° - T\Delta S° \qquad \text{(eq. 2.5)}$$

2.2.2. UV-VIS spectra and K_D determinations

Stock solutions of ferric HRP [HRP(Fe^{III})] in 100 mM sodium phosphate (pH 7.0) and ferric hPGHS-2 [hPGHS-2(Fe^{III})] in 100 mM sodium phosphate (pH 7.0) plus 1% octylglucoside were used for both spectral (Section 3.2.2.1), binding (Sections 3.2.1.2, 3.2.1.3 and 3.2.2.2) and kinetic experiments. For both spectral and binding experiments the peroxidase stock solutions were diluted to a final concentration of 2.5 μM in the following buffers: 100 mM sodium phosphate pH 7.0, 8.0, and 12.0; 100 mM TAPS pH 9.0; and 100 mM CAPS pH 10.0. 1 M stock solutions of the ligands were prepared by

weight in DMSO and serial dilutions made in the appropriate buffer. To record the UV-VIS spectra, 2 mL of 2.5 μM HRPC or hPGHS-2 was added to a 3-mL quartz cuvette and allowed to equilibrate for 15 min. Samples were mixed with a magnetic stirbar and all spectra were recorded at 25°C.

Protein-ligand titrations were performed by the successive addition of 2-μL aliquots of the appropriate concentration of ligand to the cuvettes. Solutions for BZH titrations at pH 7.0 and above were flushed extensively with N_2 gas to remove oxygen and titrations were performed in a cuvette with a septum. The observed or apparent dissociation constants ($K_{d(app)}$) were determined from least-squares fits of eq. 2.6.

$$[E-L]=\frac{[E]_{TOT}[L]}{K_{d(app)}+[L]} \qquad \text{(eq. 2.6)}$$

where $[E]_{TOT}$ is the total enzyme concentration, $[E\text{-}L]$ the concentration of bound ligand ($[E\text{-}L] = \Delta A/\Delta\varepsilon$, where ΔA is the difference in absorbance of free enzyme (E) and the E-L complex, and $\Delta\varepsilon$ is the corresponding difference in molar absorptivity), and $[L]$ the concentration of free ligand ($[L] = [L]_{TOT} - [E\text{-}L]$, or $[L] = [L]_{TOT}$ if the total ligand concentration ($[L]_{TOT}$) is much greater than $[E]_{TOT}$) (*187*). $K_{d(app)}$ values were corrected for substrate ionization ($K_d = \alpha K_{d(app)}$) by multiplying by the fraction of unionized ligand (α).

2.2.3. Determination of K_I and k_{inact} values, and partition ratios for inhibition of HRP

100 nM HRP was preincubated with 500 μM H_2O_2 and 0-5 mM hydrazide in 100 mM sodium phosphate buffer, pH 7.0, for 0.5-120 min. HRP activity was then measured

spectrophotometrically for 1 min at 450 nm with guaiacol as the chromogenic reducing substrate using a SpectraMax 190 (Molecular Devices) microtitre plate reader. The assay solution (200 μL) contained 5 mM guaiacol, 600 μM H_2O_2, and 10 nM HRP in 100 mM sodium phosphate, pH 7.0. The percent remaining activity was calculated as the ratio of the initial velocity compared to that of the control (no NSAID). Plots of percent remaining activity vs preincubation time (0.5-120 min) were produced for each hydrazide concentration (0-5 mM) and the pseudo-first-order rate constants for HRP inactivation (k_{obs}, s^{-1}) at each hydrazide concentration (0-5 mM) were calculated by a least-squares fit to equation 2.7:

$$y = a + b\exp(-k_{obs}t) \qquad \text{(eq. 2.7)}$$

where y = remaining activity, a = remaining activity at $t = \infty$ (minimum activity), and b = remaining activity at $t = 0$ (maximum activity), and t = time. The k_{obs} values obtained were then plotted vs hydrazide concentration $[I]$ and the apparent K_I and k_{inact} determined by a least-squares fit to equation 2.8:

$$k_{obs} = \frac{k_{inact}[I]}{K_I + [I]} \qquad \text{(eq. 2.8)}$$

Partition ratios were determined from remaining activity measured following a 10-min preincubation with each hydrazide because the remaining activity for the various hydrazide concentrations covered a broad range at this point. The numerical values for

the partition ratio for each hydrazide was determined by extrapolation to the x-axis in a plot of *[I]/[HRP]* vs percent remaining activity.

2.2.4. IC_{50} determination for inhibition of the POX activity of HRP and PGHS-2 by hydrazides

HRP (100 nM) was preincubated in 100 mM sodium phosphate, pH 7.0, containing 500 μM H_2O_2 and 0.001 - 50 mM hydrazide for 1 min prior to assaying activity. Activity was assayed as described in Section 2.2.3. The resulting percent remaining activity was plotted versus hydrazide concentration to generate titration curves, which were fit to equation 2.9:

$$y = \frac{(a-b)}{1+([I]/IC_{50})^c} + b \qquad \text{(eq. 2.9)}$$

where y = percent remaining activity, a = maximum percent remaining activity as inhibitor [*I*] concentration approaches zero, b = minimum percent remaining activity as [*I*] approaches ∞ and c = the slope when $[I] = IC_{50}$.

2.2.5. CO trapping of ferrous HRP

Aliquots (2-mL) of buffer were deaerated and saturated with CO by bubbling CO while stirring for 20 min in a 3-mL cuvette fitted with a septum. HRP(Fe^{III}) was added to 5.5 μM and the cuvette flushed with CO for a further 5 min. BZH stock solutions (1 M) were similarly deaerated and CO saturated. Spectra were taken before addition of BZH (to 25 mM) and at 30-s intervals following addition for a period of 30 min. An

HRP(Fe^{II})-CO standard sample was prepared for comparison by addition of 10 μL of a saturated dithionite solution to a solution of 5.5 μM HRP saturated with CO.

2.2.6. Determination of oxygen consumption

Oxygen uptake or production was measured at 25°C using a micro oxygen chamber and electrode (reaction volume 0.60 mL; Instech Laboratories, Model SYS600) coupled to a dual oxygen electrode amplifier (Instech Laboratories, Model 203). For the determination of BZH oxidation, the solutions contained 100 mM buffer (sodium phosphate, pH 7.0, 8.0, 12.0; TAPS, pH 9.0, CAPS, pH 10.0) and 25mM BZH in the presence or absence of 2.5 μM HRP.

For the H_2O_2 turnover experiments, 1 mM H_2O_2 was added (t = 0) to a solution of 100 mM sodium phosphate, pH 7.0, following by the addition of 2.5 μM HRP.

2.2.7. Determination of H_2O_2 consumption

H_2O_2 concentrations were determined using the Pierce perOXoquant kit. Aliquots (100 μL) of the solution being tested for H_2O_2 concentration were added to 1 mL of a solution containing 250 μM ammonium ferrous sulfate, 25 mM H_2SO_4, 1 mM sorbitol and 1.25 μM xylenol orange. Reactions were incubated at 25°C for 15 min prior to reading the absorbance at 560 nm. A standard curve was constructed for 1 - 100 μM H_2O_2 and the H_2O_2 concentrations of the unknowns were determined from the absorbance at 560 nm by comparison with the standard curve.

2.2.8. Isolation and identification of modified hemes from HRP

The heme extraction protocol of Ator and Ortiz de Montellano (*188*) was used with modifications as required. The effect of BZH/H_2O_2 ratios of 2:1, 1:1 and 1:2 on

HRP inactivation were investigated. The effects of 2:1, 1:1, and 1:2 PH/H_2O_2 were also determined for comparison. BZH (or PH) and H_2O_2 were added to 2.5-mL solutions of 20 μM HRP in a series of aliquots, until HRP was completely inactivated, such that the incremental concentrations of H_2O_2 and inhibitor did not exceed 2 mM to prevent damage to the enzyme. Activity was assayed as described in Section 2.2.3 2 min after each addition of BZH (or PH) and H_2O_2. Following a ~ 10 min incubation at room temperature the inactivated HRP solution was desalted on a 9 mL G-25 column (PD10, Pharmacia). The resulting 3.5 mL protein solution was acidified with 1 mL of glacial acetic acid, saturated with NaCl and the heme extracted into three 3-mL portions of ethyl acetate. The combined organic layers were washed with water, evaporated to dryness under a stream of argon and dissolved in 250 μL of HPLC solvent A (68:32:10 methanol/water/acetic acid). A 200 μL sample of the heme extraction was separated by isocratic reverse-phase HPLC on a Novapak C18 (3.9x150 mm) column at a flow rate of 1 mL/min in HPLC solvent A and monitored at 400 nm.

For analysis by mass spectrometry, samples (20 μL) of modified hemes from HRP and hPGHS-2 were separated by reverse-phase HPLC on a Hewlett Packard 1090 HPLC using a Vydac C18 (1x250 mm) column at a flow rate of 40 μL/min of solvent A. The column was connected directly to a Finnigan SSQ 7000 single quadrupole mass spectrometer fitted with an electrospray ionization source. The needle spray voltage was 4.5 kV and on-line acquisition of mass spectra was performed at a rate of 5 s/scan.

2.2.9. IC_{50} determination for inhibition of the POX activity of PGHS-2 by tepoxalin

HRP (100 nM) was preincubated in 100 mM sodium phosphate, pH 7.0, containing 5 mM guaiacol and 0.001 - 50 mM tepoxalin for 15 min prior to assaying of

activity. Activity was assayed directly in the preincubation solutions and the assay was started by the addition of 400 μM H_2O_2 and monitored at 450 nm for 1 min. The resulting percent remaining activity was plotted versus tepoxalin concentration to generate titration curves, which were fit to equation 2.9 as described in Section 2.2.4.

2.2.10. HPLC assay for hydrazides as POX reducing substrates

The relative efficiencies of a subset of hydrazides as hPGHS-2 POX reducing substrates were established by measuring the reduction of 13-HPODE to 13-HODE. The method previously described by Markey et al (*126*) was modified such that 55 nM hPGHS-2 was preincubated in 200 μL Tris buffer, pH 8.0, containing 0.05% octylglucoside and 100 μM reducing substrate at room temperature for 1 min following which the reaction was initiated by the addition of 5 μM 13-H-PODE and terminated after 1 min by the addition of 600 μL of 25% acetonitrile. A sample of 100 μL was separated by isocratic reverse-phase HPLC on a Novapak C18 (3.9x150 mm) column at a flow rate of 2 mL/min in 60:40:0.1 acetonitrile/water/acetic acid.

2.2.11. IC_{50} determination for cyclooxygenase activity

PGHS-2 (100 nM) was preincubated in a 180-μL solution of 100 mM sodium phosphate, pH 6.5, containing 1 μM heme, 1 mg/mL gelatin and 0.01 - 500 μM NSAID for 15 min at 22°C prior to the assaying of activity. The reaction was initiated by the addition of a 20-μL solution of 1 mM AA and 1 mM TMPD in assay buffer (without heme). Activity was monitored at 610 nm for 1 min and the percent remaining activity was calculated as the ratio of the initial velocity compared to that of the control (no

NSAID). The resulting percent remaining activity was plotted versus NSAID concentration to generate titration curves, which were fit to equation 2.9.

2.2.12. Fourier transform infrared (FTIR) spectroscopy

In preparation for the FTIR experiments in D_2O, hemin was added, the holoenzyme concentrated by ultrafiltration using a Centricon (Amicon), dialyzed against D_2O buffer (100 mM Sodium phosphate pD 7.0, 1% β-octylglucoside (Boehringer Mannheim)), aliquoted, and frozen immediately in liquid nitrogen. The final protein concentration was 22 mg/mL (300 μM). NSAIDs were dissolved in perdeuterated DMSO (d_6) (Aldrich) and added in stoichiometric amounts to hPGHS-2. The final DMSO concentration of the samples was 9.1%. FTIR spectra were recorded on a N_2-purged Nicolet FTIR spectrometer (Model 550) with a deuterated triglycine sulfate (DTGS) detector. The FTIR cell consisted of a temperature-controlled cell mount with CaF_2 windows (13 X 2 mm) separated by a 56-μm Teflon spacer. For thermal denaturation the temperature was ramped by 2°C between 20 and 95°C. After a 10 min interval for temperature equilibration each IR spectrum (128 scans) was recorded at 4 cm^{-1} resolution. Resolution enhancement was performed according to the method of Kauppinen et al. (*189*) using a bandwidth factor (w) of 15 cm^{-1} and a resolution factor (k) of 1.8. The spectra were baseline corrected and the integrated intensity of the amide I/I' and II bands were normalized to the tyrosine band (1508-1521 cm^{-1}) and plotted vs temperature (*190*). The T_m was taken to be the midpoint of the curve of the intensity of the 1650-1660 cm^{-1} α-helical band vs temperature.

FTIR samples in H_2O were prepared in the same manner as above to a final concentration of 30.5 mg/mL hPGHS-2 in 100 mM Sodium phosphate pH 7.0 buffer with

1% β-octylglucoside. A 6-μm teflon spacer was used to reduce absorption of water in the amide I/II region. The spectrum of buffer was acquired twice in the same cell under conditions identical to those used for hPGHS-2. The difference of these two reference spectra yielded the water vapor spectrum. The "uncorrected" protein spectrum was obtained by subtracting the buffer spectra from that of protein in buffer using subtraction criteria of Dong et al. (*191, 192*) (a straight baseline between 2000 and 1700 cm^{-1}). The water vapor spectrum was then subtracted from the "uncorrected" protein spectrum to yield the final "corrected" spectrum. In all cases, there was no observable noise in the amide I/II region of the final protein spectra so that smoothing was not required. The amide I (1700-1600 cm^{-1}) and amide II (1600-1500 cm^{-1}) regions of the spectrum were deconvolved as described above for the D_2O samples. Percent nonexchanged amide hydrogens in the D_2O samples was estimated from the ratio of the intensities of the amide II bands in D_2O and H_2O after corrections for concentration and path length.

2.2.13. Circular dichroism (CD) spectroscopy

CD experiments were performed on a Jasco model 710 CD spectrophotometer. hPGHS-2 concentration was 0.5 mg/mL (7 μM) in 100 mM sodium phosphate pH 7.0, 1% octylglucoside and diclofenac was added to stoichiometric concentrations (7 μM). CD spectra are the average of 5 scans between 184 and 280 nm in a 0.1 mm pathlength water-jacketed cell at a resolution of 0.2 nm, a bandwidth of 1.0 nm, a sensitivity of 100 mdeg, and a response time of 0.25 s. The temperature was ramped manually in 2°C intervals in the transition range and in 5°C intervals outside this range.

2.2.14. Differential scanning calorimetry (DSC)

Differential scanning calorimetry experiments were performed using the VP-DSC instrument from MicroCal at a scan rate of 60 °C/min over the temperature range 20-110°C. hPGHS-2 (0.14 mg/mL, 2μM) samples for DSC were prepared by overnight dialysis in 100 mM Sodium phosphate pH 7.0 with 1% octylglucoside. Diclofenac (11.8 μM), meclofenamic acid (7.5 μM), and L-761,164 (22.3 μM) were added and samples were incubated for 30 min at room temperature to ensure that time-dependent inhibition was complete. A baseline of buffer alone or with the appropriate NSAID was subtracted from each sample using Origin software (MicroCal).

2.2.15. Isothermal titration calorimetry (ITC) of PGHS-2

The isothermal titration calorimetry (ITC) measurements were performed using a MCS instrument from MicroCal. hPGHS-2 samples for ITC were prepared by addition of stoichiometric amounts of heme followed by 24 h dialysis in 100 mM Sodium phosphate pH 7.0 with 1% octylglucoside. NSAID solutions were prepared in dialysis buffer immediately before use to ensure minimal noise from buffer mismatch. hPGHS-2 was diluted in dialysis buffer to the appropriate concentration (0.1-0.4 mg/mL, 1-6 μM) and added to the 2.4 mL sample cell. The NSAIDs were added to the sample cell in 10-μL injections from a 250-μL syringe rotating at 400 rpm. Typically, 30 injections were made at 4 min intervals, and the heat of reaction per injection (μcal/s) was determined by integration of the peak obtained using Origin software (MicroCal). Contributions of the heat of dilution contribution to the observed heat of binding were determined by NSAID injection into the buffer only and the heat of dilution was subtracted from the observed heat of binding prior to data analysis.

The heat evolved per mole of ligand injected (kcal/mol) was plotted against the NSAID/hPGHS-2 molar ratio and the data were fitted with the Origin software (eq. 2.1) to yield the binding constant (K_a), the enthalpy of binding ($\Delta H°$), and the stoichiometry of binding, n. The Gibbs free energy of binding ($\Delta G°$, $\Delta G°=-RTlnK_a$) and the entropy of binding ($\Delta S°$, $\Delta G° = \Delta H° - T\Delta S°$) were calculated from the experimental values.

2.2.16. Active-site titration of PGHS

PGHS-2 (40μM) was dialyzed in 100 mM sodium phosphate, pH 7.0, containing 1% octylglucoside, for 6 h to remove homovanillic acid. The dialyzed PGHS-2 was subsequently diluted to 1.0 μM and preincubated with 0 - 5 μM diclofenac in 100 mM sodium phosphate, pH 7.0, containing 1% octylglucoside at 25 °C for 1 h prior to assaying. PGHS-2 (0.1 μM) activity was assayed in a solution of 100 mM sodium phosphate, pH 6.5, containing 1 mg/mL gelatin, 1 μM heme, 100 μM AA, and 100 μM N,N,N'N'-tetramethyl-p-phenyldiamine dihydrochloride (TMPD) at 25 °C and monitored at 610 nm for 1 min. The percent remaining activity was then plotted versus the diclofenac concentration in the preincubation. The active site concentration of PGHS-2 was determined to be equal to the diclofenac concentration when PGHS-2 activity reached baseline, *i.e.*, at the intersection of the two straight-line portions of the plot.

2.2.17. ^{14}C-AA incorporation into PGHS

6.0 μM PGHS-2 (3.2 μM active sites) or 3.5 μM oPGHS-1 (1.05 μM active sites) was incubated in 100 mM sodium phosphate, pH 7.0, containing 0.5% octylglucoside and 140 μM ^{14}C-AA (24 Ci/mol). At time points of 0.2 - 120 min duplicate 1.8-μg aliquots were withdrawn, mixed with SDS-PAGE sample buffer, heated at 100°C for 5 min, and

run on duplicate 8%, 1 mm SDS gels. Two identical sets of gels were thus generated and following Coomassie staining one set of gels were dried and exposed to film to produce the autoradiographs. The PGHS-2 bands were excised from the second set of gels and the gel slices were incubated in 0.5 M H_2O_2 in 50% acetonitrile for 2 days at 25°C prior scintillation counting. The CPM values obtained from scintillation counting were converted to moles of ^{14}C-AA using equation 2.10:

$$\mu Ci = (CPM \bullet 9.091 \times 10^{-7}\ \mu Ci/CPM)/24\ \mu Ci/\mu mol \qquad \text{(eq. 2.10)}$$

2.2.18. H_2O_2-dependent crosslinking of PGHS-2

PGHS-2 (10 μM) was incubated in 100 mM sodium phosphate, pH 8.0, and 0 - 100 mM H_2O_2 alone or in the presence of 2 mM phenol, for 30 min at 25°C. Mannitol (1 - 100 mM) or N-acetyltyrosinamide (10 or 100 μM) were added to some incubations to investigate radical scavenging. Following the incubation, aliquots of 10 μg PGHS-2 were mixed with SDS-PAGE sample buffer, heated at 100°C for 5 min, run on a 8%, 1-mm SDS gel, and Coomassie stained.

2.2.19. Tryptic digestion of PGHS-2

PGHS-2 (28 μg) was incubated in 4.6 M guanidinium hydrochloride containing 5 mM DTT at 65 °C for 1 h to unfold the protein and break its disulfide bonds. The sample was then cooled to 25°C and iodoacetamide was added to 20 mM and the sample was incubated for 1 h at 25°C in the dark to alkylate cysteine residues and thereby prevent disulfide shuffling. This was followed by dilution of the sample to give a guanidinium

hydrochloride concentration of 0.18 M, then 0.5 μg trypsin was added and the sample was incubated at 37°C. After 4 h a further 0.5 μg of trypsin was added and the sample was incubated overnight at 37 °C. Following tryptic digestion 2000 units of PNGase F was added and the sample incubated for a further 4 h at 37°C. Aliquots (0.7μg) were mixed with SDS loading buffer and analyzed by SDS-PAGE on a 1-mm 4 - 20% gradient gel.

3. BINDING OF AROMATIC HYDROXAMIC ACID ANALOGUES TO THE PEROXIDASE SITE OF HRP

3.1. INTRODUCTION

3.1.1. Thermodynamics of binding

The exponential growth in the number of protein crystal structures available in the past decade has allowed for a corresponding growth in other fields, including rational drug design. However, while crystal structures allow the visualization of specific interactions, being able to see an interaction provides no information about its contribution to the energy of binding (*79*). An understanding of the thermodynamic processes underlying molecular recognition is essential to successful inhibitor design. ITC measures binding interactions by detection of the heat absorbed or released during binding, and as such is more generally applicable than many other available methods (*e.g.*, equilibrium dialysis) for measuring binding affinity (*193*). Furthermore, the direct measurement of thermodynamic parameters by ITC (*194*) allows for the investigation of the driving forces involved in binding.

The affinity of a ligand for a macromolecule (*e.g.*, protein) is related to the free energy of binding (eq. 2.4) and is composed of enthalpic and entropic components (eq. 2.5). The balance of these two components determines the nature of an interaction, *i.e.* exothermic versus endothermic. An exothermic binding interaction is enthalpically driven because bond formation (*e.g.*, H-bond, salt bridge) results in the release of heat. On the other hand, an endothermic binding interaction is entropically driven because heat is absorbed to increase the randomness of the system.

The role of water is one of the key factors in protein ligand interactions and is also one of the most commonly overlooked (*79*). All protein-ligand interactions compete with interaction with water molecules. Prior to binding, both the protein and the ligand are solvated, and binding results in the loss of part of their solvation shell. Thus, desolvation plays a major role in binding interactions and the formation of an H-bond in a protein-ligand complex is an exchange process requiring the breaking of H-bonds between water and protein or the ligand or both. If the binding of a ligand simply replaces tightly-bound water molecules without yielding additional interactions, its binding affinity will be low. Conversely, the replacement of loosely-bound water molecules results in tight ligand binding, as it is both enthalpically (formation of H-bonding interactions of released water molecules with other water molecules) and entropically (increased disorder of water molecules released to the bulk solvent) favourable.

Hydrophobic interactions are not as easily visualized as H-bonds and charge-charge interactions, but specific hydrophobic interactions are often crucial to tight binding (*79*). Although there is an enthalpic component, due to H-bonding of released water molecules with other water molecules, hydrophobic interactions are generally entropically driven. This is because the loosely-bound water molecules released from hydrophobic surfaces upon binding are no longer ordered (*195*). Thus, water plays a crucial role in ligand binding, both in hydrophobic and H-bonding interactions.

Another factor involved in determining binding affinity is ligand and protein flexibility (*e.g.*, rotational, translational). Any reduction in the flexibility of either the ligand or protein residues is entropically unfavorable. For example, investigation of the binding of a series of compounds to streptavidin demonstrated that the highest binding

affinity was observed for compounds with the greatest residual mobility (*196*). Ligand flexibility is a dynamic property that is not easily estimated from a crystal structure and is often not taken into account in many modeling and docking programs (*79*). Therefore, the need for an analysis of the driving forces of ligand binding is highlighted by the difficulty in estimating the contribution of the desolvation and flexibility to binding by examination of crystal structures. Investigation of the thermodynamics of binding of a series of related compounds by ITC provides an understanding of the driving forces of binding required to complement crystal structure investigations.

3.1.2. spectroscopic properties of heme peroxidases

The chromophoric group of peroxidases is the Fe^{III} protoporphyrin IX (heme). The heme gives rise to two $\pi \rightarrow \pi^*$ electronic transitions at about 400 nm (Soret) and 500-600 nm (α, β bands). The wavelengths of these transitions are indicative of the oxidation, spin, and coordination states of the heme iron (*197*). The resting state for peroxidases [POX(Fe^{III})] is high spin (HS) because the five electrons are unpaired and distributed over the five *d* orbitals of almost equal energy (*187*).

The crystal structures of many peroxidases show a distal water molecule sitting above the Fe^{III} atom at a distance varying between 2.4 Å [CCP, (*17*)] and 5.7 Å [BP, (*12*)]. Such a distance is greater than that typical of ferric heme iron-ligand bond lengths [1.9-2.1 Å, (*198*)]; therefore, the heme iron is considered to be 5-coordinate (5-c) in heme peroxidases (*3*). The 6-coordinate (6-c) HS heme is distinguished from the 5-c HS by an increase in the Soret extinction coefficient of ~ 40% and a decrease in the intensity of the shoulder at ~380 nm, which is pronounced in the 5-c HS species (*3, 199*). The binding of BHA (Ar = ph, X = OH, Figure 3.1) to HRP(Fe^{III}) and CiP(Fe^{III}) results in a 5-c to 6-c

transition, where the distal water molecule is the sixth iron ligand (*200*). This transition is typical of substrate binding in many plant peroxidases, thereby providing a useful probe of binding. BHA in particular has been frequently used to probe the distal heme pocket of HRP and other peroxidases (*59, 61-65, 71, 73, 74, 201-205*).

3.1.3. HRP-BHA as a model complex

The ability of BHA to act as a reducing substrate of HRP (reactions 1.2 and 1.3) and compete with other reducing substrates (*63, 206*) suggests that HRP-BHA can serve as a model of a reducing-substrate complex (*61, 63, 206*). An interesting feature of BHA is its relatively tight binding to HRP (K_d = 2.4 μM), which has been attributed to polyfunctional H-bonding to residues within the distal cavity (*63*). Thus, the HRP-BHA complex is an attractive model for an investigation of the contribution of the various H-bonding and hydrophobic contacts to the binding of aromatic compounds to HRP. Furthermore, since HRP is considered one of the archetypical peroxidases (*2*), the HRP-BHA complex is also a good model for other less easily available peroxidases.

Although a wide range of spectroscopic [*e.g.*, resonance Raman (RR), UV-VIS, FTIR) and other techniques (*e.g.*, X-ray crystallography, computer modeling) have been used in numerous investigations on the binding of donor substrates to HRP, little information is available on the thermodynamics of binding. In this study the thermodynamics and binding affinities of HRP(Fe^{III}) for a series of Ar-CO-NH-X and related compounds (Figure 3.1) were investigated by ITC. The K_d values of these compounds were also determined spectroscopically to provide a comparison for ITC values. The thermodynamics of binding of these compounds to HRP are discussed in relation to the contribution to binding of specific H-bonding and hydrophobic interactions in

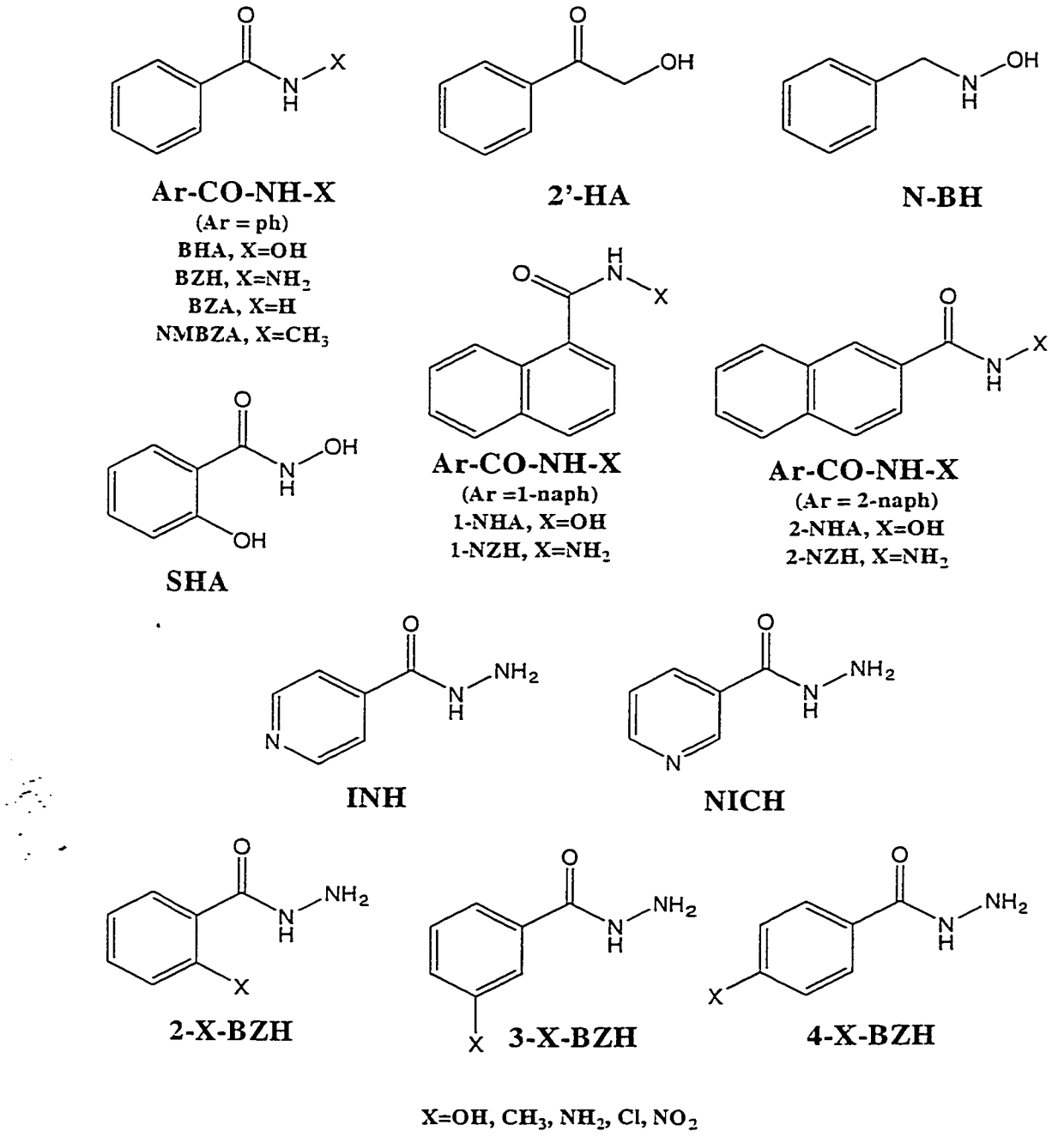

Figure 3.1. Structures of the compounds used in peroxidase binding (Chapters 3 and 5) and inhibition studies (Chapters 4 and 5).

the HRP heme cavity. The binding of a subset of compounds (BHA, SHA, 1-NHA, 2-NHA, BZH, BZA, and NMBZA) were also investigated spectroscopically over the pH range 4.0 - 12.0 for the purpose of providing further information on various binding interactions in the distal cavity of HRP.

3.2. Results

3.2.1. Thermodynamics of binding

The thermodynamics of the association between HRP and the series of aromatic compounds shown in Figure 3.1 were measured by ITC. Figure 3.2 shows the representative calorimetric titrations of HRP with BHA and N-methylbenzamide (NMBZA; Ar = ph, X = CH_3) in sodium phosphate, pH 7.0. Each peak in the binding isotherm (top panels of Figure 3.2.) represents an injection of ligand. The negative deflections from the baseline indicate that heat is evolved, showing that both binding reactions are exothermic. The enthalpy change per ligand injection was plotted as a function of the molar ratio of ligand to HRP (bottom panels of Figure 3.2), and from this plot (eq. 2.1) it was possible to determine the K_d, the stoichiometry of binding (n), and the enthalpic ($\Delta H°$) contribution to the Gibbs free energy of association ($\Delta G°$). $\Delta G°$ and the entropic ($\Delta S°$) contribution to $\Delta G°$ were calculated from equations 2.4 and 2.5, respectively.

Comparison of the titration curves for BHA and NMBZA (Figure 3.2.) highlights the difficulty, due to instrument sensitivity, in performing titrations for compounds with K_d values approaching the mM range. The steepness of an ITC titration curve is determined by the K_d and the concentration of macromolecule (HRP in this case), and is expressed by the value c (eq. 2.2, c = [HRP]/K_d, where [HRP] is the concentration of

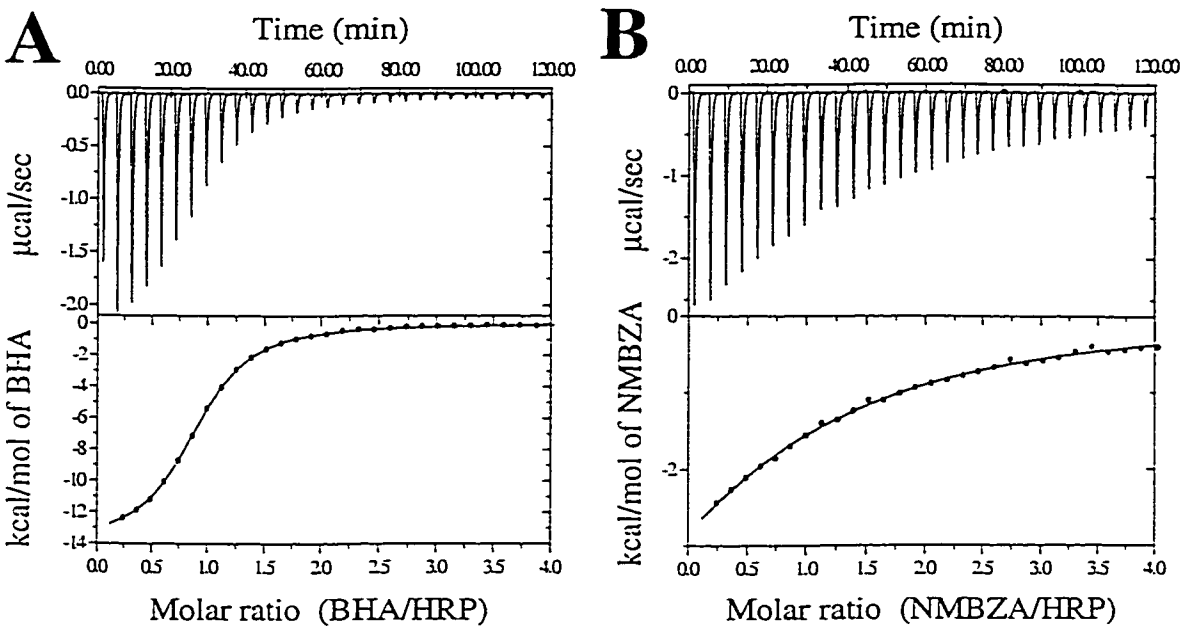

Figure 3.2. Isothermal calorimetry titration of HRP with BHA and NMBZA. (A) 33 µM HRP was titrated with 560 µM BHA and (B) 0.21 mM HRP was titrated with 3.52 mM NMBZA in 100 mM sodium phosphate, pH 7.0, at 25°C. The heat released per unit time (µcal/s) is plotted versus time where each peak corresponds to an injection of ligand (top panels). The heat of reaction per injection (kcal/mol of ligand) was determined by integration of the area under each peak using Origin software (MicroCal). This value was plotted versus the molar ratio of ligand to HRP (bottom panels) and fit with Origin software using a single binding site model (eq. 2.1).

HRP prior to the start of the experiment) (*83*). For very high c values (c > 100), the titration curve becomes rectangular, while for very low c values (c < 0.1) it becomes flat, such that in both cases estimation of K_d is less accurate. The 2.5-μM K_d [Table 3.1, (*63*)] of BHA is in the range well suited to ITC, requiring a HRP concentration of only 12.5 - 125 μM to be within the desired range (c = 5 - 50) of c values (c = 13 in Figure 3.2A). However, the K_d of NMBZA (K_d = 410 μM, Table 3.1) requires HRP concentrations of 2.1 - 21 mM to yield a c value within the specified range. As mM protein concentrations are experimentally impracticable, the HRP concentration used (*e.g.*, 207 μM HRP used in NMBZA titration, c = 0.6 in Figure 3.2.B) resulted in a shallow titration curve. This was typical of experiments for compounds with K_d values in the mM range. The experimental conditions for ITC experiments are given in Table 3A.1 of appendix 3A.

3.2.1.1. Contribution of buffer ionization to observed enthalpy of binding

The binding enthalpy measured by ITC may contain contributions from the ionization enthalpy ($\Delta H°_{ion}$) of the buffer. This is a result of proton transfer between the protein or ligand and the buffer upon binding of ligand, and is caused by pK_a changes in ionizable groups of the reactants resulting from changes in local environment upon ligand binding. Therefore, the experimentally measured enthalpy ($\Delta H°_{ITC}$) is buffer-dependent and can be expressed as:

$$\Delta H°_{ITC} = \Delta H°_{binding} + \Delta n \Delta H°_{ion} \qquad \text{(eq. 3.1)}$$

where Δn is the number of protons transferred upon binding of ligand, $\Delta H°_{ion}$ is the ionization enthalpy of the buffer and $\Delta H°_{binding}$ is the buffer-independent binding-enthalpy.

Figure 3.3 shows the experimental enthalpies for BHA, SHA (Ar = 2-OH-ph, X = OH) and 2-NHA (Ar = 2-naph, X = OH) binding to HRP in six different buffers at pH 7.0. Δn values of 0.3, 0.1, and 0.2 were determined for BHA, SHA, and 2-NHA, respectively. These values indicate that there is a small amount of proton transfer from the buffer ($\Delta n > 0$) to the complex on binding. This likely reflects protonation of the hydroxamic acids present in the anionic form, as BHA, 2-NHA and SHA have pK_a values in the 7.4 - 8.8 range, and only bind to HRP in the neutral form (*63, 207*). $\Delta H°_{binding}$ values of -14.4, -15.3, and -15.0 kcal/mol were determined for BHA, SHA, and 2-NHA, respectively, (Figure 3.3) and were found to be within 0.3 kcal/mol of the $\Delta H°_{ITC}$ values measured in 100 mM sodium phosphate, pH 7.0 (-14.1±0.07, -15.5±0.07, and -14.8±0.9 kcal/mol for BHA, SHA, and 2-NHA, respectively). This suggests that, since there is little proton transfer observed on binding at pH 7.0, correction of $\Delta H°_{ITC}$ (referred to as $\Delta H°$ from this point forward) to remove contributions due to $\Delta H°_{ion}$ are not required in phosphate buffer. Since the other compounds used in this investigation (Figure 3.1) do not have pK_a values within the pH range (6 - 7) used in this ITC study, ΔH_{ITC} values were not corrected for the negligible contribution of $\Delta H°_{ion}$.

The experimental enthalpies for BHA and 2-NHA (Ar = 2-naph, X = OH) binding to HRP in three different buffers at pH 4.0 were also plotted versus the $\Delta H°_{ion}$ (Figure 3.4). Δn values of 0.57 and 0.98 were determined for BHA and 2-NHA, respectively. These values indicate that one proton is transferred from the buffer ($\Delta n > 0$) to the complex on binding. This likely reflects protonation of the distal His42 in HRP(Fe^{III}), as this residue has been assigned a pK_a ~4 (*72*). $\Delta H°_{binding}$ values of -9.20 and -10.0 kcal/mol were determined for BHA and 2-NHA (Figure 3.4). Since proton transfer was

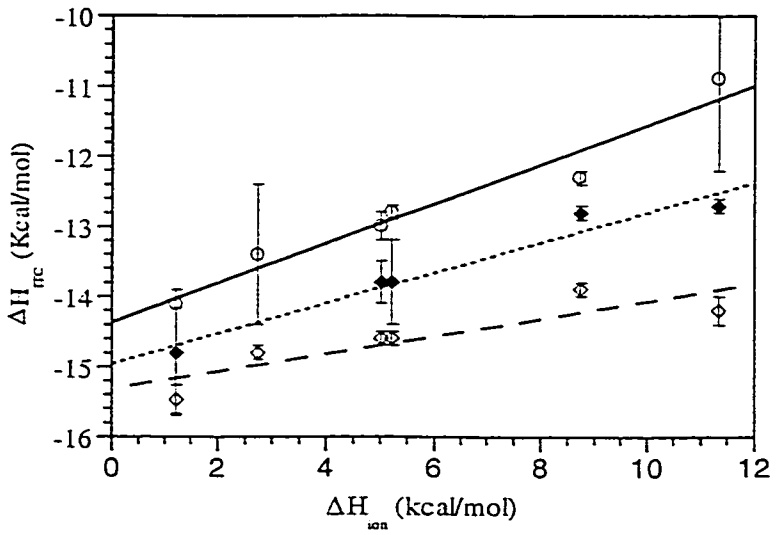

Figure 3.3. $\Delta H°_{ITC}$ **as a function of** $\Delta H°_{ion}$ **for BHA, SHA, and 2-NHA at pH 7.0 and 25 °C.** Values for Δn (0.3, 0.1, and 0.2 for BHA, SHA, and 2-NHA, respectively) and $\Delta H°_{binding}$ (-14.4, -15.3, and -15.0 kcal/mol for BHA, SHA, and 2-NHA, respectively) were determined from a fit of equation 3.1 to the plots of $\Delta H°_{ion}$ versus $\Delta H°_{ITC}$ for BHA (—), SHA (- - -) and 2-NHA (·····). The buffers and their $\Delta H°_{ion}$ (in kcal/mol) at 25 °C are as follows: sodium phosphate, 1.22 kcal/mol; PIPES, 2,74 kcal/mol; HEPES, 5.02 kcal/mol; MOPS, 5.22 kcal/mol; imidazole, 8.75 kcal/mol; Tris, 11.34 kcal/mol (H. Fukada and K. Takahashi, personal communication). Experimental data is listed in Table 3A.2 of Appendix 3A.

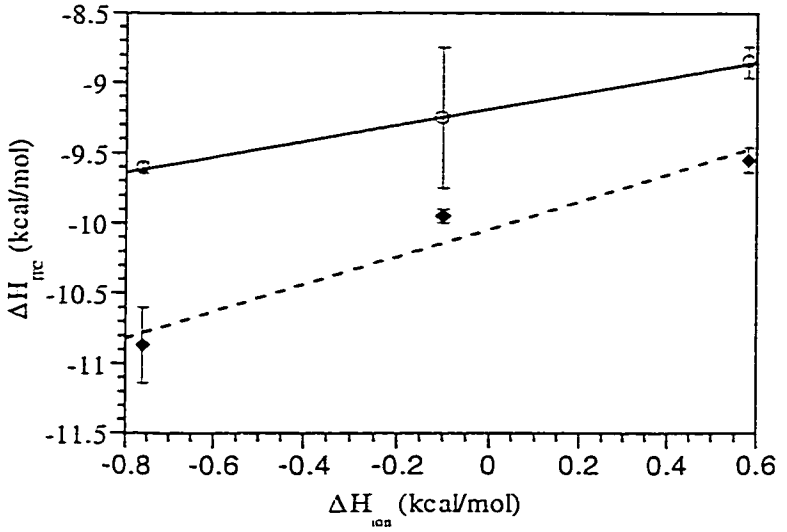

Figure 3.4. $\Delta H°_{ITC}$ **as a function of** $\Delta H°_{ion}$ **for BHA and 2-NHA at pH 4.0 and 25 °C.** Values for Δn (0.57 and 0.98 for BHA and 2-NHA, respectively) and $\Delta H°_{binding}$ (-9.20 and -10.0 kcal/mol for BHA and 2-NHA, respectively) were determined from a fit of equation 3.1 to the plots of $\Delta H°_{ion}$ versus $\Delta H°_{ITC}$ for BHA (—) and 2-NHA (- - -). The buffers and their $\Delta H°_{ion}$ (in kcal/mol) at 25 °C are as follows: sodium tartrate, -0.76 kcal/mol; sodium acetate, -0.10 kcal/mol; sodium citrate, 0.58 kcal/mol (*208*). Experimental data is listed in Table 3A.2 of Appendix 3A.

observed at pH 4.0, $\Delta H°_{ITC}$ values were found to be vary up to ±0.5 kcal/mol in relation to the $\Delta H°_{binding}$. Therefore, correction of $\Delta H°_{ITC}$ to remove contributions due to $\Delta H°_{ion}$ is required at pH 4.0 and the $\Delta H°$ values for BHA and 2-NHA binding to HRP at pH 4.0 (Table 3.1) are the corrected $\Delta H°_{binding}$ values.

3.2.1.2.Binding of aromatic hydroxamic acid analogues to HRP at pH 4.0 and 7.0

The contribution of individual H-bonding and hydrophobic contacts to binding was dissected by comparison of the thermodynamic values of the other hydroxamic acid analogues (shown in Figure 3.1) to those of BHA. The results are summarized in Table 3.1. This comparison was carried out by the calculation of $\Delta\Delta G°$ ($\Delta\Delta G° = \Delta G°_{L} - \Delta G°_{BHA}$), $\Delta\Delta H°$ ($\Delta\Delta H° = \Delta H°_{L} - \Delta H°_{BHA}$), and $T\Delta\Delta S°$ ($T\Delta\Delta S° = T\Delta S°_{L} - T\Delta S°_{BHA}$) values (Table 3.1), where the ligands (L) are: benzamide (BZA; Ar = ph, X = H), N-benzylhydroxylamine (N-BH), 2'-hydroxyacetophenone (2'-HA), SHA or 2-NHA. The $\Delta\Delta G°$, $\Delta\Delta H°$ and $T\Delta\Delta S°$ values for these compounds are represented graphically in Figure 3.5 in order to highlight the driving forces involved in the binding of these compounds relative to BHA. A positive value for $\Delta\Delta H°$ (Figure 3.5), indicates that binding of a compound is less enthalpically favourable than for BHA, while a negative value indicates that binding is more enthalpically favourable. The reverse is true for the $T\Delta\Delta S°$ values since a positive value indicates a more entropically favourable binding interaction for ligand (L) binding compared to BHA.

BHA forms 3 H-bonds within the distal POX cavity of HRP: BHA-C=O•Arg38-$N_{\eta 2}$ (2.91 Å), BHA-NH•Pro139-C=O (2.70 Å), and BHA-OH•His42-$N_{\varepsilon 2}$ (2.82 Å) (Figure 3.6) (*61*). BHA is also proposed to form 2 H-bonds to the water molecule (WAT999) within the distal cavity: BHA-OH•H_2O (3.12 Å), and BHA-C=O•H_2O

Table 3.1. Binding and thermodynamic data from pH 4.0 and 7.0 ITC experiments for aromatic hydroxamic acid analogues.

Compound	PH[c]	K_d (μM) (spec)[d]	K_d (μM) (ITC)[e]	n	ΔG°[f] (kcal/mol)	$\Delta\Delta G^{\circ}$[g] (kcal/mol)	ΔH° (kcal/mol)	$\Delta\Delta H^{\circ}$[h] (kcal/mol)	ΔS°[i] (cal/mol)	$T\Delta\Delta S^{\circ}$[j] (kcal/mol)
BZA[b]	7	2700±50	4300±91	0.75±0.07	-3.23	4.41	-9.52±0.98	4.62	-21.1	0.21
NMBZA[a]	7	410±2	360±29	0.85±0.11	-4.70	—	-8.22±1.22	—	-11.8	—
2'-HA[b]	7	~2000	13000±184	0.85±0	-2.57	5.06	-8.68±0.31	5.36	-20.5	1.30
N-BH[b]	7	—	19000±2000	0.85±0	-2.35	5.28	-7.40±0.14	6.74	-16.9	1.46
BHA[a]	4	6.4±0.04	7.3±1.0	0.86±0.19	-7.00	0.64	-9.20	4.90	-6.71	15.09
BHA[a]	7	2.5±0.01	2.5±0.05	0.90±0.003	-7.64	0	-14.1±0.07	0	-21.8	0
SHA[b]	7	11±0.1	12±0.4	0.90±0.007	-6.69	0.95	-15.5±0.16	-1.33	-29.4	-2.26
2-NHA[a]	4	0.40±0.01	0.60±0.13	0.94±0.10	-8.48	—	-10.0	—	-5.10	—
2-NHA[a]	7	0.15±0.01	0.16±0.04	1.0±0.04	-9.27	-1.63	-14.8±0.94	-0.63	-18.4	1.00

[a]ITC experiments using the MSC ITC instrument (Biotechnology Research Institute)
[b]ITC experiments using the VP ITC instrument (Structural and Functional Genomics Center, Concordia)
[c]Experiments at pH 4.0 were conducted in 100 mM tartrate, citrate and acetate buffers and the $K_{(ITC)}$ value reported is the mean of these experiments, while the ΔH value is the corrected $\Delta H^{\circ}_{binding}$. Values reported for pH 7.0 experiments are for those conducted in 100 mM sodium phosphate.
[d]Spectroscopically determined K_d values taken from Table 3.3 and shown here for comparison to K_d values determined by ITC.
[e]Kd values determined by ITC.
[f]Error in ΔG° not reported because ΔG° was determined from $K_{d(ITC)}$ (eq. 2.4).
[g]$\Delta\Delta G = \Delta G^{\circ}_{L} - \Delta G^{\circ}_{BHA}$, where ΔG°_{L} is that of the compound being compared to the binding of BHA at pH 7.0.
[h]$\Delta\Delta H = \Delta H^{\circ}_{L} - \Delta H^{\circ}_{BHA}$, where ΔH°_{L} is that of the compound being compared to the binding of BHA at pH 7.0.
[i]Error in ΔS° not reported because ΔS° was determined from ΔH° and ΔG° (eq. 2.5).
[j]$T\Delta\Delta S^{\circ} = T\Delta S^{\circ}_{L} - T\Delta S^{\circ}_{BHA}$, where $T\Delta S^{\circ}_{L}$ is that of the compound being compared to the binding of BHA at pH 7.0.

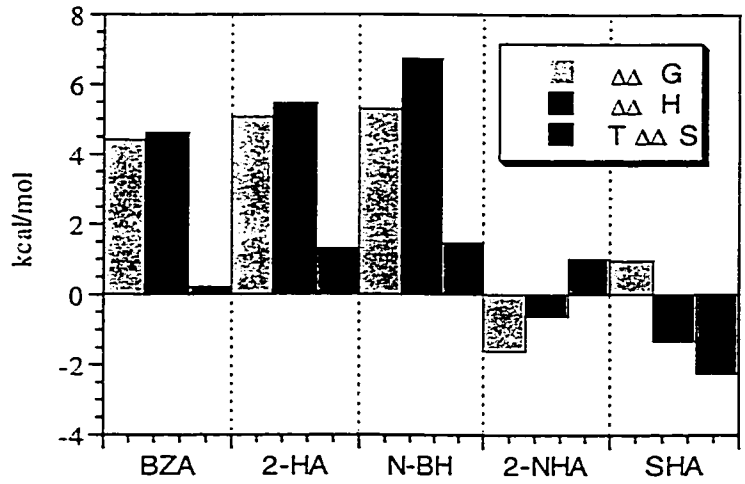

Figure 3.5. Comparison of the thermodynamic parameters for binding to HRP (Fe^{III}) of BZA, 2'-HA, N-BH, 2-NHA and SHA to that of BHA in 100 mM sodium phosphate, pH 7.0. $\Delta\Delta G°$, $\Delta\Delta H°$, and $T\Delta\Delta S°$ were calculated by subtraction of $\Delta G°$, $\Delta H°$, and $T\Delta S°$, respectively, of BHA from those of BZA, NMBZA, 2'-HA, N-BH, 2-NHA, and SHA.

(2.57 Å) (*61*). The contribution of each of the three BHA-protein H-bonds to binding was investigated with BZA, N-BH, and 2'-HA, each of which lacks the potential for the formation of a specific H-bond (Figure 3.6). These three compounds bind to HRP with K_d values 3 - 4 orders of magnitude larger than BHA (Table 3.1) and correspondingly, their overall energy of binding to HRP is lower than that of BHA ($\Delta\Delta G° = 4.41$, 5.28, and 5.06 kcal/mol for BZA, N-BH, and 2'-HA, respectively). The binding of each of these compounds is less enthalpically favourable ($\Delta\Delta H° = 4.62$, 6.74, and 5.46 kcal/mol for BZA, N-BH, and 2'-HA, respectively, Table 3.1) and more entropically favourable ($T\Delta\Delta S° = 0.21$, 1.46 and 1.30 kcal/mol for BZA, N-BH, and 2'-HA, respectively, Table 3.1) than BHA (Figure 3.5).

The distal His42 [pK_a ~4, (*72*)] is a H-bond acceptor to the hydroxyl group of BHA, suggesting that this H-bond would be eliminated when His42 is protonated. Therefore, the binding of BHA and 2-NHA to HRP was investigated at pH 4.0. The results of the binding at pH 4.0 of both BHA ($\Delta\Delta G° = 0.54$ kcal/mol, $\Delta\Delta H° = 4.49$ kcal/mol, and $T\Delta\Delta S° = 3.95$ kcal/mol as compared to BHA at pH 7.0, Table 3.1) and 2-NHA ($\Delta\Delta G° =$ 0.68 kcal/mol , $\Delta\Delta H° = 3.90$ kcal/mol, and $T\Delta\Delta S° = 3.22$ kcal/mol as compared to 2-NHA at pH 7.0, Table 3.1) showed that the overall binding energy of both of these compounds was slightly less at pH 4.0. Furthermore, their binding to HRP was much more enthalpically unfavorable and entropically favourable at pH 4.0 versus pH 7.0.

NMBZA and provides an opportunity to examine the role of hydrophobic interactions in binding. NMBZA is an amide (X = CH_3, Figure 3.1) and is thus best analyzed in comparison with the other amide BZA (X = H, Figure 3.1) rather than BHA (X = OH, Figure 3.1). Therefore NMBZA is not represented in Figure 3.5. The $\Delta\Delta G°$,

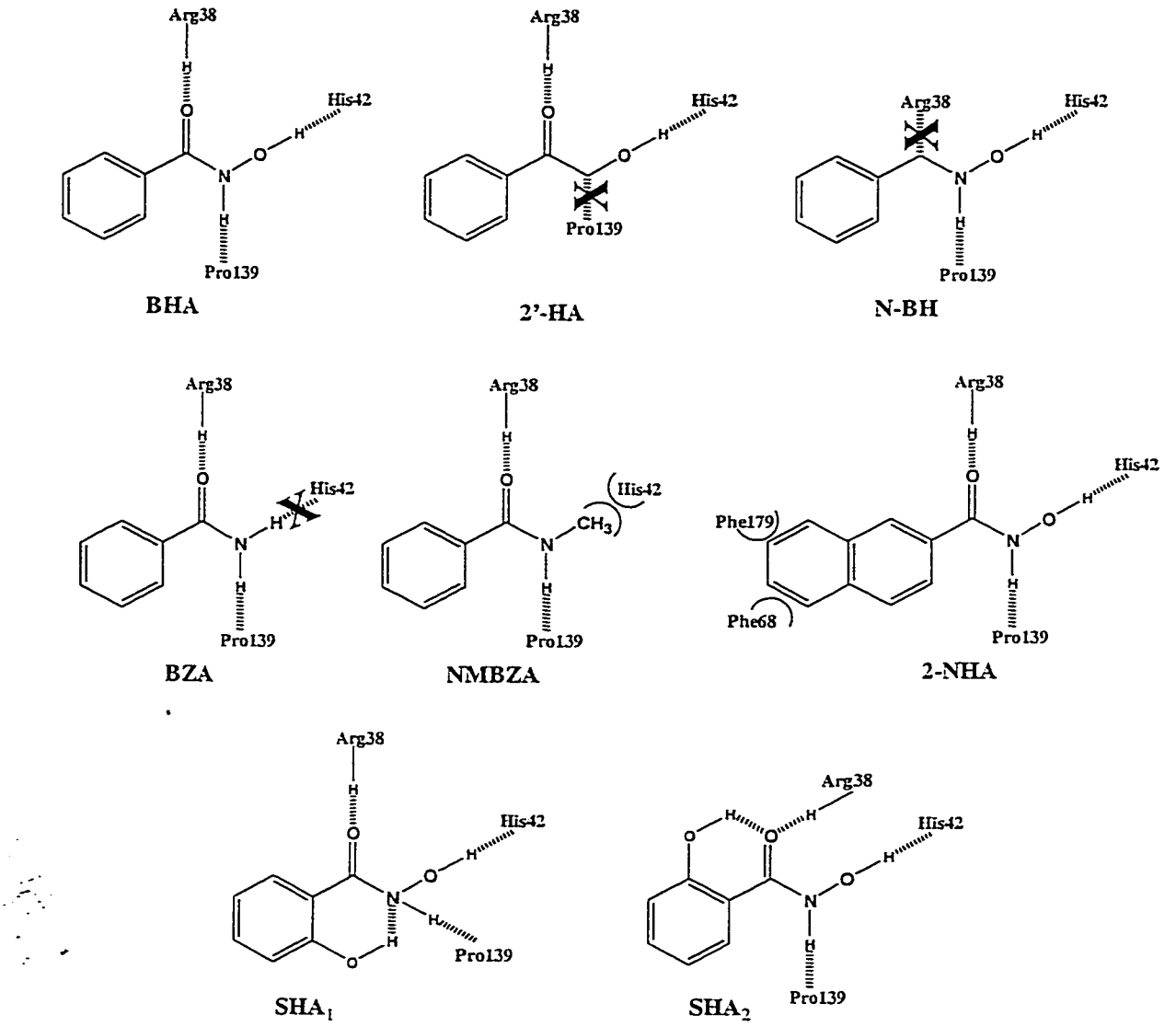

Figure 3.6. H-bonding and hydrophobic contacts between ligands and residues in the distal POX cavity of HRP. Proposed H-bonds, based on the HRP-BHA crystal structure (*61*), are represented by hashed lines, and hydrophobic or steric interactions by semicircles. X in the structures of 2'-HA, N-BH and BZA indicates the lack of a H-bond as compared with BHA. Interactions shown in the SHA_1 structure are predicted based on the MPO-SHA crystal structure (*76*), while SHA_2 is based on that of ARP-SHA (*75*).

$\Delta\Delta H°$, and $T\Delta\Delta S°$ for NMBZA binding compared to BZA are -1.47, 1.30, and 2.77 kcal/mol, respectively, indicating that NMBZA binding is more entropically driven than BZA. This is likely due to desolvation of the methyl group of NMBZA upon binding to HRP.

The tighter binding of 2-NHA as compared to BHA is also entropically driven. The $\Delta\Delta G°$, $\Delta\Delta H°$, and $T\Delta\Delta S°$ for 2-NHA binding compared to BHA are -1.63, -0.63, and 1.00 kcal/mol, respectively (Table 3.1, Figure 3.5). Both the favourable enthalpic and entropic energies of 2-NHA binding compared to BHA are likely due to desolvation of the additional aromatic ring.

SHA was the only hydroxamic acid possessing a ring substitution (2-OH) used in these experiments. Although the binding of SHA was enthalpically favourable ($\Delta\Delta H°$ = -1.33 kcal/mol, Table 3.1), it was entropically unfavorable ($T\Delta\Delta S°$ = -2.26 kcal/mol, Table 3.1) and therefore the $\Delta\Delta G°$ of SHA binding to HRP was 0.95 kcal/mol (Table 3.1) in comparison with BHA (Figure 3.5).

3.2.1.3.Effect of aromatic ring substituents on the binding of hydrazides to HRP at pH 6.0

The binding of hydrazides (Ar-CO-NH-NH_2, Figure 3.1) to HRP(Fe^{III}) was investigated at pH 6.0 to avoid the time-dependent conversion of HRP(Fe^{III}) to the oxyperoxidase form (Section 4.2.2.1, oxidation of BZH in the absence of H_2O_2) observed at pH $\geq$ 7.0 in the presence of hydrazides. The thermodynamic parameters for binding of hydrazides to HRP are summarized in Table 3.2. The $\Delta\Delta G°$ ($\Delta\Delta G° = \Delta G°_L - \Delta G°_{BZH}$), $\Delta\Delta H°$ ($\Delta\Delta H° = \Delta H°_L - \Delta H°_{BZH}$), and $T\Delta\Delta S°$ ($T\Delta\Delta S° = T\Delta S°_L - T\Delta S°_{BZH}$) values were calculated versus BZH (Table 3.2), where L is the given hydrazide (or BHA). The $\Delta\Delta G°$,

$\Delta\Delta H°$ and $T\Delta\Delta S°$ values of BHA, INH, NICH, and 2-NZH are represented graphically in Figure 3.7. As indicated in Section 3.2.1.2 (binding of aromatic hydroxamic acid analogues to HRP at pH 4.0 and 7.0), a positive $\Delta\Delta H°$ value for a given hydrazide indicates that binding is less enthalpically favourable, while a positive $T\Delta\Delta S°$ value indicates that binding is more entropically favourable than for BZH.

The overall energy of binding of 2-NZH versus BZH ($\Delta\Delta G° = -1.85$ kcal/mol, Table 3.2) is approximately the same as that for 2-NHA vs BHA ($\Delta\Delta G° = -1.63$ kcal/mol, Table 3.1). However, 2-NZH binding is more enthalpically favourable and entropically unfavorable ($\Delta\Delta H° = -2.54$ kcal/mol and $T\Delta\Delta S° = -0.67$ kcal/mol for 2-NZH versus BZH, Table 3.2) than 2-NHA ($\Delta\Delta H° = -0.63$ kcal/mol and $T\Delta\Delta S° = 1.00$ kcal/mol for 2-NHA versus BHA, Table 3.1).

The binding of INH ($\Delta\Delta G° = 1.98$ kcal/mol) and NICH ($\Delta\Delta G° = 2.17$ kcal/mol) are much weaker than what might be expected based on their structures (Figure 3.1), since the only difference between BZH and INH or NICH is the replacement of the phenyl ring of BZH with a pyridine ring. INH and NICH binding are less enthalpically favourable ($\Delta\Delta H° = 3.30$ and 4.48 kcal/mol for INH and NICH, respectively, Table 3.2), but more entropically favourable ($T\Delta\Delta S° = 1.33$ and 2.32 kcal/mol for INH and NICH, respectively, Table 3.2) than BZH (Figure 3.7).

The possibility of increasing the binding affinity of aromatic hydroxamic acid analogues for HRP was investigated using hydrazides with ring substituents on the aromatic ring. A series of hydroxyl-, methyl-, amino-, chloro-, and nitro-substituted hydrazides were chosen (Figure 3.1) and their $\Delta\Delta G°$, $\Delta\Delta H°$, and $\Delta\Delta S°$ values compared

to BZH are shown in Figure 3.8. The weak binding of the NO_2-substituted hydrazides, observed spectroscopically, prevented their use in ITC binding experiments. Comparison of the thermodynamic parameters for the binding of *ortho*-substituted benzhydrazides HRP with those of BZH shows that they bind with less energy ($\Delta\Delta G°$ of 0.98, 1.86, 1.93, and 1.68 kcal/mol, respectively for OH, CH_3, NH_2, and Cl, Table 3.2, Figure 3.8). The driving forces are different for each compound due to the H-bonding ability or hydrophobicity of each substituent. 2-OH-BZH ($\Delta\Delta H°$ = -3.94 kcal/mol, Table 3.2) binding is much more enthalpically favourable than BZH, while 2-NH_2-BZH binding is approximately enthalpically equivalent ($\Delta\Delta H°$ = -0.07 kcal/mol, Table 3.2) and both 2-CH_3-BZH ($\Delta\Delta H°$ = 1.51 kcal/mol, Table 3.2) and 2-Cl-BZH ($\Delta\Delta H°$ = 1.74 kcal/mol, Table 3.2) are enthalpically unfavorable (Figure 3.8). This suggests the formation of a H-bond by the hydroxyl moiety of 2-OH-BZH and the disturbance or disruption of existing H-bond(s) by a methyl or chloro group in the 2-position. Both 2-OH-BZH ($T\Delta\Delta S°$ = -4.92 kcal/mol, Table 3.2) and 2-NH_2-BZH ($T\Delta\Delta S°$ = -1.99 kcal/mol, Table 3.2) are less entropically unfavorable than BZH, likely due to the hydrophilic amino group and the presence of steric constraint. 2-CH_3 is also slightly entropically unfavorable ($T\Delta\Delta S°$ = -0.35 kcal/mol, Table 3.2), likely due to steric constraint. The binding of 2-CH_3-BZH is more entropically favourable than either 2-OH-BZH or 2-NH_2-BZH (Figure 3.8) because desolvation of the hydrophobic methyl group is entropically favourable. 2-Cl-BZH binding is entropically equivalent ($T\Delta\Delta S°$ = 0.06 kcal/mol, Table 3.2) to BZH.

A comparison of the thermodynamic parameters for the binding of *meta*-substituted hydrazides to HRP with those of BZH shows that they bind ($\Delta\Delta G°$ of 0, -0.06, 0.44, and 0.48 kcal/mol, respectively for OH, CH_3, NH_2, and Cl, Table 3.2) with

Table 3.2. Binding and thermodynamic data from ITC experiments for hydrazides.

Compound[ab]	K_d (μM) (spec)	K_d (μM)[d] (ITC)	n	ΔG^{oe} (kcal/mol)	$\Delta\Delta G^{of}$ (kcal/mol)	ΔH^{o} (kcal/mol)	$\Delta\Delta H^{og}$ (kcal/mol)	ΔS^{oh} (cal/mol)	$T\Delta\Delta S^{oi}$ (kcal/mol)
BHA	2.3±0.01	2.7±0.1	0.83±0.003	-7.59	2.24	-14.96±0.07	-3.23	-24.69	-0.98
BZH[c]	109±2	120±2	0.84±0.007	-5.35	0	-11.73±0.13	0	-21.41	0
2-OH-BZH	439±45	627±18	0.81±0.05	-4.37	0.98	-15.67±1.00	-3.94	-37.91	-4.92
3-OH-BZH	87±1	120±1	0.85±0.01	-5.35	0	-13.33±0.11	-1.6	-26.75	-1.59
4-OH-BZH	220±22	540±24	1.37±0.05	-4.46	0.89	-8.45±0.39	3.28	-13.38	2.39
2-CH_3-BZH	2300±50	2760±28	0.85±0	-3.49	1.86	-10.22±0.052	1.51	-22.57	-0.35
3-CH_3-BZH	76±1	108±3	0.89±0.01	-5.41	-0.06	-10.91±0.17	0.82	-18.45	0.88
4-CH_3-BHZ	118±7	143±5	0.89±0	-5.24	0.11	-11.31±0.12	0.42	-20.33	0.32
2-NH_2-BZH	2960±260	3100±220	0.89±0	-3.42	1.93	-11.8±0.6	-0.07	-28.08	-1.99
3-NH_2-BZH	250±12	250±10	0.81±0.06	-4.91	0.44	-12.09±1.01	-0.36	-24.11	-0.80
4-NH_2-BZH	303±11	231±18	0.92±0.05	-4.96	0.39	-11.14±0.68	0.59	-20.72	0.21
2-Cl-BZH	2320±80	2050±38	0.85±0	-3.67	1.68	-9.99±0.088	1.74	-21.21	0.06
3-Cl-BZH	99±4	267±14	0.82±0.06	-4.87	0.48	-9.78±0.76	1.95	-16.44	1.48

Table 3.2 continued

Compound[ab]	K_d (μM) (spec)	K_d (μM)[d] (ITC)	n	ΔG^{oc} (kcal/mol)	$\Delta\Delta G^{of}$ (kcal/mol)	ΔH^o (kcal/mol)	$\Delta\Delta H^{og}$ (kcal/mol)	ΔS^{oh} (cal/mol)	$T\Delta\Delta S^{oi}$ (kcal/mol)
4-Cl-BZH	135±5	297±9	0.85±0	-4.81	0.54	-8.17±0.098	3.56	-11.26	3.02
2-NO_2-BZH	85000±32000								
3-NO_2-BZH	9110±48								
4-NO_2-BZH	3020±1160								
INH	1100±34	3360±35	0.85±0	-3.37	1.98	-8.43±0.061	3.3	-16.95	1.33
NICH	4260±275	4620±154	0.85±0	-3.18	2.17	-7.25±0.14	4.48	-13.63	2.32
2-NZH	0.917±0.062	5.2±0.11	0.92±0.005	-7.20	-1.85	-14.27±0.11	-2.54	-23.66	-0.67

[a]All ITC experiments conducted using the VP ITC instrument (Structural Genomics Center, Concordia)
[b]All experiments conducted in 100 mM sodium phosphate, pH 6.0.
[c]Spectroscopically determined K_d value for BZH is taken from Table 3.3 and shown here for comparison to K_d values determined by ITC.
[d]Kd values determined by ITC.
[e]Error in ΔG° not reported because ΔG° was determined from $K_{d(ITC)}$ (eq. 2.4).
[f]$\Delta\Delta G^\circ = \Delta G^\circ_L - \Delta G^\circ_{BZH}$, where ΔG°_L is that of the compound being compared to BZH.
[g]$\Delta\Delta H^\circ = \Delta H^\circ_L - \Delta H^\circ_{BZH}$, where ΔH°_L is that of the compound being compared to BZH.
[h]Error in ΔS° not reported because ΔS° was determined from ΔH° and ΔG° (eq. 2.5).
[i]$T\Delta\Delta S^\circ = T\Delta S^\circ_L - T\Delta S^\circ_{BZH}$, where $T\Delta S^\circ_L$ is that of the compound being compared to BZH.

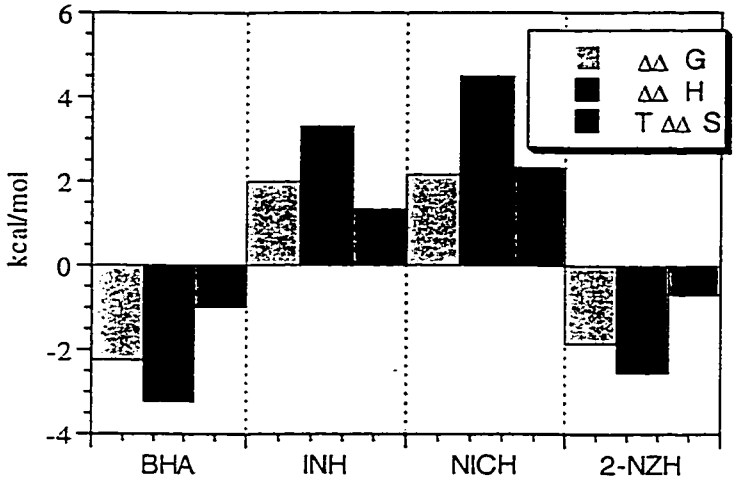

Figure 3.7. Comparison of the thermodynamics of binding to HRP(Fe^{III}) of BHA, INH, NICH, and 2-NZH with BZH in 100 mM sodium phosphate, pH 6.0. $\Delta\Delta G°$, $\Delta\Delta H°$, and $T\Delta\Delta S°$ were calculated by subtraction of $\Delta G°$, $\Delta H°$, and $T\Delta S°$, respectively, of BZH from those of BHA, INH, NICH, and 2-NZH.

approximately the same energy as BZH (Figure 3.8). However, the underlying forces are different. The binding of both 3-OH-BZH ($\Delta\Delta H° = T\Delta\Delta S° = -1.59$ kcal/mol, Table 3.2) and 3-NH_2-BZH ($\Delta\Delta H° = -0.36$ kcal/mol and $T\Delta\Delta S° = -0.80$ kcal/mol, Table 3.2) is enthalpically favourable and entropically unfavorable (Figure 3.8). In contrast, the binding of both 3-CH_3-BZH ($\Delta\Delta H° = 0.82$ kcal/mol and $T\Delta\Delta S° = 0.88$ kcal/mol, Table 3.2) and 3-Cl-BZH ($\Delta\Delta H° = 1.95$ kcal/mol and $T\Delta\Delta S° = 1.48$ kcal/mol, Table 3.2) is enthalpically unfavorable and entropically favourable compared to BZH (Figure 3.8).

A comparison of the *para*-substituted benzhydrazides with BZH shows that they also bind ($\Delta\Delta G° = 0.89$, 0.11, 0.39 and 0.54 kcal/mol, respectively for OH, CH_3, NH_2, and Cl, Table 3.2) with approximately the same energy as BZH (Figure 3.8). However, the binding of all four compounds was enthalpically unfavorable ($\Delta\Delta H° = 3.28$, 0.42, 0.59, and 3.56 kcal/mol, respectively, for OH, CH_3, NH_2, and Cl, Table 3.2) and entropically favourable ($T\Delta\Delta S° = 2.39$, 0.32, 0.21, 3.02 kcal/mol, respectively, for OH, CH_3, NH_2, and Cl, Table 3.2) compared to BZH (Figure 3.8).

The linear relationship (slope = 1.0, $r^2 = 0.60$) between $T\Delta S°$ and $\Delta H°$ observed in Figure 3.9 demonstrates that entropy-enthalpy compensation is observed for the HRP binding of the 24 aromatic hydroxamic acid analogues investigated in this study.

3.2.2. Spectroscopic survey of factors controlling binding of Ar-CO-NH-X to HRP

The change in the Soret absorption of HRP on binding of Ar-CO-NH-X provides an opportunity to complement the above ITC investigation with an independent determination of binding affinity.

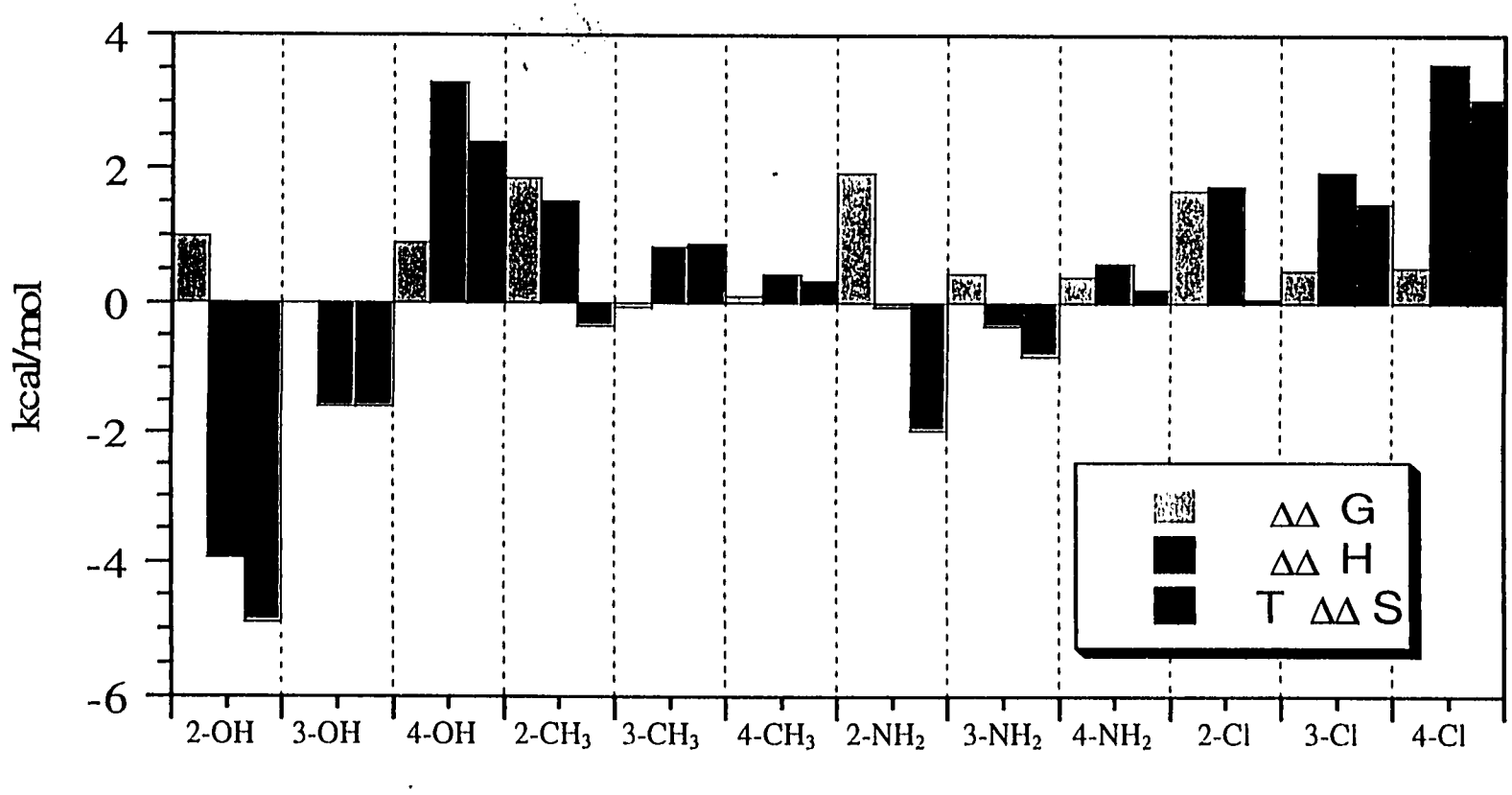

Figure 3.8. Comparison of the thermodynamics of binding to HRP of ring-substituted hydrazides with BZH in 100 mM sodium phosphate, pH 6.0. $\Delta\Delta G°$, $\Delta\Delta H°$, and $T\Delta\Delta S°$ were calculated by subtraction of $\Delta G°$, $\Delta H°$, and $T\Delta S°$, respectively, of BZH from those of the ring-substituted hydrazides

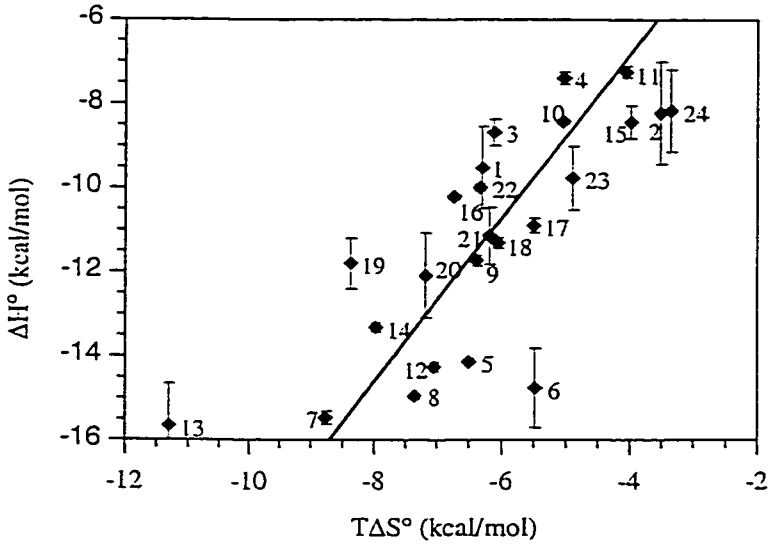

Figure 3.9. Plot of TΔS° vs ΔH° for the binding to HRP of the hydroxamic acid analogues tested. Experiments **1** - **7** were conducted in 100 mM sodium phosphate, pH 7.0, and experiments **8** - **24** were conducted in 100 mM sodium phosphate, 6.0. (**1**, BZA; **2**, NMBZA; **3**, 2'-HA; **4**, N-BH; **5**, BHA; **6**, 2-NHA; **7**, SHA; **8**, BHA; **9**, BZH; **10**, INH; **11**, NICH; **12**, 2-NZH; **13**, 2-OH-BZH; **14**, 3-OH-BZH; **15**, 4-OH-BZH; **16**, 2-CH_3-BZH; **17**, 3-CH_3-BZH; **18**, 4-CH_3-BZH; **19**, 2-NH_2-BZH; **20**, 3-NH_2-BZH; **21**, 4-NH_2-BZH; **22**, 2-Cl-BZH; **23**, 3-Cl-BZH; **24**, 4-Cl-BZH)

3.2.2.1.Effect of pH and Ar-CO-NH-X binding on the UV-VIS spectrum of HRP

Ferric HRP was incubated in the pH 3-12 buffers for 15 min to allow for equilibration before titration with ligands. The Soret maximum (402 – 404 nm) did not change appreciably with time over 15 min between pH 4.0 and 10.0, and the spectra resemble that shown in (Figure 3.10) at pH 7.0. At pH 3.0, the Soret shifted to 368 nm over the course of ~10 min. This likely indicates solvent exposure of the heme (John Wright, unpublished results) and may be due to global structural changes in the protein at pH 3, since an FTIR study found that increasing the pH from 3 to 7 had the effect of increasing α-helical content at the expense of random-loop structures (*72*). The Soret shift to 416 nm at pH 12 (Figure 3.10), in combination with the appearance of bands at 543 and 575 nm (Figure 3.10), is due to the alkaline transition (pK_a = 10.9) of HRP (*209*) which results in OH^- ligation to form 6-coordinate low-spin Fe^{III} (*210, 211*).

As previously observed (*63*), the binding of Ar-CO-NH-X to ferric HRP at pH 7.0 caused the Soret to increase in intensity and red-shift from 402 to 406 nm (Figure 3.11). Consistent with the results of Schonbaum (*63*), binding of the hydroxamic acids resulted in the greatest increase in Soret intensity (Figure 3.11). Figure 3.12 shows that at pH 12.0 the alkaline transition is inhibited in the presence of 25 mM BHA to a greater extent than in the presence of 25 mM BZA or NMBZA.

Schonbaum (*63*) suggested that the BZH side chain may interact weakly with the heme iron of ferrous HRP. In the present study, time-dependent changes in the spectra of ferric HRP were observed at pH 7.0 and above, with bands appearing at 543 and 575 nm upon addition of BZH under aerobic conditions [discussed in Section 4.2.2.1 (oxidation of BZH in the absence of H_2O_2)]. Under anaerobic conditions, no evidence was found

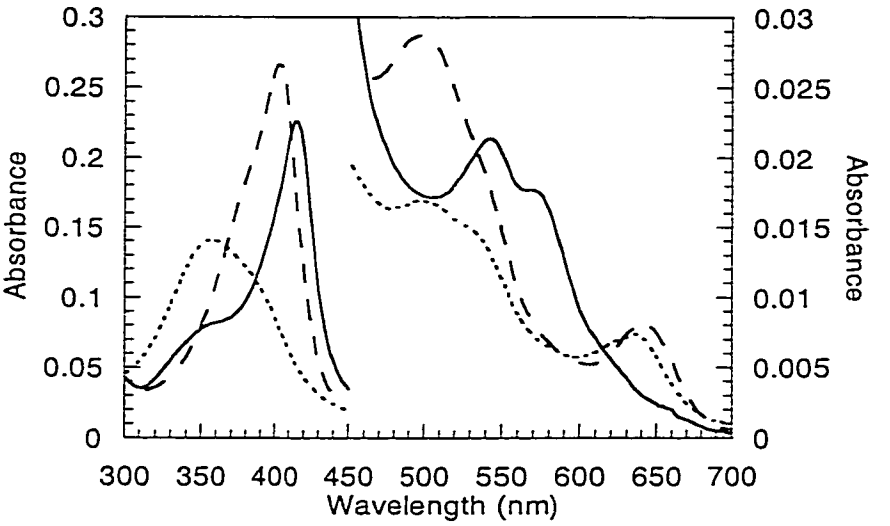

Figure 3.10. Absorption spectra of HRP(Fe^{III}) at pH 3.0 - 12.0. HRP (2.5 μM) was equilibrated for 15 min in 100 mM buffer at pH 3.0 (·····) (sodium tartrate), and pH 7.0 (- - -) and 12.0 (—) (sodium phosphate) prior to spectral acquisition.

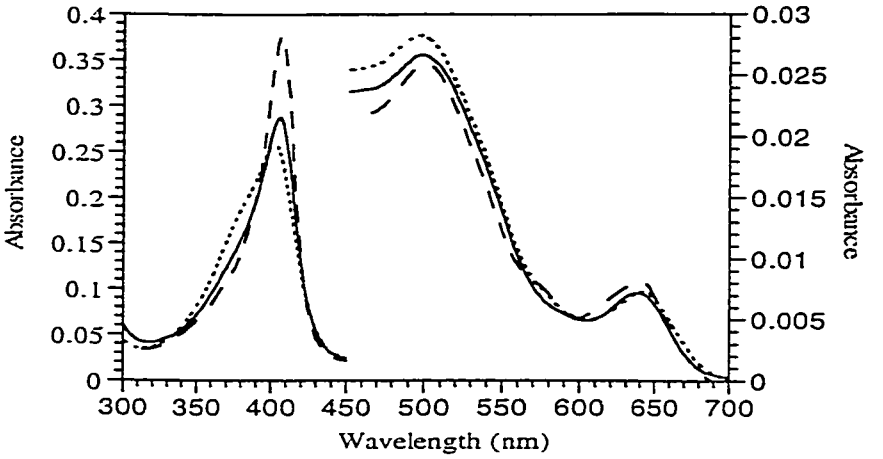

Figure 3.11. Effect of Ar-CO-NH-X on the Soret absorption of HRP at pH 7.0. HRP (·····, 2.5 μM) in 100 mM sodium phosphate, pH 7.0, and in the presence of 25 mM BHA (- - -) and BZA (—).

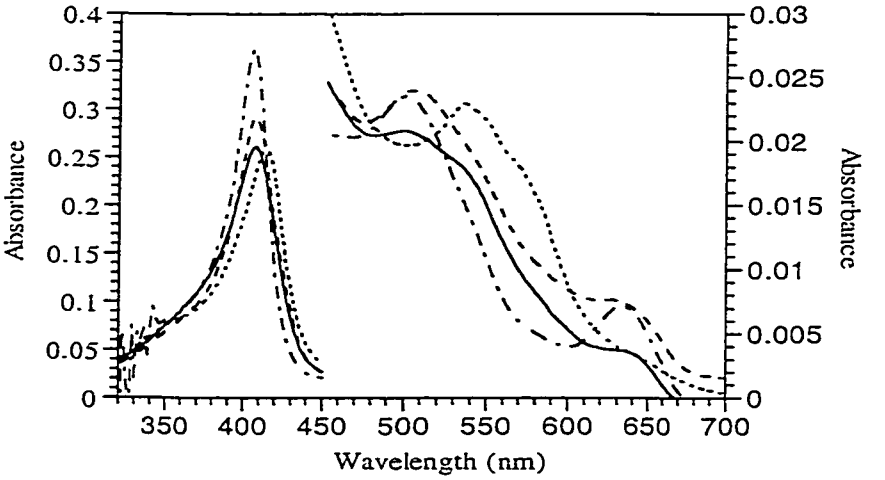

Figure 3.12. Effect of Ar-CO-NH-X on the Soret absorption of HRP at pH 12.0. HRP (·····, 2.5 μM) in 100 mM sodium phosphate, pH 12.0, and in the presence of 25 mM BHA (- · - · -), BZA (—), and NMBZA (- - -).

for the formation of a low-spin species and the HRP-BZH and HRP-BHA spectra between pH 7.0 and 10.0 were similar. Stable spectra were not recorded for HRP-BZH at pH 12.0 because of the sensitivity of the samples to trace amounts of O_2 in the N_2-purged cuvettes.

The spectrum of HRP in the presence of 20 μM tepoxalin is shown in Figure 3.13. Tepoxalin is a hydroxamic acid inhibitor of the COX activity of PGHS and has also been suggested to inhibit the POX activity, via chelation of the heme iron (*212*). Its effect on HRP was to decrease (1.6%) and slightly blue-shift the Soret. There were no changes observed in the 450 - 650 nm region (Figure 3.13). These observations suggest that tepoxalin does not bind close enough to the heme in HRP to significantly perturb its environment.

3.2.2.2. Spectroscopic determination of Ar-CO-NH-X binding to HRP at pH 4.0 - 12.0

A representative titration of HRP with BHA at pH 7.0 is shown in Figure 3.14, and the apparent dissociation constants ($K_{d(app)}$) from the titration of HRP with the 7 Ar-CO-NH-X over the pH range 4-12 are presented in Table 3.3. The $K_{d(app)}$ values of two amides (BZA and NMBZA), which are not expected to H-bond to the distal His42, and BZH increased slightly (1.5 – 7-fold) at pH 4.0 compared to pH 7. Furthermore, since neither BZH nor the aromatic amides ionize over the pH range (4 - 12) investigated here (*63*) and the hydroxamic acids remain in their neutral forms at pH 4.0 (*63*), the small increases in the Ar-CO-NH-X $K_{d(app)}$ values at low pH are likely due to structural changes in the protein (*72*).

The 4 hydroxamic acids bound to HRP most tightly between pH 4 and 8 ($K_{d(app)}$ = 0.15–36 μM). The 14 - 68-fold increase in the BHA, 1-NHA and 2-NHA $K_{d(app)}$ values at

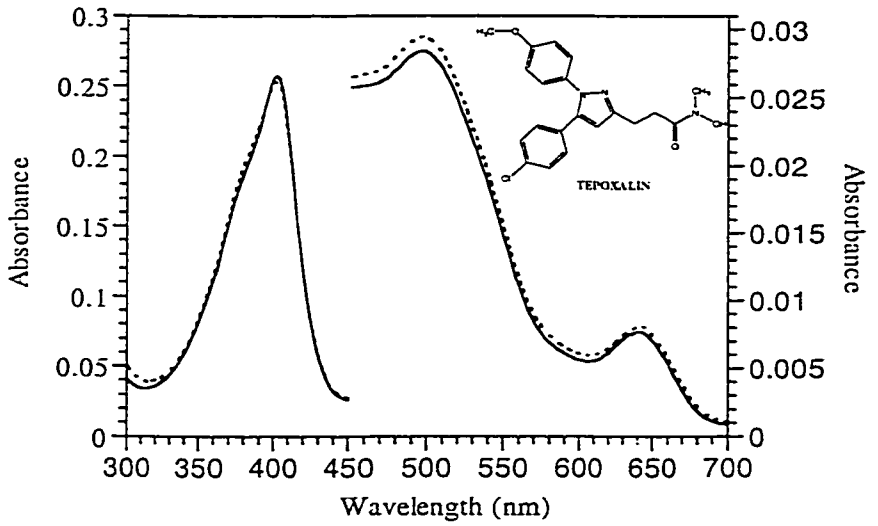

Figure 3.13. Effect of tepoxalin on the Soret of HRP. HRP (—, 2.5 μM) was equilibrated for 15 min in 100 mM sodium phosphate, pH 7.0, prior to addition of 20 μM tepoxalin (·····).

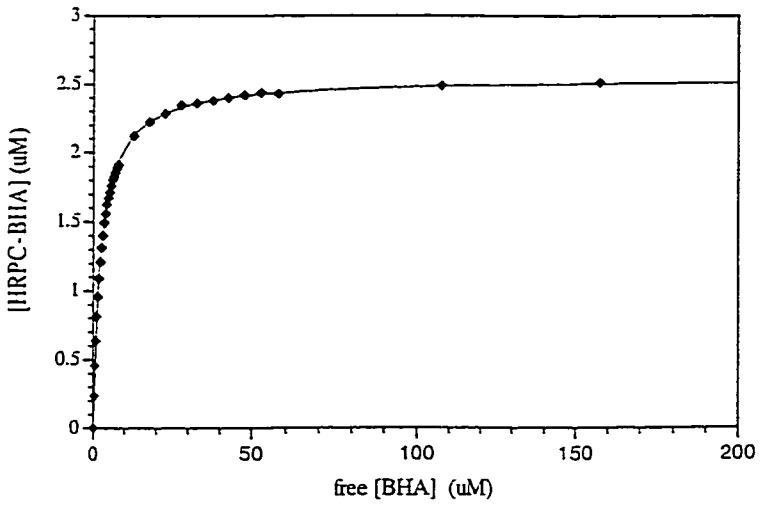

Figure 3.14. Titration of HRP(Fe^{III}) with BHA at pH 7.0. 2.5 μM HRP(Fe^{III}) was equilibrated for 15 min in 100 mM sodium phosphate at pH 7.0 at 25°C prior to titration with BHA. The concentration of bound ligand ([HRP-BHA] = $\Delta A/\Delta\varepsilon$) was determined from the change in absorbance at 406 nm on addition of BHA; $\Delta\varepsilon = 49\ mM^{-1}cm^{-1}$ for free and BHA-bound HRP and free [BHA] = $[BHA]_T$ – [HRP-BHA].

pH 10.0 compared to neutral pH reflects the inability of their ionized forms to bind to HRP and indicates that ligand ionization must be taken into consideration in the calculation of K_d (*63*) (Table 3.3). When the fraction of unionized substrate (α_{HA}) is taken into account, the BHA K_d ($= \alpha_{HA}K_{d(app)}$) shows little variation in the pH 4-12 range (Table 3.4). The corrected K_d values for 1- and 2-NHA, calculated using the reported pK_a of 7.7 (*207*), decrease significantly with increasing pH (Table 3.4). However, when the pK_a of 8.8 reported for BHA (*63*) was used, the corrected NHA K_d values show little variation over the pH range 4-12, similarly to BHA (Table 3.4). Since the BHA and NHA side chains should exhibit similar pK_a values and are expected to bind to the residues in the active site of HRP in a similar manner [Table 3.1, (*61*)], the pK_a of NHA is likely higher than the literature value (*207*).

Free SHA exhibits pK_{a1} and pK_{a2} at 7.4 and 10.0, respectively (Figure 3.15) and the former number agrees with the literature value of 7.43 (*207*). pK_{a2} (10.0) is assigned to the ring hydroxyl because it is unlikely that the pK_a of this group would be lowered by ~2.5 pH units from the value of 9.95 in phenol. The SHA K_{d1} value ($K_{d1} = \alpha_{H_2A}K_{d(app)}$) for binding of the neutral form (H_2A) only to HRP showed little variation with pH (Table 3.4), but the K_{d12} [$K_{d12} = (\alpha_{HA^-} + \alpha_{H_2A})K_{d(app)}$] value, which reflect both H_2A and HA^- binding, increased significantly at alkaline pH (Table 3.4), indicating that only the neutral form of SHA binds to HRP. Both the BHA K_d at pH 12.0 and the SHA K_{d1} at pH 10.0 are slightly smaller than their values at pH 7.0; however, this difference may be due to increased error in the determination of $K_{d(app)}$ under conditions of weak binding since the observed values are in the mM range (Table 3.3) in both cases.

Table 3.3. **Apparent dissociation constants, $K_{d(app)}$ (μM), for Ar-CO-NH-X binding to ferric HRP at pH 4 – 12**

pH	BZH[a]	BZA (mM)[b]	NMBZA	BHA	SHA	1-NHA	2-NHA
4.0	362±5	5.4±0.1	2.8±0.02x10^3	6.4±0.04	18±0.1	36±0.9	0.40±0.01
5.0	154±5	3.8±0.1	595±6	3.3±0.02	9.2±0.1	25±0.4	0.24±0.01
6.0	109±2	2.6±0.05	376±3	2.3±0.01	7.7±0.04	20±0.3	0.16±0.004
7.0	90±2	2.7±0.05	411±2	2.5±0.01	11±0.1	25±0.3	0.15±0.01
8.0	85±2	2.8±0.06	400±2	2.8±0.01	30±0.1	31±0.5	0.22±0.006
9.0	83±1	2.8±0.04	359±2	21±1	313±15	93±5	1.1±0.1
10.0	204±12	3.3±0.04x10^3	301±1	174±3	1.1±0.1x10^3	403±20	2.0±0.03
12.0		9.2±0.4x10^3	2.0±0.05x10^3	2.1±0.3x10^3			387±21

[a] $K_{d(app)}$ values determined under anaerobic conditions since HRP-BZH exhibits time-dependent spectra in air (see text).
[b] Note: $K_{d(app)}$ values for BZA are in mM.

Table 3.4. Dissociation constants (K_d)[a] (μM) corrected assuming only the neutral form of Ar-CO-NH-OH binds to ferric HRP at pH 4 –12

pH	BHA[b]	SHA[c]	SHA^- +SHA[d]	1-NHA[e]	2-NHA[e]	1-NHA[f]	2-NHA[f]
4.0	6.4	18	18	36	0.38	36	0.39
5.0	3.3	9.2	9.2	25	0.24	25	0.24
6.0	2.3	7.4	7.7	20	0.16	20	0.16
7.0	2.5	7.9	11	25	0.15	21	0.13
8.0	2.4	6.0	30	27	0.19	10	$7.2x10^{-2}$
9.0	8.0	7.0	285	36	0.42	4.4	$5.2x10^{-2}$
10.0	10.4	1.3	531	24	0.12	2.0	$1.0x10^{-2}$
12.0	1.2				0.23		$1.9 x10^{-2}$

[a] $K_d = \alpha K_{d(app)}$ where α is the fraction of hydroxamic acid in the neutral form and $K_{d(app)}$ the apparent dissociation constant from Table 3.3.
[b] K_d assuming a pK_a of 8.8 for BHA (*63*).
[c] K_d assuming only the neutral form of SHA binds to HRP, and a pK_{a1} of 7.4 for SHA.
[d] K_d assuming both neutral and singly ionized forms of SHA bind to HRP, and $pK_{a1} = 7.4$ and $pK_{a2} = 10.0$ for SHA.
[e] K_d assuming a pK_a of 8.8 for NHA (see text).
[f] K_d assuming a pK_a of 7.7 for NHA (see text).

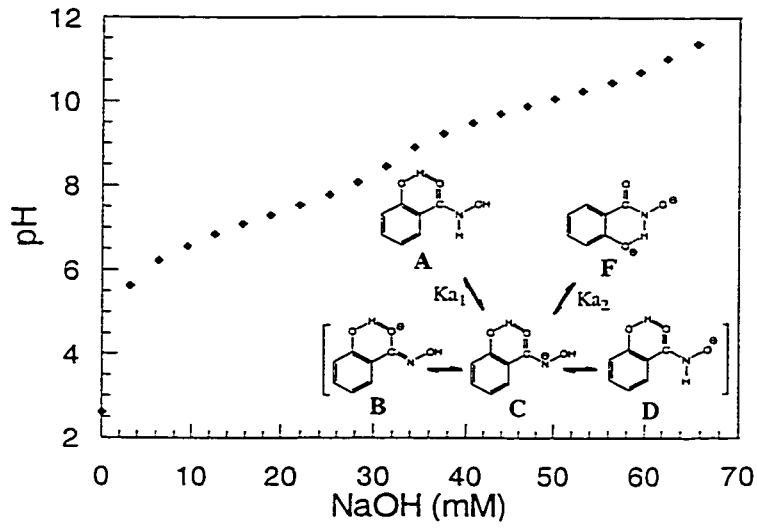

Figure 3.15 pK_a titration for SHA. 40 mM SHA was titrated with 1.0M NaOH in the presence of 1% DMSO. Lower right corner shows tautomeric forms of singly ionized SHA. The pK_a values were determined independently by fitting the plot to equation 2.9.

3.3. Discussion

3.3.1. Driving forces underlying the tight binding of BHA

The majority of peroxidase-substrate interactions are weak, with K_d values in the mM range (*62*). Therefore, the comparatively tight binding of BHA to HRP [K_d = 2.5 μM, Table 3.3, (*63*)] makes it an excellent model system with which to investigate the thermodynamic contributions of the various H-bonding and hydrophobic interactions formed by BHA in the distal heme cavity of HRP. As discussed in Section 3.1.1 (thermodynamics of binding), the formation of H-bonds and the desolvation of hydrophobic surfaces are two of the major driving forces in protein-ligand binding interactions. However, there are other factors involved (*e.g.*, ligand or protein flexibility and steric or electronic repulsion) which complicate prediction and interpretation of the thermodynamic parameters of ligand binding.

3.3.1.1. H-bonding of the hydroxamic acid group

There has been considerable debate in the literature over the H-bond contacts made by BHA in the distal heme cavity of HRP. Much of the nuclear magnetic resonance (NMR) spectroscopy work to date implicates His42 due to the presence of NOE connectivities between BHA and the distal His42 (*64-69*). However, a computer model of the HRP-BHA complex showed that the BHA side chain H-bonded exclusively to Arg38 (*70*). Furthermore, the low affinity of the R38K mutant for BHA supports the importance of Arg38 in BHA binding (*71*). An FTIR study of the ferrous ArCONHX-HRP-CO ternary complexes provided further evidence for H-bonding between BHA and Arg38 by demonstrating that the ν(CO) frequencies of BHA and BZH complexes are 6 – 15 cm^{-1} higher than those of the BZA and NMBZA complexes. The higher frequencies

could arise due to competition between CO and the hydroxamic acid side chain for H-bonding to Arg38 (*72*).

The decreased affinity of the His42 and Arg38 mutants (H42L, K_d = 2.9 mM; H42R, K_d = 6.8 mM; R38G, K_d = 10.4 mM; R38L, K_d > 12.1 mM) for BHA, however, supports the role of both of these residues in BHA binding (*73*). Examination of the crystal structure (*61*) indicates that BHA is involved in 5 H-bonds in the distal cavity of HRP: BHA-C=O•Arg38-$N_{\eta 2}$, BHA-NH•Pro139-C=O, BHA-OH•His42-$N_{\varepsilon 2}$, BHA-OH•H_2O, and BHA-C=O•H_2O. Similar H-bonds were observed in the *Arthromyces ramosus* peroxidase (ARP)-BHA complex (*74*).

Although the interactions involved in binding have been identified in the HRP-BHA crystal structure (*61*), their contributions to the energy of binding cannot be inferred. A comparison of the thermodynamics of binding of BHA to a series of HRP mutants, or the binding of a series of BHA analogues to wild-type HRP is required to determine the contribution to the binding energy of the various H-bonding and hydrophobic interactions in the HRP-BHA complex. While both approaches are acceptable, the advantage of the latter is that there is no risk of structural changes in the protein. Examples of other studies investigating the thermodynamics of binding of a series of related compounds are the binding of 8 pyridine nucleotide substrates to dihydrodipicolinate reductase (*213*) and the binding of phosphonamide-, phosphonate- and phosphinate-containing inhibitors to thermolysin (*214*).

3.3.1.1.1. Use of BZA, 2'-HA and N-BH to isolate the contribution to binding of specific HRP-BHA H-bonds

Each of the three compounds selected (BZA, N-BH and 2'-HA) to probe the H-bonding interactions of the hydroxamic acid group of BHA in the distal heme cavity of HRP lack the potential to form one of the three H-bonds observed in the HRP-BHA structure (*61*). BZA, N-BH and 2'-HA were observed to bind 3 - 4 orders of magnitude less tightly than BHA ($\Delta\Delta G^\circ$ ~ 4.5 - 5.5 kcal/mol, Table 3.1), confirming the proposed role of these H-bonds in binding (Figure 3.6). This is in agreement with the 3 - 4 order of magnitude increase in the K_d of BHA for His42 and Arg38 HRP mutants compared to wild-type HRP (*73*). As expected, the binding of BZA, 2'-HA and N-BH is more entropically favourable ($T\Delta\Delta S^\circ$ ~1 - 1.5 kcal/mol, Table 3.1, Figure 3.5) than BHA. The reason for this is that each of these three compounds is more hydrophobic than BHA because each lacks one of the hydrophilic H-bonding groups of BHA. The less entropically favourable binding of BHA relative to BZA, 2'-HA, and N-BH is compensated by the large and favourable enthalpy of binding of BHA in relation to these compounds ($\Delta\Delta H^\circ$ ~4.5 - 7 kcal/mol, Table 3.1, Figure 3.5). Therefore, as originally suggested by Schonbaum (*63*), polyfunctional H-bonding is largely responsible for the tight binding of BHA.

The formation of a neutral H-bond in water generally contributes 1.9 - 3.0 kcal/mol and 0.5 - 1.5 kcal/mol to the ΔH° and ΔG°, respectively, to the energy of ligand binding to a protein. In contrast, the contribution of a charged H-bond to the ΔH° and ΔG° of ligand binding has been observed to be as high as 8.3 kcal/mol and 4.7 kcal/mol, respectively (*79, 215-218*). The $\Delta\Delta H^\circ$ value of 4.62 kcal/mol for BZA (Table 3.1) is

close to the estimated value for two neutral H-bonds (1.9 - 3.0 kcal/mol), and is consistent with the loss of two neutral H-bonds formed by the hydroxyl moiety of BHA (BHA-OH•His42 and BHA-OH•H_2O) on BZA binding. The $\Delta\Delta H$ value of 6.74 kcal/mol (Table 3.1) for the binding of N-BH to HRP in relation to BHA binding is consistent with previous estimates of the contribution of a charged H-bond to binding [*e.g.*, 8.3 kcal/mol, (*218*)]. Arg38 is expected to be protonated at pH 7.0, resulting in the formation of a charged H-bond between the C=O moiety of BHA and Arg38. However, as the C=O moiety of BHA is also observed to H-bond to the distal water molecule, the exact contribution of the BHA-C=O•Arg38 H-bond cannot be determined from this study. Nonetheless, it is evident that the C=O group is extremely important to the tight binding of BHA, such that the K_d of N-BH is an order of magnitude higher than that of BZA. The $\Delta\Delta H°$ value (5.36 kcal/mol, Table 3.1) for the binding of 2'-HA relative to BHA was greater than expected for the single, neutral H-bond (~1.9 - 3.0 kcal/mol, (*217*)) formed by the N-H group of BHA and the carbonyl backbone of Pro139. Furthermore, the N-H group is not expected to form any other H-bonds within the distal heme cavity of HRP (Figure 1.3). That being so, the reason for the large $\Delta\Delta H°$ of 2'-HA relative to BHA is not apparent. However, experimental error may be a factor due to the difficulty in fitting ITC curves (Figure 3.2) when the c value approaches 0.1, as is the case for both 2'-HA and N-BH (Table 3A.1).

Comparison of the thermodynamics of binding of BHA and BZH yields additional information on the contribution of the BHA-OH•His42 H-bond to binding. The values obtained in this study for the binding of BHA ($\Delta H°$ = -15.0 kcal/mol at pH 6.0 and $\Delta H°$ = -14.1 kcal/mol at pH 7.0) and BZH ($\Delta H°$ = -11.7 kcal/mol at pH 6.0) were

comparable to those observed by Nakatani et al. (*82*) for the binding of BHA ($\Delta H°$ = -13.9 kcal/mol) and BZH (BZH, $\Delta H°$ = -10.1 kcal/mol) at to HRP pH 7.0. The pK_a of BZH (~12) is much higher than that of BHA (8.8) (*63*) resulting in the formation of a stronger H-bond for BHA-OH•His42 than for BZH-NH_2•His42 ($\Delta\Delta H°$ = -3.23 kcal/mol for BHA as compared to BZH, Table 3.2). This value demonstrates that the BZH-NH_2•His42 H-bond provides only ~1.5 kcal/mol to the energy of binding, as the $\Delta\Delta H$ of BZA, which lacks this H-bond, is 4.62 kcal/mol compared to BHA (Table 3.1). This indicates that the presence of a good H-bond donor is required to form a strong H-bond to the distal His42.

3.3.1.1.2. Use of pH to isolate the contribution to binding of specific HRP-BHA H-bonds

It was not possible to isolate the thermodynamic contribution to binding of the BHA-OH•His42 H-bond from that of the BHA-OH•H_2O H-bond by comparing the binding of BHA to that of BZA. Therefore, BHA binding was also investigated by ITC at pH 4.0 since the protonated His42, which reportedly has a pK_a ~4 (*72*), is not expected to act as a H-bond acceptor from the OH group of BHA. The binding energy of both BHA ($\Delta\Delta G°$ = 0.54 kcal/mol at pH 4.0 versus 7.0, Table 3.1) and 2-NHA ($\Delta\Delta G°$ = 0.68 kcal/mol at pH 4.0 versus 7.0) was found to be slightly less at pH 4.0. Furthermore, BHA ($\Delta\Delta H°$ = 4.49 kcal/mol, and $T\Delta\Delta S°$ = 3.95 kcal/mol at pH 4.0 versus 7.0, Table 3.1) and 2-NHA ($\Delta\Delta H°$ = 3.90 kcal/mol, and $T\Delta\Delta S°$ = 3.22 kcal/mol at pH 4.0 versus 7.0) binding was less enthalpically favourable and more entropically favourable at pH 4.0 compared to pH 7.0. The large values of $\Delta\Delta H°$ for both BHA and 2-NHA are close to the $\Delta\Delta H°$ (4.62

kcal/mol, Table 3.1) for BZA compared to BHA at pH 7.0, suggesting that the hydroxyl group of BHA does not H-bond, or forms a weak H-bond to the distal His42 at pH 4.0. The observation that proton transfer likely results in the protonation of the distal His42 in the HRP-BHA complex at pH 4.0 explains the lack of an H-bond between BHA-OH and His42, since the protonated His42 would not be expected to act as an H-bond acceptor.

The spectroscopic survey of binding of Ar-CO-NH-X in the pH 4.0 - 7.0 range yielded additional information required for interpretation of the entropically favourable binding of BHA and 2-NHA at pH 4.0 versus 7.0. All Ar-CO-NH-X were observed to bind 2 –7-fold more weakly at pH 4.0 than at pH 7.0 (Table 3.3), including BZA (X = H) and NMBZA ($X = CH_3$), which do not possess an X group capable of H-bonding to either His42 or the distal water molecule. Thus, it is likely that increases in the $K_{d(app)}$ values at pH 4.0 are at least partially due to structural changes in the protein. In reporting on the X-ray structure of HRP, Gajhede et al. (*11*) speculated that extremes of pH would likely affect the position of the distal His42 due to breaking of the H-bonding network between it and one of the calcium ions. Although the structure of HRP at pH 4.0 is unknown, it is possible that the active site is more solvent-exposed. Therefore, the binding of BHA or 2-NHA at pH 4.0 would be expected to cause the release of extra water molecules to the bulk solvent and be entropically favourable, as was observed.

Investigation of Ar-CO-NH-X binding in the pH 7.0 - 12.0 range provided insight as to how these compounds suppress the alkaline transition of HRP. Free ferric HRP undergoes a spin-state transition at pH 10.9, going from 5-coordinate high-spin to 6-coordinate low-spin (*209*) (pH 12 spectrum, Figure 3.10) due to OH^- ligation to Fe^{III} (*210, 211*). Hydroxide is a relatively weak-field ligand, and the formation of a low-spin

complex in alkaline HRPC had been attributed to H-bond donation by hydroxide to the distal His42 (*210*). From the temperature dependence of the RR spectra, it was suggested that OH^- acts as a H-bond acceptor from the distal Arg38 in HRPC rather than a H-bond donor (*211*). More recent evidence supports the concerted involvement of both distal residues, suggesting that His42 acts as a H-bond acceptor, while Arg38 is required for stabilization of the OH^- ligand (*73*).

Schonbaum (*63*) reported that BZA binding depressed the alkaline transition of HRP with a $pK_{a(app)}$ given by:

$$pK_{a(app)} = pK_{a(AT)} + \log\left(1 + \frac{[L]_{TOT}}{K_d}\right) \qquad \text{(eq. 3.2)}$$

where $pK_{a(AT)}$ is the pK_a of the alkaline transition for free HRP, L_{TOT} is the total ligand concentration, and K_d is dissociation constant for the binding of the ligand to HRP at pH 7.0. Using K_d values for the substrates in Table 3.4, the expected $pK_{a(app)}$ values for HRP in the presence of 25 mM BHA, NMBZA and BZA (Figure 3.12) are 15.0, 12.7 and 11.9, respectively. The spectrum of HRP-BHA at pH 12.0 is similar to that at pH 7.0 as expected, since the $pK_{a(app)}$ for the HRP-BHA complex is 15.0. In the presence of 25 mM BZA the pH 12.0 spectrum can be fit to a sum of the HRP-BZA and alkaline HRP spectra, consistent with a $pK_{a(app)} = 11.9$ (Figure 3.16). Based on $pK_{a(app)} = 12.7$, the HRP-NMBZA spectrum at pH 12.0 would be expected to closely resemble that at pH 7.0, and an examination of Figure 3.12 reveals that this is the case.

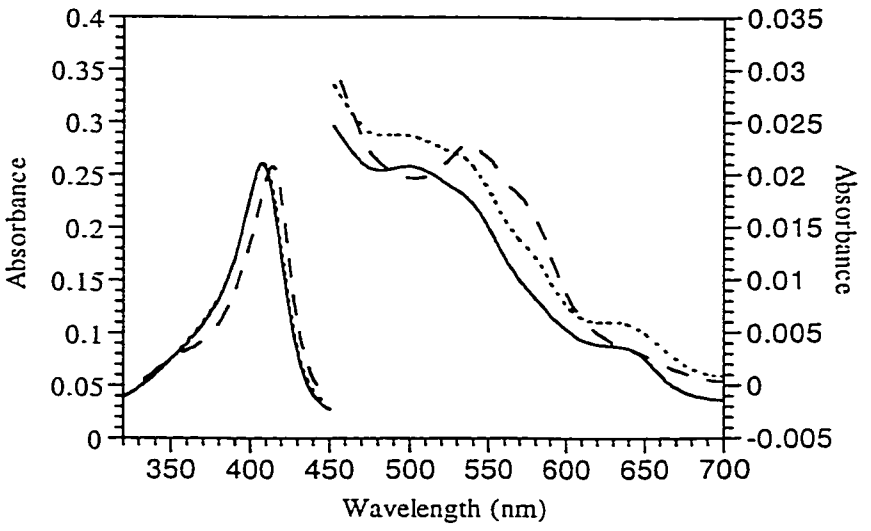

Figure 3.16. Experimentally observed and calculated spectra for the HPR-BZA complex at pH 12.0. The calculated spectrum for the HRP-BZA complex at pH 12.0 (·····) was obtained on the basis that the pK_a(app) of 11.9 calculated (eq. 3.2) for the alkaline transition of HRP in the presence of 25 mM BZA. The experimental spectra of 2.5 μM free HRP in 100 mM sodium phosphate, pH 12.0 (- - -) and in the presence of 25 mM BZA (—) are shown for comparison.

Schonbaum (*63*) also suggested that hydroxamate anions do not bind to HRP. This is consistent with the results presented here, since the $K_{d(app)}$ values for BHA, 1-NHA, and 2-NHA increased by 61-, 13-, and 9-fold, respectively, between pH 8.0 and pH 10.0 (Table 3.3). SHA was examined in more detail because it has two groups that ionize (pK_{a1} = 7.4 and pK_{a2} = 10.0, Figure 3.15) within the pH 4.0 - 12.0 range. Table 3.3 reveals a large (28-fold) increase in SHA $K_{d(app)}$ between the pH values (7.0 and 9.0) that bracket its pK_{a1}. This is consistent with binding of the neutral form only, as was observed for the other hydroxamic acids and is confirmed by the lack of change in the corrected K_d values for SHA between pH 7.0 - 9.0 (Table 3.4). Figure 3.15 shows three possible tautomers of singly ionized SHA (SHA^-) with the negative charge located on the carbonyl oxygen (Figure 3.15, Form ***B***), on the N atom (Figure 3.15, Form ***C***) or on the hydroxamate O atom (Figure 3.15, Form ***D***). Tautomers ***B*** through ***D*** are also representative of the singly ionized forms of BHA, 1-NHA, and 2-NHA, although the intramolecular H-bond is not present for these. Each of these tautomers is incapable of forming one of the three H-bonds observed in the HRP-BHA complex (to His42, Arg38, and Pro139), thus explaining the low affinity of HRP for SHA^- and other ionized Ar-CO-NH-X.

3.3.1.2.Role of hydrophobic interactions in the binding of aromatic hydroxamic acid analogues to HRP

While the formation of H-bonds to distal cavity residues provides a large enthalpic driving force for binding, other factors cannot be ignored. A comparison of BHA binding [K_d = 2.5 μM, Table 3.3, (*63*)] with that of acetohydroxamic acid [K_d = 62 mM, (*63*)] reveals a $\Delta\Delta G°$ of 5.45 kcal/mol. The binding of acetohydroxamic acid is too

weak to measure by ITC. However, since these two compounds have the same H-bonding capacity, it would seem likely that the large difference in binding energy is due largely to the presence of the hydrophobic phenyl ring of BHA. Desolvation of the phenyl ring, as well as liberation of water molecules within the distal cavity is both entropically and enthalpically favourable as released water molecules form H-bonds with the bulk solvent. The role of hydrophobic interactions in the binding of ligands to HRP is also shown by the binding of 2-NHA, NMBZA, 3-CH_3-BZH and 4-CH_3-BZH (Figures 3.5 and 3.8), as the binding of each of these compounds is entropically favourable.

The binding of NMBZA to HRP ($\Delta\Delta G°$ = -1.47 kcal/mol, $\Delta\Delta H°$ = 1.30 kcal/mol and $T\Delta\Delta S°$ = 2.77 kcal/mol, as compared to BZA) is more entropically driven and less enthalpically favourable than BZA. The loss of binding enthalpy for NMBZA compared to BZA is likely due to destabilization of H-bond(s) in the distal cavity resulting from the presence of the bulky methyl group of NMBZA (Figure 3.1). The large entropic contribution is due to desolvation of the methyl group of NMBZA and results in its tighter binding than BZA. Thus, desolvation of the methyl group is the driving force for the 7-fold tighter binding of NMBZA compared to BZA.

Desolvation is also responsible for the greater binding energy and more entropically favourable binding of 2-NHA to HRP ($\Delta\Delta G°$ = -1.63 kcal/mol, $T\Delta\Delta S°$ = 1.00 kcal/mol, Table 3.1) compared to BHA. The 2-NHA side chain has the same potential for H-bond formation as BHA; therefore, the additional enthalpy ($\Delta\Delta H°$ = -0.63 kcal/mol for 2-NHA versus BHA) is likely due to H-bonding of released water molecules with the bulk solvent. Comparison of the crystal structures for HRP and the HRP-BHA complex shows that Phe68, which is located at the opening of the distal cavity, is flexible

and can be flipped away from the entrance to the distal pocket (open conformation) or flipped down and partially blocking the entrance (closed conformation) (*11, 61*). It is not known whether this flexibility is involved in substrate binding, and it may be responsible for the two binding modes for BHA in the ternary HRP•CN•BHA complex of BHA observed by NMR (*64*). It was suggested by Henriksen et al. (*61*) that the binding of 2-NHA could be accommodated with Phe68 in the open conformation. This restriction in the flexibility of Phe68 would be entropically unfavorable, resulting in a lower $T\Delta\Delta S°$ than what might be expected on the basis of desolvation alone. Therefore, the low $T\Delta\Delta S°$ of the additional phenyl ring of 2-NHA (1.00 kcal/mol compared to BHA) in contrast with that of the methyl group of NMBZA ($T\Delta\Delta S° = 2.77$ kcal/mol compared to BZA) is likely due to the loss of flexibility of HRP residues in the HRP-2-NHA complex.

3.3.2. Effect of Ar-CO-NH-X ring substituents on binding to HRP(Fe^{III})

Interpretation of the thermodynamic binding parameters for SHA is challenging because of the two possible binding modes (Figure 3.6). Davey et al. (*76*) observed that in the MPO-SHA complex, the 2-OH group of SHA is positioned to form an intramolecular H-bond with the NH group of the hydroxamic acid side chain. If this conformation of SHA (SHA_1, Figure 3.6) occurs in the HRP-SHA complex, it would position the ring OH in proximity with the backbone carbonyl of Pro139, possibly resulting in steric or electronic repulsion between these groups. In contrast, the ARP-SHA structure shows a 180 degree rotation around the C1-C7 bond (Figure 1.3) to place the ring OH in proximity with the C=O moiety of the hydroxamic acid side chain (*75*) such that an intramolecular H-bond could be formed between the two oxygen atoms. If

this conformation (SHA_2, Figure 3.6) is adopted by SHA in the HRP-SHA complex, the 2-OH group would be positioned in proximity to Arg38.

Given its low pK_{a1} (7.4; Figure 3.15), SHA should form a stronger H-bond to the distal His42, as observed for BHA vs BZH, resulting in a greater binding affinity relative to BHA. However, the K_d of SHA was observed to be ~ 4-fold greater than that of BHA (Tables 3.1 and 3.3). The 2-OH group of SHA does provide an enthalpic advantage ($\Delta\Delta H°$ = -1.33 kcal/mol, Table 3.1) compared to BHA, possibly due to the formation of an H-bond by the 2-OH. The 2-OH group of SHA is predicted to be an H-bond donor in the intramolecular H-bond in both the SHA_1 and SHA_2 conformations shown in Figure 3.6. Since the 2-OH group cannot donate an H-bond to both the NH group of the hydroxamic acid side chain and to the backbone carbonyl of Pro139, the $\Delta\Delta H°$ of -1.33 kcal/mol observed for SHA binding to HRP compared to BHA supports the formation of an H-bond with Arg38. Therefore, the thermodynamic data supports the binding of SHA to HRP in the SHA_2 conformation (Figure 3.6), which was observed for the ARP-SHA complex (*75*)

Desolvation of the hydrophilic 2-OH group is expected to be at least partially responsible for the entropically unfavorable binding of SHA ($T\Delta\Delta S°$ = -2.26 kcal/mol, Table 3.1) versus BHA. However, other factors are involved, including the intramolecular H-bond of SHA, which makes it more rigid than BHA (*75, 76, 219*). This is expected to provide an entropic advantage to the binding of SHA because less ligand flexibility is lost on binding of SHA to HRP compared to BHA. The magnitude of the relative contributions of ligand flexibility and desolvation to the entropy of SHA binding to HRP is difficult to estimate. It is also possible that the presence of the 2-OH group

may result in a more constrained conformation for some active site residue(s), contributing to the unfavorable entropy of SHA binding.

Comparison of the binding of the ring-substituted hydrazides to HRP revealed that the *ortho*-substituted hydrazides generally had the lowest binding energies (Figure 3.8). The rationale for the weak binding of these compounds depends on the H-bonding capacity of the *ortho* group. Observation of a trend for 2-OH-BZH ($\Delta\Delta H°$ = -3.94 kcal/mol and $T\Delta\Delta S°$ = -4.92 kcal/mol, Table 3.2) and 2-NH_2-BZH ($\Delta\Delta H°$ = -0.07 kcal/mol and $T\Delta\Delta S°$ = -1.99 kcal/mol, Table 3.2), similar to the one observed for SHA, suggests that the above explanation for SHA binding is also true for these compounds. However, since the amino group of 2-NH_2-BZH can donate two H-bonds, it could bind to HRP in either the SHA_1 or SHA_2 conformations (Figure 3.6). The role of steric or electronic repulsion in the weak binding of SHA, 2-OH-BZH and 2-NH_2-BZH is supported by the very weak binding of the bulky 2-NO_2-BZH (K_d = 85 mM, Table 3.2).

In contrast to 2-OH-BZH and 2-NH_2-BZH, 2-CH_3-BZH and 2-Cl-BZH are incapable of forming an intramolecular H-bond between the *ortho* group and the hydrazide side chain. Furthermore, steric constraint between the ring substituent and the hydrazide side chain likely causes these compounds to be nonplanar. The binding of these nonplanar hydrazides may result in strain on the H-bonds formed by the hydrazide side chain within the distal cavity, thus causing the observed reduction in the enthalpy of binding of 2-CH_3-BZH ($\Delta\Delta H°$ = 1.51 kcal/mol, Table 3.2) and 2-Cl-BZH ($\Delta\Delta H°$ = 1.74 kcal/mol, Table 3.2) compared to BZH.

At a glance, the presence of a hydroxyl, methyl, amino or chloro substituent in the *meta* position appears to have little effect on binding because the $\Delta G°$ of binding of these

compounds to HRP is within 0.5 kcal/mol of that of BZH. However, a closer look uncovers the role in binding of groups in the *meta* position (Figure 3.8). 3-OH-BZH ($\Delta\Delta H° = T\Delta\Delta S° = -1.59$ kcal/mol) and 3-NH_2-BZH ($\Delta\Delta H° = -0.36$ kcal/mol and $T\Delta\Delta S° = -0.80$ kcal/mol) are both enthalpically favourable and entropically unfavorable. It is possible that these hydrophilic groups are able to form a weak H-bond with the backbone carbonyl of Pro139 (Figure 3.17) resulting in their small enthalpic advantage over BZH. Alternatively, they may form an H-bond to the aromatic ring of Phe68 (Figure 3.17), which is in proximity to the *meta*-position of BHA in the HRP-BHA structure (*61*). Aromatic rings have been shown to be H-bond acceptors, forming H-bonds about half as strong as a neutral H-bond (*220*). The entropic disadvantage of 3-OH-BZH and 3-NH_2-BZH as compared to BZH is likely due to the hydrophilic nature of their ring substituents.

The binding of both 3-CH_3-BZH ($\Delta\Delta H° = 0.82$ kcal/mol and $T\Delta\Delta S° = 0.88$ kcal/mol) and 3-Cl-BZH ($\Delta\Delta H° = 1.95$ kcal/mol and $T\Delta\Delta S° = 1.48$ kcal/mol) to HRP are enthalpically unfavorable in comparison with BZH, possibly due to steric hindrance resulting in increased strain on existing H-bonds. 3-CH_3-BZH and 3-Cl-BZH are both entropically favourable compared to BZH. This is likely due to the desolvation of the hydrophobic methyl group for 3-CH_3-BZH, whereas the reason is not apparent from the evidence available for 3-Cl-BZH.

Examination of the HRP-BHA structure shows that C4 of the BHA aromatic ring is 3.70 Å and 3.93 Å from the phenyl rings of Phe68 and Phe179, respectively (Figure 3.17). Binding of 4-CH_3-BZH ($\Delta\Delta H° = 0.42$ kcal/mol and $T\Delta\Delta S° = 0.32$ kcal/mol) and 4-NH_2-BZH ($\Delta\Delta H° = 0.59$ kcal/mol and $T\Delta\Delta S° = 0.21$ kcal/mol) are only slightly

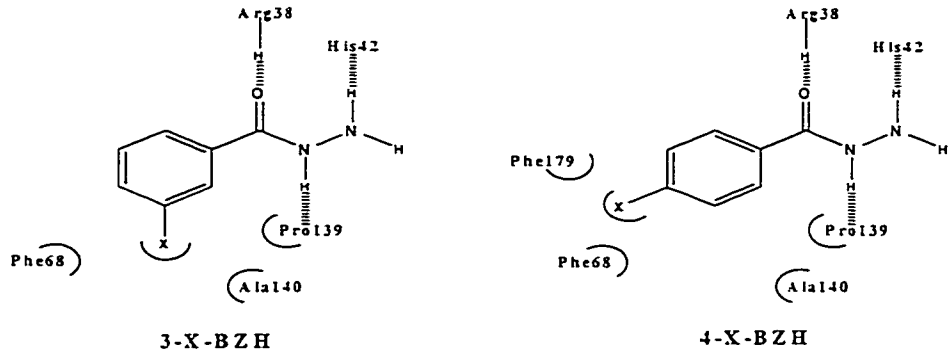

Figure 3.17. Proposed H-bonding and hydrophobic contacts of ring-substituted hydrazides in the distal POX cavity of HRP based on the HRP-BHA structure. H-bonds are represented by hashed lines and hydrophobic or steric interactions by semicircles.

enthalpically unfavorable and entropically favourable. In contrast, the binding of 4-OH-BZH ($\Delta\Delta H^\circ$ = 3.28 kcal/mol and $T\Delta\Delta S^\circ$ = 2.39 kcal/mol) and 4-Cl-BZH ($\Delta\Delta H^\circ$ = 3.56 kcal/mol and $T\Delta\Delta S^\circ$ = 3.02 kcal/mol) are very enthalpically unfavorable and entropically favourable. This suggests that one of the H-bonds formed by BZH in the distal heme cavity of HRP is not present in 4-OH-BZH and 4-Cl-BZH and is compensated by the increased flexibility of the complex.

3.3.3. Binding of other Ar-CO-NH-X to HRP

The binding of isoniazid and the related compound, nicotinic hydrazide, was investigated to probe the reason for their 10 - 40-fold weaker binding to HRP compared to BZH (Table 3.2). Both of these compounds are structurally similar to BZH (Figure 3.1), with the only difference being replacement of the phenyl ring of BZH with a pyridine ring. The unfavorable binding enthalpy of INH ($\Delta\Delta H^\circ$ = 3.30 kcal/mol) and NICH ($\Delta\Delta H^\circ$ = 4.48 kcal/mol) compared to BZH suggests the loss of a H-bond. While the loss of a H-bond may result in less constrained conformation ($T\Delta\Delta S^\circ$ = 1.33 kcal/mol and 2.32 kcal/mol for INH and NICH, respectively), the gain in entropy is inadequate to compensate for the enthalpic loss, and the overall energy of binding is reduced ($\Delta\Delta G^\circ$ = 1.98 kcal/mol and 2.17 kcal/mol for INH and NICH, respectively) compared to BZH.

The binding of 1-NHA and tepoxalin to HRP was investigated spectroscopically because their low solubility precluded the use of ITC. Although desolvation and H-bonding potential are expected to be the same for the two naphthoic hydroxamic acids, 2-NHA binds ~170-fold more tightly than 1-NHA (Table 3.4). Examination of the HRP-BHA complex (*61*) shows that Phe179 partially blocks the entrance of the distal cavity, resulting in steric hindrance with bulky substrates. 2-NHA is able to bind because it

enters the distal cavity in an end-on fashion, which is not possible for 1-NHA (Figure 3.1). Consequently, the decreased binding affinity of 1-NHA is likely an entropic effect due to steric constraint.

The small change in the Soret band observed in the presence of tepoxalin (Figure 3.13) indicates that it does not greatly disturb the heme environment in HRP. Since tepoxalin does not inhibit HRP (*212*), it is likely that the hydroxamic acid group of tepoxalin is restricted from accessing the distal cavity of HRP due to steric hindrance.

3.3.4. Entropy-enthalpy compensation

Enthalpy-entropy compensation is commonly observed for ligand binding to proteins in aqueous solutions and has been generally regarded as a property of water (*221*). However, it has been suggested that enthalpy-entropy compensation is actually a property of all weak intermolecular interactions and that H-bonding in aqueous solution is just the most frequently encountered in living systems (222). Release of structured water molecules (desolvation) from the interacting surfaces results in an entropy gain that is compensated by loss in enthalpy due to enthalpically weaker H-bonds in bulk water (*221*). The result is that $\Delta H°$ and $\Delta S°$ change proportionally, while $\Delta G°$ is less affected. The linear relationship ($r^2 = 0.6$) between $\Delta H°$ and $\Delta S°$ for all 24 of the compounds tested shows that this phenomenon occurs for the binding of aromatic hydroxamic acid analogues to HRP (Figure 3.9).

3.4. APPENDIX 3A. EXPERIMENTAL CONDITIONS AND RAW DATA FOR ITC EXPERIMENTS

Table 3A.1. Experimental conditions for ITC experiments

Compound	pH	c	[HRP] (mM)	[ligand] (mM)
BZA[b]	7 (NaPi)	0.22	0.938	35.0
NMBZA[a]	7 (NaPi)	0.58	0.207	3.52
2-HA[b]	7 (NaPi)	0.068	0.879	30.0
N-BH[b]	7 (NaPi)	0.06	1.14	40.0
BHA[a]	4 (tartrate)	11	0.0678	1.15
BHA[a]	4 (citrate)	11	0.0832	1.41
BHA[a]	4 (acetate)	8.3	0.0678	1.15
BHA[a]	7 (Tris)	6.9	0.0137	0.233
BHA[a]	7 (imidazole)	16	0.0576	0.979
BHA[a]	7 (MOPS)	10	0.0314	0.534
BHA[a]	7 (HEPES)	7.8	0.0273	0.464
BHA[a]	7 (PIPES)	10	0.0131	0.223
BHA[a]	7 (NaPi)	13	0.0330	0.560
BHA[b]	7 (NaPi)	26	0.0660	0.896
SHA[a]	7 (Tris)	4.2	0.0562	0.955
SHA[a]	7 (imidazole)	16	0.318	5.41
SHA[a]	7 (MOPS)	9.4	0.107	1.82
SHA[a]	7 (HEPES)	8.5	0.138	2.34
SHA[a]	7 (PIPES)	4.3	0.0510	0.867
SHA[b]	7 (NaPi)	7.7	0.085	1.16
2-NHA[a]	4 (tartrate)	20	0.0100	0.170

Table 3A.1 continued.

Compound	pH	c	[HRP] (mM)	[ligand] (mM)
2-NHA[a]	4 (citrate)	45	0.0245	0.417
2-NHA[a]	4 (acetate)	27	0.0203	0.345
2-NHA[a]	7 (TRIS)	65	0.0154	0.262
2-NHA[a]	7 (Imidazole)	55	0.0178	0.303
2-NHA[a]	7 (MOPS)	35	0.00750	0.128
2-NHA[a]	7 (HEPES)	32	0.0110	0.187
2-NHA[a]	7 (PIPES)	93	0.0240	0.409
2-NHA[a]	7 (NaPi)	16	0.00260	0.0442
BHA[b]	6 (NaPi)	21	0.0560	0.950
BZH[b]	6 (NaPi)	2.6	0.310	10.0
2-OH-BZH[b]	6 (NaPi)	0.49	0.310	10.0
3-OH-BZH[b]	6 (NaPi)	2.6	0.310	10.0
4-OH-BZH[b]	6 (NaPi)	0.68	0.365	8.00
2-CH_3-BZH[b]	6 (NaPi)	0.33	0.905	30.0
3-CH_3-BZH[b]	6 (NaPi)	2.9	0.310	10.0
4-CH_3-BZH[b]	6 (NaPi)	2.2	0.310	10.0
2-NH_2-BZH[b]	6 (NaPi)	0.10	0.310	10.0
3-NH_2-BZH[b]	6 (NaPi)	0.62	0.155	5.00
4-NH_2-BZH[b]	6 (NaPi)	1.6	0.365	8.00
2-Cl-BZH[b]	6 (NaPi)	0.37	0.761	30.0
3-Cl-BZH[b]	6 (NaPi)	0.94	0.250	8.00
4-Cl-BZH[b]	6 (NaPi)	0.84	0.250	8.00
INH[b]	6 (NaPi)	0.18	0.597	10.15

Table 3A.1 continued.

Compound	pH	c	[HRP] (mM)	[ligand] (mM)
NICH[b]	6 (NaPi)	0.16	0.721	30.0
2-NZH[b]	6 (NaPi)	5.5	0.0287	0.490

[a]ITC experiments using the MSC ITC instrument (Biotechnology Research Institute)
[b]ITC experiments using the VP ITC instrument (Structural Genomics Center, Concordia)

Table 3.A2. Data from ITC experiments for BHA and 2-NHA at pH 4.0 and BHA, SHA and 2-NHA at pH 7.0

Compound	PH	$K_{d(ITC)}$ (μM)	n	ΔG^{oc} (kcal/mol)	ΔH^{o} (Kcal/mol)	ΔS^{od} (cal/mol)
BHA[a]	4 (tartrate)	6.2±0.1	1.06±0.002	-7.10	-9.60±0.04	-8.39
BHA[a]	4 (acetate)	8.2±0.15	0.85±0.003	-6.93	-9.30±0.50	-7.95
BHA[a]	4 (citrate)	7.4±0.32	0.68±0.01	-7.00	-8.90±0.11	-6.38
BHA[a]	7 (TRIS)	2.0±0.6	0.91±0.08	-7.77	-10.9±1.3	-10.5
BHA[a]	7 (IMID)	3.7±0.1	0.87±0.003	-7.41	-12.3±0.07	-16.4
BHA[a]	7 (HEPES)	3.5±0.15	1.19±0.01	-7.45	-13.0±0.15	-18.6
BHA[a]	7 (MOPS)	3.1±0.12	1.04±0.007	-7.51	-12.8±0.12	-17.8
BHA[a]	7 (PIPES)	3.3±0.5	0.83±0.04	-7.47	-13.4±0.95	-19.9
BHA[a]	7 (NaPi)	2.5±0.05	0.90±0.003	-7.64	-14.1±0.07	-21.7
BHA[b]	7 (NaPi)	2.9±0.06	0.88±0.002	-7.55	-14.2±0.05	-22.3
SHA[a]	7 (TRIS)	13.3±0.4	0.85±0.01	-6.65	-14.2±0.21	-25.3
SHA[a]	7 (IMID)	19.8±0.7	0.81±0.004	-6.41	-13.9±0.11	-25.1
SHA[a]	7 (MOPS)	11.4±0.3	0.84±0.004	-6.74	-14.6±0.09	-26.4

Table 3A.2 continued

Compound	pH	$K_{d(ITC)}$ (μM)	n	ΔG^{oc} (kcal/mol)	$\Delta H°$ (Kcal/mol)	ΔS^{od} (cal/mol)
SHA[a]	7 (HEPES)	16.3±0.3	0.91±0.004	-6.53	-14.6±0.08	-27.1
SHA[a]	7 (PIPES)	11.8±0.3	0.87±0.006	-6.72	-14.8±0.14	-27.1
SHA[b]	7 (NaPi)	12.3±0.4	0.90±0.007	-6.69	-15.5±0.16	-29.6
2-NHA[a]	4 (tartrate)	0.500±0.06	0.93±0.02	-8.59	-10.9±0.27	-7.75
2-NHA[a]	4 (citrate)	0.540±0.04	0.85±0.005	-8.55	-9.6±0.09	-3.52
2-NHA[a]	4 (acetate)	0.750±0.05	1.05±0.005	-8.35	-10.0±0.09	-5.53
2-NHA[a]	7 (TRIS)	0.238±0.014	1.02±0.004	-9.03	-12.7±0.08	-12.3
2-NHA[a]	7 (IMID)	0.323±0.016	1.03±0.004	-8.85	-12.8±0.07	-13.3
2-NHA[a]	7 (MOPS)	0.217±0.056	1.01±0.02	-9.09	-13.8±0.61	-15.8
2-NHA[a]	7 (HEPES)	0.342±0.062	1.06±0.02	-8.82	-13.8±0.33	-16.7
2-NHA[a]	7 (PIPES)	0.257±0.017	1.03±0.004	-8.99	-12.7±0.07	-12.4
2-NHA[a]	7 (NaPi)	0.158±0.04	1.04±0.04	-9.27	-14.8±0.94	-18.6

[a]ITC experiments using the MSC ITC instrument (Biotechnology Research Institute).
[b]ITC experiments using the VP ITC instrument (Structural and Functional Genomics Center, Concordia)
[c]Error in ΔG° not reported because ΔG° was determined from $K_{d(ITC)}$ (eq. 2.4).
[d]Error in ΔS° not reported because ΔS° was determined from ΔH° and ΔG° (eq. 2.5).

4. INACTIVATION OF HRP BY HYDRAZIDES

4.1. INTRODUCTION

The potential of selective POX inhibitors to reduce toxicity caused by the generation of free radicals and other oxidants by peroxidases was discussed in Section 1.4 (peroxidase inhibition). However, the ability of many peroxidases to oxidize a wide range of organic compounds makes the design of selective, reversible inhibitors that will not be oxidized, exceedingly difficult. Therefore, mechanism-based inhibitors are an attractive alternative for peroxidase inhibition. A mechanism-based inhibitor is one that is chemically transformed into the inactivating species by the target enzyme and which inactivates the enzyme by covalent modification prior to its release from the active site (*154*).

Alkyl- and arylhydrazines (R-NH-NH_2) are peroxidase inhibitors which result in covalent heme modification and have been used to probe active-site topology in a number of peroxidases (*188, 223-228*). Arylhydrazines are oxidized by peroxidases to highly reactive radical species (via reactions such as 1.2 and 1.3) which can be incorporated at the heme or in its vicinity, thereby preventing further peroxidase substrate turnover (*228*). Hydrazides (R-CO-NH-NH_2) are related compounds that are also known to be inhibitors of peroxidases (*157, 229, 230*); however, while their mechanism of inhibition is likely similar to that of hydrazines, it has not yet been investigated in detail.

Several hydrazine and hydrazide derivatives have been used therapeutically, including isoniazid (tuberculosis antibiotic), iproniazid (tranquilizer), isocarboxazid, mebanazine, phenelzine (monoamine oxidase inhibitors), hydralazine (antihypertensive), and phenylhydrazine (PH; control of polycythemia vera). However, many of these are no

longer in use due to the severe side-effects, which include hemolysis, liver damage, lupus erythematosus and base-pair mutation resulting from bioactivation (*231-235*). These side effects can be due to bioactivation by other enzymes as a result of the lack of specificity of these compounds or the release of activated inhibitor by the target enzyme. If release of the activated inhibitor occurs more readily than inactivation of the target enzyme, the result is a high partition ratio. The partition ratio is the number of inhibitor molecules turned over and released as product per turnover leading to enzyme inactivation (*154*). The radicals released from hydrazine and hydrazide oxidation are likely capable of attacking lipids, nucleic acids, and other proteins *in vivo*. Therefore, partition ratios approaching zero, *i.e.*, no product release, would be ideal for any hydrazine or hydrazide to be developed as a potential therapeutic agent.

A relatively low partition ratio of ~12 has been reported for HRP inhibition by PH (*188*). However, PH is known to undergo autooxidation at pH 7.0 to produce superoxide both in the presence of heme or a heme protein or in a heme-free medium (*236*). As a result, PH would be an ineffective therapeutic because it is too labile and because of the toxicity of radicals and superoxide produced during its autooxidation (*229*). In contrast, hydrazides, like INH and NICH, undergo autooxidation very slowly and require activation by a peroxidase (*229*). Therefore, hydrazides may prove to be more effective than hydrazines in the development of inhibitors for specific peroxidases.

Hydrazides have been suggested to be mechanism-based inhibitors of the mammalian peroxidase MPO (*158*). The distinguishing feature of a mechanism-based inhibitor is that the target enzyme chemically transforms the pro-inhibitor into the inactivating species and inactivation occurs prior to the release of this species from the

enzyme (*154*). However, while release and rebinding of the activated inhibitor do not occur prior to enzyme inactivation for a mechanism-based inhibitor, release of this species is possible and results in a partition ratio greater than zero. In contrast, following activation, a metabolically-activated inhibitor is released from the activating enzyme and leads to inactivation by returning to the active site of the same enzyme or a different enzyme (*154*). The hydrazide INH is an example of a metabolically-activated inhibitor, as it has been shown to inactivate enoyl reductase, inhA, following activation and release by the peroxidase/catalase (KatG) of *Mycobacterium tuberculosis* (*160*). Despite the fact that INH is still the most important drug worldwide for the treatment of tuberculosis (*159*), it results in severe side effects including allergic and autoimmune syndromes (*e.g.*, lupus, erythamatosus-like syndrome, rheumatic syndrome) and hepatitis (*159, 237, 238*). Therefore, although INH does not act therapeutically as a peroxidase inhibitor, it provides a good example of the need to ensure that a potential class of peroxidase inhibitors (*e.g.*, hydrazides) are mechanism-based, rather than metabolically-activated. This highlights the requirement for an investigation of hydrazide autooxidation and the mechanism of peroxidase inhibition by hydrazides prior to the assessment of their potential as therapeutic agents.

The mechanism of HRP inactivation by phenylhydrazine has been thoroughly investigated (*188, 223*). Therefore, HRP was also used in this study to probe the mechanism of peroxidase inhibition by hydrazides. The autooxidation of the simplest aromatic hydrazide, BZH, and mechanism of inactivation of HRP by BZH was investigated in detail in this study to provide insight into the mechanism of HRP inhibition by hydrazides and the suitability of hydrazides as peroxidase inhibitors.

Additionally, a series of aromatic hydrazides varying in the size of the aromatic ring system and the type and position of aromatic-ring substituents (shown in the lower portion of Figure 3.1.) was examined. IC_{50} values as well as K_I and k_{inact} values and partition ratios were determined for the hydrazide series to determine the factors that contribute to the effective inhibition of HRP. Since HRP is an archetypical peroxidase (2) these results are expected to be applicable to other peroxidases, including PGHS.

4.2. RESULTS

4.2.1. Kinetics of HRP inactivation by hydrazides

4.2.1.1. Is BZH a mechanism-based inhibitor of HRP?

Silverman (*154*) has delineated the 7 criteria generally observed for mechanism-based inhibitors:

1. Time-dependence
2. Saturation kinetics
3. Substrate protection
4. Irreversibility
5. Stoichiometry of inactivation
6. Activation of the inhibitor by the target enzyme
7. Inactivation occurs prior to release of activated species

To investigate whether hydrazides are mechanism-based inhibitors of HRP, a series of experiments based on the criteria listed above were conducted. In the first experiment, HRP activity was monitored over time at BZH concentrations ranging from 12.5 - 500 μM to evaluate the time-dependence of inhibition (criterion 1) and whether the inactivation displayed saturation kinetics (criterion 2). In the absence of BZH, HRP activity was also observed to decrease with an observed rate constant of (k_{obs}) of 0.031 min^{-1} due to H_2O_2-dependent inactivation (Figure 4.1A). However the enzyme retained 75% of its activity after 40 min. The decline in the remaining activity of HRP over time

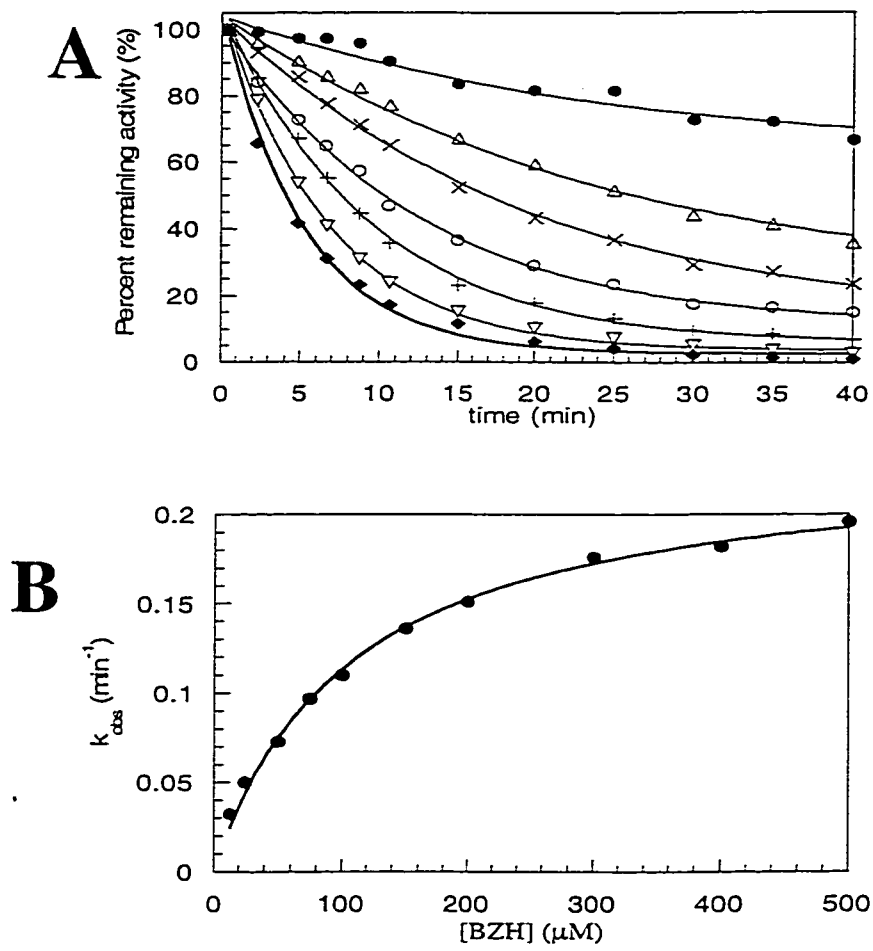

Figure 4.1. Kinetics of HRP inactivation by BZH. 100 nM HRP was preincubated in 100 mM sodium phosphate, pH 7.0, containing 500 μM H_2O_2 and 0 to 500 μM BZH (•, 0 μM; Δ, 12.5 μM; X, 25μM; O, 50 μM; +, 100 μM; ∇, 200 μM; ♦, 500 μM) and assayed at time points between 0.5 and 45 min. The assay mixture contained 100 mM sodium phosphate, pH 7.0, 500 μM H_2O_2 and 5 mM guaiacol as described in Section 2.2.3. (**A**) Plots of remaining activity versus time were fit to equation 2.7 to determine k_{obs} at each BZH concentration. (**B**) The k_{obs} values thus obtained were plotted versus [BZH] and fit to equation 2.8 to yield values for K_I (105 μM) and k_{inact} (0.23 min^{-1}).

for a given BZH concentration (Figure 4.1A) and the leveling off of k_{obs} at BZH concentrations approaching 500 μM (Figure 4.1B) indicate that both criteria 1 and 2 are met by BZH.

In the second experiment, the ability of BZH to compete with guaiacol as a reducing substrate at the active site of HRP (reactions 1.2 and 1.3) was investigated (criterion 3) (*154*). Increasing concentrations of guaiacol were added to a series of preincubations of containing 100 nM HRP, 500 μM H_2O_2, and 500 μM BZH in 100 mM sodium phosphate, pH 7.0. In the absence of guaiacol, k_{obs} was 0.066 min^{-1}, while in the presence of 250 μM guaiacol it was reduced to 0.046 min^{-1}. In the presence of 500 μM guaiacol, k_{obs} was 0.015 min^{-1}, indicating almost complete protection at a 1:1 ratio of guaiacol/BZH (Figure 4.2). Thus, that criterion 3 is met for BZH.

The fourth criterion for a mechanism-based inhibitor is irreversibility, usually due to covalent attachment of the inhibitor to the enzyme. An exception would be a tight, noncovalent complex that is stable to dialysis or gel filtration (*154*). Therefore, the inactivated enzyme will not be reactivated by the removal of excess inhibitor because it is not in equilibrium with the free enzyme and inhibitor. In the third experiment, the HRP sample was desalted to remove excess BZH by gel filtration following incubation with 500 μM H_2O_2 and 500 μM BZH for 1.5 h. HRP was found to be completely inactivated by BZH and H_2O_2 and to remain inactivated (Figure 4.3); therefore, BZH meets criterion 4. Although the control (500 μM H_2O_2, no BZH) lost ~75% activity over the course of the experiment, inactivation of the sample containing both H_2O_2 and BZH was complete. Both samples were found to remain inactivated following desalting (Figure 4.3). Inactivation of HRP by H_2O_2 is likely due to heme destruction resulting in the open-ring

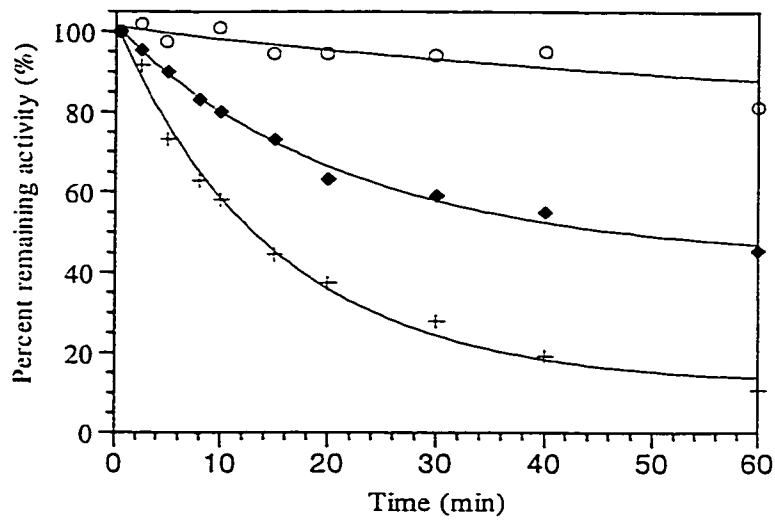

Figure 4.2. Protection by guaiacol against HRP inactivation by BZH. 100 nM HRP was preincubated in 100 mM NaPi, pH 7.0, containing the donor substrate, guaiacol (+, 0 μM, k_{obs} = 0.066 min^{-1}; ♦, 250 μM, k_{obs} = 0.046 and O, 500 μM, k_{obs} = 0.015 min^{-1}), 500 μM H_2O_2 and 500 μM BZH in 100 mM sodium phosphate, pH 7.0, and assayed at time points between 0.5 and 60 min. Activity was measured in an assay mixture containing 100 mM sodium phosphate, pH 7.0, 500 μM H_2O_2 and 5 mM guaiacol as described in Section 2.2.3.

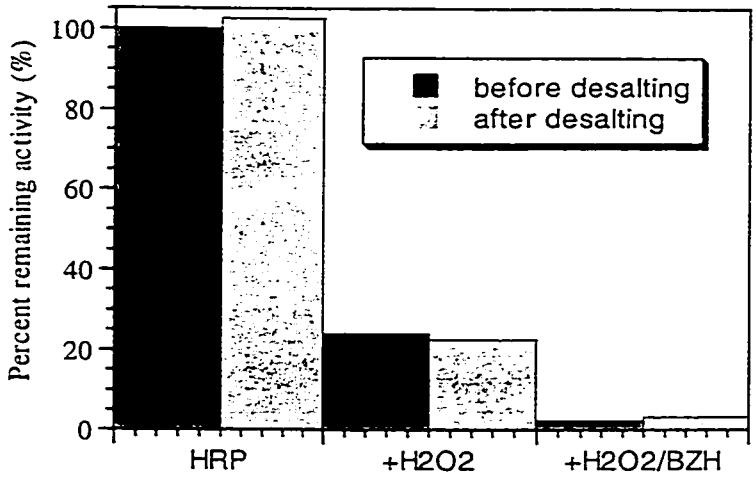

Figure 4.3. Irreversibility of HRP inactivation by BZH and H_2O_2. 100 nM HRP was preincubated for 1.5 h in 100 mM sodium phosphate, pH 7.0, alone (HRP), or containing either 500 μM H_2O_2 (+H_2O_2) or 500 μM H_2O_2 and 500 μM BZH (+H_2O_2/BZH). Following preincubation samples were desalted (PD10, Pharmacia). Activity was measured immediately before and after desalting. The assay mixture contained 100 mM sodium phosphate, pH 7.0, 500 μM H_2O_2 and 5 mM guaiacol as described in Section 2.2.3.

porphyrin, biliverdin (Section 4.2.2.2, mechanism of HRP inactivation by BZH and H_2O_2). Therefore, it is not surprising that desalting did not reactivate the H_2O_2-treated HRP in the control (Figure 4.3).

Determination of the stoichiometry of inactivation (criterion 5) generally requires the use of a labeled inhibitor (*e.g.*, radioactively labeled) and was not investigated here. However, further insight is provided into both the stoichiometry and the involvement of a BZH-activation step (criterion 6) from the types of modifications observed in BZH-inactivated HRP (Section 4.2.2.2, mechanism of HRP inactivation by BZH and H_2O_2).

In order for an inhibitor to be considered as mechanism-based, the activated species must not be released and rebound prior to inactivation (criterion 7). If release of the activated species occurs prior to inactivation then the activated species can build up in solution so that the rate of inactivation of a second aliquot of enzyme would be expected to be faster than that of the initial aliquot. To determine whether BZH meets this criterion, HRP was incubated with 500 μM H_2O_2 and 500 μM BZH until only ~10% activity remained (1 h). To this solution a fresh aliquot of HRP was added and activity was measured for the same period of time (Figure 4.4). The k_{obs} values for the first and second aliquots of HRP (Figure 4.4) are of 0.15 and 0.14 min^{-1}, respectively, indicating that no long-lived activated species are present in the reaction mixture. However, the ability to detect the release of activated species in this manner depends on their reactivity and very reactive species are expected to have short half-lives. Therefore, the possibility of HRP inactivation due to release and attack of an activated species of short half-life cannot be ruled out.

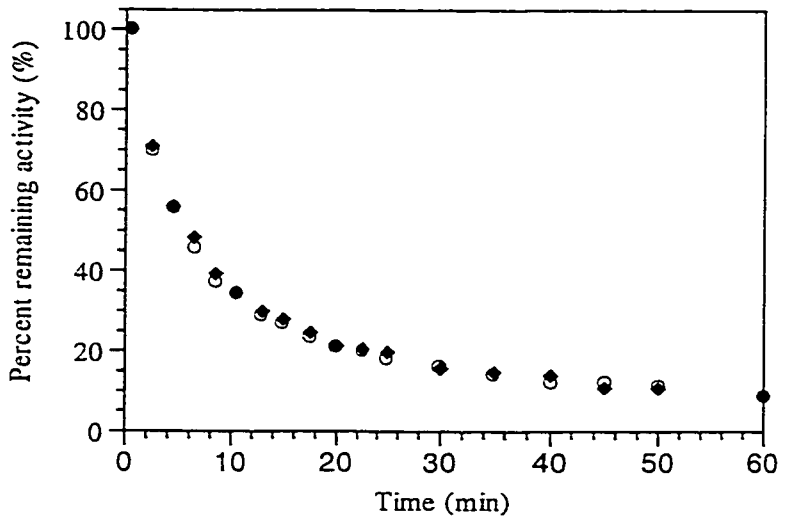

Figure 4.4. Effect of released BZH oxidation product on fresh HRP. 100 nM HRP (O) was incubated for 1 h in 100 mM sodium phosphate, pH 7.0, containing 500 μM H_2O_2 and 500 μM BZH, following which (◆) fresh HRP (100 nM) was added to the reaction mixture and incubated for 1 h. Activity was measured in an assay mixture containing 100 mM sodium phosphate, pH 7.0, 500 μM H_2O_2 and 5 mM guaiacol as described in Section 2.2.3.

4.2.1.2. Comparison of HRP inactivation by a series of hydrazides

All 24 of the hydrazides tested (Figure 3.1, X = NH_2) were observed to exhibit similar time-dependence and saturation kinetics as shown for BZH in Figure 4.1. The plot of the observed first-order rate constants (k_{obs}) for loss of HRP activity versus hydrazide concentration (Figure 4.1B) could be fit by equation 2.8 in which K_I is the concentration of inactivator that produces half the maximal rate of inactivation and k_{inact} is the observed inactivation rate constant:

$$E + I \underset{}{\overset{K_I}{\rightleftharpoons}} EI \xrightarrow{k_{inact}} EI^* \qquad \text{(Scheme 4.1)}$$

The K_I and k_{inact} values are summarized in Table 4.1 for the hydrazides shown in Figure 3.1. 2-NZH, 1-NZH, and 2-NH_2-BZH exhibit the highest values of k_{inact}, with all others being 1-2 orders of magnitude lower (Table 4.1). The ratio of K_I to K_d for the hydrazides tested (Table 4.1) falls within 0.1 - 10 for most of the hydrazides tested, the only notable exceptions being 2-NZH and NICH.

The partition ratio is the number of molecules leading to product per inactivation event, or the turnover number (number of inhibitor molecules required for complete inactivation) minus one. Therefore, it provides an estimate of the efficiency of a given compound as a mechanism-based inhibitor. The partition ratios for inactivation of HRP were determined by titration because it is one of the simplest methods. HRP (100 nM) was preincubated for 10 min with 500 μM H_2O_2, and 0-5 mM hydrazide (0 - 500 μM for BZH and 2-NZH) and the remaining activity plotted versus [hydrazide]/[HRP]. Extrapolation of the lower-ratio, linear portion of this plot to 0% remaining activity yielded the turnover number (partition ratio + 1) after 10 min (Figure 4.5, Table 4.1).

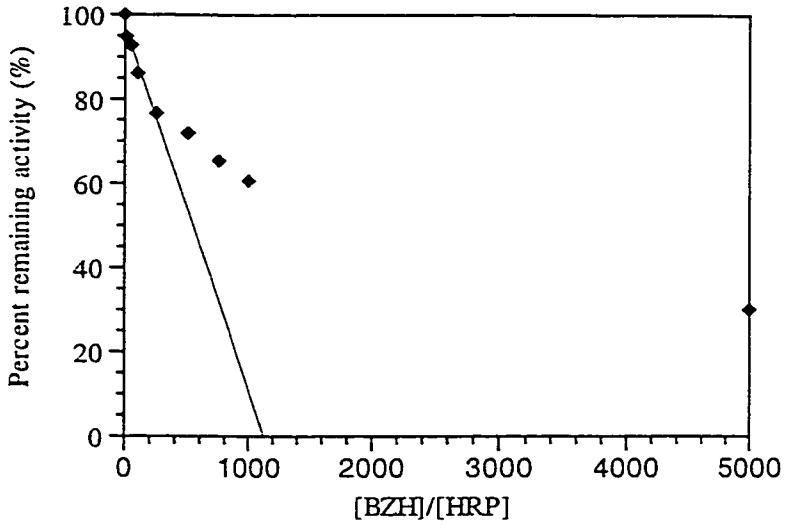

Figure 4.5. Inactivation of HRP as a function of the BZH to enzyme ratio. 100 nM HRP was preincubated for 10 min in 100 mM NaPi, pH 7.0, containing 500 μM H_2O_2 and 12.5 to 500 μM BZH. Percent remaining activity (determined as described in Section 2.2.3) is plotted versus [BZH]/[HRP]. The partition ratio was determined from the x-intercept (0% activity) of a linear fit to the initial linear portion of the curve.

Table 4.1. Partition ratios, K_I and k_{inact}, and IC_{50} values for the inactivation of HRP by hydrazides

Inhibitor	Partition ratio at 10 min ($x10^{-3}$)[a]	K_I (mM)[b]	K_{inact} (min^{-1})[b]	IC_{50} (mM)[c]	K_I/K_d[d]
BZH	1.1	0.11	0.23	6.9±0.4	0.96
2-OH-BZH	16	0.55	0.078	49±7	1.2
3-OH-BZH	0.58	0.41	0.16	5.9±0.8	4.7
4-OH-BZH	0.14	0.024	0.57	5.9±1.1	0.11
2-CH_3-BZH	0.67	4.5	0.84	56±26	1.9
3-CH_3-BZH	0.37	0.88	0.43	4.9±0.5	12
4-CH_3-BZH	0.20	0.32	0.33	6.2±2.6	2.7
2-NH_2-BZH	0.13	0.28	1.4	0.59±0.17	0.094
3-NH_2-BZH	0.30	0.92	0.40	12±2	3.7
4-NH_2-BZH	0.14	0.10	0.62	9.0±2.0	0.33
2-Cl-BZH	6.4	1.8	0.12	95±70	0.76
3-Cl-BZH	0.51	1.1	0.33	11±3	11
4-Cl-BZH	0.37	1.4	0.58	16±4	10
2-NO_2-BZH	35	5.5	0.025	92±22	0.064
3-NO_2-BZH	0.92	1.8	0.62	38±12	0.19
4-NO_2-BZH	0.42	1.4	0.65	14±2	0.46
1-NZH	0.22	0.40	1.7	3.4±0.6	
2-NZH	0.11	0.15	6.8	0.048±0.022	158
3-OH-2-NZH[e]	—	—	—	3.3±1.2	—
INH	4.7	0.44	0.046	29±6	0.40
NICH	16	0.11	0.053	78±23	0.025

[a]Partition ratio for inactivation of HRP after a 10-min incubation with 500 μM H_2O_2 and varying hydrazides concentrations.
[b]K_I and k_{inact} calculated as described in Section 2.2.3.
[c]Preincubation conditions for IC_{50} determinations were 100 nM HRP, 100 μM H_2O_2, and 10^{-2}-10^5 μM hydrazide in 100 mM sodium phosphate, pH 7.0, for 1 min at 25°C. IC_{50} calculated as described in Section 2.2.4. IC_{50} values are the mean ± standard deviation (S.D.) of at least three experiments.
[d]K_I/K_d calculated using K_d values from Table 3.2.
[e]Partition ratio, K_d, K_I and k_{inact} could not be determined for 3-OH-2-NZH due to its low solubility.

The plots deviate from a straight line at high [hydrazide]/[HRP] ratios due to substrate or product protection (*154*). The lowest partition ratio was that of 2-NZH at 110. The other hydrazides exhibit partition ratios generally ~10-50-fold higher, with the exception of 2-OH-BZH, 2-Cl-BZH and 2-NO_2-BZH, for which the partition ratios are 2-3 orders of magnitude larger than 2-NZH.

IC_{50} values were also determined for the inhibition of HRP by the hydrazides (Table 4.1). The IC_{50} is the concentration of inhibitor required for 50% inhibition. IC_{50} plots of BZH, 2-NZH, and 2-NH_2-BZH are shown in Figure 4.6.

The reactivity of aromatic donor compounds can be related to the electron-donating or -withdrawing capacity of their ring-substituents (*157*). The quantitative relationship between the reactivity of an aromatic side-chain and the nature of other ring substituents is indicated by the Hammett substituent constant (σ) where a positive or negative σ is indicative of an electron-withdrawing or donating substituent, respectively (*239*). The IC_{50} values for HRP inactivation by *meta*- and *para*-substituted hydrazides (Figure 4.7) show a slight correlation with σ constants. The effect of the electronic character of the ring substituents on HRP inactivation is represented by ρ, the slope of the plot in Figure 4.7, and $\rho = 14$ for HRP, indicating that the ability of hydrazides to inhibit HRP is only slightly increased by the presence of electron donating ring substituents.

4.2.2. Mechanism of HRP inactivation by BZH

4.2.2.1. Oxidation of BZH in the absence of H_2O_2.

In the absence of H_2O_2 at pH 7.0 and above, HRP(Fe^{III}) underwent spectral changes in both the Soret and visible regions in the presence of BZH. Figure 4.8 shows the partial formation of a low-spin heme species at pH 10.0 within 30 s of BZH addition,

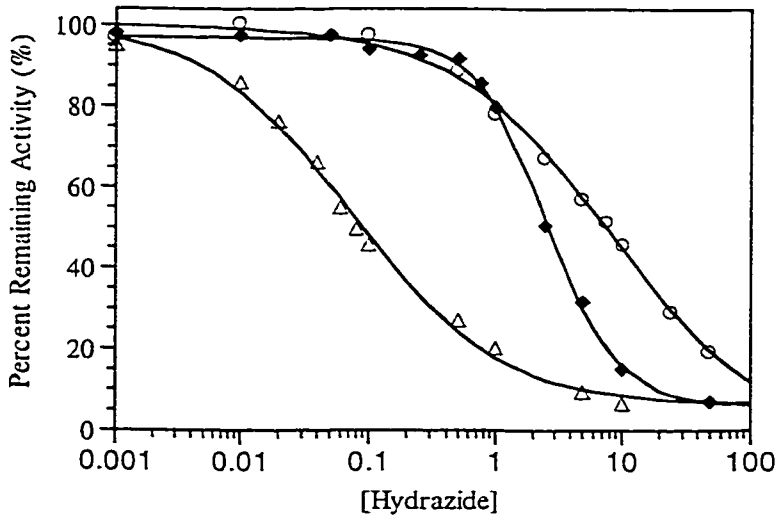

Figure 4.6. IC_{50} titrations for inhibition of HRP by 2-NZH, BZH, and 2-NH_2-BZH. 100 nM HRP was preincubated in 100 mM sodium phosphate, pH 7.0, containing 500 μM H_2O_2 and 0.001 - 50 mM of 2-NZH (Δ), BZH (O) or 2-NH_2-BZH (♦) for 1 min prior to assaying of activity in 100 mM sodium phosphate containing 500 μM H_2O_2 and 5 mM guaiacol, as described in Section 2.2.3. Titration curves were fit to equation 2.9 as described in Section 2.2.4.

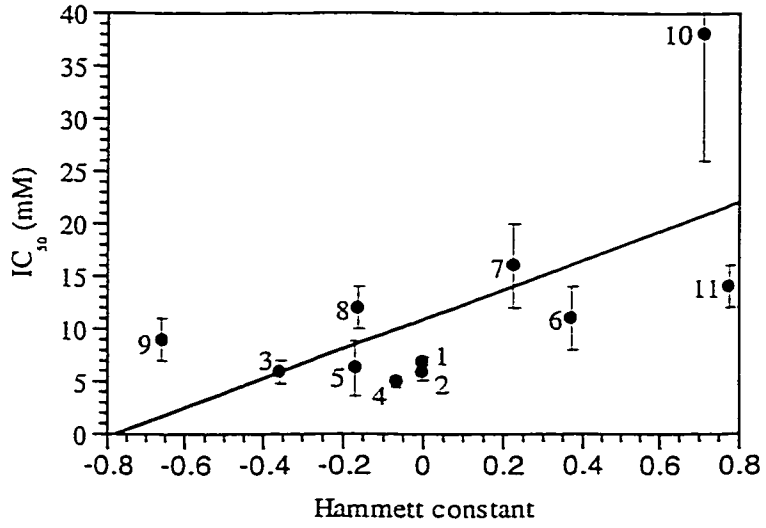

Figure 4.7. Plot of Hammett constants versus IC_{50} values for inactivation of HRP by hydrazides. Hammett substituent constants are from Jaffe, 1953 (*239*). IC_{50} values are the means ±S.D. of at least three experiments (**1**, BZH; **2**, 3-OH-BZH; **3**, 4-OH-BZH; **4**, 3-CH_3-BZH; **5**, 4-CH_3-BZH; **6**, 3-Cl-BZH; **7**, 4-BZH, **8**, 3-NH_2-BZH; **9**, 4-NH_2-BZH; **10**, 3-NO_2-BZH; **11**, 4-NO_2-BZH).

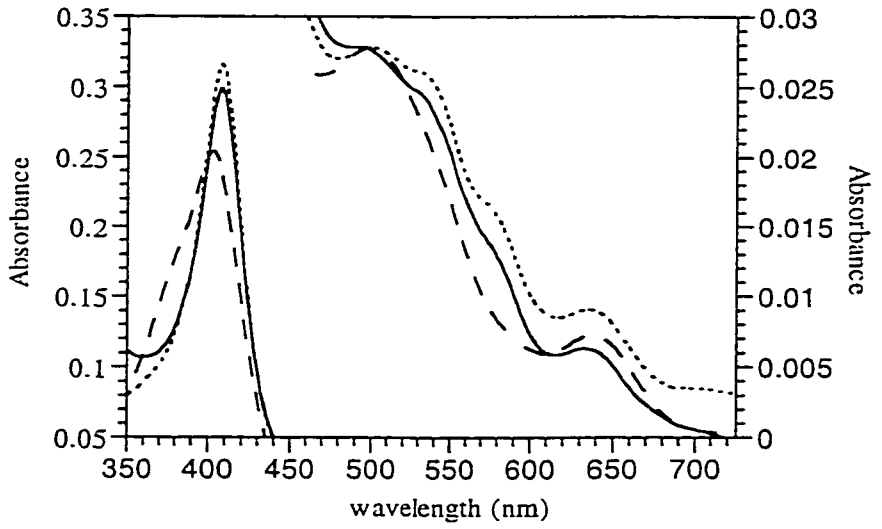

Figure 4.8. Effect of BZH on the absorption spectrum of HRP(Fe^{III}) at pH 10.0.

Following a 15-min aerobic equilibration of 2.5 μM HRP in 100 mM CAPS, pH 10.0, the t = 0 min (- - -) spectra was acquired, 25 mM BZH was added, and spectra [shown at t = 0.5 (····) and 30 min (—)] were recorded over 30 min, as described in Section 2.2.2.

as evidenced by the presence of bands at 543 and 577 nm in the visible region of the HRP spectrum. The low-spin heme slowly decayed back to the high-spin HRP-BZH complex (Figure 4.8). Addition of BZH to HRP solutions under anaerobic conditions did not result in any formation of low-spin heme (data not shown).

The peaks at 543 and 577 nm, in addition to a Soret shift from 402 to 408 nm in the presence of BZH (Figure 4.8), indicate that some HRP Compound III (Fe^{II}-O_2) is formed at pH 10.0 (*240*). Two possible mechanisms for the role of BZH in Compound III formation are presented in Figure 4.9. Mechanism 1 involves the generation of $O_2^{-\bullet}$ by abstraction of an electron from the BZH^- anion by O_2 followed by binding of $O_2^{-\bullet}$ to HRP(Fe^{III}) to generate compound III. In mechanism 2 direct electron transfer from the BZH^- anion to HRP(Fe^{III}) yields HRP(Fe^{II}) which then binds O_2 to generate compound III.

Since HRP(Fe^{II}) is a postulated intermediate in mechanism 2, CO was used to trap any Fe^{II} formed. Figure 4.10 shows that ~50% of HRP is trapped as the Fe^{II}-CO adduct after 10 min at pH 10.0 in the presence of BZH. Higher percentages were trapped with increasing pH (data not shown), suggesting that it is the BZH^- rather than the neutral form of BZH [pK_a = 12.5, (*63*)] that donates an electron to HRP(Fe^{III}).

Mechanism 1 predicts O_2 consumption by BZH^- in the absence of HRP, whereas mechanism 2 predicts that O_2 consumption requires the presence of HRP. Hence, O_2 consumption was monitored directly using a Clark electrode (Section 2.2.6). In the presence of both HRP and BZH, O_2 consumption was observed to increase with increasing pH (Figure 4.11), while no O_2 consumption was observed over the pH range 7 - 12 in the absence of HRP (pH 12.0 data shown in Figure 4.11). Therefore, both the CO

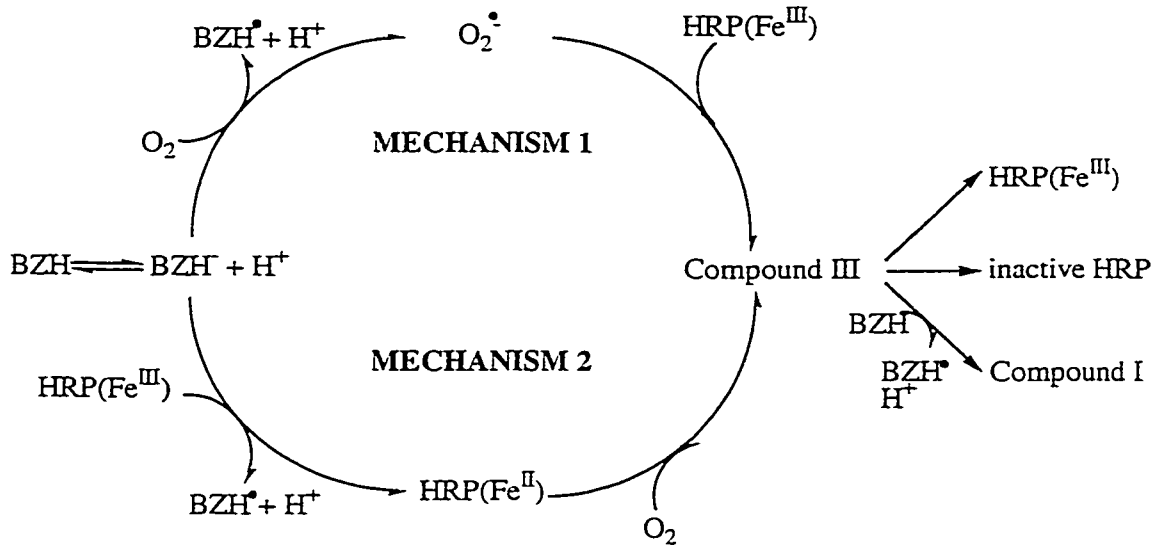

Figure 4.9. Possible mechanisms for the role of BZH^- in HRP Compound III formation in the absence of added H_2O_2.

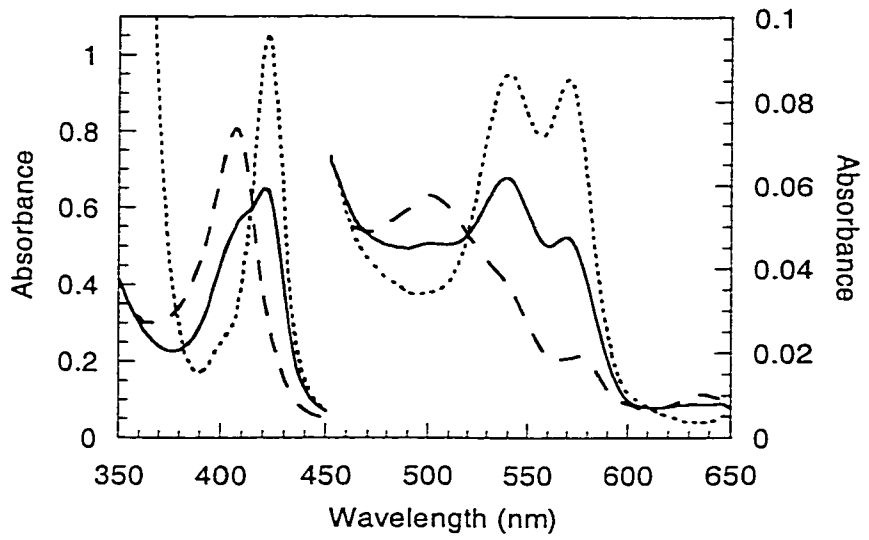

Figure 4.10. CO-trapping of HRP(Fe^{II}) in the presence of 25 mM BZH at pH 10.0. Solutions of 5.5 μM HRP(Fe^{III}) and 1 M BZH were made anaerobic and CO-saturated by flushing with CO for 30 min in 100 mM CAPS, pH 10.0, as described in Section 2.2.5. Spectra were recorded immediately following addition of 25 mM BZH to the HRP solution (- - -) and after 10 min (—). These are compared to the spectrum of the anaerobic HRP(Fe^{II})-CO adduct (····) prepared by the addition of 10 μL of a saturated dithionite solution to a solution of 5.5 μM HRP saturated with CO.

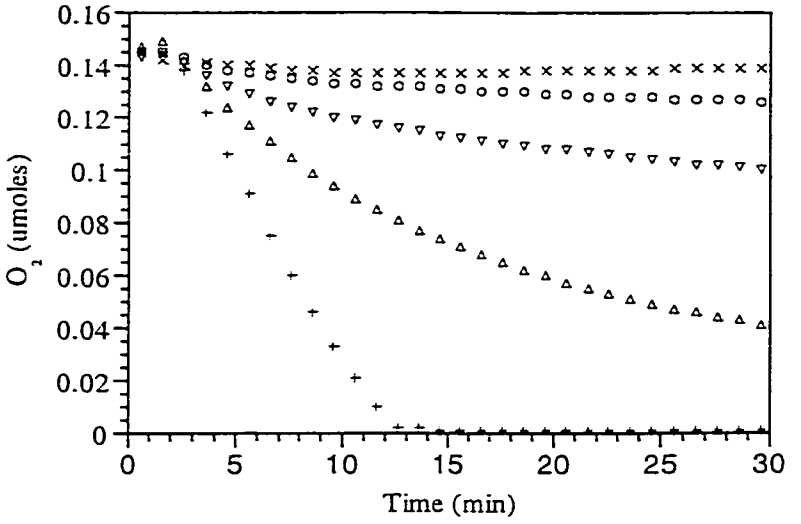

Figure 4.11. Effect of HRP and pH on O_2 consumption in BZH-containing solutions. Solutions of 2.5 μM HRP in 100 mM sodium phosphate pH 7.0 (O), 8.0 (∇), 12.0 (+), 100 mM CAPS pH 10.0 (Δ), and 100 mM sodium phosphate, pH 12.0, only (X) were added to the electrochemical cell (600 μL) and measurement of O_2 was commenced. At t = 1 min 25 mM BZH was added to the cell. The O_2 concentration was measured as described in Section 2.2.6 using a Clark oxygen electrode over the course of 30 min.

trapping and O_2 consumption results support the direct reduction of HRP(Fe^{III}) to HRP(Fe^{II}) by BZH^- followed by O_2 binding to the ferrous enzyme to form Compound III (mechanism 2). The absence of measurable BZH autooxidation in a heme-free medium (pH 12.0 data in Figure 4.11), in combination with the low levels of BZH oxidation at neutral pH (pH 7.0 data in Figure 4.11) in the presence of HRP, indicate that autooxidation may not be a serious problem in the development of hydrazides as potential therapeutics. This is in contrast to phenylhydrazine, which has been shown to undergo autooxidation and heme-induced oxidation at neutral pH (*236*).

At pH 7.0 and above, the presence of 25 mM BZH was observed to result in a Soret shift that was more pronounced than in the presence of 2.5 mM BZH (data not shown). This, in combination with the observed pH-dependence, demonstrates that Compound III formation is increased by conditions that increased the availability of the singly ionized form of BZH [pK_a = 12.5; (*63*)]. The increasingly negative reduction potential of HRP(Fe^{III})→HRP(Fe^{II}) with increasing pH (*241*), predicts that if neutral BZH were the reductant, Compound III formation would be expected to decrease with increasing pH.

4.2.2.2. Mechanism of HRP inactivation by BZH and H_2O_2

The results of Section 4.2.1 (kinetics of HRP inactivation by hydrazides) suggest that BZH is a mechanism-based inhibitor of HRP and that modification of the aromatic group results in compounds with IC_{50} values in the μM range (2-NH_2-BZH and 2-NZH, Table 4.1). These findings, in combination with the lack of autooxidation of BZH (Section 4.2.2.1), indicate that hydrazides are a promising family of compounds for development as specific peroxidase inhibitors. Therefore, the mechanism of HRP

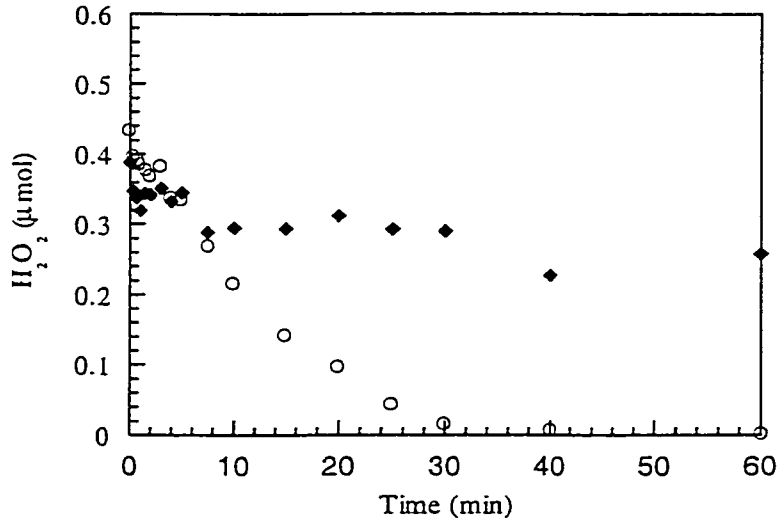

Figure 4.12. Effect of BZH on H_2O_2 consumption by HRP. A 600-µM solution of 2.5 µM HRP was incubated in 100 mM sodium phosphate, pH 7.0, containing 1 mM H_2O_2 in the presence (♦) and absence (O) of 25 mM BZH. Aliquots removed for H_2O_2 determination over the course of 1 h. H_2O_2 concentration was measured using the PerOXoquont kit (Pierce), as described in Section 2.2.7.

inactivation by BZH and H_2O_2 was further investigated to determine the nature of the HRP-activated BZH species (criterion 6).

HRP is capable of catalactic turnover, that is using H_2O_2 as both an oxidizing and reducing substrate to produce O_2 and H_2O, in the absence of its normal reducing substrates (*242*). HRP (2.5 μM) was incubated with 1 mM H_2O_2 in 100 mM sodium phosphate and over the course of 30 min the H_2O_2 concentration decreased to less than 10 μM. This demonstrates that HRP is able to disproportionate at least 400 molar equivalents of H_2O_2 (Figure 4.12) via catalactic H_2O_2 turnover (reactions 4.1, 4.2 and 4.3), to produce ~1 molecule of O_2 (figure 4.13B) for every 2 molecules of H_2O_2 consumed (Figure 4.12).

$$POX^{III} + H_2O_2 \rightarrow \text{Compound I} + H_2O \qquad \text{(reaction 4.1)}$$

$$\text{Compound I} + H_2O_2 \rightarrow \text{Compound II} + \bullet OOH \qquad \text{(reaction 4.2)}$$

$$\text{Compound II} + \bullet OOH \rightarrow POX^{III} + O_2 + H_2O \qquad \text{(reaction 4.3)}$$

The catalactic turnover of H_2O_2 by HRP is accompanied by loss of Soret absorption, formation and decay of Compound III (Soret at 417 nm and visible bands at 543 and 577 nm), and growth of a previously reported band at 670 nm (*243*) (Figure 4.13A). Intensity at 580 nm (Compound III) and 670 nm, as well as O_2 consumption were plotted versus time to facilitate the interpretation of the data (Figure 4.13B). The 670-nm intensity was observed to plateau by 30 min (Figure 4.13B), and H_2O_2 consumption (Figure 4.12) and production of O_2 (Figure 4.13B) followed a similar pattern. Compound III (580 nm) was observed to peak at ~3.5 min and decay with time at times greater than this (Figure 4.13B).

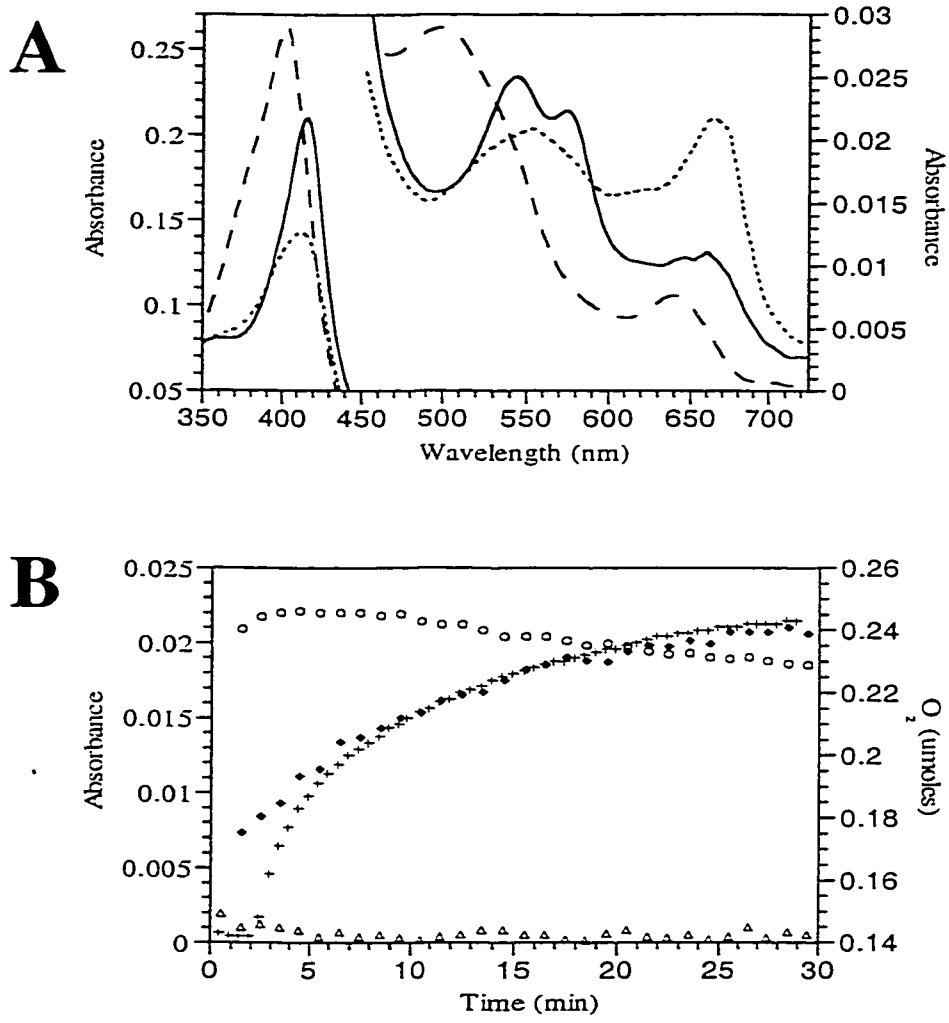

Figure 4.13. Catalactic activity, HRP Compound III and p-670 formation in the presence of excess H_2O_2. HRP (2.5 μM) solutions were equilibrated in 100 mM sodium phosphate, pH 7.0, for 15 min prior to addition of 1 mM H_2O_2. Recording of absorption spectra commenced at 30 s prior to H_2O_2 addition. (**A**) Spectra are shown at t = 0 min (- - -), 3.5 min (——) and 30 min (····). (**B**) The absorption maxima plotted versus time correspond to those of Compound III (O, 580 nm), the 670-nm species (♦, 670 nm) and isoporphyrin (Δ, 820 nm) (see text). O_2 concentration (+) was monitored using a Clark electrode, as described in Section 2.2.6 starting at 2 min prior to H_2O_2 addition.

In the presence of both 1 mM H_2O_2 (400 molar equivalents) and 25 mM BZH, O_2 was consumed (Figure 4.14) and the H_2O_2 consumption was only ~15% that observed in the absence of BZH (Figure 4.12). The HRP species with 670 nm absorption (p-670) formed more quickly in the presence of BZH and was observed to plateau in ~ 10 min (Figure 4.14). A second band of low intensity at ~ 820 nm was formed within the initial mixing time and decayed over 30 min (Figure 4.14). A similar band at ~820 nm was found to result from isoporphyrin, the cation radical generated on attack of heme by the phenylhydrazine-generated radical, when HRP was incubated with H_2O_2 and phenylhydrazine (*223*). The lack of absorption at 820 nm in the absence of BZH (Figure 4.13B), supports the conclusion that this band is due to isoporphyrin formation in the presence of BZH.

Insight into the mechanism of HRP inactivation by BZH and H_2O_2 can be obtained from the stoichiometry of inactivation. Since each molecule of H_2O_2 contains two oxidizing equivalents, if only a 1-electron oxidation of BZH is required for inactivation of HRP, a 2:1 ratio of BZH/H_2O_2 would be expected to be optimal. The partition ratio of BZH (1100, Table 4.1) indicates the number of BZH molecules oxidized by HRP per inactivation event. Comparison of the partition ratios for BZH and H_2O_2 provides an estimate of the ratio of BZH/H_2O_2 required for HRP inactivation. Therefore, the partition ratio for H_2O_2 in HRP inactivation by BZH and H_2O_2 was determined as described in Section 4.2.1.2 (Comparison of HRP inactivation by a series of hydrazides), but in this case the BZH concentration was kept fixed at 1 mM while the H_2O_2/HRP ratio was varied. A value of 2440 was obtained, which is approximately 2-fold higher than the partition ratio for BZH, indicating that a 1:2 ratio of

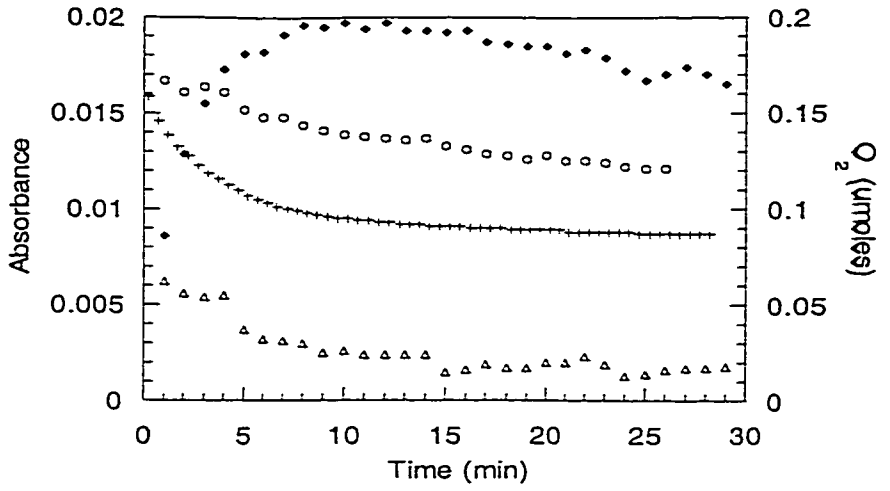

Figure 4.14. Catalactic activity, HRP Compound III and p-670 formation in the presence of excess H_2O_2 and BZH. HRP (2.5 μM) was equilibrated in 100 mM sodium phosphate, pH 7.0, for 15 min prior to addition of 1 mM H_2O_2 and 25 mM BZH (t = 0). O_2 concentration (+) was monitored using a Clark electrode, as described in Section 2.2.6. The absorption maxima plotted correspond to those of Compound III (O, 580 nm), p-670 (♦, 670 nm), and isoporphyrin (Δ, 820 nm) (see text).

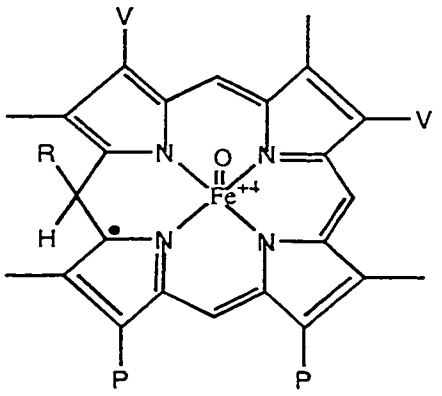

Figure 4.15 Structure of isoporphyrin proposed by Ator et al. (*223*). Vinyl and propionic groups are represented by V and P, respectively.

BZH/H_2O_2 is required. This suggests that a 3- or 4-electron oxidization is required to convert BZH to the species that inactivates HRP. Similarly, Ator and Ortiz de Montellano (*188*) determined that 2 molecules of H_2O_2 per molecule of PH were required for HRP inactivation.

Despite the similarity between the results of this study and those of Ator et al. (*188*), the curvature of the partition ratio plots (Figure 4.5) casts doubt on the accuracy of the partition ratios and the 1:2 ratio of BZH/H_2O_2 thus obtained. Therefore, the effect of BZH/H_2O_2 molar ratios of 2:1, 1:1 and 1:2 on HRP inactivation were investigated. The effects of 2:1, 1:1, and 1:2 PH/H_2O_2 were also determined for comparison. BZH and H_2O_2 were added to 2.5-mL solutions of 20 μM HRP in a series of aliquots such that the incremental concentrations of H_2O_2 and inhibitor did not exceed 2 mM to prevent damage to the enzyme (Figure 4.16). Inactivation by 1:2 BZH/H_2O_2 was most rapid, requiring only two increments of 1 mM BZH/2 mM H_2O_2 for complete inactivation. 1:1 BZH/H_2O_2 required three increments of 1 mM BZH/1 mM H_2O_2. In contrast, HRP inactivation by 2:1 BZH/ H_2O_2 was inefficient, requiring six increments of 2 mM BZH/1 mM H_2O_2 for complete inactivation. A similar trend was observed for HRP inactivation by PH (Figure 4.17). The 1:2 PH/ H_2O_2 ratio was found to be the most efficient for HRP inactivation, requiring only three increments of 1 mM PH/2 mM H_2O_2. In contrast, both 1:1 and 2:1 PH/ H_2O_2 were not completely inactivated even in the presence of concentrations of over 10 mM PH and over 5 mM H_2O_2. Incomplete inactivation of HRP by PH and H_2O_2 was also observed by Ator et al. (*188*) and attributed to product inhibition. Following inactivation the BZH- and PH-treated HRP samples were used for

heme extraction to identify possible heme adducts, such as those observed for PH-inactivated HRP by Ator et al. (*188*).

Criterion 6 of Silverman's list (*154*) of the 7 criteria generally observed for mechanism-based inhibitors states that a mechanism-based inhibitor must be activated by the target enzyme. The increased rate of HRP inactivation observed with increasing H_2O_2:BZH ratios (Figure 4.16) supports the requirement for BZH oxidation by HRP Compound I or II. However, isolation of BZH-modified HRP is required for proof of BZH activation. Ator et al. (*188*) observed the formation of heme adducts in PH-treated HRP. Therefore, heme was extracted from HRP that had been completely inactivated by 2:1, 1:1 and 1:2 BZH/H_2O_2 (as described in the legend of Figure 4.16) according to the protocol of Ator et al. (*188*). Heme extracts were analyzed by reversed-phase HPLC, monitored at 400 nm (Figure 4.18), and spectra at selected time points for 1:1 BZH/ H_2O_2 are shown in Figure 4.19. Peak **1** (2.1 min, Figure 4.18) was identified as p-670 by examination of its UV-VIS spectrum (Figure 4.19A), which has a strong absorbance centered at 680 nm. An *m/z* of 583 was determined by ESI-MS for this species, identifying it as biliverdin, an open ring porphyrin lacking iron (Figure 4.20). p-670 (peak **1**) was observed to increase with increasing H_2O_2:BZH ratios (Figure 4.18). However, since the Soret of p-670 is blue-shifted to 365 nm, its concentration relative to that of unmodified heme (peak **4**) is underestimated by the 400-nm HPLC traces shown in Figure 4.18. Peaks **2** (2.5 min), **4** (3.6 min) and **5** (5.1 min) of Figure 4.18 have similar Soret and visible absorption bands (Figure 4.19B, C, D) and *m/z* values of 632, 616 and 720, respectively, identifying them as hydroxylheme, heme, and benzoylheme

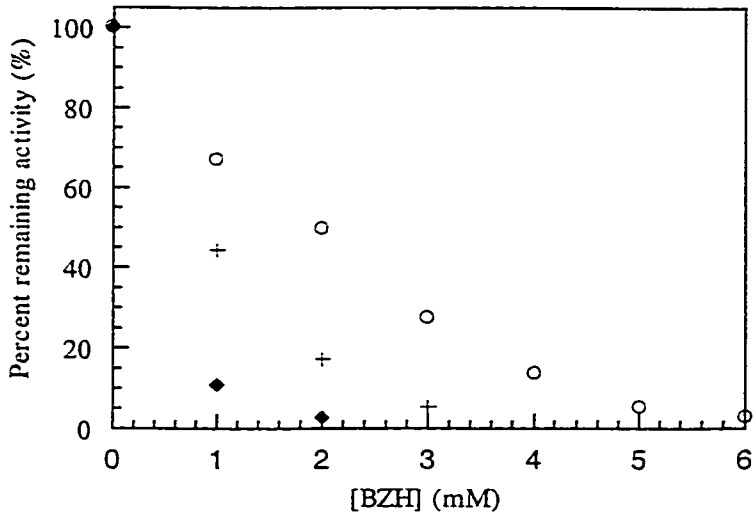

Figure 4.16. Effect of BZH/H_2O_2 ratio on inactivation of HRP. To a solution of 20 μM HRP in 100 mM sodium phosphate, pH 7.0, a series of BZH/H_2O_2 aliquots were added to increment their concentration as follows: 1 mM BZH/0.5 mM H_2O_2 (O, 2:1), 1 mM BZH/1 mM H_2O_2 (Δ, 1:1), or 1 mM BZH/2 mM H_2O_2 (♦, 1:2). Activity was measured 2 min following aliquot addition according to the method described in Section 2.2.3 and plotted versus total BZH concentration.

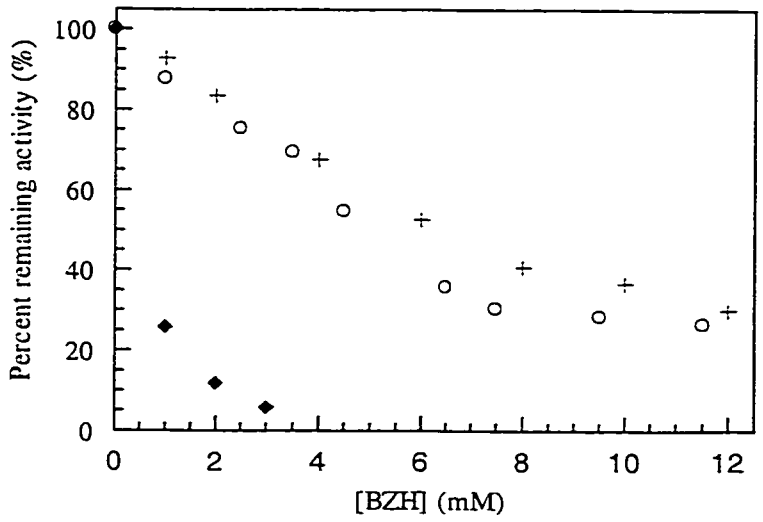

Figure 4.17. Effect of PH/H_2O_2 ratio on inactivation of HRP. To a solution of 20 μM HRP in 100 mM sodium phosphate, pH 7.0, a series of PH/H_2O_2 aliquots were added to increment their concentration as follows: 1 mM PH/0.5 mM H_2O_2 (O, 2:1), 1 mM PH/1 mM H_2O_2 (Δ, 1:1), or 1 mM PH/2 mM H_2O_2 (◆, 1:2). Activity was measured 2 min following aliquot addition according to the method described in Section 2.2.3 and plotted versus total PH concentration.

Figure 4.18. Reversed-phase HPLC chromatograms of the heme species extracted from BZH-treated HRP. A 2.5-mL solution containing 20 μM HRP in 100 mM sodium phosphate, pH 7.0, was inactivated by addition of successive aliquots of (**A**) 1 mM BZH/1 mM H_2O_2 (1:1), (**B**) 1 mM BZH/0.5 mM H_2O_2 (2:1), or (**C**) 1 mM BZH/2 mM H_2O_2 (1:2) at 2 min intervals until HRP was completely inactivated as described in Figure 4.16. (**D**) As a control, a 2.5-mL of 20 μM HRP in 100 mM sodium phosphate, pH 7.0, was incubated for 12 min at room temperature prior to heme extraction. Following their complete inactivation, the HRP solutions were desalted and the heme extracted according to the procedure described in Section 2.2.8. The extracted heme was dissolved in 250 μL of HPLC solvent A (68:32:10 methanol/water/acetic acid), and 200 μL was separated by isocratic reversed-phase HPLC on a Novapak C18 (3.9x150 mm) column at a flow rate of 1 mL/min in HPLC solvent

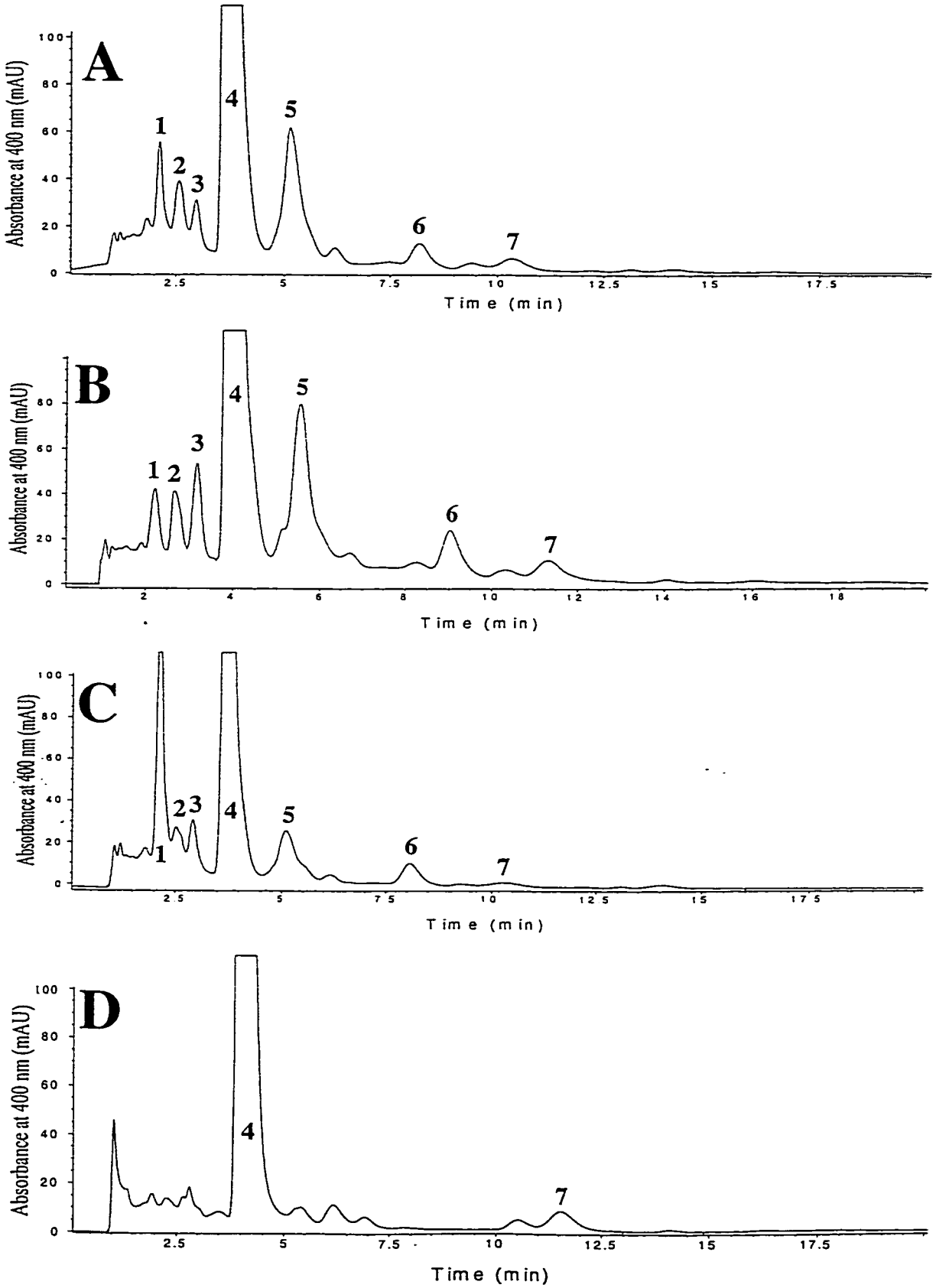
A
B
C
D
Absorbance at 400 nm (mAU)
Time (min)
1
2
3
4
5
6
7

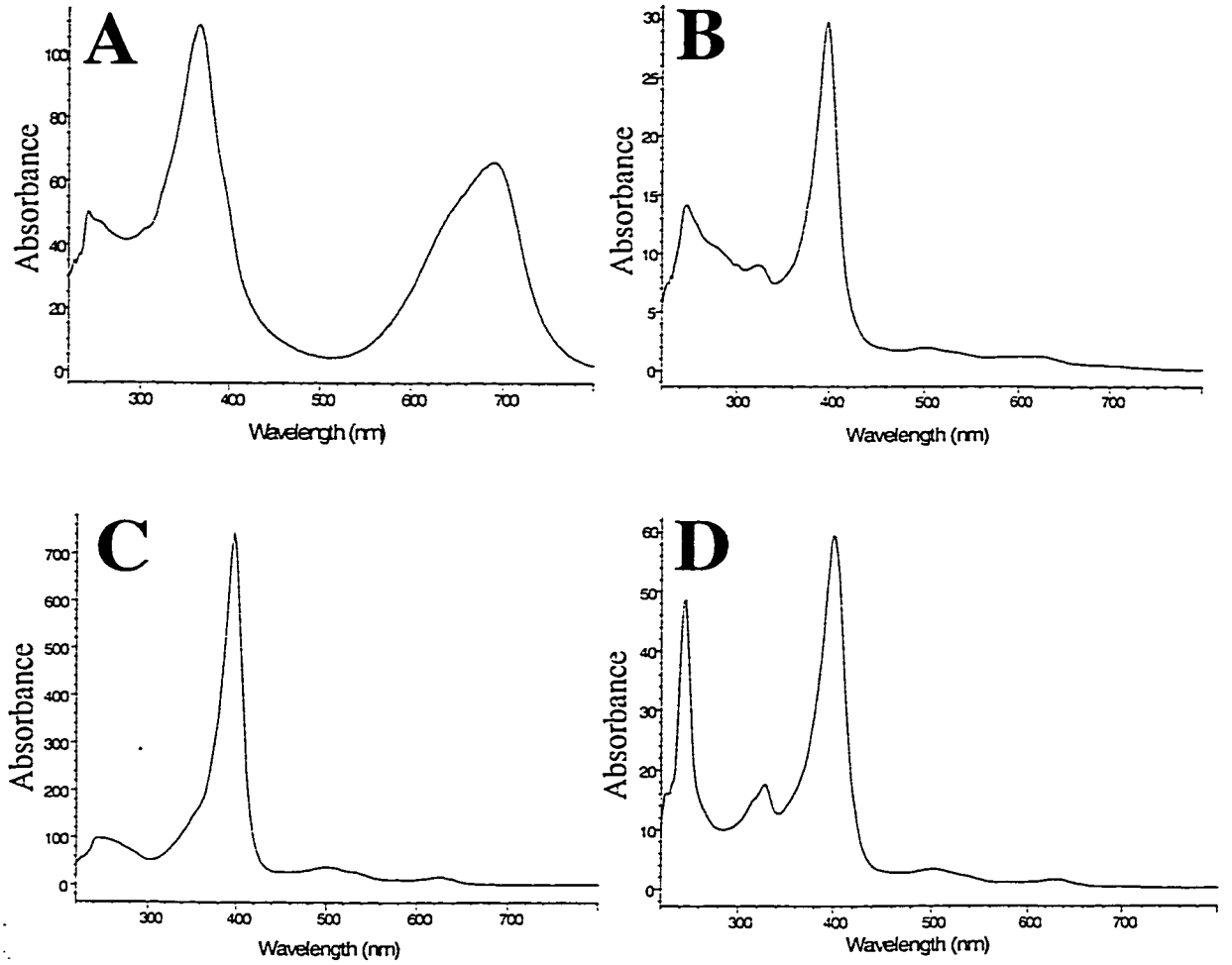

Figure 4.19 Absorbance spectra of BZH-inactivated HRP heme species. Absorbance spectra for peaks **1**, **2**, **4** and **5** of the 400-nm HPLC trace shown in Figure 4.18A. Peaks at 2.1 (**1**, spectrum **B**), 2.6 (**2**, spectrum **C**), 3.6 (**4**, spectrum **D**), 5.1 (**5**, spectrum **E**), min are assigned to biliverdin (p-670), hydroxyl and benzoyl heme adducts, respectively, based on their molecular weights. Peaks at 2.9, 8.3, and 11.5 min were not identified.

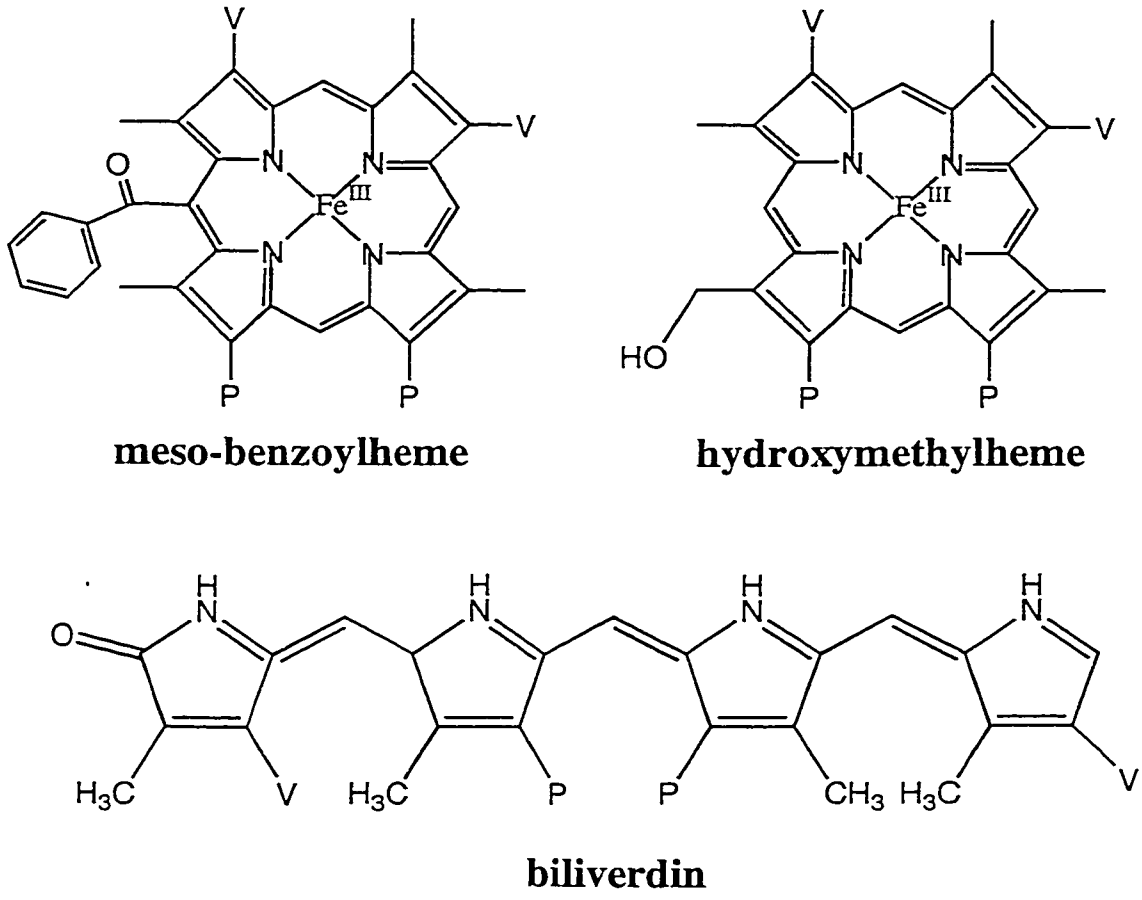

Figure 4.20. Proposed structures of the heme species extracted from BZH-treated HRP.

(Figure 4.20). In contrast to p-670, hydroxyl and benzoyl heme adduct formation was observed to be maximal with a 2:1 ratio of BZH/H_2O_2. The peaks at 2.9 (**3**), 8.3 (**6**) and 11.5 (**7**) min in Figure 4.18 exhibit absorption spectra similar to heme (Figure 4.19B & C), but could not be identified by ESI-MS. Mainly unmodified heme (peak **4**) was extracted from the control HRP sample (Figure 4.18D). Peak **7** was also observed in the control extract (Figure 4.18D), suggesting that it is an impurity.

As a control, heme was extracted from HRP incubated in the presence of PH and H_2O_2 (in 1:2 and 2:1 ratios). Peaks **2**, **4**, and **5** of Figure 4.21 were identified as hydroxylheme (m/z = 632), heme (m/z = 616), and phenylheme (m/z = 692) in agreement with a study by Ator et al. (*188*) which identified these adducts as 8-hydroxymethylheme and δ-meso-phenylheme. As was observed for BZH, the ratio of PH to H_2O_2 was observed to have an effect on heme modification. HRP completely inactivated by 1:2 PH/H_2O_2 showed >50% heme modification in comparison with <50% for HRP completely inactivated by a 2:1 ratio of PH/H_2O_2 (Figure 4.21).

4.3. Discussion

4.3.1. Mechanism of inactivation of HRP by BZH

4.3.1.1. Nonspecific oxidation and autooxidation of BZH

One of the requirements in the development of hydrazides as a class of useful peroxidase inhibitors is that the oxidation step(s), which result in activation of the hydrazide, should occur at the active site of the target peroxidase. Autooxidation and oxidation under nonturnover conditions should be minimal to prevent the generation of reactive radical species capable of modifying other proteins, DNA or lipids *in vivo*. The lack of O_2 consumption in BZH solutions at pH 7.0 and above (pH 12.0 data shown in

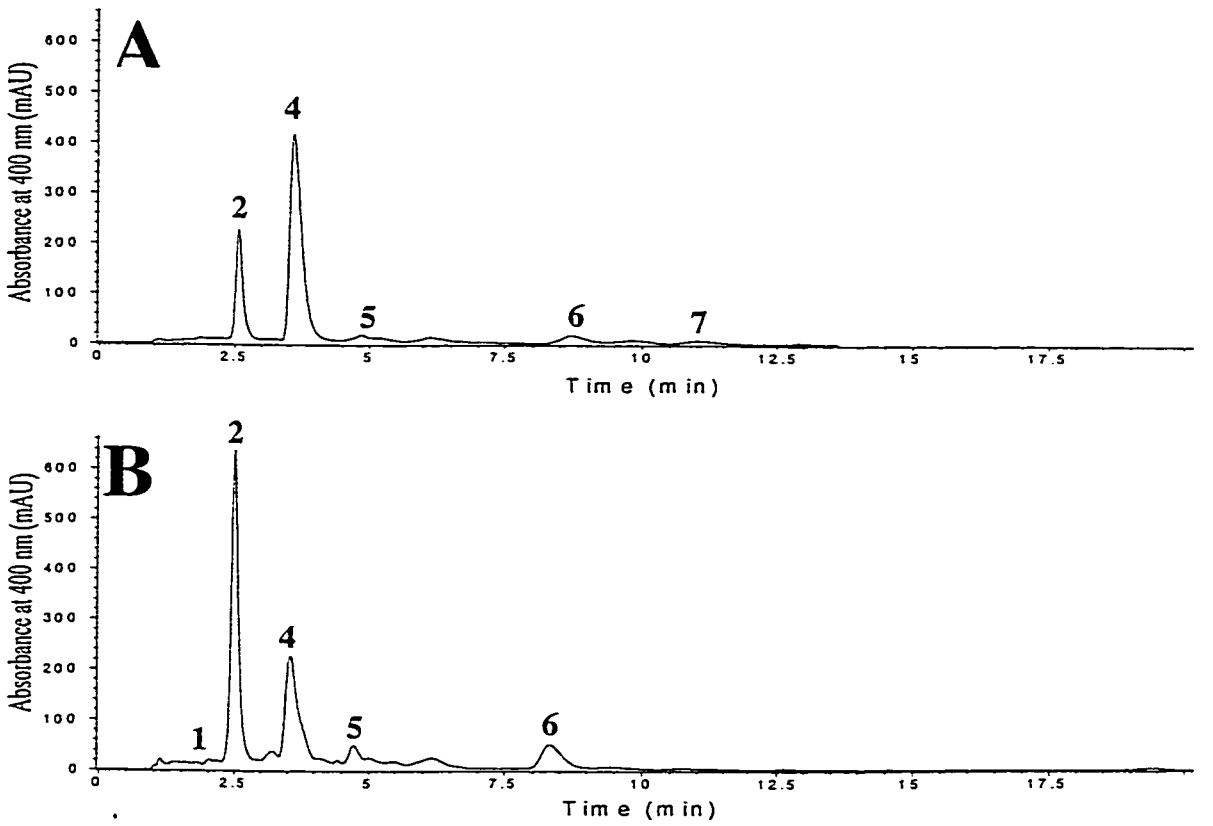

Figure 4.21. Reversed-phase HPLC chromatogram of the heme extracted from PH-treated HRP. A 2.5-mL solution containing 20 μM HRP in 100 mM sodium phosphate, pH 7.0, was inactivated by addition of successive aliquots of (**A**) 2 mM PH/1 mM H_2O_2 (2:1) and (**B**) 1 mM BZH/2 mM H_2O_2 (1:2) at 2 min intervals until HRP was completely inactivated as described in Figure 4.17. Following their complete inactivation, the HRP solutions were desalted and the heme extracted according to the procedure described in Section 2.2.8. The extracted heme was dissolved in 250 μL of HPLC solvent A (68:32:10 methanol/water/acetic acid), and 200 μL was separated by isocratic reversed-phase HPLC on a Novapak C18 (3.9x150 mm) column at a flow rate of 1 mL/min in HPLC solvent

Figure 4.11) in the absence of HRP indicates that BZH does not undergo significant autooxidation in a heme-free medium. Catalysis of BZH oxidation was investigated in the presence of HRP at pH 7.0 - 12.0. A species with a red-shifted Soret (408 nm) and visible bands at 543 and 577 nm was formed upon addition of BZH to HRP(Fe^{III}) (Figure 4.8), suggesting the partial formation of HRP Compound III (Fe^{II}-O_2) [Soret band at 417 nm and visible bands at 543 and 577 nm (*240*)], via the oxidation of BZH^-. Compound III could be formed by 2 mechanisms: (1) reaction of HRP(Fe^{III}) with $O_2^{-\bullet}$, or (2) reaction of HRP(Fe^{II}) with O_2 (Figure 4.9). Mechanism 2 is supported by both CO-trapping (Figure 4.10) and O_2-consumption (Figure 4.11) results, and the pH and BZH concentration-dependence data (Section 4.2.1.1, oxidation of BZH in the absence of H_2O_2) indicate that it is BZH^- which directly reduces HRP(Fe^{III}) to HRP(Fe^{II}). In spite of the high BZH concentrations (25 mM) used in these experiments only slight O_2 consumption was observed at pH 7.0, where BZH is largely present as the neutral form [pK_a = 12.5, (*63*)]. Therefore, at pH 7.0 and below, BZH undergoes minimal heme catalyzed oxidation in the absence of H_2O_2, and this warrants the further investigation of hydrazides as potential peroxidase inhibitors.

The interaction of HRP(Fe^{III}) with BZH^- and O_2 to produce Compound III and the fate of Compound III in the absence of H_2O_2 are summarized in Figure 4.22. In the absence of reducing substrates, Compound III (Fe^{II}-O_2) can eliminate either $O_2^{-\bullet}$ or O_2 to form HRP(Fe^{II}) or HRP(Fe^{III}), respectively. However, since BZH (or BZH^-) can act as a reducing substrate, Compound III can be returned to HRP(Fe^{III}) via three 1-electron oxidations of BZH with Compound I and Compound II as intermediates and H_2O as a final product. Neither isoporphyrin nor p-670 were observed for the interaction of HRP

and BZH in the absence of H_2O_2. This is likely due to the limiting O_2 concentration (~250 μM O_2 in buffer at 25°C (*244*)), which is only ~100-fold in excess of the HRP concentrations used (2.5 μM) in the spectroscopic experiments. Alternatively, it is possible that only Compound I is capable of further oxidation of $BZH^{\bullet}$. The partition ratio of 1100 determined for BZH (Table 4.1) in the presence of H_2O_2, suggests that the level of BZH turnover in the absence of H_2O_2 would be inadequate to result in significant levels of heme modification and, as shown in Figure 4.8, the majority of the HRP returns to the native HRP(Fe^{III}) form when the O_2 is consumed.

4.3.1.2. Mechanism of HRP inactivation by BZH and H_2O_2

The time-dependence (Figure 4.1A), saturation kinetics (Figure 4.1B), susceptibility to substrate protection (Figure 4.2), and irreversibility (Figure 4.3) of HRP inactivation by BZH and H_2O_2 fulfill criteria 1 - 4 of the 7 (listed in Section 4.2.1, kinetics of HRP inactivation by hydrazides) delineated by Silverman (*154*) for a mechanism-based inhibitor. However, since these criteria may also be met by a very tight-binding reversible inhibitor, they are necessary but, not sufficient to prove that BZH is a mechanism-based inhibitor of HRP. The stoichiometry of inactivation (criterion 5) was not investigated here due to the requirement for labeled BZH. Ator et al. (*188*) observed the incorporation of 2 radiolabeled phenyl moieties per enzyme molecule in PH-treated HRP. One of the phenyl moieties was incorporated at the heme, resulting in the δ-meso-phenylheme adduct, while the other was incorporated into the protein (*188*). The identity of the protein adduct was not determined by Ator et al. (*188*). The incorporation of more than one labeled phenyl moiety suggests that formation of an amino acid adduct. Since it is possible for a mechanism-based inhibitor to have a

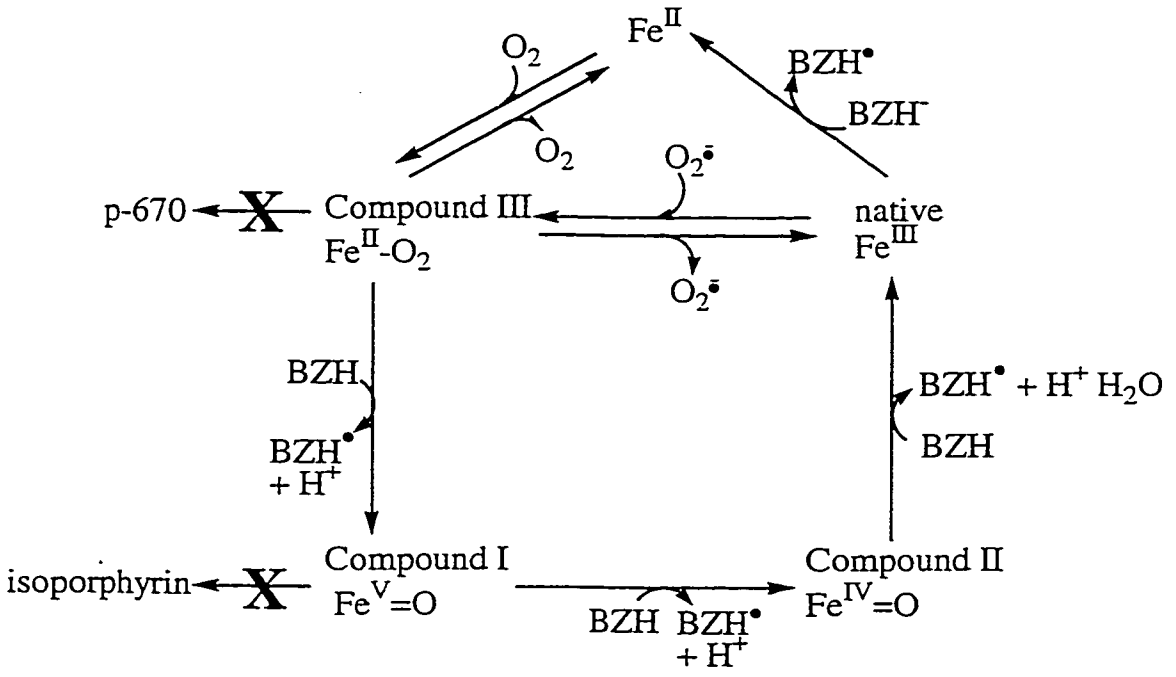

Figure 4.22. Proposed mechanism for O_2 consumption by HRP and BZH in the absence of H_2O_2. Compound III formed by the reduction of HRP(Fe^{III}) by BZH^- followed by reaction with O_2 can be reduced by BZH or (BZH^-) to return to the resting state HRP(Fe^{III}) via Compounds I and II. Alternatively, Compound III can release O_2 or $O_2^{-\bullet}$ to return to HRP(Fe^{II}) or HRP(Fe^{III}), respectively.

partition ratio greater than zero, the 2:1 phenyl/HRP stoichiometry determined by Ator et al. (*188*) does not identify PH, and by inference BZH, as a metabolically-activated rather than a mechanism-based HRP inhibitor.

Of the 7 criteria listed by Silverman [(*154*), Section 4.2.1], the sixth (activation of inhibitor by the target enzyme) and seventh (inactivation occurs prior to release of the activated species) are key in the definition of a mechanism-based inhibitor and are not generally observed for tight-binding, reversible inhibitors. However, the formation of a metabolite that is a tight-binding inhibitor is one example of an exception to these criteria. Activation of BZH by HRP (criterion 6) in the presence of H_2O_2 was demonstrated here by the requirement for H_2O_2 (Figure 4.16) and the isolation of the benzoylheme adduct (Figures 4.18). Although the isolation of the benzoylheme adduct demonstrates that BZH is activated by HRP, and thus satisfies criterion 6, this is not sufficient to distinguish between mechanism-based and metabolically-activated mechanisms for HRP inhibition by BZH. This distinction is addressed by criterion 7, which requires that HRP inactivation occurs prior to release of activated BZH for BZH to be considered as a mechanism-based inhibitor. The results shown in Figure 4.3 demonstrate that there are no long-lived (*i.e.*, $t_{1/2} \geq 1$ h) activated BZH species released from the HRP active site that can inactivate a second molecule of HRP. However, they do not rule out species with half-lives much less than 1 h. Therefore, the results presented here, while not conclusive, support the classification of BZH as a mechanism-based inhibitor of HRP.

One of the main reasons for investigating the mechanism of heme adduct formation in BZH-treated HRP was the identification of any steps in the mechanism that

could provide evidence for or against the classification of BZH as a mechanism-based inhibitor. A second reason was that an understanding of the mechanism is a necessary step in the development of any class of compounds as potential therapeutics. There are two possible mechanisms for the generation of the activated BZH species, the benzoyl radical (**5**, Figure 4.23). In the mechanism proposed by Sinha et al. (*245*) for INH, following a 1-electron oxidation of BZH, diimide (NH=NH) is rapidly eliminated by the $BZH^{\bullet}$ radical (**2**, Figure 4.23) to produce the benzoyl radical (**5**). In the mechanism proposed by Ator et al. (*188*) for PH activation, three 1-electron oxidations are required prior to elimination of N_2 to produce the benzoyl radical (**5**). The consumption of 2 molecules of H_2O_2 per molecule of BZH observed here (Section 4.2.2.2) suggests that benzoyl-radical formation likely occurs via a mechanism similar to that proposed by Ator et al. (*188*) for PH. In this mechanism, one molecule of H_2O_2 generates HRP Compound I which oxidizes BZH to generate the diazene (**3**, Figure 4.23). A second H_2O_2 molecule regenerates Compound I (*188*), which oxidizes the diazene to the diazene radical (**4**, Figure 4.23), from which N_2 is released to produce the benzoyl radical (**5**), the activated form of BZH. This mechanism is supported by the observation that the efficiency of HRP inactivation increases with increasing H_2O_2/BZH ratios (2:1>1:1>>1:2, Figure 4.16).

The diazene (**3**) can be generated by a single 2-electron oxidation or two 1-electron oxidations of BZH. Under aerobic conditions (Figure 4.14), any $BZH^{\bullet}$ (Figure 4.23) released could be scavenged by O_2 to produce superoxide and the diazene (**3**) or other hydroxylated products. Any diazene formed by $BZH^{\bullet}$ oxidation would also have to

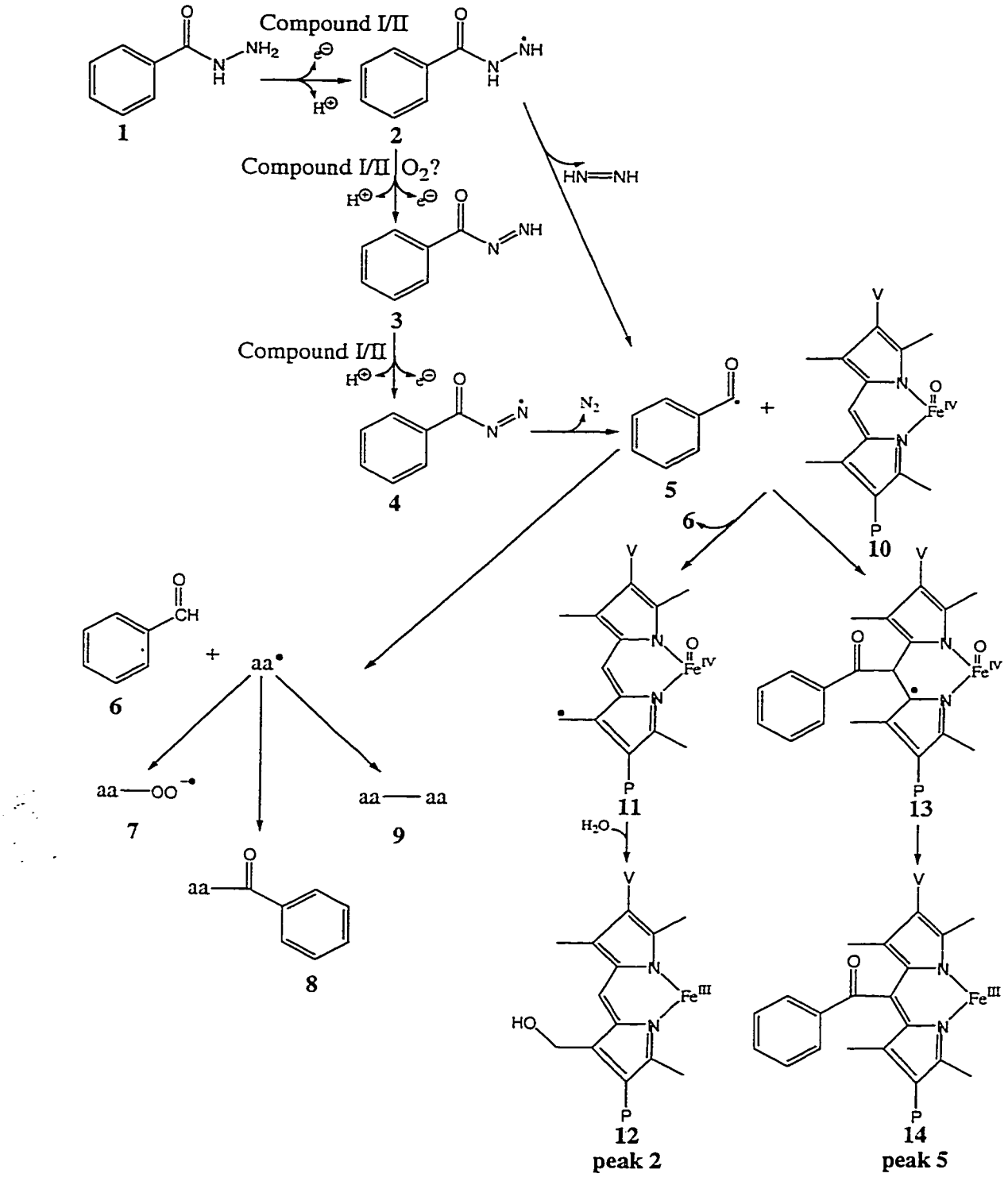

Figure 4.23. Mechanisms of BZH oxidation and attack on HRP.

compete with BZH for the active site of HRP. Figure 4.4 demonstrates that there are no species in solution with $t_{1/2} \geq 1$ h, indicating that the diazene concentration likely does not build up. The diazene (**3**, Figure 4.23) must be further activated by Compound I or II since the benzoyl radical resulting from loss of N_2 from the diazene radical is the activated species that results in HRP inactivation. Therefore, the classification of BZH as a mechanism-based inhibitor depends on whether the diazene radical (**4**, Figure 4.23) is released prior to its decomposition to the benzoyl radical (**5**, Figure 4.23) and N_2. It is unlikely that the benzoyl radical would be released prior to attack at the active site of HRP for two main reasons: (1) scavenging by O_2 under aerobic conditions or attack on other sites on the protein would be rapid and likely prevent the return of the benzoyl radical to the active site, and (2) the benzoyl radical lacks the hydrazide side chain and therefore, is expected to have a much lower binding affinity for HRP than BZH. These observations, in combination with the low partition ratio of 2-NZH (110, Table 4.1), which binds more tightly than the other hydrazides investigated (Table 3.2), suggests that the diazene radical (**4**) and the benzoyl radical (**5**) are not released and rebound prior to HRP inactivation. Therefore, the indirect evidence provided by this study suggests that BZH or the diazene is a mechanism-based inhibitor of HRP.

Ator et al. (*223*) observed the growth and decay of a band at 820 nm during the inactivation of HRP by PH and H_2O_2 and assigned it to the isoporphyrin cation transiently formed following attack of the phenyl radical on Compound II (*223*). The observation of a similar band (820 nm) and its decay during the reaction of HRP with BZH and H_2O_2 (Figure 4.14), in addition to the isolation of δ-meso-benzoylheme (peak **5**, Figure 4.18), suggest that an isoporphyrin intermediate (**13**, Figure 4.23) leads to

arylation (**14**, Figure 4.23) of the heme in the HRP/BZH/H_2O_2 reaction. The lack of transient absorption at 820 nm for HRP in the absence of BZH (Figure 4.13B) provides further evidence that this band is hydrazide-derived.

Rapaport et al. (*246*) proposed a mechanism for the production of both benzoyl and phenyl radicals as products of BZH oxidation in DMSO under alkaline conditions. However, mass spectrometry demonstrated that the benzoylheme adduct ($m/z = 720$) rather than the phenylheme adduct ($m/z = 692$) is formed by BZH-treated HRP. Therefore, CO is not released prior to heme adduct formation and the benzoyl radical is the reactive intermediate responsible for HRP inactivation. This confirms expectations, as the benzoyl radical is more stable than the phenyl radical (T. Scaiano, personal communication).

A hydroxyl heme adduct was also observed in the inactivation of HRP by H_2O_2 and PH [peak **2**, Figure 4.21, (*188*)] although to a much greater extent than observed here for BZH (Figure 4.18). This hydroxylated adduct arises from abstraction of a hydrogen atom from C8 by the phenyl radical to form a methylene radical, which is then oxidized to the cation by internal transfer of the unpaired electron to the porphyrin radical cation of Compound I or the ferryl iron of Compound II followed by addition of water (*188*). Ator et al. (*188*) suggested that 8-hydroxymethyl and δ-meso-phenyl heme adducts were the only heme adducts observed for PH-treated HRP because the rest of the heme is shielded by the protein. This is supported by the HRP crystal structure, which shows that the majority of the heme is not solvent exposed (*11*). Therefore, it is likely that the hydroxyl and benzoyl heme adducts isolated in this study from BZH-treated HRP are 8-hydroxymethylheme and δ-meso-benzoylheme.

The hydroxymethylheme (**12**, Figure 4.23) and benzoylheme (**14**, Figure 4.23) adducts are minor heme products of BZH-inactivated HRP (Figure 4.18). Additionally, little p-670 formation was observed for HRP-inactivation with 2:1 BZH/H_2O_2 (Figure 4.18B). These observations suggest that other pathways play a major role in HRP inactivation by BZH and H_2O_2. Ator et al. (*188*) proposed that in the inactivation of HRP by PH and H_2O_2, modification of the protein may be more extensive than heme modification, and this is likely also true for the BZH reaction. Potential pathways for protein modification are delineated in Figure 4.23. Abstraction of a hydrogen atom from an amino acid residue (aa, Figure 4.23) by the benzoyl radical (**5**, Figure 4.23) produces a protein based radical aa$^{\bullet}$ (Figure 4.23). It is also possible that BZH$^{\bullet}$ (**2**, Figure 4.23) or the diazene radical (**4**, Figure 4.23) could react with an amino acid residue to produce aa$^{\bullet}$ (Figure 4.23) This aa$^{\bullet}$ radical may then react with either O_2, another benzoyl radical, or another protein radical to produce a protein-linked peroxyl radical (**7**, Figure 4.23), a benzoyl-protein adduct (**8**, Figure 4.23) or an intermolecular or intramolecular protein crosslink (**9**, Figure 4.23), respectively. The formation of a phenyl-protein adduct was detected by Ator et al. (*188*), although it was not localized.

Ator et al. (*223*) proposed that in PH-inactivated HRP, the presence of the bulky aromatic group of δ-meso-phenyl heme would block access of reducing substrates to the HRP distal heme cavity, while allowing H_2O_2 to enter (*223*). Compound I thus formed could spontaneously decompose to Compound II which can then react with another molecule of H_2O_2 to produce Compound III (*242*). However, HRP is capable of consuming H_2O_2 via its catalactic activity to return the enzyme to the HRP(Fe^{III}) resting state with a rate constant of $5x10^2$ $M^{-1}s^{-1}$ (*242*). The consumption of H_2O_2 (Figure 4.12)

and production of O_2 (Figure 4.13B) observed here for HRP in the presence of excess H_2O_2 and no reducing substrate are consistent with catalactic activity; for example, 0.6 μmol H_2O_2 was converted to ~0.25 μmol O_2 in 30 min by HRP. However, in the presence of BZH, HRP is converted to Compound III (Figure 4.14), the major decay product of which was observed to be p-670 rather than HRP(Fe^{III}). This suggests that the heme environment of HRP is destabilized by the formation of BZH adducts such that the efficiency of catalactic H_2O_2 turnover is reduced. The destabilization may be a result of BZH-derived adducts formed near the active site or conformational changes in the enzyme as a result of adduct formation.

Ator and Ortiz de Montellano (*188*) also proposed that meso-arylation by PH resulted in an increased sensitivity of the heme to H_2O_2-mediated degradation since only 70% as much heme in PH-treated HRP was recovered as compared to control HRP samples, which contained no H_2O_2 or PH. However, in contrast to BZH-treated HRP, p-670 formation was not observed for PH-treated samples and biliverdin was not isolated by reversed-phase HPLC of their reaction products (Figure 4.21, (*188*)).

4.3.2. Factors controlling inactivation and specificity

The slope (ρ) of the Hammett plot (σ versus IC_{50} values) in Figure 4.7 is 14, indicating that the ability of benzhydrazides to inactivate HRP increases slightly with the electron-donating capacity of the substituents on the aromatic ring. However, with the exception of the IC_{50} for 3-NO_2-BZH, which has a high error (38 ± 12 mM, Table 4.1) because its IC_{50} value is too high to measure reliably, the IC_{50} values of all the *meta*- and *para*-substituted hydrazides vary by only 3-fold or less. If 3-NO_2-BZH is excluded from Figure 4.7, the resulting ρ value is only 5.4. Therefore, the trend is so slight that there is

essentially no effect of the electron-donating capacity of ring substituents on the IC_{50} values of the *meta*- and *para*-substituted hydrazides tested here. IC_{50} reflects both K_I, and k_{inact}, which themselves comprise many rate constants; thus, the effect of the Hammett constants cannot be assigned to a specific step. Plots of σ versus K_I and k_{inact} yielded ρ values of 1.2 and 0.073, respectively (data not shown), indicating that these values are similarly unaffected by the electron-donating capacity of ring substituents.

Bulky and/or negatively charged (*e.g.*, 2-CH_3-BZH and 2-NO_2-BZH) substituents in the *ortho*-position were observed here to result in increased IC_{50} values for inhibition of HRP. This is likely due to the confined active site of HRP (*11*). In contrast, an amino group in this position resulted in a decrease in the IC_{50} value, as compared to BZH, possibly due to the electron-donating capacity of this group.

K_I and k_{inact} values (Scheme 4.1), as well as partition ratios (at 10 min) were determined for HRP inhibition by a series of hydrazides. These data, in addition to the IC_{50} values (Table 4.1), indicate that with the exception of 2-NZH, the hydrazides tested are poor inhibitors of HRP. The ability of 2-NZH to efficiently inactivate HRP is due to its low partition ratio, which in turn is likely due to its ability to bind tightly to HRP (K_d = 5.2 μM, Table 3.2). Low partition ratios are necessary in the design of selective inhibitors so that the production of radicals *in vivo* can be minimized because any radicals released may cause the modification of other proteins, DNA or lipids. An inactivator selective for the target peroxidase with a partition ratio near zero will have the properties of high specificity and low toxicity desired for a drug. An example of a mechanism-based inhibitor currently in use therapeutically that has been shown to have low toxicity is the thyroid peroxidase inhibitor propylthiouracil (*247*).

Assuming that the diazene is the species ultimately activated by HRP, Scheme 4.2 is proposed:

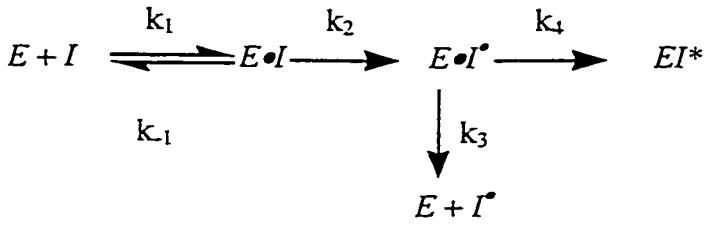

(Scheme 4.2)

Rapid binding of the diazene, *I*, to the H_2O_2-oxidized catalytic intermediates (Compound I or II) of HRP, followed by 1-electron oxidation of *I* and release of N_2 to give a radical species, $I^{\bullet}$, which attacks the porphyrin ring or the protein to form $E{\bullet}I^*$ or is released to the solvent.

The observed K_I and k_{inact} (Scheme 4.1) can be expressed in terms of the rate constants for the individual steps in Scheme 4.2 as follows (*154*):

$$k_{inact} = \left(\frac{k_2 k_4}{k_2 + k_3 + k_4}\right) \qquad \text{(eq. 4.1)}$$

$$K_I = \left(\frac{k_{-1} + k_2}{k_1}\right)\left(\frac{k_3 + k_4}{k_2 + k_3 + k_4}\right) \qquad \text{(eq. 4.2)}$$

$$K_d = \frac{k_{-1}}{k_1} \qquad \text{(eq. 4.3)}$$

If formation of the enzyme-inhibitor complex ($E{\bullet}I$) is rapid then the rate of enzyme inactivation can be expected to show saturation with increasing inhibitor concentration as the enzyme is converted completely to the $E{\bullet}I$ form (*154*), as was observed for BZH in Figure 4.1. Since the hydrazide partition ratios (k_3/k_4) are much greater than zero this indicates that k_3 (rate of $I^{\bullet}$ release) exceeds k_4 (rate of HRP

inactivation). Comparison of K_I and K_d (Table 4.1) values is also informative since if k_2 is much smaller than k_4, K_I (equation 4.2) is equal to K_d (equation 4.3). K_I was found to be within a factor of 10 of K_d for most of the hydrazides tested, with the exception of 2-NZH and NICH (Table 4.1). Therefore, since $K_d \approx K_I$, then k_4 must exceed k_2 and, since the partition ratios for all compounds were greater than zero, k_3 exceeds k_4. Thus, overall $k_3 > k_4 > k_2$, indicating that for these compounds diazene oxidation (k_2) is the rate limiting step in HRP inactivation. Scheme 4.2 is a simplified scheme, which assumes that binding and 1-electron oxidation of the diazene are the rate-limiting steps in HRP inactivation. However, as discussed in Section 4.3.1.2 (Mechanism of HRP inactivation by BZH and H_2O_2), the hydrazide must first bind to HRP and undergo a 2-electron oxidation to the diazene. If diazene oxidation is not the rate-limiting step, clearly the rate constants in Scheme 4.2 will describe more complex steps.

5. INHIBITION OF THE PEROXIDASE ACTIVITY OF PROSTAGLANDIN SYNTHASE-2

5.1. INTRODUCTION

Most xenobiotic metabolism *in vivo* occurs in the liver and is a result of the cytochrome P450 monooxygenases located there (*248*). However, *in vivo* investigations have revealed the role of the POX activity of PGHS in both bioactivation and detoxification of chemicals in extrahepatic tissues with low monooxygenase (P450) activity such as urinary bladder, renal medulla, skin, and lung. PGHS-dependent bioactivation of xenobiotics has been implicated in carcinogenesis, pulmonary- and nephrotoxicity, and teratogenicity (*146-148*). Development of inhibitors of the POX activity of PGHS could aid in further defining the role of this activity *in vivo* and in decreasing the toxic effects of xenobiotic activation. The determination of contacts important in the binding of ligands to the PGHS-2 POX site will aid in the development of such inhibitors.

The inhibitory effects of most current NSAIDs are limited to the COX activity of PGHS and are assumed not to affect the POX activity (*161, 162*). However, tepoxalin, an NSAID that was first identified as a joint COX/5-lipoxygenase inhibitor (*249*), was reported also to be an inhibitor of the POX activity of ovine PGHS-1 (oPGHS-1) (*212*). Based on the observation that increasing heme concentration resulted in a reduction in the level of POX inhibition, Tam et al. (*212*) proposed that chelation of the heme iron by the hydroxamic acid group of tepoxalin was the likely mechanism for POX inhibition. In light of the fact that many compounds referred to as peroxidase inhibitors are actually

POX reducing substrates (*152, 153*), the binding of tepoxalin to the PGHS-2 POX site and its effectiveness as a reducing substrate were investigated.

The ability of most heme peroxidases to oxidize a wide array of compounds makes the development of reversible inhibitors that will not be oxidized difficult. Therefore, the investigation of selective mechanism-based inhibitors, such as hydrazides, may be a more viable alternative to reversible inhibitors for the inhibition of peroxidases. However, due to the covalent nature of the hydrazide-inactivated peroxidase adducts (Section 4.2.2.2, Mechanism of HRP inactivation by BZH and H_2O_2), hydrazides are not ideal therapeutic agents from a pharmaceutical viewpoint (M.D. Percival, personal communication). Therefore, these compounds are unlikely to be used therapeutically on a long-term basis. In spite of this, hydrazides, like hydrazines, can be useful probes of peroxidase active-site topology, and PGHS-2-specific hydrazides could also provide information on the role of this activity and the effects of its inhibition *in vivo*. Recent findings have shown that 4-NH_2-BZH (Figure 3.1) is an effective MPO inhibitor (*157, 158, 250*). This, in combination with the current use of the peroxidase-activated hydrazide INH as a therapeutic agent in the treatment of tuberculosis (*159*), emphasizes the need for investigations on the selectivity to hydrazides and their effect on other mammalian peroxidases.

The series of aromatic hydrazides used in the HRP study in Section 4.2.1.2 (Comparison of HRP inactivation by a series of hydrazides) (Figure 3.1), including 4-NH_2-BZH and INH, were also investigated here to determine the factors that contribute to the effective and selective inhibition of PGHS. The results are compared with those for

HRP (Section 4.2.1.2), which was used as an archetypical peroxidase in this work to probe the selectivity of the hydrazides tested.

5.2. RESULTS

5.2.1. Effect of pH on the UV-VIS spectrum of PGHS-2

The spectrum of PGHS-2 was examined at pH 3 - 12. The spectra at pH 4 - 10 are identical to the pH 7.0 spectrum shown in Figure 5.1, with a Soret maximum at 404 nm. At pH 3.0, the Soret blue-shifted to 378 nm (Figure 5.1) within ~5 min. This blue-shift, similar to that observed for HRP at pH 3.0 (Figure 3.10), suggests an increase in the solvent exposure of the heme of PGHS-2 at pH 3.0 as compared to pH 7.0. The broadening of the Soret at pH 12.0 is also indicative of increased solvent exposure of the heme, although to a lesser extent than that observed at pH 3.0 (Figure 5.1). The absence of Soret red-shifting and of α/β bands in the visible region reveals that PGHS-2 does not undergo a high- to low-spin transition at pH $\leq$12.0, unlike HRP (Figure 3.10). It is of interest that lactoperoxidase (LPO) exhibits a transition to a 6-coordinate, low-spin heme with a pK_a of 12.2 (*251*).

5.2.2. Binding of Ar-CO-NH-X to the peroxidase site of PGHS-2

In comparison to HRP, the effect of Ar-CO-NH-X binding on the absorption spectrum of PGHS-2 is small. For example, binding of saturating SHA to PGHS-2 results in a ~10% decrease in Soret absorbance (Figure 5.2) compared to a ~48% increase for the HRP-BHA complex (Figure 3.11). BHA and SHA binding to MPO, LPO and IPO have also been observed to result in small changes in their visible spectra (*81, 153, 252*). At pH 7, the $K_{d(app)}$ of PGHS-2 for SHA (475 μM) is greater than that of MPO (2 μM), IPO (2 μM), and LPO (70 μM). The latter three mammalian peroxidases have been

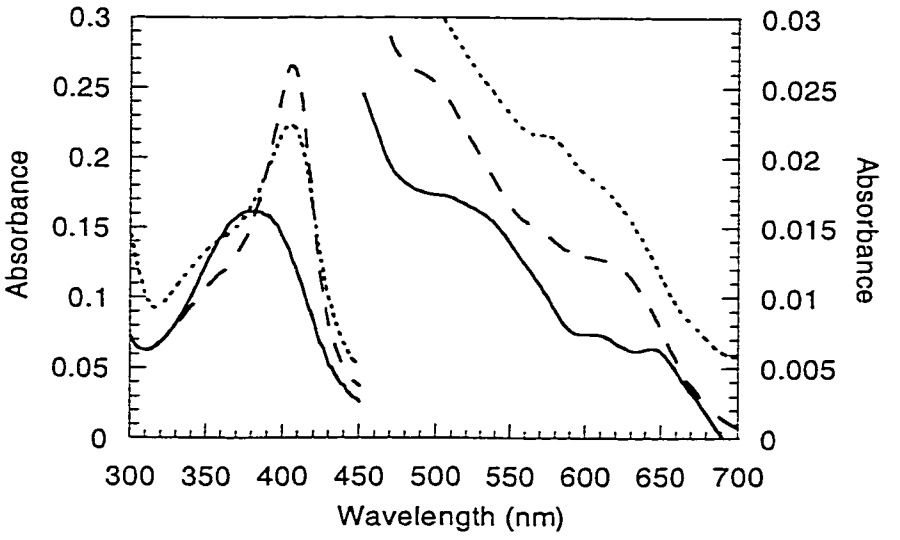

Figure 5.1. Absorption spectra of PGHS-2 at pH 3.0 - 12.0. PGHS-2 (2.5 μM) was incubated for 15 min in 100 mM sodium tartrate, pH 3.0 (—); sodium phosphate, pH 7.0 (- - -) and 12.0 (·····) prior to acquisition of the spectra, as described in Section 2.2.2.

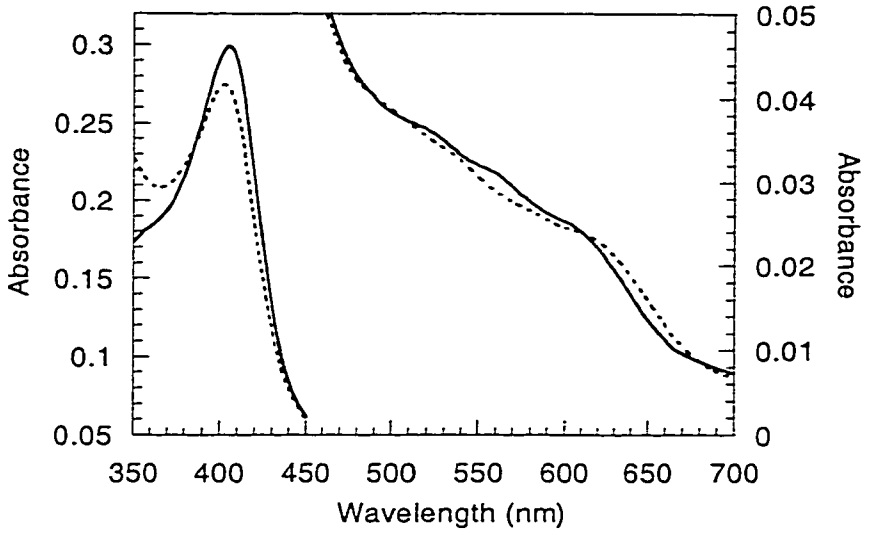

Figure 5.2. Effect of SHA on the UV-VIS spectrum of PGHS-2. PGHS-2 (2.5 μM) was incubated for 15 min in (—) 100 mM sodium phosphate, pH 7.0, prior to the addition of (·····) 2.5 mM SHA, as described in Section 2.2.2.

reported to bind SHA ~10^3-fold more tightly than BHA at pH 7, and the same trend is observed for PGHS-2 as the $K_{d(app)}$ for BHA (~42 mM) is ~10^2-fold greater than that for SHA. BZA and NMBZA, at 25 mM, have no effect on the visible spectrum of PGHS-2. BZH had a only a slight effect on the PGHS-2 spectrum and the presence of 2.5 mM BZH caused only a 1.6% decrease in the Soret intensity at 404 nm, as compared to the 8.5% decrease observed for 2.5 mM SHA at this wavelength (Figure 5.2). As with HRP-BZH, the PGHS-2-BZH spectra undergo time-dependent changes at pH 7.0 and above.

5.2.3. Mode of PGHS-2 peroxidase inhibition by tepoxalin

The spectra of PGHS-2 alone and in the presence of 20-μM tepoxalin are shown in Figure 5.3. The Soret intensity was decreased (2.4%) and slightly red-shifted and there were no changes observed in the 450 - 650 nm region. These observations suggest that tepoxalin does not bind close enough to the heme of PGHS-2 to significantly perturb its environment. Tepoxalin is not soluble at concentrations greater than 50 μM, but it is unlikely that its $K_{d(app)}$ is above this value since an IC_{50} of 25 μM was determined here for its inhibition of PGHS-2 POX, as described in Section 2.2.9. An IC_{50} of 4 μM was reported for oPGHS-1 POX inhibition by tepoxalin (*212*).

The ability of tepoxalin to act as a PGHS-2 POX reducing substrate was investigated by the method of Markey et al. (*126*) with 13-H-PODE as a peroxide substrate, as described in Section 2.2.10. 13-H-PODE is reduced to the alcohol, 13-HODE by the POX activity of PGHS-2 and the amount of conversion depends on the efficiency of the POX reducing substrate present. An index of efficiency (*I*) has been defined for PGHS-2 reducing substrates such that I = [13-HODE]/([13-HODE] + [13-H-PODE]), where [13-HODE] is the concentration of the alcohol produced during the POX

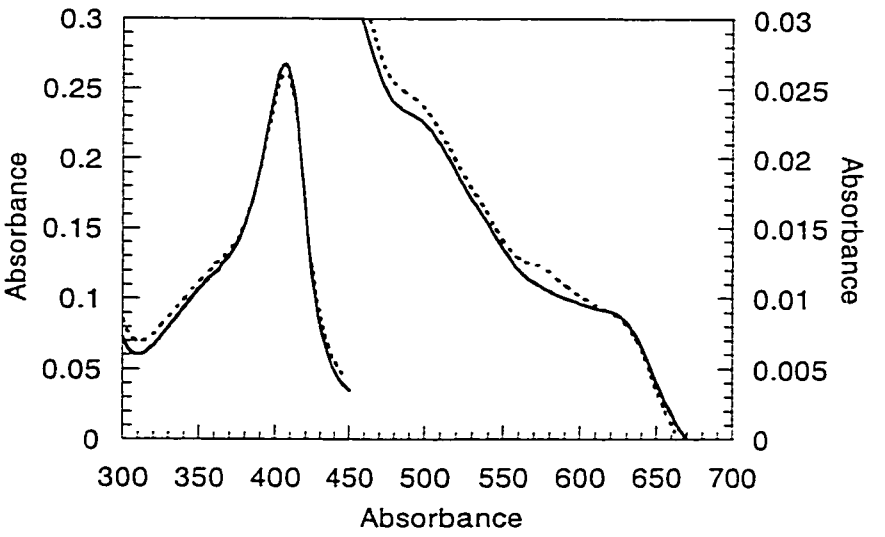

Figure 5.3. Effect of tepoxalin on the Soret absorption of PGHS-2. PGHS-2 (2.5 μM) was incubated for 15min in (—) 100 mM sodium phosphate, pH 7.0, prior to the addition of (·····) 20 μM tepoxalin, as described in Section 2.2.2.

cycle and [13-H-PODE] the remaining peroxide cosubstrate (*126*). Epinephrine and indomethacin were assayed in addition to tepoxalin as these are reported to be good and poor oPGHS-1 substrates with high and low ***I*** values, respectively (*126*). In this study, tepoxalin ($I = 0.77$) was found to be a good PGHS-2 reducing substrate, approaching epinephrine ($I = 0.97$), which was one of the best of 49 substrates tested with oPGHS-1 (*126*). In contrast, indomethacin ($I = 0.21$) was not a substrate, as it resulted in a level of 3-H-PODE conversion similar to that of control sample ($I = 0.24$), which contained DMSO (used to dissolve the reducing substrates) but no reducing substrate.

5.2.4. Inactivation by hydrazides

The rapid autoinactivation of PGHS-2 POX activity in the presence of H_2O_2 alone (Section 7.2.2, peroxide-dependent inactivation of the POX activity of PGHS-2) precluded the determination of K_I and k_{inact} for this activity. Therefore, IC_{50} values were used for comparative studies of hydrazide selectivity for PGHS-2 (Table 5.1) and HRP (Section 4.2.1.2, Comparison of HRP inactivation by a series of hydrazides). With the exception of 2-NZH ($IC_{50} = 48$ μM), all the hydrazides tested have IC_{50} values in the 0.59-92 mM range for HRP. In contrast, only INH ($IC_{50} = 1.5$ mM) and 2-NO_2-BZH ($IC_{50} = 76$ mM) (Table 5.1) have IC_{50} values for PGHS-2 approaching mM concentrations. 2-NZH has the lowest IC_{50} value for both peroxidases [48 μM for HRP (Table 4.1) and 1.6 μM for PGHS-2 (Table 5.1)].

As previously discussed in Section 4.2.1.2 (Comparison of HRP inactivation by a series of hydrazides), the reactivity of aromatic donor compounds can be related to the electron-donating or -withdrawing capacity of their ring-substituents (*157*). The quantitative relationship between the reactivity of an aromatic side-chain and the nature

Table 5.1. IC_{50} values for PGHS-2 inhibition by hydrazides

Hydrazide	PGHS-2 IC_{50} (μM)[a]	Selectivity IC_{50}HRP/IC_{50}PGHS-2
1-NZH	5.9±0.2	576
2-NZH	1.6±0.03	30
3-OH-2-NZH	9.1±1.7	363
INH	$1.5x10^3$±$0.4x10^3$	19
NICH	78±12	1000
BZH	5.2±0.6	1327
2-CH_3-BZH	36±3	1555
3-CH_3-BZH	6.4±1.5	766
4-CH_3-BZH	4.2±1.0	1476
2-OH-BZH	7.3±1.9	6712
3-OH-BZH	4.8±0.5	1229
4-OH-BZH	5.3±0.5	1113
2-Cl-BZH	43±11	2209
3-Cl-BZH	3.9±1.1	2821
4-Cl-BZH	4.5±0.2	3556
2-NH_2-BZH	13±5	45
3-NH_2-BZH	9.5±2.8	1263
4-NH_2-BZH	16±4	563
2-NO_2-BZH	$7.6x10^4$±$3.1x10^4$	1.2
3-NO_2-BZH	20±5	1900
4-NO_2-BZH	130±12	108

[a]Preincubation conditions were 1 μM PGHS-2, 100 μM H_2O_2 and 10^{-2}-10^5 μM hydrazide in 100 mM sodium phosphate, pH 7.0, 0.5% octylglucoside, for 1 min at 25 °C. IC_{50} calculated as described in Section 2.2.4. IC_{50} values are the mean ± S.D. of at least three experiments.
[b]IC_{50} values for HRP used in the calculation of selectivity were taken from Table 4.1.

of other ring-substituents is indicated by the Hammett substituent constant (σ) where a positive or negative σ is indicative of an electron-withdrawing or donating substituent, respectively (*239*). The IC_{50} values for PGHS-2 inactivation by *meta*- and *para*-substituted hydrazides show only a slight correlation with σ constants (Figure 5.4) if 3-NO_2-BZH and 4-NO_2-BZH are excluded. The effect of the electronic character of the ring substituents is represented by ρ, the slope of the plot in Figure 5.4 and $\rho = -9.8$ for PGHS-2.

The ability of a selection of hydrazides to act as reducing substrates for the peroxidase activity of PGHS-2 was also investigated using the 13-H-PODE procedure described in Section 5.2.3 (Mode of PGHS-2 POX inhibition by tepoxalin), which gives an indirect estimation of reducing substrate efficiency. 3-OH-2-NZH ($I = 0.76$) was the most efficient reducing substrate, while 2-OH-BZH ($I = 0.54$) was less efficient, and 2-NZH ($I = 0.36$), BZH ($I = 0.35$), INH ($I = 0.37$), and NICH ($I = 0.32$) were only slightly (8 - 13%) above background ($I = 0.24$).

5.3. Discussion

5.3.1. pH dependence of PGHS-2 spectra.

The Soret maximum for PGHS-2 is 404 nm over the pH range 4-12 (Figure 5.1). The broadening and blue-shifting (to 378 nm) of the Soret at pH 3.0 is suggestive of solvent-exposed heme. The absence of a red-shifted Soret at pH 12.0 indicates that, unlike HRP (Figure 3.10), PGHS-2 does not undergo an alkaline transition below pH 12.0. However, the decrease in molar absorptivity from 106 at pH 7.0 to 89 $mM^{-1}cm^{-1}$ at pH 12.0, in combination with the presence of a broad shoulder at ~350 nm (Figure 5.1), suggests increased solvent exposure at pH 12.0. Evidence from EPR, MCD and RR

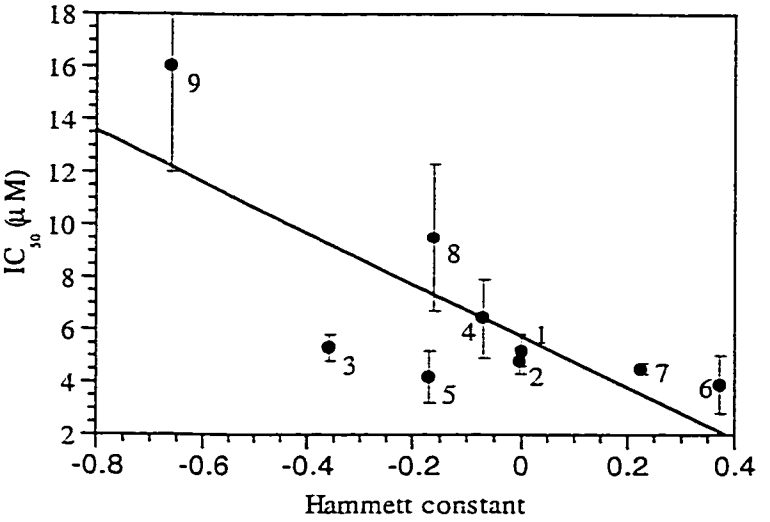

Figure 5.4. Plot of Hammett constants vs IC_{50} values for inactivation of PGHS-2 by hydrazides. Hammett substituent constants are from Jaffe, 1953 (*239*). IC_{50} values are the mean±S.D. of at least three experiments, determined as described in Section 2.2.4. (**1**, BZH; **2**, 3-OH-BZH; **3**, 4-OH-BZH; **4**, 3-CH_3-BZH; **5**, 4-CH_3-BZH; **6**, 3-Cl-BZH; **7**, 4-BZH, **8**, 3-NH_2-BZH; **9**, 4-NH_2-BZH) .

suggests that the distal His207 is weakly coordinated to the Fe^{III} as a sixth ligand in oPGHS-1 at pH 7.2 (*253*). Using RR and CD, Gaspard et al. (*254*) speculated that both His207 and a distal water molecule are possible sixth Fe^{III} ligands in oPGHS-1. Competition with His207 would lower the water-occupancy of a site close to the Fe^{III} in PGHS. This, in combination with the replacement of the distal Arg38 in HRP, which stabilizes the OH^- ligand in alkaline HRP (*73*), with Gln203 in PGHS-2, may inhibit a high- to low-spin transition in PGHS-2 below pH 12.0.

5.3.2. Binding of aromatic hydroxamic acids to PGHS-2

The recent crystal structure of the MPO-SHA complex (*76*) confirms that SHA does bind in the distal heme cavity and elucidates the reason for the relatively small spectral perturbations caused by SHA binding to MPO in relation to BHA binding to HRP. SHA binding eliminates the three waters closest to the Fe^{III} from the distal heme pocket of MPO (*76*). In contrast, a water molecule remains in the distal cavity of the HRP-BHA (*61*) complex and is pushed close enough to the Fe^{III} (2.6 Å) by BHA to become the sixth iron ligand (*61*), resulting in a large Soret perturbation (Figure 3.11).

Despite differences in active-site water molecules, similar H-bonding patterns are observed for the hydroxamic acid side chain in both HRP-BHA and MPO-SHA. In MPO the side-chain hydroxyl H-bonds to the distal His95 (His42 in HRP) and the carbonyl H-bonds to the distal Gln91 (Arg38 in HRP). PGHS and MPO share common distal residues in the POX site including the distal histidine (His207 in PGHS, His95 in MPO) and glutamine (Gln203 in PGHS, Gln91 in MPO) (*15*). Therefore, His207 is expected to accept an H-bond from the hydroxyl, and Gln203 to donate an H-bond to the carbonyl group of hydroxamic acids bound to PGHS. Assuming that the MPO-SHA complex is

representative of that of PGHS and other mammalian peroxidases, the absence of a distal water molecule positioned to be a sixth Fe^{III} ligand would explain why the Soret shift on Ar-CO-NH-X binding to PGHS-2 (Figure 5.2) is much smaller than that observed for HRP (Figure 3.11).

The 10^2-10^3-fold smaller K_d values of the mammalian peroxidases, MPO, LPO, IPO (*81, 153, 252*) and PGHS-2 (K_d = 475 μM and 42 mM for SHA and BHA, respectively), for SHA compared to BHA can also be rationalized from the MPO-SHA structure. The SHA ring hydroxyl replaces the H-bonds formed by W3, an active-site water molecule that is expelled from the distal heme cavity upon SHA binding. Hence, it was suggested by Davey and Fenna (*76*) that elimination of W3 with no compensatory H-bond formation would explain the weaker binding of BHA, which lacks the 2-OH group of SHA. The lack of water molecules in the available coordinates for oPGHS-1, mPGHS-2, and hPGHS-2 precludes a comparison of the H-bonding networks in the distal heme cavities of PGHS and MPO; however, these networks are expected to be similar given the high degree of active-site conservation in the mammalian peroxidases (*15, 76*).

Comparison of the H-bonds formed in the HRP-BHA and MPO-SHA complexes also offers some insight into the weaker binding of aromatic hydroxamic acids to MPO and PGHS than to HRP. The charged BHA-C=O•Arg38 H-bond of HRP was determined to contribute ~1.5 kcal/mol (Table 3.1) more to the energy of BHA binding than the neutral BHA-OH•His42 H-bond. The distal Arg of HRP is replaced in MPO and PGHS by the neutral Gln. Therefore, the H-bond formed between the carbonyl group of the hydroxamic acid side chain and Gln203 of PGHS is expected to be weaker and at least

partially responsible for the ~43-fold weaker binding ($\Delta\Delta G^\circ$ = 2.3 kcal/mol) of SHA to PGHS-2 (K_d = 475 μM) as compared to HRP (K_d = 11 μM, Tables 3.1 and 3.3)

5.3.3. Tepoxalin: substrate or inhibitor?

Hydroxamic acids are known to chelate metal ions, an example being the BHA-Fe^{III} complex for which there is a crystal structure (*255*). Examples of pharmaceutical targeting of metalloenzymes with hydroxamic acids are varied and include inhibition of metalloproteases (*256-262*), lipoxygenases (*263-265*), tyrosinase (*266*), urease (*267-269*), and ribonucleotide reductase (*270*). The crystal structure of human neutrophil collagenase complexed with a peptidomimetic hydroxamate inhibitor reveals bidentate coordination of the catalytic zinc by the hydroxamate hydroxyl and carbonyl oxygens (*256*). Preparation of hydroxamic acid derivatives, such as tepoxalin, of known inhibitors of 5-lipoxygenase has also been attempted (*249, 263-265*). Although inhibition of heme peroxidases by hydroxamic acids has been reported, an example being SHA inhibition of MPO (*151*), the mechanism of inhibition is not due to chelation as in collagenase (*256*), but to competition as a substrate with the chromogenic donor being monitored (*152, 153*).

It has been proposed that the mechanism of PGHS POX inhibition by tepoxalin is via chelation of the heme Fe^{III} (*212*). This is unlikely since the effect of 20 μM tepoxalin on the Soret of PGHS-2 is small (Figure 5.3) despite the IC_{50} value of 25 μM determined here for PGHS-2 inhibition by tepoxalin. Also, tepoxalin was determined to be almost equivalent to epinephrine (*126*) in its efficiency as a POX reducing substrate. Thus, tepoxalin is expected to act as an effective competitive inhibitor of N,N,N',N'-tetramethyl-p-phenylenediamine dihydrochloride (TMPD) oxidation by PGHS POX in the experiments of Tam et al. (*212*). It is also possible that the radical product produced

by tepoxalin oxidation inhibits PGHS by covalently modifying the enzyme to prevent further turnover. N-arylhydroxamic acids have been shown to be activated by peroxidases to products which can form DNA and protein adducts (*271*), suggesting that this may also be possible for tepoxalin. However, the efficiency observed in this investigation of tepoxalin as a reducing substrate for the POX activity of PGHS-2 suggests that either the tepoxalin radical product does not inactivate the POX activity or that inactivation is inefficient and has a high partition ratio.

5.3.4. Development of hydrazides as specific PGHS-2-POX inhibitors

The ability of a subset of hydrazides to act as reducing substrates for PGHS-2 was investigated. This was done indirectly by observing their effect on PGHS-2 turnover of the peroxide 13-HPODE, which is increased in the presence of a reducing substrate. There is no apparent relationship between the IC_{50} values determined for inhibition of PGHS-2 by a given hydrazide and its efficiency as a POX reducing substrate. For example, INH and 2-NZH possess essentially identical efficiencies as reducing substrates but their IC_{50} values differ by almost 500-fold (Table5.1). With the exception of the ring-hydroxylated compounds (I = 0.54 and 0.76 for 2-OH-BZH and 3-OH-2-NZH, respectively), the presence of hydrazides resulted in a level of 13-HPODE reduction by PGHS-2 only slightly above the background. The ability of hydrazides to act as reducing substrates of the POX activity of PGHS-2 is likely affected by several factors including binding affinity, efficiency as a reducing substrate and the rate of inactivation. The results of Section 5.3.2 (binding of aromatic hydroxamic acids to PGHS-2) suggest that the presence of the hydroxyl group in the position *ortho* to the hydroxamic acid group results in tighter binding. Therefore, the ability of 2-OH-BZH and 3-OH-2-NZH to act as

good reducing substrates of PGHS-2 may be a result of their affinity for the POX site. In Section 4.2.1.2 (comparison of HRP inactivation by a series of hydrazides) 2-NZH was reported to have the highest k_{inact} for HRP inactivation of the 24 hydrazides tested (Table 4.1). Although k_{inact} values were not determined here for PGHS-2, it is likely that the low turnover of 13-H-PODE with 2-NZH as a reducing substrate was due to inactivation of the enzyme. This is supported by the ~ 5-fold lower IC_{50} value for 2-NZH (1.6μM, Table 5.1) compared to 2-OH-BZH (7.3 μM, Table 5.1) and 3-OH-2-NZH (9.1 μM, Table 5.1). While POX inactivation may be partially responsible for the low 13-H-PODE turnover observed for BZH, INH and NICH, it is also possible that these three compounds are poor reducing substrates of the POX activity of PGHS-2, particularly INH and NICH.

The results shown here demonstrate that aromatic hydrazides are effective inhibitors of the POX activity of PGHS-2 with IC_{50} values ranging from 1.6-130 μM (Table 5.1), with the exception of INH (IC_{50} = 1.5 mM, Table 5.1) and 2-NO_2-BZH (IC_{50} = 76 mM, Table 5.1). The Hammett ρ value determined from the slope of the plot of σ versus IC_{50} in Figure 5.4 is -9.8. This demonstrates that the electronic character of the substituents has only a marginal effect on their ability to inactivate PGHS-2. The negative ρ value indicates that rather than resulting in increased inactivation, electron-donating substituents cause an increase in the IC_{50} values of the compounds tested. It is possible that the hydrazides with electron-donating ring-substituents provide a slight protection of the POX activity against H_2O_2-induced inactivation.

Comparison of PGHS-2 and HRP IC_{50} values (of those compounds in the μM to low mM range) for methyl, hydroxyl, chloro, amino, and nitro-substituted benzhydrazides indicates some trends in PGHS-2 selectivity (Table 5.1). The greatest

increases in PGHS-2 selectivity were observed for 3-OH-2-NZH and 2-OH-BZH, which were ~12-fold and ~5-fold more PGHS-2 selective than 2-NZH and BZH, respectively (Table 5.1). This is likely due to the more confined active site of HRP (*11*) in comparison to PGHS-2 (*97-99*), in addition to the preference of PGHS-2 (Section 5.3.2) for a hydroxyl group in the *ortho*-position.

The results presented here (Table 5.1) suggest that investigation of the effects of ring substituents on the selectivity of 2-NZH (or other large aromatic hydrazides) could lead to the development of a PGHS-2-specific POX inhibitor. Kettle et al. (*157*) found 4-NH_2-BZH to be the best inhibitor in a series of hydrazides of MPO, by a factor of 2 - 3-fold. In contrast, 4-NH_2-BZH was observed here to be one of the poorest inhibitors of PGHS-2 by a factor of ~4, a similarly small margin as that observed by Kettle et al. (*157*) for MPO. Neither 2-OH-BZH nor 3-OH-2-NZH were tested by Kettle et al. (*157*) for MPO, therefore, a comparison between the selectivity of MPO and PGHS-2 is not possible.

6. NSAID BINDING TO THE CYCLOOXYGENASE SITE OF PROSTAGLANDIN SYNTHASE-2

6.1. INTRODUCTION

6.1.1. Spectroscopic methods for the investigation of dynamic aspects of protein structure

X-ray crystallography has played a crucial role in the recent advances in structural biology (*272, 273*). However, one drawback of X-ray structures is that they are inherently static and therefore, cannot provide information about the dynamic properties of proteins in solution. These dynamic properties are more effectively investigated using spectroscopic techniques including NMR, FTIR and CD (*272*). NMR is an attractive technique because it provides detailed structural information; however, it is limited to proteins of not more than ~ 40 kDa (*273*). Therefore, the dynamic structural properties of larger proteins must be investigated by other means, including FTIR and CD spectroscopies. Differential scanning calorimetry (DSC) is also a useful technique for the investigation of conformational stability, as it can be used to determine thermodynamic parameters.

6.1.1.1. Fourier transform infrared spectroscopy

The potential of infrared spectroscopy for the investigation of protein structure has been recognized for several decades (*274, 275*). A combination of the availability of computerized FTIR instrumentation and the development of techniques for resolution enhancement (*276*) has resulted in the increased application of this technique for the prediction of secondary structure over the past 15 years (*272*). An additional advantage

of FTIR is that it can be used to investigate the conformational stability of proteins via denaturation studies (*e.g.*, thermal denaturation).

The two regions of the FTIR spectrum examined in this study are the amide I (amide I' in D_2O) and amide II (amide II' in D_2O). The amide I/I' (1600-1700 cm^{-1}) bands arise from the carbonyl C-O stretching mode [ν(CO)] of the peptide backbone (*277*). The sensitivity of ν(CO) to small variations in H-bonding and molecular geometry makes the amide I/I' bands useful probes of secondary structure (*272, 278, 279*). Curvefitting of the deconvolved amide I/I' envelope assists in visualizing the component bands, and if the absorbtivities of the individual secondary structure elements are assumed to be the same, the number of residues in a given secondary structure can be estimated from its band area (*192, 272*). Comparison of spectra in ^1H_2O and ^2H_2O helps in assigning overlapping bands since those arising from rapidly exchanging random-coil structures generally red-shift up to 10 cm^{-1} in ^2H_2O (*280*), while the more slowly exchanging α-helices characteristically undergo much smaller red-shifts (*281, 282*).

The amide II band (centered at 1546 cm^{-1}) arises from N-H in-plane bending of the peptide backbone. $^1H \mid ^2H$ exchange occurs on transfer of a protein to ^2H_2O and the amide II (N-^{1}H) red-shifts from 1546 cm^{-1} to 1457 cm^{-1} (amide II', N-^{2}H). Unexchanged protons result in residual amide II absorption, the intensity of which depends on the solvent accessibility of the protein core (*283, 284*).

6.1.1.2. Circular dichroism spectroscopy

Circular dichroism is a phenomenon that results from the interaction of circularly polarized light with chromophores that contain a chiral center or are located in an asymmetrical environment (*285*). In the investigation of protein secondary structure by

CD spectroscopy, the chromophore examined is generally the peptide backbone. In the far-UV region (190 – 240 nm) the peptide backbone has a weak transition ($n \rightarrow \pi^*$) centered at 210 nm and an intense transition ($\pi \rightarrow \pi^*$) centered at 190 nm (*286*). Left- and right-circularly polarized light is absorbed to different extents by proteins due to the presence of protein structures (e.g. α-helix, β-strand), providing a useful tool of secondary structure estimation in solution. CD can also be used as a probe of conformational stability via monitoring the effects of chemical or thermal denaturation on protein structural elements (*286*).

6.1.1.3. Differential scanning calorimetry

DSC measures the specific heat of a system as a function of temperature, relative to a reference solution. Although calorimetry provides no information about the conformation of a protein, it does detect the transition from one conformation to another during folding or unfolding, since this involves the disruption of numerous weak forces (*e.g.*, H-bonds, electrostatic interactions, hydrophobic interactions). An additional advantage of DSC is that it can be used to determine the thermodynamic parameters contributing to the conformational stability of a protein (*287*).

6.1.2. Effect of NSAID binding on the structure and conformational stability of PGHS-2

Nonsteroidal antiinflammatory drugs (NSAIDs) inhibit the COX activity of PGHS and thereby block the production of prostanoids from AA at the first step in their generation (*168, 288*). With the exception of acetylsalicylic acid (ASA), NSAIDs can be divided into 2 groups: the reversible inhibitors such as ibuprofen, and the time-dependent inhibitors such as indomethacin, flurbiprofen, and diclofenac (*162, 167, 168*).

Time-dependent inhibition is a two-step process in which rapid equilibrium binding is followed by a slower isomerization to a non-covalent, slowly reversible complex (*169, 170*). The isomerization step has been suggested to involve a protein conformational change (*169*); however, more recent evidence argues against this. Results of a study using inhibitor-induced (indomethacin, DuP-697, NS-398, ketoprofen, ibuprofen, and diclofenac) changes in the intrinsic fluorescence of PGHS-2 as a probe confirmed the two-step mechanism for the binding of time-dependent inhibitors, but did not support the idea that the isomerization step involves a major change in the inhibitor binding mode (*172*). Similarly, using CD spectroscopy, Kulmacz (*289*) observed that binding of indomethacin to oPGHS-1 caused negligible change in secondary structure. Comparison of the crystal structures of the free and NSAID-ligated (flurbiprofen, indomethacin and SC-558) forms of mPGHS-2 has also shown that with the exception of residues 118 - 122 at the mouth of the COX site, NSAID binding has little effect on the secondary and overall structure of PGHS (*98*). Recent studies on the Y341F (hPGHS-2 numbering, Tyr355 of oPGHS-1) mutant of PGHS-2 suggest that it is the equilibrium between two possible H-bonding networks at the entrance of the COX site (Arg513-Glu524-Tyr355 and Arg120-Glu524-Tyr355) that results in time-dependent inhibition (*290*).

Although NSAID binding does not result in any significant changes in secondary structure (*98*), limited proteolysis has revealed that it does alter the local conformational stability in oPGHS-1. The Arg277 region of oPGHS-1 is protected from attack by trypsin in the presence of heme or time-dependent NSAIDs (indomethacin, flurbiprofen, meclofenamic acid) and to a slightly lesser degree by reversible NSAIDs (flufenamic acid

and ibuprofen) (*173*). Arg277 is approximately 35 and 20 Å away from the NSAID binding site and the heme, respectively (Figure 1.5). Therefore, the reduction in protease-sensitivity observed on NSAID binding indicates reduced conformational flexibility in the loop containing Arg277 rather than competition between trypsin and NSAIDs for a common binding site (*289, 291*). This finding highlights the fact that a static picture of substrate-protein and inhibitor-protein interactions is emerging from crystallographic and mutagenesis studies, while the dynamics of these interactions are still not completely understood (*132*).

Since PGHS-2 lacks a similarly situated trypsin cleavage site, Guo et al. (*291*) constructed the P263R (hPGHS-2 numbering, Arg277 in oPGHS-1) mutant to examine protease-sensitivity in PGHS-2. However, both PGHS-2 and its P263R mutant are resistant to trypsin and proteinase K digestion (*291*), thus impeding the use of protease sensitivity as a probe of the effects of inhibitor binding on the conformational flexibility of PGHS-2. The spectroscopic methods, FTIR and CD, are sensitive probes of conformational stability, via denaturation studies, and have the additional advantage of not requiring conveniently placed proteolytic cleavage sites. Therefore, FTIR and CD were used in this study to investigate the effect of NSAID binding on the structure and conformational stability of PGHS-2 and to seek differences between reversible and time-dependent inhibitors. These studies were complemented with DSC in an effort to determine thermodynamic parameters for the increase in the conformational stability caused by NSAID binding.

Ligand binding is known to have a stabilizing effect on protein structure (*292, 293*). Therefore, to determine whether NSAID binding affinity was correlated with the

observed increase in conformational stability, ITC was used here to determine the affinity and energetics of binding of a subset of the more soluble NSAIDs, including both reversible and time-dependent compounds. Despite the usefulness to drug design of an understanding of the driving forces underlying binding, there have been no studies reporting the thermodynamics of NSAID binding to PGHS-2.

The available crystal structures of PGHS-2-NSAID complexes show that the binding contacts within the COX site are variable (*132*). Therefore, the inhibitors selected for this study (Figure 6.1) were chosen to include commonly studied compounds of diverse structure, and represent 5 families of inhibitors: the sulfonamides (NS-398), indoles (indomethacin), furanones (DFU), profens (ibuprofen and flurbiprofen), and fenamates (diclofenac, L-761,164, meclofenamic acid, and flufenamic acid). Four representatives of the fenamate family were selected because previous studies have indicated that meclofenamic acid and diclofenac have different modes of binding as compared to other NSAIDs (*172, 294*).

6.2. Results

6.2.1. Effect of NSAID binding on the secondary structure of PGHS-2

Free PGHS-2 was dialyzed for 16 h versus ^2H_2O buffer prior to NSAID addition to allow for $^1H|^2H$ exchange of rapidly exchanging groups. However, PGHS-2 did not undergo complete $^1H|^2H$ exchange without irreversible denaturation (data not shown). Therefore, the residual amide II intensity of PGHS-2 in ^2H_2O results from buried and/or strongly H-bonded amide protons (*295*). The percentage of unexchanged amide protons, calculated from the ratio of amide II intensity in ^2H_2O and ^1H_2O was ~48±3.3%, which is close to the 45% secondary structure estimated from the crystal structures of mPGHS-2

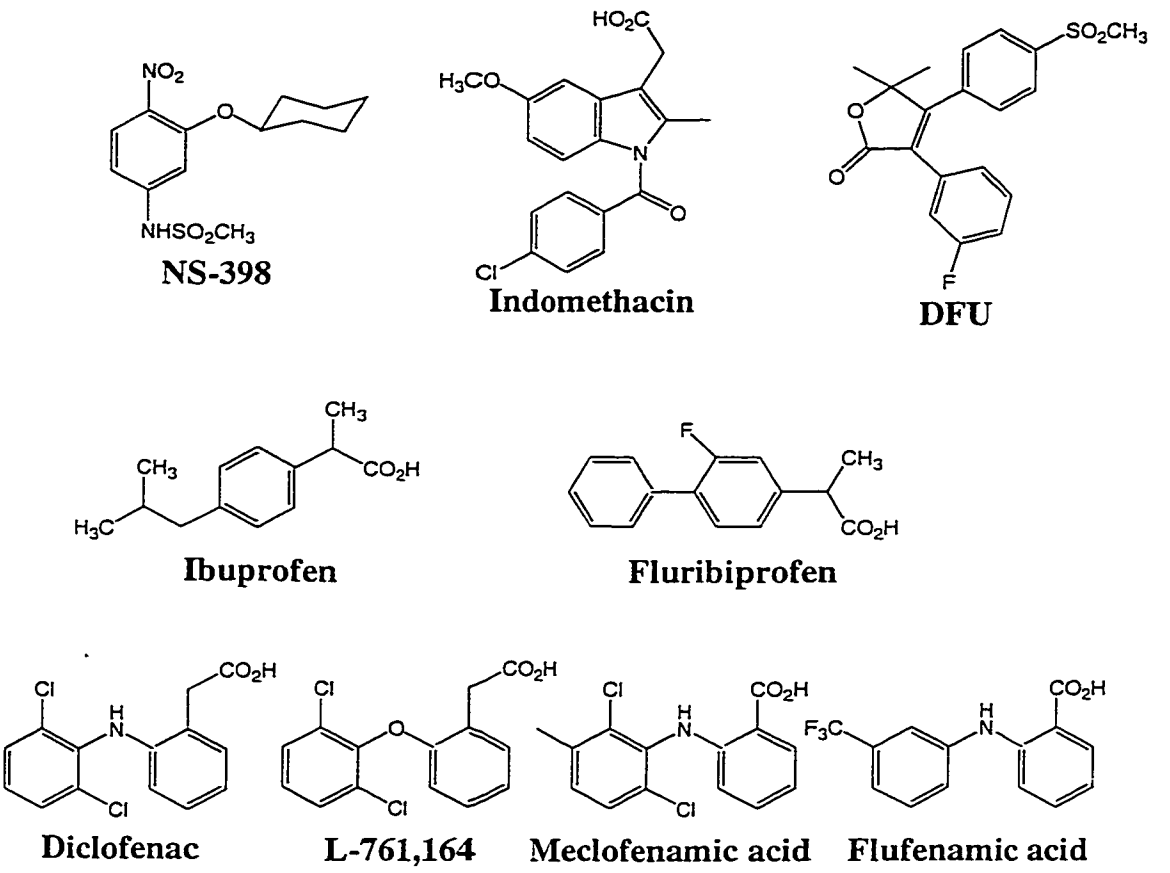

Figure 6.1. Structures of the PGHS inhibitors used in this study.

and oPGHS-1 (43% α-helix, 2% β-sheet) (*15, 98*). The lack of additional $^1H|^2H$ exchange on NSAID binding suggests that binding does not result in exposure of unexchanged regions of PGHS-2.

Examination of the deconvolved amide I/I' region of the spectra of unliganded PGHS-2 (Figure 6.2) shows that it is composed of several component bands. Based on literature assignments (*272, 278*) bands at 1666, 1676, 1685, and 1697 cm^{-1} in ^1H_2O that red-shift ≥ 7 cm^{-1} in ^2H_2O were tentatively assigned to loops and turns (Table 6.1). These bands collectively comprise ~46% of the amide I intensity. The 1685 and 1697cm^{-1} bands also have a contribution to absorption from β-sheet structures, although for PGHS-2 [~ 2% β-sheet, (*98*)] this is likely negligible compared to the absorption of loops and turns. This is confirmed by the weak 1630 cm^{-1} band in ^1H_2O, which is assigned to β-sheet structures, and comprises only 3% relative intensity (Table 6.1) (*272, 278*). An interesting observation is the shift of one of the bands assigned to turns from 1666 cm^{-1} in ^1H_2O to 1631 cm^{-1} in ^2H_2O. A red-shift of this magnitude cannot be ascribed to simple mass effects and other possibilities include unequal contributions from N^1H and N^2H deformation to the normal modes, or sensitivity of the dihedral angle of this type of turn to deuteration (*280, 296, 297*). Absorption in the amide I region below 1630 cm^{-1} (1%) was attributed to side chain absorption (Table 6.1), likely due to Asn, Gln and Tyr (*295*). Absorption at 1617 cm^{-1} may also be due to intermolecular β-sheets, which are characteristic of aggregation (*298*). However, while the presence of aggregated structures cannot be ruled out, it is unlikely in the high detergent concentrations (1% octylglucoside) used here.

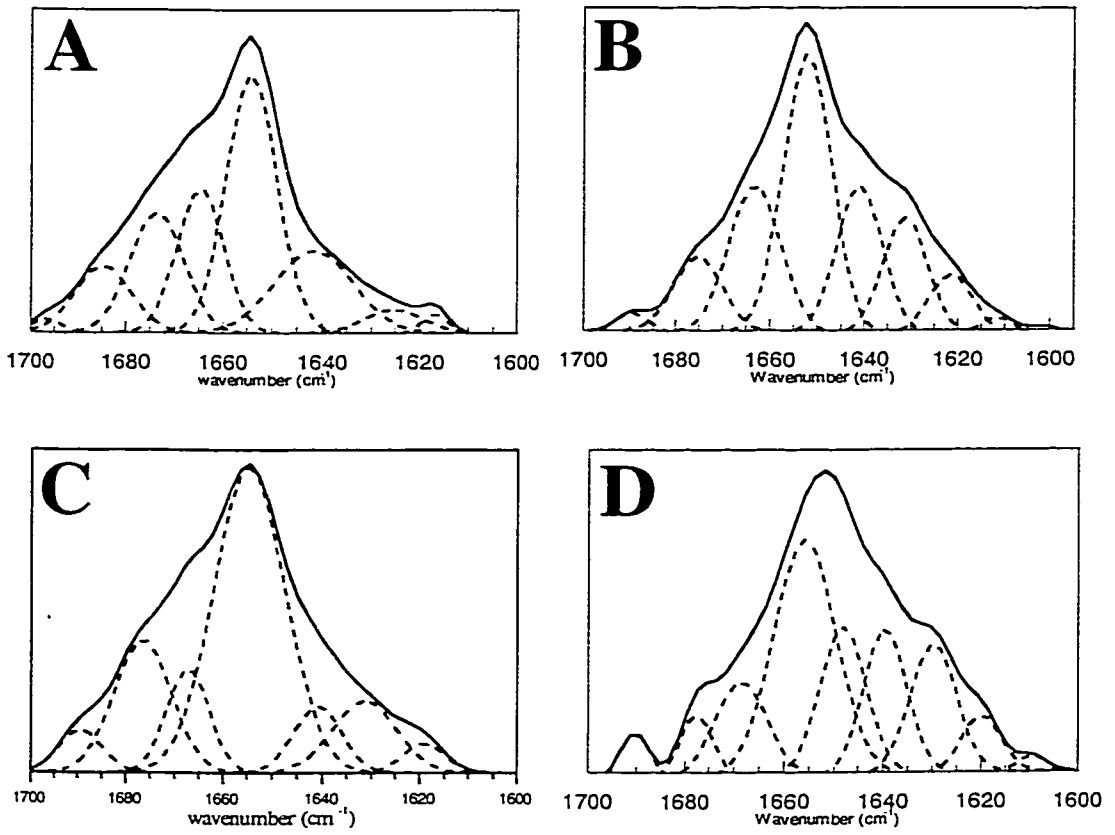

Figure 6.2. Effect of diclofenac on the amide I/I' region of PGHS-2. FTIR spectra between 1600 - 1700 cm^{-1} of PGHS-2 (300 μM in ^2H_2O and 424μM in ^1H_2O) in 100 mM sodium phosphate, pH 7.0, 1% octylglucoside, with 9.1% DMSO in (**A**) ^1H_2O and (**B**) ^2H_2O and in the presence of equimolar diclofenac in (**C**) ^1H_2O and (**D**) ^2H_2O were deconvolved (w = 15, k = 1.8) and curvefit using Peaksolve (Galactic).

Table 6.1. Peak positions and relative intensities of amide I/I' component bands of PGHS-2 in $^{1}H_2O$ and after 16 h exchange in $^{2}H_2O$

$^{1}H_2O$ + DMSO		16 h in $^{2}H_2O$ + DMSO		
Band position (cm-1)	Band area (%)	Band position (cm^{-1})	Band area (%)	Assignment[a]
1697	2	1690	2	β-sheet/Turn
1685	8	1675	9	β-sheet/Turn
1676	17	1663	18	Turn
1666	19	1631	13	Turn
1654	30	1652	33	α-helix
1641	19	1641	16	Random/α-helix
1630	3	1622	6	β-sheet
1617	2	1612	3	Sidechain/Aggregation

[a]band assignments based on literature (*272, 278, 281, 282*).

The 1654 cm^{-1} band in ^1H_2O red-shifts only 2 cm^{-1} in ^2H_2O and is assigned to α-helical absorption (Table 6.1) (*272, 281, 282*). The relative intensity of this band is only ~30% in ^1H_2O and ^2H_2O in comparison to 43% α-helical structures observed in the crystal structure of mPGHS-2 (*98*). However, α-helical absorption is also observed at 1641 cm^{-1} and is associated with more solvent-exposed helices (*299-301*). Therefore, an additional 13% helical absorption is likely present under the broad 1641 cm^{-1} band in both ^1H_2O and ^2H_2O, and the remaining intensity at 1641 cm^{-1} (6% in ^1H_2O and 3% in ^2H_2O) is assigned to random structure. The shift of ~13% of the helical absorption to 1641 cm^{-1} due to solvent exposure is likely due to the presence of the COX channel, which allows access of solvent molecules to helices at the core of the protein.

Comparison of the ^1H_2O curvefitting results in the absence and presence of 9.1% DMSO (Table 6.2) shows ~1 - 5% variations in the intensity of all bands and a decrease of 6% in the intensity of the 1617 cm^{-1} band corresponding to absorbance from Asn, Gln and Tyr side chains (*295*) or aggregated structures (*298*). Similarly small changes (1 - 3%) were observed upon addition of DMSO to PGHS-2 in ^2H_2O (Table 6.3). This indicates that the 9.1% DMSO concentrations required for FTIR experiments has negligible effect on PGHS-2 secondary structure. The slightly larger changes in band intensities in ^1H_2O as compared to ^2H_2O may arise in part from subtraction errors when subtracting the large absorption due to water in the amide I region.

No trends were observed for the effects of reversible versus time-dependent inhibitors on PGHS-2 secondary structure. With the exception of diclofenac (Figure 6.2) and meclofenamic acid, addition of inhibitors had little effect on the amide I/I' bandshapes and the α-helical content of PGHS-2 in ^2H_2O (Table 6.3). In ^2H_2O

Table 6.2. Effect of DMSO, diclofenac, meclofenamic acid, and flufenamic acid on relative intensities (%) of the amide I component bands in the FTIR spectra of PGHS-2 in ^1H_2O

Centre (cm^{-1})	^1H_2O (%)	+ DMSO[a] (%)	Diclofenac[a] (%)	Meclofenamic acid[a] (%)	Flufenamic acid[a] (%)	Assignment[b]
1697	1	2				β-sheet/Turn
1685	6	8	6	8	11	β-sheet/Turn
1676	12	17	13	15	11	Turn
1666	17	19	14	22	22	Turn
1654	27	30	46	47	31	α-helix
1641	18	19	9	6	21	Random/α-helix
1630	11	3	9	1	3	β-sheet
1617	8	2	3	1	1	Sidechain/ Aggregation

[a]9.1% DMSO added.
[b]band assignments based on literature (*272, 278, 281, 282*).

Table 6.3. Effect of DMSO, diclofenac, meclofenamic acid, and flufenamic acid on peak positions and relative intensities (%) of the amide I' component bands of PGHS-2 in ^2H_2O

Centre (cm^{-1})	^2H_2O (%)	+ DMSO[a] (%)	Diclofenac[a] (%)	Meclofenamic acid[a] (%)	Flufenamic acid[a] (%)	Assignment[b]
1690	2	2	3	2	2	β-sheet/Turn
1675	9	9	5	7	7	β-sheet/Turn
1663	21	18	15	20	22	Turn
1657			21			α-helix
1652	33	33		41	37	α-helix
1650			23			α-helix
1641	18	16	15	10	9	α-helix/Turn
1630	11	13	12	15	16	Turn
1622	4	6	5	4	5	β-sheet
1612	2	3	1	2	3	Sidechain/ Aggregation

[a]9.1% DMSO added
[b]band assignments based on literature (*272, 278, 281, 282*).

flufenamic acid binding resulted in a ~4% increase in the 1652 cm^{-1} helical band at the expense of the 1641 cm^{-1} band. The amide I' (Table 6.3) curvefitting results for flufenamic acid are representative of those obtained in the presence of L-761, 164, flurbiprofen, ibuprofen, DFU, indomethacin, and NS-398. Therefore, binding of most of the inhibitors resulted in only small changes in the α-helical structure of PGHS-2. Due to the difficulty in subtracting the large absorption of ^1H_2O in the amide I region from the much smaller protein absorption only flufenamic acid, meclofenamic acid and diclofenac were investigated in ^1H_2O for comparison with ^2H_2O results. There was only a very slight change (1%) in the 1654 cm^{-1} helical band in ^1H_2O of PGHS-2 on binding of flufenamic acid, in agreement with the ^2H_2O results.

The effect of meclofenamic acid binding to PGHS-2 in ^1H_2O was to increase the intensity of the 1654 cm^{-1} amide I band from 30% to 47%, while the 1641 cm^{-1} band decreased in intensity from 19% to 6% (Table 6.2). Similar effects were observed in ^2H_2O (Table 6.3). This confirms the assignment of 1641-cm^{-1} intensity to α-helical absorption for free PGHS-2 and indicates that meclofenamic acid binding decreases the solvent exposure of some of the α-helices in PGHS-2.

Similarly, diclofenac binding increased the 1652 cm^{-1} helical absorption (from 30% to 46%) at the expense of the 1641-cm^{-1} band (from 19% to 9%) in ^1H_2O (Table 6.2, Figure 6.2A versus C). Interestingly, in ^2H_2O, diclofenac binding resulted in splitting of the amide I' helical absorption into components at 1650 and 1657 cm^{-1} with 23% and 21% intensity, respectively (Table 6.3). Together these two bands comprise 44% of amide I' absorption, similar to the value of 43% helical content estimated from the crystal structure of free PGHS-2 (*98*). Splitting of the amide I' intensity to yield a higher

frequency component reveals that diclofenac is more effective than the other NSAIDs in reducing the solvent exposure of certain α-helical structures. Alternatively, splitting of the α-helical absorbtion into two component bands may be due to changes in the strength of H-bonding in some helices. High frequency α-helical absorption 1(1667 cm^{-1}) has been reported for bacteriorhodopsin (*302*) and was proposed to be due to weaker H-bonding in the helices involved, with a consequent increase in the amide I carbonyl stretching force constant (*303*). The risk of overinterpreting the curvefitting data prevents a detailed discussion of the effects of diclofenac binding on other structural elements.

In contrast to FTIR amide I/I' spectra, the presence of diclofenac has little effect on the UV/CD spectra of PGHS-2. Addition of diclofenac shifts the UV peak minimum from 208.5 to 209.5 nm and marginally decreases intensity at 220 (0.6%). However, the overall spectral shape remains the same (Figure 6.3). The negligible effect of diclofenac binding on the CD spectrum of PGHS-2 observed here (Figure 6.3) is in agreement with previous results indicating that indomethacin binding also had a negligible effect on the CD spectrum of oPGHS-1 (*289*). Therefore, no other NSAIDs were investigated here by CD spectroscopy.

6.2.2. Effect of NSAIDs on the conformational stability of PGHS-2

6.2.2.1. FTIR and CD-monitored thermal denaturation of PGHS-2

Insight into the effect of NSAIDs on PGHS-2 in conformational stability and flexibility was obtained from the FTIR-monitored thermal denaturation of PGHS-2 and its NSAID complexes in ^2H_2O. The stacked FTIR amide I' spectra over the temperature range 22 - 90 °C in Figure 6.4A reveal that free PGHS-2 maintains much of its helical

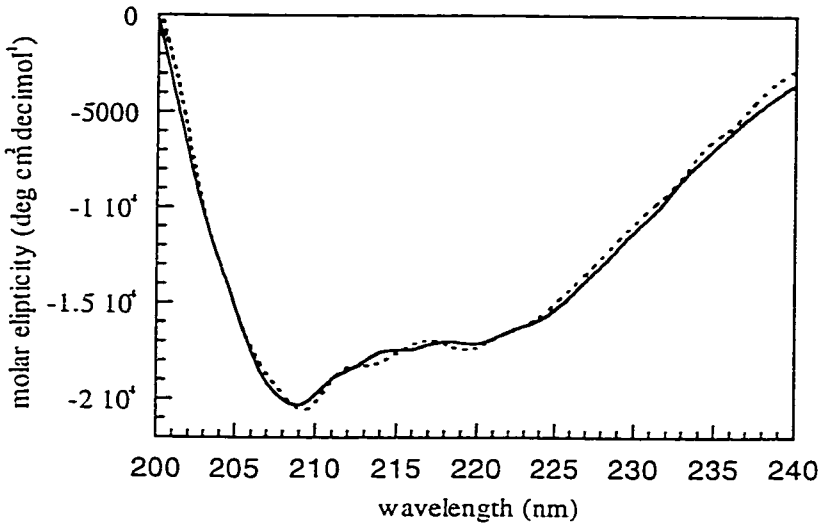

Figure 6.3. CD spectra of free and diclofenac-bound PGHS-2. CD spectra of 6.9 μM PGHS-2, free (solid line) and in the presence of stoichiometric diclofenac (dotted line), were recorded at 20°C in 100 mM sodium phosphate, pH 7, containing 1% octylglucoside and 9.1% DMSO, as described in Section 2.2.13.

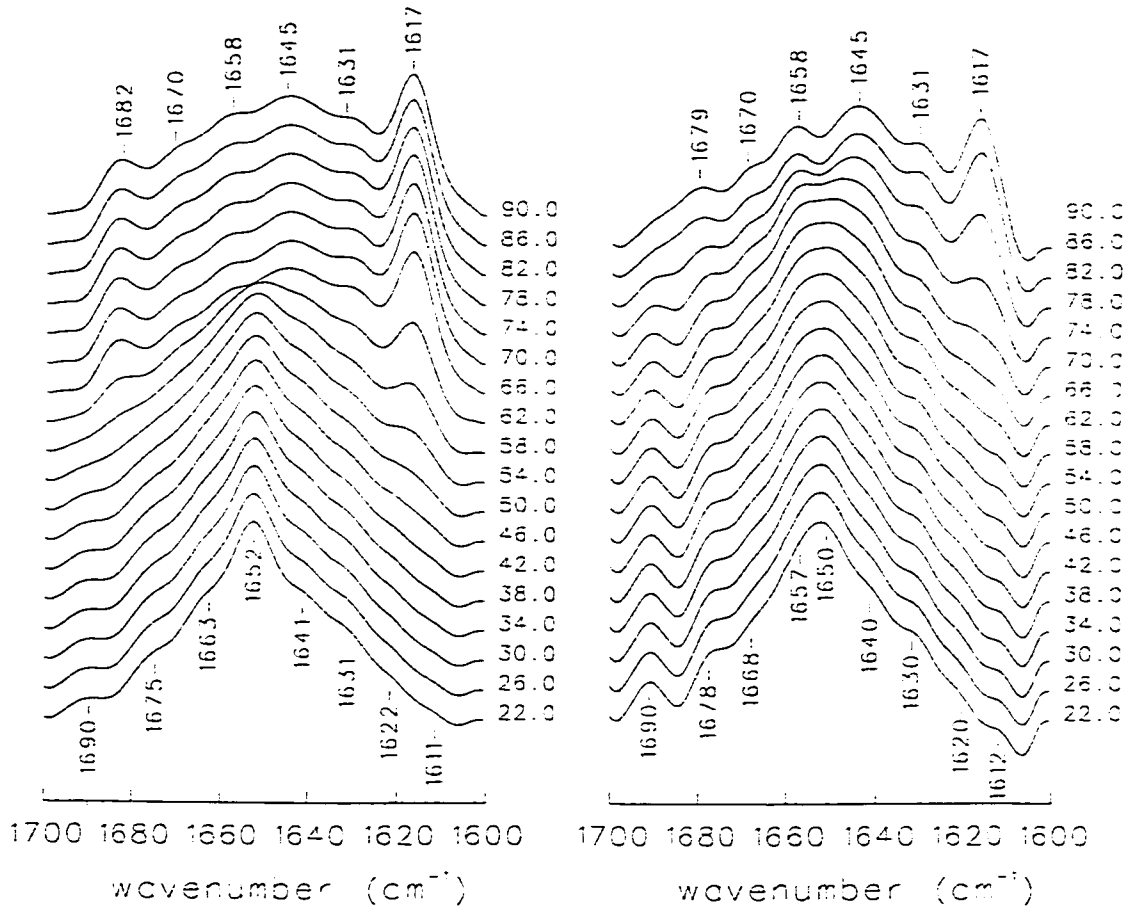

Figure 6.4. Effect of diclofenac on the FTIR spectrum of PGHS-2 during thermal denaturation. Deconvolved (w = 15, k = 1.8) amide I' region of the FTIR spectra of 300 μM PGHS-2 in 100 mM sodium phosphate buffer, pD 7.0, 1% octylglucoside, with 9.1% DMSO (d6) (**A**) alone and (**B**) with equimolar diclofenac were deconvolved and stacked using RAMOPN and GPLOTC (*189*).

structure up to 58°C followed by the abrupt loss of secondary structure between 58 and 66°C. Above 66°C no further spectral changes are evident in the amide I' region of the spectrum of PGHS-2.

A more detailed examination of the FTIR-monitored thermal denaturation of PGHS-2 is possible from the plot of the integrated intensity of the α-helical band (1650-1660 cm^{-1}) versus temperature shown in Figure 6.5A. This plot demonstrates that there is negligible decrease in the intensity of the 1650-1660 cm^{-1} helical band between 20 and 40°C. Between ~40 and 58°C there is a gradual loss of α-helical absorption followed by a more abrupt loss between 58 and 66°C. There appears also to be a small transition at ~ 50°C, which is not discussed in detail here due to the risk of overinterpretation of the data. However, this transition may reflect the onset of aggregation occurs at 50°C as evidenced by the appearance of bands characteristic of protein aggregation (intermolecular β-sheet formation) at 1616 and 1684 cm^{-1} (Figure 6.4) (*298*). The regions of PGHS-2 responsible for the biphasic decrease in helical absorption between 40 and 66°C are not obvious. A recent investigation of PGHS-1 and -2 stability in guanidinium hydrochloride showed that dimer dissociation into monomers occurs prior to unfolding of monomers (*304*). Therefore, the spectral changes in the 40-58°C range may be a result of increased solvent exposure of previously buried α-helices due to subunit dissociation.

When the stacked amide I/I' spectra are examined for the thermal denaturation of PGHS-2 in the presence of NS-398, indomethacin, DFU, ibuprofen, flurbiprofen, and L-761,164 (data not shown) the pattern closely resembles that of vehicle alone (DMSO, Figure 6.4A). In contrast, while flufenamic acid and meclofenamic acid produced a

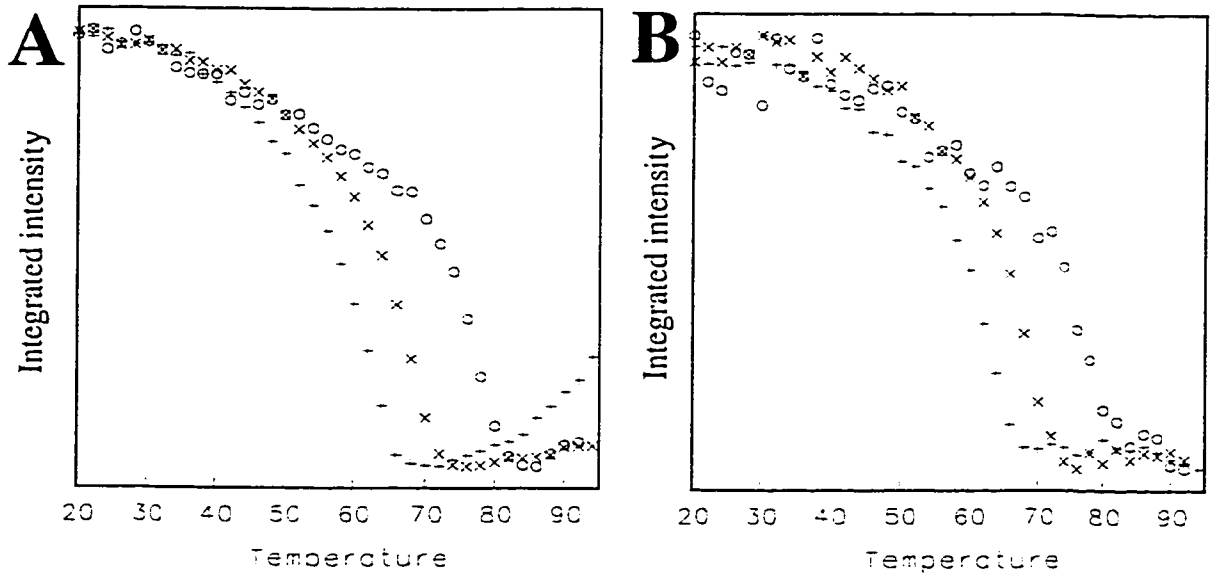

Figure 6.5. Effect of L-761,164 and diclofenac binding on the conformational stability of PGHS-2. PGHS-2 (300 μM) in 100 mM sodium phosphate, pD 7.0, 1% octylglucoside, with 9.1% DMSO (d6) (+), or an equimolar concentration of L-761,164 (X) or diclofenac (o) was thermally denatured. Spectra were deconvolved (w =15, k = 1.8) and the integrated intensity of the (**A**) α-helical (1650-1660 cm^{-1}) and (**B**) amide II (1540-1560 cm^{-1}) bands were plotted versus temperature.

pattern similar to that observed in the presence of diclofenac (Figure 6.4B). In all cases (Figure 6.4) some residual structure remains at high temperatures, as is evidenced by the presence of a band at 1658 cm^{-1}. However, in the presence of meclofenamic acid, flufenamic acid, and diclofenac (Figure 6.4B) there is no obvious point at which secondary structure collapses and the band at 1658 cm^{-1} is much more pronounced at 90°C, suggesting that these compounds have a unique stabilizing effect on PGHS-2.

Figure 6.5A shows the effect of L-761,164 (representative of flurbiprofen, ibuprofen, indomethacin, DFU and NS-398) and diclofenac (representative of meclofenamic acid and flufenamic acid) binding on the intensity of α-helical absorption (1650 - 1660 cm^{-1}) during thermal denaturation of PGHS-2. Of note is the temperature at which the transition between slow and rapid loss of α-helical absorption occurs. In the case of flurbiprofen, (~43°C), ibuprofen (~43°C), indomethacin (~41°C), DFU (~41°C), NS-398 (~41°C) (data not shown), and L-761,164 (~44°C, Figure 6.5A) this transition temperature is only slightly higher than that of free PGHS-2 (~ 40°C, Figure 6.5A). In sharp contrast, the temperature of this transition is elevated for diclofenac (~67°C, Figure 6.5A), flufenamic acid (~58°C) and meclofenamic acid (~48°C), suggesting that these compounds stabilize certain α-helical structures and possibly prevent dimer dissociation at lower temperatures. T_m values are reported in Table 6.4 for the midpoints of the abrupt phase of loss of α-helical intensity. T_m values for the increase in the intensity of the 1616 cm^{-1} aggregation band were also determined (data not shown) and are identical to the values shown in Table 6.4 for the decrease of α-helical intensity. Inhibitors fall into three categories with respect to their effect on T_m ($\Delta T_m = T_{mNSAID} - T_{mPGHS-2}$, where$T_{mPGHS-2}$ is that of free PGHS-2): those resulting in slight (ΔT_m = 4.5 - 5°C), intermediate (ΔT_m = 7 -

8.5 °C) and large (ΔT_m = 16°C) stabilization of PGHS-2 α-helical structure. The degree of stabilization afforded by NSAID binding is unrelated to time-dependency as both reversible and time-dependent inhibitors are found in the first two categories. The third category is comprised of diclofenac alone, which exhibits a ΔT_m close to double that of the other compounds tested (Table 6.4). Since no K_d or thermodynamic parameters are available for the binding of these NSAIDs to PGHS-2, their IC_{50} values are listed in Table 6.4. There is no apparent correlation between T_m and IC_{50} for these compounds. This is not surprising as IC_{50} values for PGHS inhibition vary widely depending on experimental conditions (*e.g.*, AA concentration, preincubation time, presence of detergent) (Marc Ouellet, personal communication).

Examination of the integrated intensity of the amide II band (1540-1550 cm^{-1}) shows that this band decreases in intensity due to amide $^1H|^2H$-exchange with increasing temperature (Figure 6.5B). This occurs as expected, since the loosening and eventual loss of secondary structure in PGHS-2 (Figure 6.5A) allows buried hydrogens, which were previously inaccessible, to exchange with the ^2H_2O solvent. The plot of amide II intensity versus temperature (Figure 6.5B) is almost superimposable with that of the helical intensity (Figure 6.5A), and for free PGHS-2 transition temperatures are observed at ~40, ~58 and T_m (66°C). The more gradual $^1H|^2H$ exchange between 40 - 58 °C is likely due to dimer dissociation and exposure of loops, turns, and random structures, while the abrupt loss of amide II intensity above 58°C is assigned to exchange of hydrogens involved in H-bonding within α-helices.

The thermal denaturation of PGHS-2 was also monitored by CD spectroscopy. Plots of CD molar elipticity at 220 nm versus temperature for PGHS-2 free and in the

Table 6.4. Effect of NSAID binding on the T_m for the high-temperature phase of loss of α-helical absorption of PGHS-2.

NSAID	T_m (amide I) (°C)	ΔT_m (°C)[a]	IC_{50} (μM)[b]
None	62.0		
L-761,164	66.5	4.5	1.10
Flufenamic acid	70.0	8	0.30
Meclofenamic acid	70.5	8.5	0.14
Diclofenac	78	16	0.04
Ibuprofen	67	5	0.06
DFU	67	5	0.84
NS-398	69	7	0.17
Flurbiprofen	70	8	0.02
Indomethacin	71	9	0.50

[a]ΔT_m values were calculated by subtraction of the T_m (62.0°C) of free PGHS-2 from that of inhibitor-bound PGHS-2 for each NSAID.
[b]IC_{50} values determined by Marc Ouellet as described in Section 2.2.11.

presence of diclofenac (Figure 6.6) demonstrate that loss of helical structure mirrors that observed by FTIR (Figure 6.4A). For free PGHS-2 the elipticity at 220nm changes slowly until ~60 °C followed by an abrupt increase in molar elipticity between ~60 and 70 °C. Above ~70 °C there are no further changes in the molar elipticity at 220 nm. The small increase in the transition temperatures observed by CD, as compared to FTIR (T_m = 65°C and 62°C) is likely a concentration effect, as the PGHS-2 concentration in FTIR experiments was ~40-fold greater than that used in CD experiments. Aggregation is a greater driving force in thermal denaturation at high protein concentrations, and this was also observed for cytochrome *c* (*280*). In the presence of diclofenac the abrupt increase in 220-nm elipticity occurs between ~74 and 84 °C (T_m = 79°C).

6.2.2.2. DSC-monitored thermal denaturation of PGHS-2

The aggregation of PGHS-2 in combination (Figure 6.4) with the complexity of the denaturation process (Figures 6.5 and 6.6) and the irreversibility of the FTIR-monitored thermal denaturation of PGHS-2 preclude the calculation of thermodynamic denaturation parameters. Therefore, the effect of L-761,164 and diclofenac binding on PGHS-2 was also monitored by DSC, which requires lower (μM range) protein concentrations that are less conducive to aggregation. Hadden et al. (*190*) were the first to observe that the T_m values for loss of secondary structure observed for thermal denaturation monitored by FTIR were comparable to the midpoints observed in DSC transitions. DSC thermograms for free PGHS-2 and in the presence of diclofenac and L-761,164 are shown in Figure 6.7. The truncation of the DSC thermograms following the unfolding transition is a result of aggregation. Therefore, even at low PGHS-2 concentrations (2 μM) aggregation precludes a quantitative analysis of the

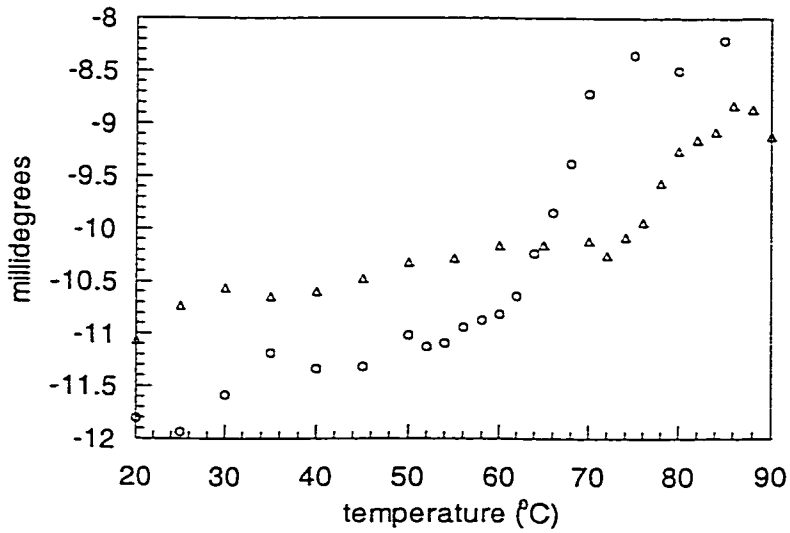

Figure 6.6. Effect of diclofenac on the PGHS-2 UV/CD intensity at 220 nm versus temperature. CD spectra of 6.9 μM PGHS-2 free (o) and in the presence of stoichiometric diclofenac (Δ) were recorded during thermal denaturation, as described in Section 2.2.13, and the intensity at 220 nm (α-helical structure) was plotted versus temperature.

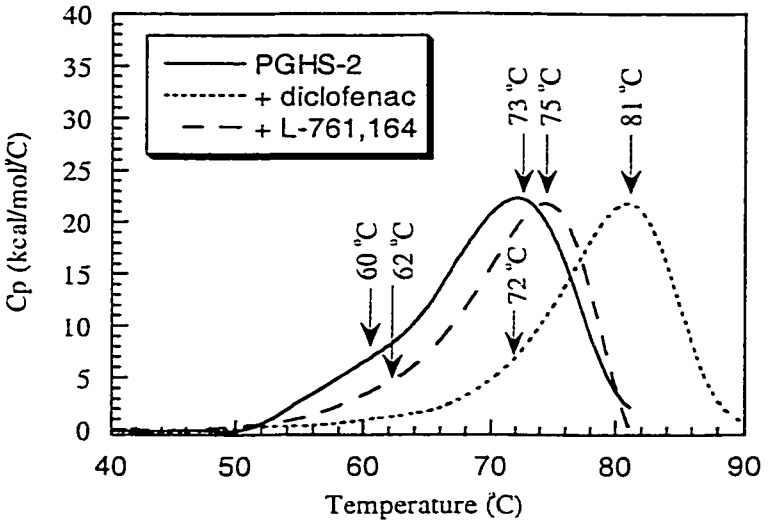

Figure 6.7. DSC thermograms of free and L-761,164- and diclofenac-bound PGHS-2. DSC thermograms (—) 2.0 μM PGHS-2 (in 100 mM sodium phosphate, pH 7.0, 1% octylglucoside, with 9.1% DMSO), and in the presence of stoichiometric (- - -) L-761,164 and (·····) diclofenac were recorded during thermal denaturation.

thermodynamics of unfolding. However, a determination of the midpoint (T_m) of the transitions provided some insight into the structural changes observed by FTIR. In the absence of inhibitor, PGHS-2 shows overlapping transitions with T_m values of 60 and 73°C. The 73°C transition parallels the 62°C T_m observed by FTIR and therefore is expected to be due to loss of the remaining secondary structure. The 10°C higher T_m estimated from the DSC thermogram (2 μM PGHS-2) compared to FTIR amide I/I' (300 μM PGHS-2) is likely a concentration effect, similar to that observed with CD (T_m = 65°C, 6.9 μM PGHS-2). However, another possible factor is differences in temperature detection by these instruments. DSC-monitored denaturation predicts the same trend as FTIR for PGHS-2, with stabilization due to diclofenac binding (ΔT_m = 8 °C) being much greater than that of L-761,164 (ΔT_m = 2 °C).

6.2.3. Isothermal titration calorimetry of NSAID binding to PGHS-2

It is well known that ligand binding has a stabilizing effect on proteins that can be correlated with the strength of ligand binding (*292, 293*). It is not possible to elucidate from the FTIR, CD and DSC data whether differences in effects of the NSAIDs tested here on the thermal denaturation of PGHS-2 are due to their strength of binding or differences in their binding modes. Therefore, a subset of the NSAIDs shown in Figure 6.1 were selected for investigation by ITC.

The 4 fenamates (diclofenac, meclofenamic acid, flufenamic acid, and L-761,164) were chosen for ITC analysis because they comprise both reversible and time-dependent inhibitors and they are relatively buffer soluble. Additionally, this was considered to be an interesting group of compounds for which to investigate the thermodynamics of binding because of the unique effects of meclofenamic acid and diclofenac (Figure 6.2C

and D) on secondary structure and of diclofenac on conformational stability (Figure 6.4B). Furthermore, previous studies of PGHS-2 inhibition by NSAIDs suggest that some fenamates (meclofenamic acid and diclofenac) bind differently from other NSAIDs (*294, 305-307*). NS-398 (sulfonamide class) was also selected for comparison because it was the most buffer-soluble of the remaining NSAIDs in Figure 6.1. Solubility in buffer is an important factor in ITC since the use of an organic cosolvent like DMSO results in heats of mixing that obscure the heat resulting from ligand binding. This becomes increasingly important at the low enzyme concentrations (low μM range) required to measure accurate K_d values for tight binding (nM range) ligands, such as many NSAIDs, because the heat evolved approaches the lower limits of detection.

The raw and integrated ITC curves for the titration of PGHS-2 with diclofenac and L-761-164 are shown in Figure 6.8. These curves are representative of those obtained for the 5 NSAIDs tested. The concentrations used and the c and n values are summarized in Table 6.5. The thermodynamic parameters for binding were determined, as described in Section 2.2.1, and are presented in Table 6.6.

A comparison of the enthalpies and entropies for the five NSAIDs investigated (Table 6.6) exemplifies the differences in their thermodynamics of binding. Examination of the structures of diclofenac and L-761,164 (Figure 6.1) highlights the importance of the nitrogen bridging the two phenyl rings. Although the only difference between these 2 compounds is the substitution of the NH in diclofenac by an oxygen atom in L-761,164, the binding of diclofenac is 8.64 kcal/mol more enthalpically favourable than L-761,164 (Table 6.6). Of particular note is that the thermodynamic parameters for meclofenamic acid (time-dependent) and flufenamic acid (reversible) binding are very similar

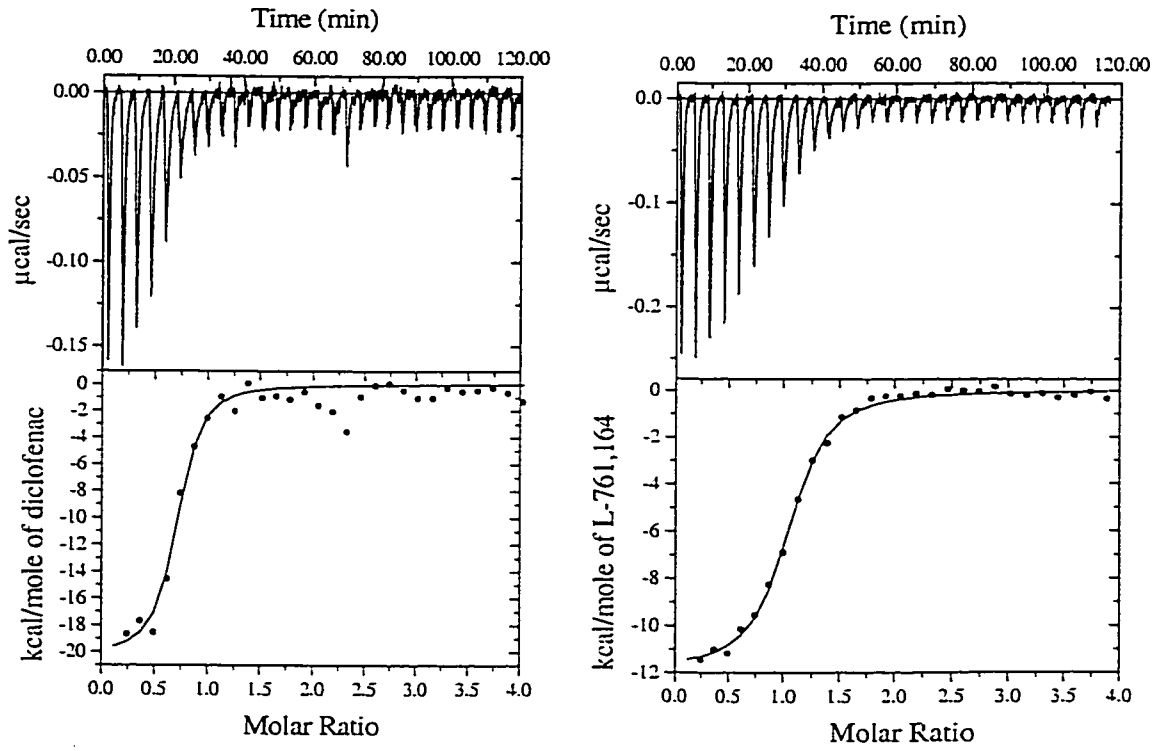

Figure 6.8. Microcalorimetric titration of PGHS-2 with diclofenac and L-761,164. (A) 2.5 µM PGHS-2 was titrated with 42.5 µM diclofenac and (B) 5.5 µM PGHS-2 was titrated with 93.5 µM L-761,164 in 100 mM sodium phosphate, pH 7.0, 1% octylglucoside at 25°C, as described in Section 2.2.15. The heat released per unit time (µcal/s) is plotted versus time where each peak corresponds to an injection of ligand (top panels). The heat of reaction per injection (kcal/mol of ligand) was determined by integration of the area under each peak using Origin software (MicroCal). This value was plotted versus the molar ratio of ligand to PGHS-2 (bottom panels) and fit with Origin software using a single binding site model (eq. 2.1, Section 2.2.1).

Table 6.5. Experimental parameters for ITC analysis of NSAID binding to PGHS-2

NSAID	[PGHS-2] (μM)	[NSAID] (μM)	c[a]	n[b]
Diclofenac	2.5	42.5	52	0.68±0.02
Meclofenamic acid	1.4	23.8	197	1.22±0.04
Flufenamic acid	2.5	42.5	64	0.56±0.03
L-761,164	5.5	93.5	35	1.02±0.01
NS-398	1.7	28.9	30	1.09±0.04

[a]c values are discussed in Section 3.2.1.
[b]n is the observed stoichiometry of binding between the NSAID and PGHS-2 (Section 2.2.1).

Table 6.6. Binding constants and thermodynamic parameters for ITC of inhibitor binding to PGHS-2.

NSAID[a]	K_d (nM)	$\Delta G°$[b] (kcal/mol)	$\Delta H°$ (kcal/mol)	$\Delta S°$[c] (cal/mol)	T_m (FTIR)[d] (°C)
Diclofenac	47.9±17.5	-9.98	-20.22±1.07	-34.36	16
Meclofenamic acid	20.9±10.0	-10.47	-13.26±0.68	-9.36	8.5
Flufenamic acid	38.9±22.7	-10.10	-12.89±0.88	-9.36	8
L-761,164	173.9±15.4	-9.22	-11.82±0.15	-8.72	4.5
NS-398	95.2±26.3	-9.57	-12.19±0.54	-8.73	7

[a]ITC experiments using the MSC ITC instrument (Biotechnology Research Institute). Experiments were conducted in 100 mM sodium phosphate, pH 7.0, 1% octylglucoside.
[b]Error in $\Delta G°$ not reported because $\Delta G°$ was determined from $K_{d(ITC)}$ (eq. 2.4).
[c]Error in $\Delta S°$ not reported because $\Delta S°$ was determined from $\Delta H°$ and $\Delta G°$ (eq. 2.5).
[d]data from Table 6.4
[e]data from Figure 6.7

(Table 6.6). Hence, time-dependency is not reflected in the enthalpy or entropy of binding. Examination of the $\Delta H°$ and $\Delta S°$ values in Table 6.6 demonstrates that entropy-enthalpy compensation is observed for the binding of these five NSAIDs to PGHS-2, as was observed for the binding of aromatic hydroxamic acid analogues to HRP in Figure 3.9.

6.3. Discussion

6.3.1. Secondary structure of PGHS-2 and the effect of NSAID binding

As expected, curvefitting of the amide I/I' spectrum of PGHS-2, in agreement with the X-ray structure (*97-99*), showed that the enzyme is predominantly α-helical. A quantitative analysis of amide I/I' absorption arising from turns, loops, and random structures risks overinterpretation of the data. However, the sensitivity of peptide ν(CO) to variations in H-bonding patterns (*e.g.*, environment, angle) makes it an excellent probe of defined structural elements (e.g. α-helices and β-sheets). This is reflected in the splitting of the amide I/I' α-helical absorption of PGHS-2 into two regions (1654 and 1641 cm^{-1} in $^{1}H_2O$ and 1652 and 1641 cm^{-1} in $^{2}H_2O$), indicative of more (1641 cm^{-1}) and less (1652/4 cm^{-1}) solvent-exposure of helices. Although PGHS-2 is a large globular protein, the solvent exposure of ~13% of its α-helices (Table 6.1) is not surprising. It likely results from the surface-location of helical membrane-binding domain, and the solvent accessibility of the core of the protein due to the COX channel and, to a lesser degree, the POX cleft. Therefore, its sensitivity to solvent exposure makes the amide I/I' α-helical absorption a useful tool for probing tertiary and quaternary structure, in addition to secondary structure.

NSAID binding resulted in a large increase (~16%, Tables 6.2 and 6.3) in amide I/I' α-helical absorption in the 1650-1660 cm^{-1} region for meclofenamic acid and diclofenac, and a smaller increase (~4%) for the other inhibitors investigated. In contrast, the negligible effect of diclofenac on the CD spectrum of PGHS-2 observed here is in agreement with a previous study which showed that indomethacin also has little effect on the CD spectrum of oPGHS-1 (*289*). This is consistent with X-ray data which have shown that NSAID binding does not involve large changes in secondary structure (*98*). The crystal structure supports the assignment of ~13% of the absorption of the 1641 cm^{-1} band to α-helices and indicates that NSAID binding results in a reduction in solvent accessibility, likely due to a reduction in solvent access to the COX channel, and formation of a more compact protein structure with a reduction in conformational stability. Similar results were observed in $^{1}H|^{2}H$ exchange studies on transferrins and lactoferrins (*190*) which showed that, in agreement with X-ray scattering (*308*) and hydrodynamic studies (*309*), ligand binding resulted in more compact protein structures. If the mobility of the loop containing Arg277 is restricted as a result of this type of general tightening of the protein structure, this would explain the reduction in susceptibility of PGHS to proteolysis observed upon NSAID binding (*289*). Since conformational flexibility is a dynamic protein property, it is not easily inferred from static crystal structures. Therefore, it is not surprising that changes in the conformational stability of PGHS-2 on NSAID binding were observed here by FTIR, CD and DSC, despite crystal structure data indicating that NSAID binding causes no change in the overall structure of PGHS-2.

No trends were observed in curvefitting results (Tables 6.2 and 6.3) for reversible versus time-dependent inhibitors. This is not surprising for three reasons: (1) comparison of the X-ray structures of the unliganded and NSAID-bound forms of mPGHS-2 has shown that the secondary structure of only five residues (118-122, PGHS-1 numbering) is changed on NSAID binding (*98*), (2) time-dependency has been postulated to be the result of an equilibrium between two three-residue H-bonding networks at the mouth of the COX cavity (*290*), and (3) tryptophan fluorescence quenching by bound NSAIDs shows that there is no major change in the inhibitor binding mode during the isomerization to the tightly-bound form for time-dependent inhibitors (*172*).

6.3.2. Effect of NSAIDs on PGHS-2 conformational stability

FTIR-monitored thermal denaturation of PGHS-2 showed almost complete loss of native structure at temperatures above 66°C (Figure 6.5). Similar FTIR-monitored thermal denaturation experiments have been performed on HRP and CCP (*310*). Like PGHS-2, HRP is glycosylated and possesses multiple disulfide bridges, whereas CCP is not glycosylated and has no disulfide bridges. Nonetheless, the thermal denaturation pattern of PGHS-2 resembles that of CCP (*310*), since HRP maintains its secondary structure up to 80°C. Holzbaur et al. (*310*) suggested that the stability of HRP is due largely to its 2 bound calcium ions and its 4 disulfide bridges, which are dispersed throughout the polypeptide. Although PGHS-2 contains no calcium ions, it possesses 5 disulfide bridges; however, 3 of these are intradomain in the small EGF-like domain and there are no intradomain disulfide bridges within the (~55 kDa) catalytic domain (*98*). Therefore, the location of the disulfides in PGHS-2 suggests that they are less capable of stabilizing the overall structure than the more dispersed disulfides of HRP.

NSAID binding to PGHS-2 causes changes not only in the degree of solvent accessibility of the protein core as detected by curvefitting of the amide I/I' band (Figure 6.2), but also in the conformational stability of the enzyme. The loss of amide II intensity with temperature parallels loss of helical intensity during thermal denaturation of the binary complexes (Figures 6.5, 6.6 and 6.7). In a similar study, the increase in T_m observed upon the binding of ADP or ATP to mitochondrial F1 and was postulated to be due to tightening of the bonds between the neighboring α and β subunits (*311*). The observation here that the slow phase of secondary structure loss (40-58°C) is shifted to higher temperatures in the presence of NSAIDs (Figure 6.5) suggests that increases in the T_m of PGHS-2 upon NSAID binding are due to stabilization of the PGHS-2 dimer, thus protecting it from dissociating and unfolding. This is supported by a recent report (*304*) that dimer dissociation occurs prior to loss of secondary structure in guanidinium hydrochloride denaturation of PGHS-1 and -2.

Kulmacz (*173*) observed that time-dependent NSAIDs resulted in slightly increased protection against limited proteolysis of oPGHS-1 compared to reversible NSAIDs. However, no trends were observed here for reversible versus time-dependent inhibitors (Table 6.4) in their effect on the conformational stability of PGHS-2. This is in agreement with a more recent study of limited proteolysis which found that trypsin resistance is a reflection of the initial association of both reversible and time-dependent inhibitors with oPGHS-1(*312*). Interestingly, diclofenac resulted in a ~2 - 4-fold increase in the conformational stability of PGHS-2 as compared to the other NSAIDs investigated (Table 6.4). This, in combination with the curvefitting data (Figure 6.2), suggests that diclofenac binding results in reduced solvent accessibility, possibly by

tightening contact between the monomers. It has been suggested that diclofenac and meclofenamic acid possess different binding modes from other NSAIDs because they do not inhibit either ASA-acetylated PGHS-2 or the S516M mutant (PGHS-2 numbering) (*294*). ASA acetylates PGHS-2 on Ser516 (PGHS-2 numbering, Ser530 in oPGHS-1) and blocks the production of PGG_2. However, both ASA-acetylated PGHS-2 and the S516M mutant can still turn over AA to produce 15-(R)-hydroperoxy-eicosatetraenoic acid (15-HPETE) (*305*). This activity can be blocked by NSAID binding, with the exception of diclofenac and meclofenamic acid (*294*).

6.3.3. Thermodynamics of NSAID binding to PGHS-2

Knowledge of the magnitude and sign of the enthalpy and entropy of binding allow for an evaluation of the contribution of the various interactions involved in ligand binding. It is difficult to interpret these values for a single ligand-enzyme complex (*e.g.*, PGHS-2-diclofenac) because of the large number of interactions involved. However, comparison of a series of structurally related compounds, like the fenamates tested in this study, can reveal the underlying thermodynamic forces controlling binding (*213*).

Arg106 (PGHS-2 numbering, Arg120 in oPGHS-1) has been shown to be important in binding the carboxylate group of carboxylate-containing NSAIDs (*307*). It is less crucial to PGHS-2 inhibition by the two fenamates, meclofenamic acid and diclofenac (*307*), suggesting that their mode of binding is different from other carboxylate-containing NSAIDs. However, the crystal structure of PGHS-2 complexed with meclofenamic acid demonstrates the presence of a salt bridge between the carboxylate group of meclofenamic acid and Arg106 of PGHS-2. Additionally, a recent study modeling the binding of a group of fenamates, including meclofenamic acid,

flufenamic acid, and diclofenac to PGHS-1 suggests that the carboxylate group of these compounds forms an electrostatic interaction with the guanidinium group of Arg120 (oPGHS-1 numbering) (*313*). Additional support for this binding model is demonstrated by the inability of meclofenamic acid and diclofenac to inhibit either PGHS-2 acetylated by ASA at Ser516 (PGHS-2 numbering) or the S516M mutant. This suggests that these compounds bind similarly to the profens, with the chlorine-substituted ring in proximity of Ser516 and the carboxylate group closer to the mouth of the COX channel, such that steric hindrance occurs between the chlorine substituents and acetylated Ser516 (*172, 294*). The thermodynamic data on the binding of the fenamates investigated in this study is interpreted using the model proposed by Pouplana et al. (*313*).

The placement of the chlorine atoms in diclofenac and meclofenamic acid (Figure 6.1) has the effect of restricting the rotation of the aromatic rings relative to each other, resulting in an almost perpendicular arrangement between the two aromatic rings (*313*). The difference in the binding of diclofenac, compared to the other fenamates investigated, is likely due to a combination of the perpendicular arrangement of the aromatic rings and the additional methylene group, which extends the reach of the carboxylate group. Since salt bridges are electrostatic interactions, and extension of the carboxylate group toward Arg106 would increase the strength of the salt bridge. However, since the chlorine atoms reduce the rotation of the aromatic rings relative to each other, this salt bridge likely forces diclofenac into a position that is entropically unfavorable. Therefore, it is possible that the enthalpic advantage of the salt bridge and the entropic disadvantage of the resulting constrained conformation balance such there is no overall effect on the free energy of binding. In meclofenamic acid, the carboxylate

moiety is attached directly to the nonchlorinated ring (Figure 6.1), likely resulting in a weaker salt bridge to Arg106 ($\Delta H°$ = -20.22 and –13.26 kcal/mol for diclofenac and meclofenamic acid, respectively) and a less constrained conformation (ΔS = -34.36 and –9.36 cal/mol for diclofenac and meclofenamic acid, respectively).

Diclofenac binding is much more enthalpically favourable and entropically unfavorable ($\Delta\Delta H°$ = -8.4 kcal/mol and $T\Delta\Delta S°$ = -7.64 kcal/mol) compared to L-761,164. Examination of the structures of diclofenac and L-761,164 (Figure 6.1) demonstrates that the only difference between these two compounds is the substitution of the NH group, which bridges the two phenyl rings in diclofenac, by an oxygen atom in L-761,164. It is possible that the large differences in $\Delta\Delta H°$ and $T\Delta\Delta S°$ between diclofenac and L-761,164 are due to loss of an H-bond formed by the NH group. However, it is likely more complicated because the large difference in the enthalpy of binding suggests that a charged H-bond (Section 3.3.1.1.1, Use of BZA, 2'-HA and N-BH to isolate the contribution to binding of specific HRP-BHA H-bonds) is formed by diclofenac and not by L-761,164. H-bond donation of the ring-bridging NH group to a negatively charged Glu or Asp residue is not possible since there are no Glu or Asp residues within the COX channel. Therefore, replacement of the NH group of diclofenac with an oxygen atom may result in an unfavorable interaction (*i.e.*, electronic repulsion) which causes a shift in the binding mode and weakening of the salt bridge between the carboxylate group of L-761,164 and Arg106.

The enthalpy of binding for the reversible NSAID, flufenamic acid (-12.89 kcal/mol), is quite similar to that of the time-dependent NSAID, meclofenamic acid (-13.26 kcal/mol), from which it differs (Figure 6.1) by the absence of chlorine substituents

and the replacement of the methyl group by a trifluoromethyl group. This suggests that the 2 chlorine atoms do not play a major role in binding and that time-dependency is not related to the enthalpy or entropy of binding. The similarity in the energetics of meclofenamic acid, flufenamic acid, L-761,164, and NS-398 binding suggests that despite differences in the relative arrangement of their rings, these compounds bind in the same orientation within the COX channel. This is supported by the recent modeling study of NS-398 binding to PGHS-2, in which the carboxylate group of NS-398 was observed to be in proximity with Arg106 (*314*).

7. INACTIVATION OF PROSTAGLANDIN SYNTHASE-2

7.1. INTRODUCTION

A consensus has emerged, based on the protective effect of reducing substrates, that the irreversible loss of PGHS activity occurs as the result of an unstable protein radical intermediate generated during POX or COX catalysis (*57, 58*). Although the identity of this radical is unknown, support for the existence of at least one other radical, in addition to that located on Tyr385, is provided by the presence of endogenous reductants within PGHS, the ability of the inactive Y385F mutant of PGHS-1 to form a tyrosyl radical and EPR studies demonstrating the formation of a second tyrosyl radical in the presence of bound inhibitor (*122, 141, 142, 144, 315, 316*). The detection of tyrosyl radical(s) in addition to that located on Tyr385, suggests crosslinking via dityrosine formation as a possible mechanism of inactivation. LPO, another member of the mammalian peroxidase superfamily, has recently been shown to undergo dityrosine crosslinking leading to oligomeric forms in the presence of H_2O_2 (*50*). Although the dimeric and trimeric forms of LPO retain full activity (*50*), this need not necessarily be the case for other peroxidases, as crosslinking could result in conformational changes that inactivate the enzyme or block substrate access.

There are several tyrosine residues in PGHS-2 and those considered the most likely to be involved in intermolecular dityrosine formation are shown in Figure 7.1. Tyr402 and Tyr409 are 17 and 13 Å, respectively, from the heme iron and 14 and 21 residues, respectively, from the proximal His388. Therefore, electron transfer through the peptide backbone from one or both of these surface-exposed tyrosines to the heme iron would

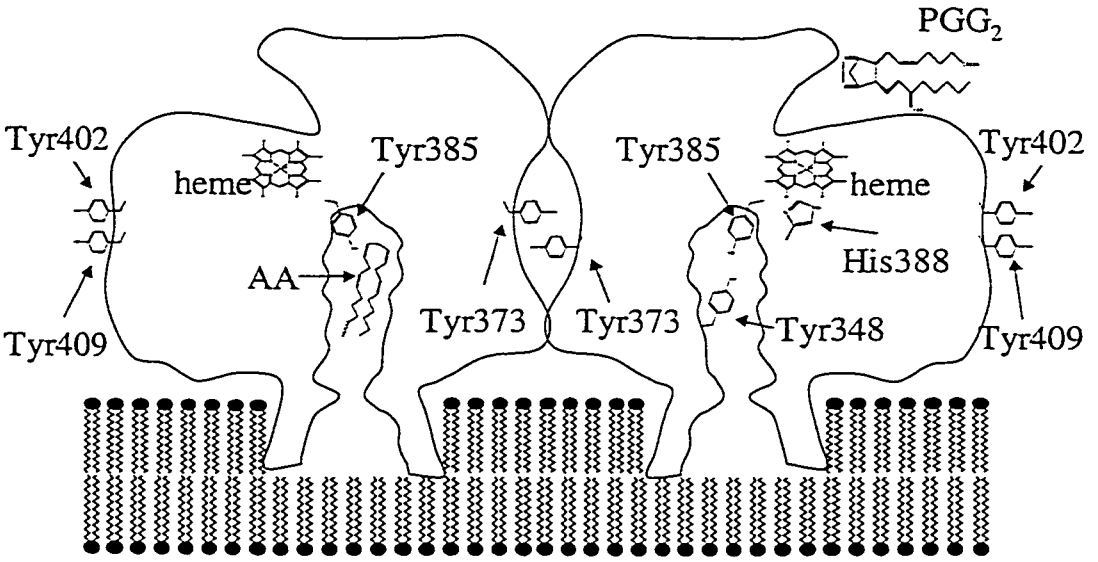

Figure 7.1. Location of exposed tyrosine residues in PGHS. Cross-section of Figure 1.5 showing the central pore at the dimeric interface (PGHS-1 numbering).

result in the formation of tyrosyl radicals that could form dityrosine crosslinks.

Another tyrosine, Tyr373, is particularly interesting because it is located among the residues lining the central pore of the dimeric interface (Figure 7.1). Tyr373 is 29 Å through space from the heme iron, but only 15 residues from the proximal histidine, thus electron transfer through the peptide backbone is conceivable. Although the aromatic rings of the Tyr373 residues from the two monomers are ~11 Å apart in the crystal structure of mPGHS-2 (*98*), their location at the surface of the central pore may allow them enough flexibility to rotate and come into contact, thus allowing for the formation of an intermolecular dityrosine crosslink between the monomers. This is similar to the situation recently observed in LPO, in which a Tyr289-Tyr289 dityrosine crosslink is formed at the subunit interface between LPO monomers (*50*).

Another possible mechanism of inactivation could involve enzyme modification by activated substrate species There are several radical intermediates involved in COX catalysis (Figure 1.6). The reactive nature of these intermediates raises the possibility that COX inactivation occurs via substrate incorporation. As a preliminary step, ^{14}C-AA was used to probe whether substrate incorporation occurs and if so, in what ratio. A similar study with oPGHS-1 showed that stoichiometric incorporation of ^{14}C-AA does occur, but on a 30-fold longer time-scale (~ 60 min) than COX inactivation (~ 2 min) suggesting that incorporation of reactive intermediates is not the major mechanism of COX inactivation (*181*). Although stoichiometric ^{14}C-AA incorporation suggests nonrandom attachment, the residue(s) modified were not determined by Kulmacz (*181*). Investigation of both crosslinking and incorporation of intermediates require peptide

mapping to identify the modified residues; therefore, suitable conditions for PGHS-2 digestion were developed in this work.

7.2. RESULTS

7.2.1. AA incorporation as a potential mechanism of COX inactivation

The conditions used here to investigate ^{14}C-AA incorporation into PGHS-2 (6 μM PGHS-2 and 140 μM ^{14}C-AA) were similar to those used by Kulmacz (6 μM oPGHS-1 and 140 μM ^{14}C-AA) (*181*). The COX active-site concentration in a 1 μM solution of PGHS-2 was determined to be 0.54 μM from an active-site titration with diclofenac shown in the Ackermann-Potter plot in Figure 7.2. This was produced by plotting the activity of 1 μM COX samples, preincubated with 0 - 5 μM diclofenac, versus diclofenac concentration. The concentration of COX active sites equals the diclofenac concentration required to decrease the COX activity to background levels, and was observed to be 0.54 μM (Figure 7.2). This indicates that either the estimation of protein concentration is inaccurate or that 46% of the protein did not bind diclofenac. Assuming that enzyme that does not bind diclofenac is inactive, the Ackermann-Potter plot corrects for any inactive enzyme present in the starting material.

PGHS-2 (6 μM, 3.2 μM active-sites) was incubated for 2 h in 100 mM sodium phosphate, pH 7.0, containing 0.5% octylglucoside and 140 μM ^{14}C-AA (24 Ci/mol). At time points of 0.2 - 120 min, duplicate 1.8-μg aliquots were withdrawn and analyzed by SDS-PAGE. Two identical sets of gels were generated and one set was used to prepare the autoradiograph shown in Figure 7.3. The PGHS-2-containing bands were excised from the second set of gels and the ^{14}C-AA content determined by scintillation counting

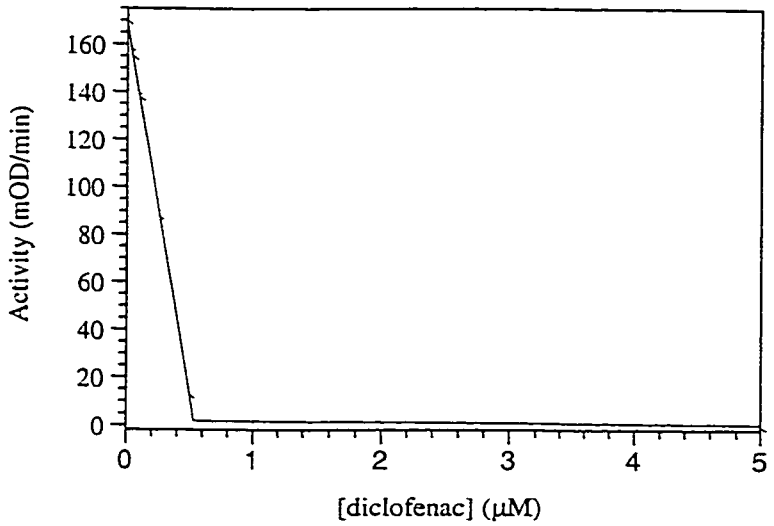

Figure 7.2. Ackermann-Potter plot of PGHS-2 active site titration. Following 6 h dialysis in 100 mM sodium phosphate, pH 7.0, 1% octylglucoside, to remove homovanillic acid, 1.0 μM PGHS-2 was preincubated with 0 - 5 μM diclofenac at 25 °C for 1 h. The COX activity of 0.1 μM PGHS-2 in 100 mM sodium phosphate, pH 6.5, containing 1 mg/mL gelatin, 1 μM heme, 100 μM AA, and 100 μM TMPD was determined at 25 °C for 1 min. The concentration concentration of active COX sites (0.54 μM) equals the diclofenac concentration at which the COX activity reaches the baseline, *i.e.*, at the intersection of the two straight-line portions of the plot.

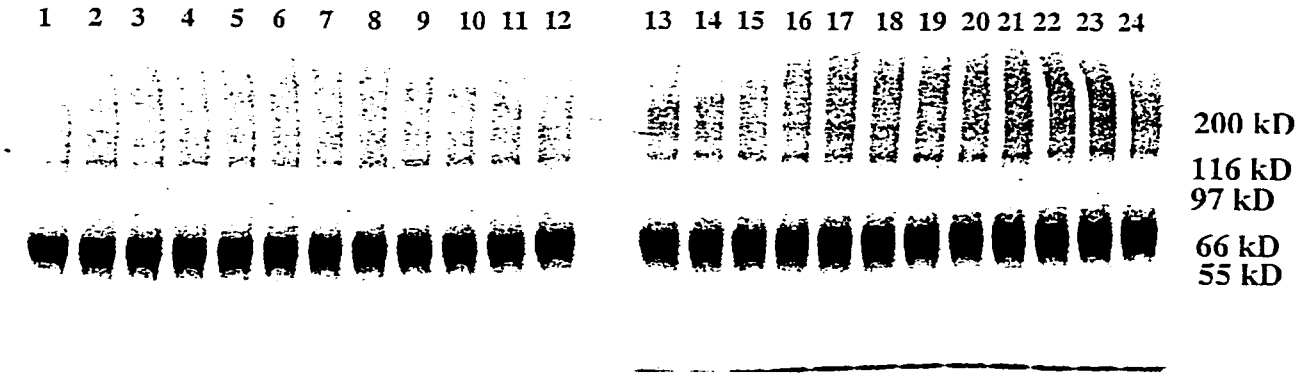

Figure 7.3. Incorporation of ^{14}C-AA into PGHS-2 versus time. A PGHS-2 sample containing 3.2 μM active COX sites was incubated in 100 mM sodium phosphate, pH 7.0, containing 0.5% octylglucoside and 140 μM ^{14}C-AA (24 Ci/mol). At time points of 0.2 - 120 min 1.8-μg aliquots were withdrawn, mixed with SDS-PAGE sample buffer, heated at 100°C for 5 min, and run on 8%, 1-mm SDS-PAGE gels. Following Coomassie staining, one set of gels were dried and exposed to film to produce the autoradiographs: lane 1, 12 s; lane 2, 20 s; lane 3, 30 s; lane 4, 40 s; lane 5, 50 s; lane 6, 60 s; lane 7, 80 s; lane 8, 100 s; lane 9, 2.0 min; lane 10, 2.5 min; lane 11, 3.0 min; lane 12, 3.5 min; lane 13, 4.0 min; lane 14, 4.5 min; lane 15, 5.0 min; lane 16, 7.5 min; lane 17, 10 min; lane 18, 15 min; lane 19, 20 min; lane 20, 30 min; lane 21, 40 min; lane 22, 60 min; lane 23, 90 min; lane 24, 120 min.

(Table 7A.1). ^{14}C-AA incorporation was complete prior to the first time point (12 s) and did not change between 12 s and 120 min (Figure 7.3). This is in contrast to the previous report by Kulmacz (*181*), in which ^{14}C-AA incorporation into oPGHS-1 was observed to require ~ 1 h to plateau at a ratio of 1 mol ^{14}C-AA per mol oPGHS-1 (*181*). The stoichiometry of ^{14}C-AA incorporation (Table 7A.1) observed in this study was ~ 1.2 ± 0.075 mol ^{14}C-AA per mole of COX active sites for all time points. In a parallel experiment, 6 μM PGHS-2 was preincubated in 100 mM sodium phosphate, pH 7.0, 0.15% octylglucoside, containing 200 μM AA and the COX activity declined to 10% of the control (no AA in the preincubation) within the mixing time (10 s). Since the time required for inactivation of its COX activity is essentially the same as that required for stoichiometric incorporation of ^{14}C-AA, PGHS-2 likely incorporates AA within the COX channel in a nonrandom manner.

There is a difference of at least 300-fold in the time determined in this study for stoichiometric incorporation of ^{14}C-AA into PGHS-2 (less than 12 s) and that reported previously for oPGHS-1 (~ 60 min) (*181*). This may be due to isoform differences or to experimental differences (*e.g.*, Kulmacz does not report the use of detergent although it is required to solubilize PGHS). Therefore, ^{14}C-AA incorporation into oPGHS-1 (Cayman Chemical Company) was also investigated in this study. The concentration of active COX sites in a 3.5 μM oPGHS-1 sample was determined by titration with diclofenac (Ackermann-Potter data not shown) to be 1.05 μM. Figure 7.4 shows that stoichiometric incorporation of ^{14}C-AA into oPGHS-1 occurs within ~ 5 - 10 min and does not increase between ~ 10 - 120 min. However, most of the incorporation (~ 75%)

Figure 7.4. Incorporation of ^{14}C-AA into oPGHS-1 versus time. oPGHS-1 (3.5 μM, 1.05 μM active site) was incubated in 100 mM sodium phosphate, pH 7.0, containing 0.5% octylglucoside and 140 μM ^{14}C-AA (24 Ci/mol). At time points between 17 s - 120 min duplicate 0.25 μg aliquots were withdrawn, mixed with SDS-PAGE sample buffer and treated as described in Figure 7.3. (**A**) Autoradiograph: Lane 1, 17 s; lane 2, 24 s; lane 3, 30 s; lane 4, 40 s; lane 5, 50 s; lane 6, 60 s; lane 7, 80 s; lane 8, 100 s; lane 9, 2.0 min; lane 10, 2.5 min; lane 11, 3.0 min; lane 12, 3.5 min; lane 13, 4.0 min; lane 14, 4.5 min; lane 15, 5.0 min; lane 16, 7.5 min; lane 17, 10 min; lane 18, 15 min; lane 19, 20 min; lane 20, 31 min; lane 21, 40 min; lane 22, 63 min; lane 23, 90 min; lane 24, 120 min. (**B**) Stoichiometry of incorporation (ratio of ^{14}C-AA:active PGHS-2 COX sites) from Table 7A.2 (appendix 7A) was plotted versus incubation time.

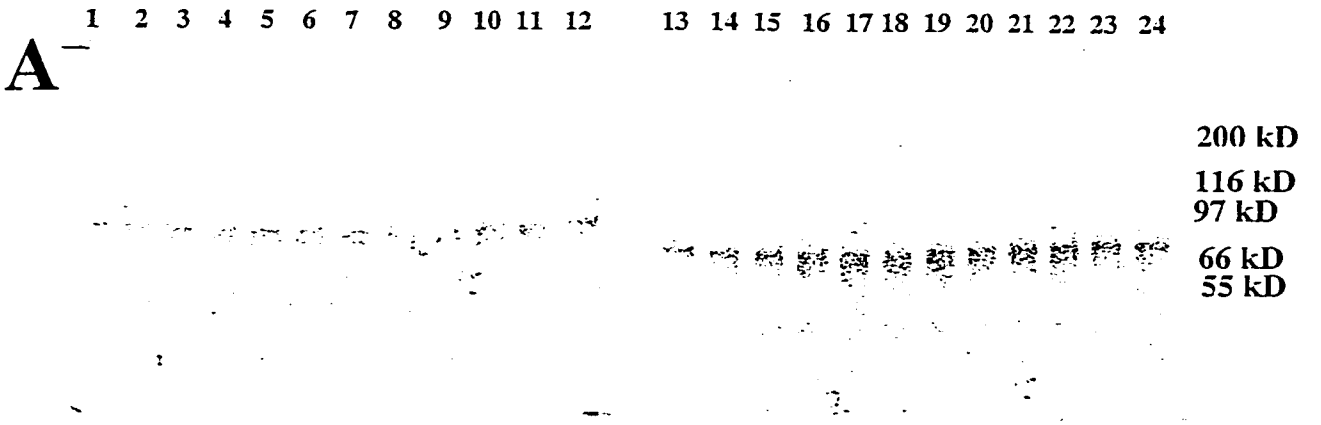
A
1 2 3 4 5 6 7 8 9 10 11 12 13 14 15 16 17 18 19 20 21 22 23 24
200 kD
116 kD
97 kD
66 kD
55 kD

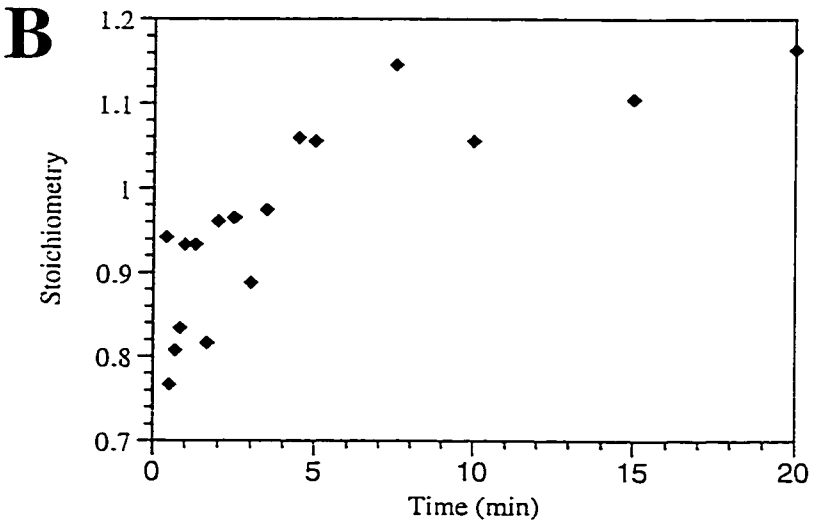
B
Stoichiometry
1.2
1.1
1
0.9
0.8
0.7
0
5
10
15
20
Time (min)

into oPGHS-1 occurs prior to the first time point (17 s). This is in contrast to previous finding that incorporation of AA into oPGHS-2 requires 1 h for completion (*181*).

In Figure 7.3 incubation of PGHS-2 with AA is seen to result in the formation of higher molecular weight bands which gradually increase in intensity with time. The effect of AA and the POX reducing substrate TMPD on the oligomerization of PGHS-2 are shown in Figure 7.5. In the presence of AA alone (lane 3, Figure 7.5) faint bands of ~140 and ~210 kDa are produced, which correspond to the molecular weights of the dimeric and trimeric forms of PGHS-2.

There are two likely mechanisms for AA-dependent crosslinking of PGHS-2: (1) levuglandins (*317, 318*) and (2) dityrosine formation (*50, 51*). In an aqueous environment PGH_2, the product of PGHS, is unstable and is converted spontaneously to a variety of products including the levuglandins, LGD_2 and LGE_2 (Figure 7.6) (*319*). These compounds have been shown to covalently modify surface lysine residues (Figure 7.6) and to cause protein and DNA crosslinking (*317, 318, 320*). PGHS-2 has several surface-exposed lysine residues that could be involved in crosslinking via levuglandins. Alternatively, as discussed in Section 7.1, there are several tyrosine residues in PGHS-2 (Figure 7.1) that may be involved in crosslinking. Both CCP and LPO have been recently observed to undergo H_2O_2-dependent crosslinking via dityrosine formation (*50, 51*). To distinguish between the two mechanisms, further experiments were conducted using H_2O_2 as a POX substrate, thus eliminating any crosslinking due to levuglandin formation.

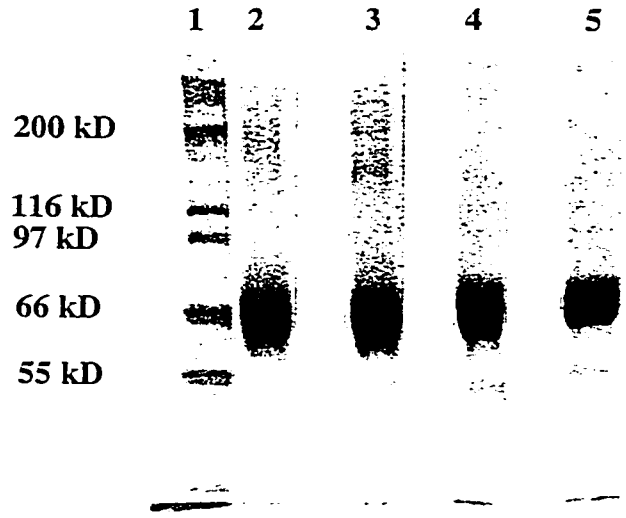

Figure 7.5. Effect of AA and TMPD on the crosslinking of PGHS-2. 6.6 μM PGHS-2 was incubated in 100 mM sodium phosphate, pH 6.5, alone and with 20 μM AA and/or 20 μM TMPD for 30 min at 25 °C. Aliquots of 10 μg were mixed with SDS-PAGE sample buffer, heated at 100°C for 5 min, run on a 8%, 1-mm SDS gel, and Coomassie stained. Lane 1, molecular weight markers; lane 2, 10 μg of PGHS-2 incubated with both AA and TMPD; lane 3, 10 μg of PGHS-2 incubated with AA only; lane 4, 10 μg of PGHS-2 incubated with TMPD only; lane 5, 10 μg of PGHS-2 incubated without either substrate.

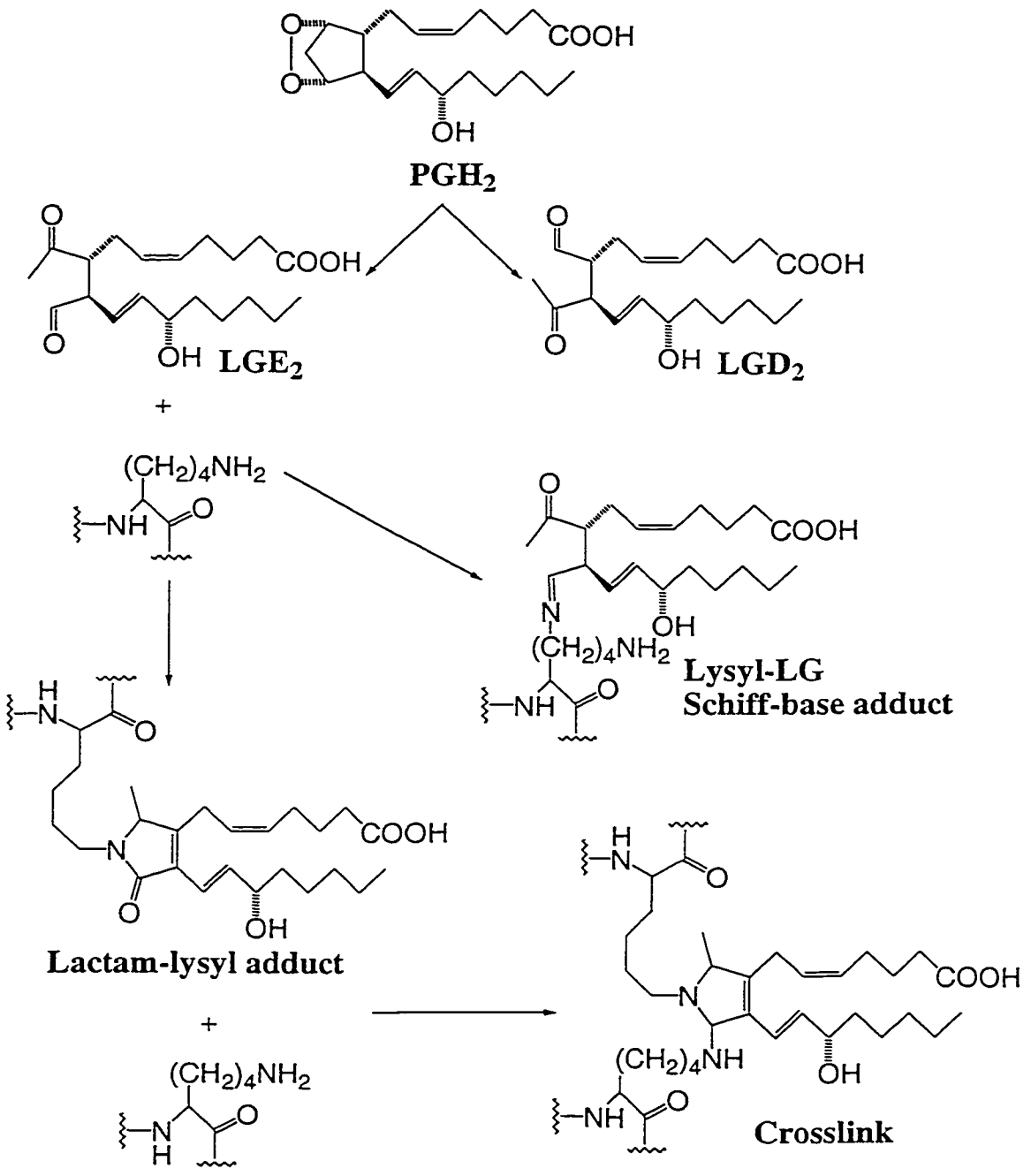

Figure 7.6. Levuglandin-based mechanism for AA-dependent PGHS-2 crosslinking. Crosslinking and lysine modification by LGE_2 are shown as an example and are also possible for LGD_2 (*317, 318, 321*).

7.2.2. Peroxide-dependent inactivation of the POX activity of PGHS-2

When PGHS-2 was incubated in the presence of 50 - 1000 molar equivalents of H_2O_2, a faint dimeric band (~ 140 kDa) was visible (lanes 1 - 4, Figure 7.7) and a trimeric band (~ 210 kDa) became apparent at 1000 molar equivalents (lane 4, Figure 7.7). In contrast to LPO, for which maximum yields of the dimeric and trimeric forms were 49% and 5%, respectively, in the presence of 4 molar equivalents of H_2O_2 without reducing substrate (*50*), only a small percentage of PGHS-2 is converted to oligomeric forms. At 10^4 molar equivalents of H_2O_2 oligomeric forms were not observed and the monomeric form is less defined (lane 5, Figure 7.7). The presence of phenol, a reducing substrate, may slightly induce the formation of oligomeric forms as seen by the reduction of the monomeric band and the presence of dimeric, trimeric, and undefined bands of greater than 200 kDa in the presence of 2 mM phenol and 100 - 1000 molar equivalents of H_2O_2 (lanes 10 - 13, Figure 7.7).

The radical scavenger mannitol was found to have no effect on PGHS-2 oligomer formation either in the absence (lanes 3 - 5, Figure 7.8) or presence of phenol (lanes 13 - 15, Figure 7.8). This suggests that any radicals formed are located in an environment that is inaccessible to mannitol. The effect of N-acetyltyrosinamide (NATA) was also investigated and observed to have no effect of H_2O_2-dependent PGHS-2 oligomerization either in the absence (lanes 1 and 2, Figure 7.8) or presence of phenol (lanes 11 and 12, Figure 7.8). At pH 8.0, the same extent of oligomerization was observed in Tris (lanes 7, 10, 16 and 19, Figure 7.8) and sodium phosphate buffers (lanes 8 and 17, Figure 7.8). Only in borate, pH 10.0, was a slight

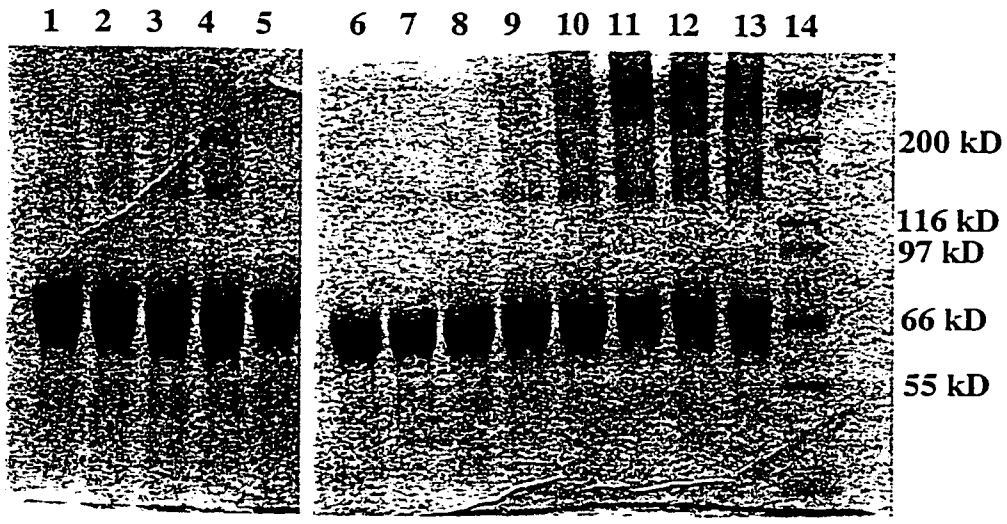

Figure 7.7. SDS-PAGE analysis of the effect of H_2O_2 concentration and phenol on PGHS-2 crosslinking. 10 μM PGHS-2 was incubated in 100 mM Tris, pH 8.0 and 0 - 100 mM H_2O_2 for 30 min at 25°C. Aliquots of 10 μg were mixed with SDS-PAGE sample buffer, heated at 100°C for 5 min, run on a 8%, 1-mm SDS gel, and Coomassie stained. Lanes 1 - 5, no phenol and 0.5, 1, 5, 10, and 100 mM H_2O_2; lanes 6 - 13, 2 mM phenol and 0, 0.01, 0.1, 0.5, 1, 2, 5, and 10 mM H_2O_2; lane 14, molecular weight markers.

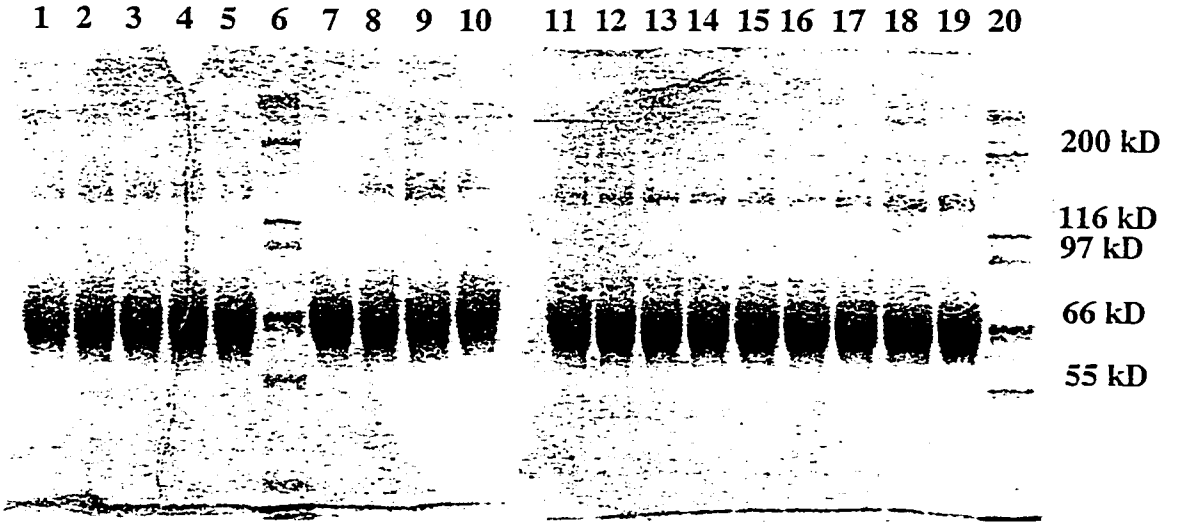

Figure 7.8. Effect of pH, phenol, and radical scavengers on PGHS-2 crosslinking. All incubations contained 10 μM PGHS-2 and were carried out for 30 min at 25 °C. Aliquots of 10 μg were mixed with SDS-PAGE sample buffer, heated at 100°C for 5 min, run on a 8%, 1-mm SDS gel, and Coomassie stained. Lanes 1 and 2, 100 mM sodium phosphate, pH 8.0, and 200 μM H_2O_2 and 100 and 10 μM N-acetyltyrosinamide, respectively; lanes 3 - 5, 100 mM sodium phosphate, pH 8.0, and 200 μM H_2O_2 and 100, 10, 1 mM mannitol, respectively; lanes, 6 and 20, molecular weight markers; lanes 7 and 10, 100 mM Tris, pH 8.0, and 200 μM H_2O_2; lane 8, 10 mM sodium phosphate, pH 8.0, and 200 μM H_2O_2; lane 9, 100 mM borate, pH 10.0, and 200 μM H_2O_2; lanes 11 - 15, same as lanes 1 - 5 but with 2 mM phenol; lanes 16 -19, same as lanes 7 - 10 but with 2 mM phenol.

increase in dimerization observed both in the absence and presence of phenol (lanes 9 and 18, Figure 7.8).

The finding that the majority of PGHS-2 is not covalently crosslinked in the presence of a range of H_2O_2 concentrations (Figures 7.7 and 7.8) suggests that oligomerization is not responsible for its H_2O_2-dependent inactivation. PGHS-2 (0.5 μM) was observed to be completely inactivated by the addition of 25 μM H_2O_2 (50 molar equivalents) in the absence of a reducing substrate. The presence of guaiacol as a reducing substrate resulted in complete protection of the POX activity of PGHS-2 against H_2O_2-dependent inactivation (Figure 7.9). The sensitivity of PGHS-2 to H_2O_2 may be due in part to its inability to carry out the catalactic conversion of H_2O_2 (to H_2O and O_2) to the same extent as other, less H_2O_2-labile, peroxidases (*e.g.*, HRP). Figure 7.10 demonstrates that when 2 μM peroxidase (PGHS-2 or HRP) is incubated with 200 μM H_2O_2, O_2 is evolved via catalactic activity ($2H_2O_2 \rightarrow O_2 + 2H_2O$). PGHS-2 is capable of catalactic turnover of less than 100 molar equivalents of H_2O_2, (Figure 7.10) in comparison to HRP, which is able to turnover in excess of 400 molar equivalents of H_2O_2 (Section 4.2.2.2). The addition of a second aliquot of 200 μM H_2O_2 (at ~ 6.5 min) resulted in negligible O_2 production by PGHS-2. This is in agreement with the results shown in Figure 7.9, which showed that 50 molar equivalents of H_2O_2 was sufficient to completely inactivate the POX activity of PGHS-2 in the absence of a reducing substrate.

Although intermolecular or intersubunit dityrosine formation resulting in oligomerization is likely not responsible for POX inactivation, it is possible that intramolecular crosslinking may be involved (Figure 7.1). Peptide mass mapping should allow the identification of amino acid residues modified in both AA-dependent COX and

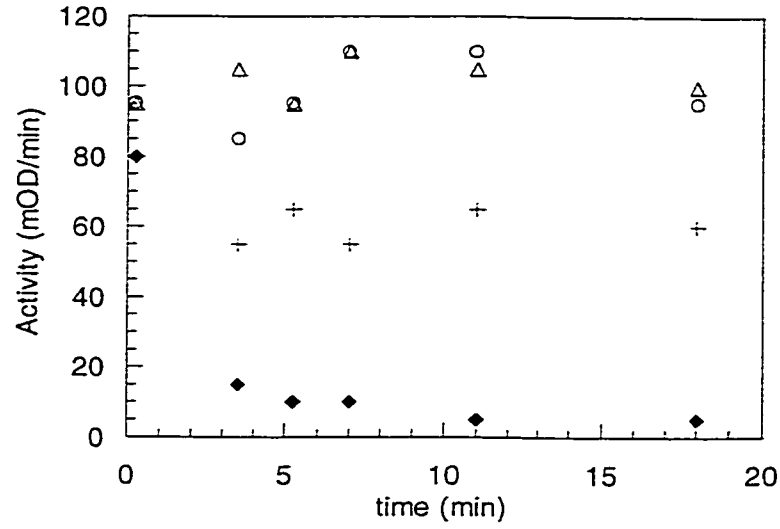

Figure 7.9. Inactivation of PGHS-2 POX activity by H_2O_2 and protection by guaiacol. 0.5 μM PGHS-2 was preincubated in 100 mM sodium phosphate, pH 7.0, with (O) 6.25 μM H_2O_2, (+) 12.5 μM H_2O_2, (♦) 25 μM H_2O_2 and (Δ) 25 μM H_2O_2 with 5 mM guaiacol for 0.25 - 18 min at 25°C prior to assaying POX activity in 100 mM sodium phosphate, pH 7.0, containing 500 μM H_2O_2 and 5 mM guaiacol as described in Section 2.2.3.

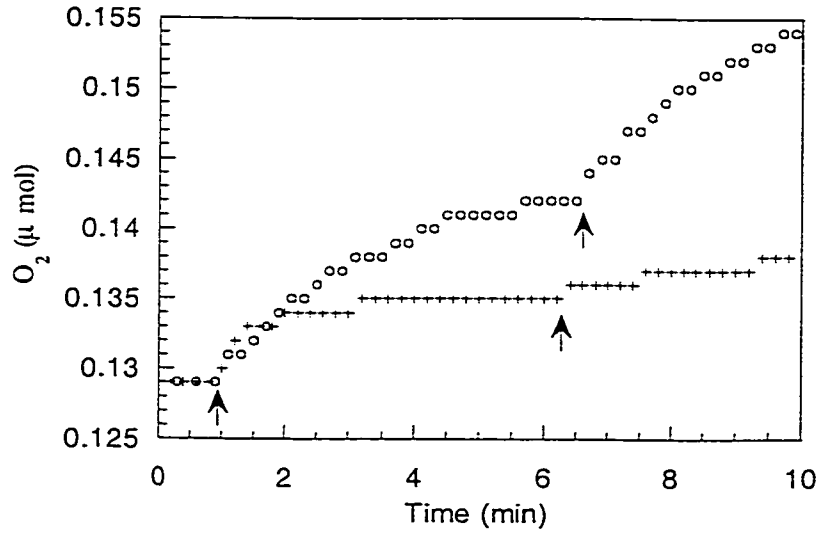

Figure 7.10. Comparison of catalactic H_2O_2 turnover by PGHS-2 and HRP. 2 μM (1.2 nmol) HRP (O) or PGHS-2 (+) were incubated in 100 mM sodium phosphate, pH 7.0, at 25°C and aliquots of 200 μM H_2O_2 were added at ~ 1 and ~ 6.5 min (at arrows). O_2 production (μmol) was measured as described in Section 2.2.6.

H_2O_2-dependent POX inactivation. PGHS-2 possesses a number of features that make it a difficult target for peptide mass mapping: (1) it is highly resistant to proteolytic digestion (*172*), (2) it requires the presence of detergent (*186*) to remain soluble as it has a large hydrophobic surface area and has a tendency to aggregate and bind very tightly to reversed-phase chromatography columns (data not shown), (3) PGHS-2 contains two free Cys residues and five disulfide bonds, which must be broken and capped to prevent disulfide shuffling, and (4) the enzyme is heterogeneously glycosylated (*322*), thus requiring deglycosylation to produce a peptide mass map that can be interpreted accurately (Dr. J. Kelly, personal communication). A digestion protocol was developed which eliminated complications due to these factors. Figure 7.11 shows that both deglycosylation (lane 5) and tryptic digestion (lanes 1, 2 and 6) of PGHS-2 were successful using this protocol. Time constraints did not allow for peptide mass mapping.

7.3. Discussion

Stoichiometric incorporation of ^{14}C-AA into PGHS-2 was observed here to be a rapid process, complete within 12 s (Figure 7.3). Incorporation of ^{14}C-AA into oPGHS-1 was observed in this study to require ~ 5 - 10 min to plateau at a level of one mol of ^{14}C-AA per mol of oPGHS-1 (Figure 7.4). This is in contrast to the observation by Kulmacz (*181*) that stoichiometric ^{14}C-AA incorporation into oPGHS-1 required ~1 h to plateau. The rapid, stoichiometric incorporation of ^{14}C-AA observed in this study correlates with the rapid inactivation of PGHS observed here under similar conditions, suggesting that inactivation via attack of an activated substrate metabolite may be a predominant mechanism. The lack of increase in labeling between 12 s -120 min (Figure 7.3)

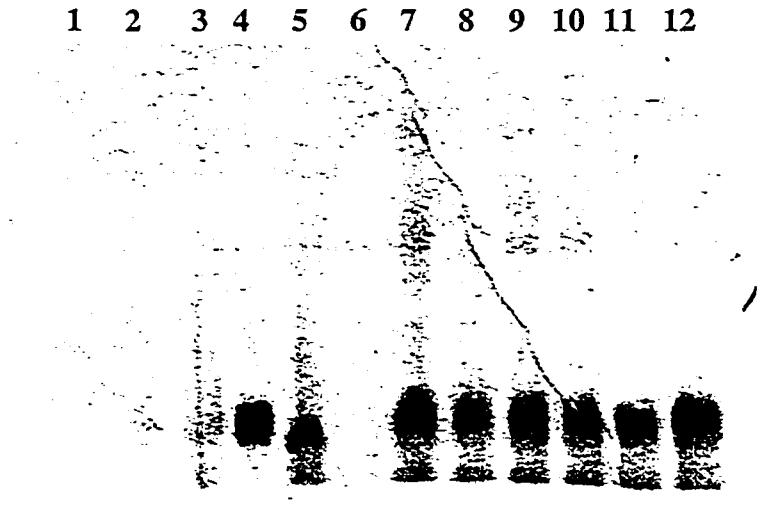

Figure 7.11. SDS analysis of tryptic digestion of PGHS-2. 28 μg PGHS-2 was incubated in 4.6 M guanidinium hydrochloride containing 5 mM DTT at 65 °C for 1 h then cooled to 25°C. Following the addition of 20 mM iodoacetamide, the sample was incubated for 1 h at 25°C in the dark. The sample was then diluted to give a guanidinium hydrochloride concentration of 0.18 M, 0.5 μg trypsin was added and the sample was incubated at 37°C. Aliquots (0.7 μg) were mixed with SDS loading buffer and analyzed by SDS-PAGE on a 1-mm 4 - 20% gradient gel (lane 12, 0.5 h; lane 11, 1 h; lane 10, 1.5 h; lane 9, 2 h; lane 8, 2.5 h; lane 7, 3 h). After 4 h a further 0.5 μ g of trypsin was added and the sample was incubated overnight at 37 °C (lanes 2 and 6). Following tryptic digestion 2000 units of PNGase F was added and the sample incubated for a further 4 h (lane 1). A sample was also prepared with PNGase F addition prior to trypsin (lane 5 - 0.7 μg PGHS-2 following 4 h PNGase F treatment, lane 3 - 0.7 μg PGHS-2 following PNGase F and tryptic digestion). For comparison 0.35 μg of undigested PGHS-2 is shown in lane 4.

supports nonrandom incorporation, likely the COX or POX active site.

Interestingly, while no increase in intensity was observed for the monomeric PGHS-2 band, ^{14}C-AA labeling of oligomeric bands increased in intensity between 0.2 - 120 min (Figure 7.3). In the presence of AA, oligomerization may result from either levuglandin crosslinking (Figure 7.6) or intermolecular dityrosine formation. A similar degree of crosslinking was observed in experiments using H_2O_2 as a substrate (Figures 7.7 and 7.8) as in the presence of AA (Figure 7.5). This suggests that crosslinking in PGHS-2 occurs as a result of POX turnover rather than via levuglandin generation from COX turnover (Figure 7.6).

The negligible degree of intermolecular crosslinking observed both in the presence of AA (Figures 7.3, 7.4 and 7.5) and H_2O_2 (Figures 7.7 and 7.8) indicates that electron transfer from surface tyrosines is not an efficient process in PGHS-2, as compared to CCP and LPO. Therefore, intermolecular crosslinking does not contribute to either AA-dependent or H_2O_2-dependent PGHS-2 inactivation. Furthermore, although LPO undergoes significant intermolecular crosslinking via dityrosine formation in the presence of H_2O_2, the resulting oligomeric forms of LPO are fully active (*50*).

The recent finding by Wu et al. (*58*) that PGHS inactivation likely commences with compound I, supports the consensus that radical intermediates generated in POX or COX catalysis lead to inactivation. This is consistent with the ability of POX-reducing substrates to protect against H_2O_2-dependent inactivation (Figure 7.9) and the inefficient catalactic turnover of H_2O_2 by PGHS-2 (Figure 7.10). Although the results of this study demonstrate that intermolecular crosslinking is not responsible for H_2O_2-dependent PGHS-2 inactivation, there are other possible mechanisms involving radical species.

Formation of an intrasubunit dityrosine crosslink that either blocks substrate access or causes a change in conformation is a possible mechanism. For example, Tyr348 is located in the COX channel at 2.7 Å from Tyr385, and Tyr348-Tyr385 crosslinking would block access to the COX channel. The possibility of a relationship between PGHS inactivation and conformational changes in the enzyme has been raised by Mevkh et al. (*323*). The results of a study investigating the modification of His residues in PGHS using diethylpyrocarbonate (DEPC) demonstrated that only 7 His residues were modified by DEPC in native PGHS, while 18 His residues were modified by DEPC in the inactivated enzyme. Based on these results, Mevkh et al. (*323*) suggested that dramatic changes in the protein structure either cause or occur as a result of PGHS inactivation.

7.4. APPENDIX 7A. SCINTILLATION COUNTING RESULTS FOR PGH-2 AND OPGHS-1

Table 7.1 Scintillation counting and stoichiometry of ^{14}C-AA incorporation into PGHS-2.

Lane[a]	^{14}C-AA (CPM)[b]	^{14}C-AA (μCi) ($x10^{-4}$)[c]	^{14}C-AA (mol) ($x\ 10^{-11}$)[d]	PGHS-2 (mol) ($x\ 10^{-11}$)[e]	Stoichiometry[f]
1	788	7.16	2.98	2.56	1.166
2	724	6.58	2.74	2.56	1.0713
3	764	6.95	2.89	2.56	1.1305
4	830	7.55	3.14	2.56	1.2281
5	726	6.60	2.75	2.56	1.0742
6	825	7.50	3.13	2.56	1.2207
7	837	7.61	3.17	2.56	1.2385
8	810	7.36	3.07	2.56	1.1985
9	811	7.37	3.07	2.56	1.2
10	791	7.19	3.00	2.56	1.1704
11	715	6.50	2.71	2.56	1.058
12	883	8.03	3.34	2.56	1.3065
13	888	8.07	3.36	2.56	1.3139
14	881	8.01	3.34	2.56	1.3036
15	840	7.64	3.18	2.56	1.2429
16	891	8.10	3.38	2.56	1.3184
17	812	7.38	3.08	2.56	1.2015
18	816	7.42	3.09	2.56	1.2074
19	780	7.09	2.95	2.56	1.1541

Table 7A.1 continued

Lane[a]	^{14}C-AA (CPM)[b]	^{14}C-AA (μCi) ($x10^{-4}$)[c]	^{14}C-AA (mol) ($x\ 10^{-11}$)[d]	PGHS-2 (mol) ($x\ 10^{-11}$)[e]	Stoichiometry[f]
20	849	7.72	3.22	2.56	1.2562
21	759	6.90	2.88	2.56	1.1231
22	788	7.16	2.98	2.56	1.166
23	842	7.65	3.19	2.56	1.2459
24	824	7.49	3.12	2.56	1.2192

[a]lanes correspond to those shown in Figure 7.3.
[b]scintillation counting results for PGHS-2-containing gel slices
[c]μCi calculated from CPM using equation 2.10
[d]activity of ^{14}C-AA was 24 Ci/mol
[e]8 μL of 3.6 μM PGHS-2 loaded in each lane
[f]stoichiometry expressed as mol ^{14}C-AA per mol PGHS-2

Table 7.2. Scintillation counting and stoichiometry of ^{14}C-AA incorporation into oPGHS-1.

Lane[a]	^{14}C-AA (CPM)[b]	^{14}C-AA (μCi) ($x\ 10^{-4}$)[c]	^{14}C-AA (mol) ($x\ 10^{-11}$)[d]	oPGHS-1 (mol) ($x\ 10^{-12}$)[e]	Stoichiometry[f]
1	273	2.48	10.3	8.40	1.23
2	209	1.90	7.92	8.40	0.942
3	170	1.55	6.44	8.40	0.767
4	179	1.63	6.78	8.40	0.807
5	185	1.68	7.01	8.40	0.834
6	207	1.88	7.84	8.40	0.933
7	207	1.88	7.84	8.40	0.933
8	181	1.65	6.86	8.40	0.816
9	213	1.94	8.07	8.40	0.960

Table 7A.2 continued

Lane[a]	^{14}C-AA (CPM)[b]	^{14}C-AA (μCi) (x 10^{-4})[c]	^{14}C-AA (mol) (x 10^{-11})[d]	oPGHS-1 (mol) (x 10^{-12})[e]	Stoichiometry[f]
10	214	1.95	8.11	8.40	0.965
11	197	1.79	7.46	8.40	0.888
12	216	1.96	8.18	8.40	0.974
13	290	2.64	11.0	8.40	1.31
14	235	2.14	8.90	8.40	1.06
15	234	2.13	8.86	8.40	1.06
16	254	2.31	9.62	8.40	1.15
17	234	2.13	8.86	8.40	1.06
18	245	2.23	9.28	8.40	1.10
19	258	2.35	9.77	8.40	1.16
20	205	1.86	7.77	8.40	0.924
21	238	2.16	9.02	8.40	1.07
22	243	2.21	9.20	8.40	1.10
23	236	2.15	8.94	8.40	1.06
24	329	2.99	12.5	8.40	1.48

[a]lanes correspond to those shown in Figure 7.4.
[b]scintillation counting results for PGHS-2-containing gel slices
[c]μCi calculated from CPM using equation 2.10
[d]activity of ^{14}C-AA was 24 Ci/mol
[e]8 μL of 3.6 μM PGHS-2 loaded in each lane
[f]stoichiometry expressed as mol ^{14}C-AA per mol PGHS-2

8. CONCLUSIONS AND FUTURE DIRECTIONS

8.1. CONCLUSIONS

PGHS-POX-dependent bioactivation of xenobiotics has been implicated in carcinogenesis, pulmonary- and nephrotoxicity, and teratogenicity (*146-148*). Development of inhibitors of the POX activity of PGHS could aid in further defining the role of this activity *in vivo* and in decreasing the toxic effects of xenobiotic activation. Knowledge of the underlying thermodynamic driving forces is key to understanding the roles of the various H-bonding and hydrophobic interactions in binding and could provide valuable insight in the design of selective peroxidase inhibitors.

Peroxidases typically bind reducing substrates weakly, with K_d values in the millimolar range. However, the binding of BHA to HRP [K_d = 2.4 μM, (*63*)] is a notable exception (*62*) and has provided a useful tool for probing the local environment of the aromatic donor binding site. Since the distal catalytic residues of heme peroxidases are highly conserved (*4*), the HRP-BHA complex can be expected to be a good model of substrate binding in other peroxidases. This is confirmed by the recent X-ray structures of the ARP-BHA, ARP-SHA and MPO-SHA complexes (*74-76*).

The results of the ITC investigation of the contribution to binding of each of the H-bonding and hydrophobic interactions observed in the HRP-BHA complex reveal the significance of H-bonding interactions in the distal heme cavity. BHA binding was shown to be enthalpically driven, with the H-bond to Arg38 providing the largest contribution (6.74 kcal/mol). The important role of hydrophobic interactions in binding is apparent in the more enthalpically and entropically favorable binding of 2-NHA relative to BHA. The tight binding of 2-NHA in combination with an examination of the

effect on binding of chloro, amino, hydroxyl and nitro substituents on the aromatic ring of BZH suggests that increased binding affinity will result from the introduction of hydrophobic groups in the *meta* and *para* positions.

The design of specific, reversible peroxidase inhibitors is challenging due to the low specificity demonstrated by most peroxidases for reducing substrates and the difficulty of designing an inhibitor that will not be oxidized by the peroxidase. Another option in peroxidase inhibition is the development of mechanism-based inhibitors. The mechanism of HRP inactivation by phenylhydrazine has been thoroughly investigated (*188, 223*). Therefore, HRP was also used in this study to probe the mechanism of peroxidase inhibition by BZH. Since HRP is an archetypical peroxidase (*2*) these results are expected to be applicable to other peroxidases, including PGHS.

It is proposed that the diazene, generated by the 2-electron oxidation of BZH, is a mechanism-based inhibitor of HRP. Inactivation of HRP by BZH results in heme adduct formation, heme destruction and likely protein adduct formation. Prior activation of BZH to produce the diazene is required, but this is not the result of autooxidation at pH 7.0 since HRP is required for BZH activation. The lack of BZH autooxidation ensures that the diazene will be generated only in the location required for inactivation of the target peroxidase. This is necessary to avoid the nonselective inhibition of other enzymes. The presence of an electron-donating amino group in the position *ortho* to the hydrazide group and the presence of the additional aromatic ring of 2-NZH, which increased the binding affinity, were observed to result in decreased IC_{50} values and increased k_{inact} values for HRP inactivation, as compared to BZH. These guidelines will be useful in the

design of a selective inhibitor for the archetypical peroxidase, HRP. A selective inhibitor of HRP would be useful for investigation of the role of this enzyme *in vivo*.

The binding of aromatic hydroxamic acid analogues to the POX site of PGHS-2 was investigated here by UV-VIS spectroscopy, using changes in the Soret absorption band as a probe of binding. The results highlight the role of the distal Gln203 in defining the distal-cavity characteristics of PGHS-2. The replacement of the distal Arg38 of HRP with the uncharged Gln203 in PGHS results in both the lack of an alkaline transition below pH 12.0 and the weaker binding of aromatic hydroxamic acids. The weak binding of reducing substrates by the POX site of PGHS-2 makes the design of tight binding compounds, as potential inhibitors, more challenging. Additionally, the finding that tepoxalin is a reducing substrate of PGHS-2 rather than an inhibitor, highlights the difficulty in designing specific, tight-binding, reversible inhibitors for PGHS-2 POX that will not be oxidized by this activity. The μM-range IC_{50} values determined here for the inhibition of the POX activity of PGHS-2 by hydrazides suggests that this may be a more viable alternative. The finding in this study that 4-NH_2-BZH was among the poorest inhibitors of PGHS-2, while Kettle et al. (*157*) found it to be one of the most effective inhibitors of MPO (IC_{50} = 2 μM for MPO), reveals that peroxidase-specific hydrazide-based inhibitors can be developed.

Although the binding of NSAIDs to PGHS does not result in any significant changes in secondary structure (*98*), limited proteolysis has revealed that it does alters the local conformational stability in oPGHS-1. The Arg277 region of oPGHS-1 is protected from attack by trypsin in the presence of heme or time-dependent NSAIDs (indomethacin, flurbiprofen, meclofenamic acid) and to a slightly lesser degree by

reversible NSAIDs (flufenamic acid and ibuprofen) (*173*). Investigation of the effects of NSAID binding on the structure and conformational stability of PGHS-2 by FTIR shows that, while changes in solvent accessibility and flexibility occur, these are unrelated to the phenomenon of time-dependency. Diclofenac binding caused the most marked conformational stabilization and reduction in solvent accessibility. Previous studies have also indicated that diclofenac has a different mode of binding as compared to other NSAIDs (*172, 294*). To probe the reason for the distinct effects observed for diclofenac, and to a lesser extent for meclofenamic acid, the thermodynamics of binding of the four fenamates were investigated by ITC. The results revealed that diclofenac binding is very entropically unfavorable. This may be responsible for the greater reduction in the conformational flexibility of the PGHS-2-diclofenac complex compared to other NSAIDs.

A consensus has emerged, based on the protective effect of reducing substrates, that the irreversible loss of PGHS activity is due to the generation of an unstable radical during POX or COX catalysis (*57, 58*). There are several radical intermediates involved in COX catalysis (Figure 1.6). The reactive nature of these intermediates raises the possibility that COX inactivation occurs via substrate incorporation. The stoichiometric (one mol ^{14}C-AA per mol of PGHS-1 or -2) incorporation of ^{14}C-AA into both PGHS-1 and -2 observed here suggest a specific site of attachment, likely within the COX active site. The rapid (less than 12 s for PGHS-2 and ~ 5-10 min for oPGHS-1) incorporation of ^{14}C-AA observed under the conditions used here (6 μM PGHS-2 or 3.5 μM oPGHS-1 and 140 μM ^{14}C-AA) correlates with the rapid inactivation of PGHS also observed here. This suggests that activated substrate intermediates may be involved in COX inactivation.

Support for the existence at least one other protein radical, in addition to that located on Tyr385, is provided by: (1) the presence of endogenous reductants within PGHS, (2) the ability of the inactive Y385F mutant of PGHS-1 to form a tyrosyl radical and (3) EPR studies demonstrating the formation of a second tyrosyl radical in the presence of bound inhibitor (*122, 141, 142, 144, 315, 316*). The detection of tyrosyl radical(s) in addition to that located on Tyr385 suggests that crosslinking via dityrosine formation as a possible mechanism of inactivation. Negligible intermolecular crosslinking was observed in this study in the presence of either AA or H_2O_2, indicating that this is not a major mechanism of PGHS-2 inactivation, and that crosslinking likely results from POX turnover rather than levuglandin crosslinks. Investigation of both crosslinking and incorporation of intermediates require peptide mapping to identify the modified residues; therefore, suitable conditions for PGHS-2 digestion were developed in this work.

8.2. Future directions

The work described in this thesis contributes significantly to the understanding of the binding of reducing substrates by peroxidases and the development of selective peroxidase inhibitors. It also suggests a number of experimental paths to pursue. The investigation of the thermodynamics of binding of 24 aromatic hydroxamic acid analogues to HRP provides an excellent basis for modeling or docking studies of the binding of these compounds to HRP, PGHS-2 and other peroxidases, based on existing crystal structure data.

The investigation of HRP inactivation by hydrazides provides evidence that these compounds are good candidates for development as peroxidase inhibitors. The results

presented here indicate that these compounds are mechanism-based inhibitors. However, further evidence is required to provide conclusive proof of the mechanism. Future experiments would include peptide mapping to identify amino acid adducts and the determination of the stoichiometry of inactivation. Additionally, isolation of hydrazide oxidation products is required to verify the mechanism of hydrazide activation proposed here (Figure 4.23).

Comparison of the IC_{50} values for HRP versus PGHS-2 inactivation by the series of aromatic hydrazides investigated here demonstrated that PGHS-2 is more susceptible to inactivation than HRP. Most of the hydrazides tested demonstrated similar peroxidase selectivity as BZH. However, the placement of an amino group in the *ortho*-position increased the HRP selectivity ~20-fold, while a hydroxyl group in this position increased the PGHS-2 selectivity 5 - 12-fold. The addition of a second aromatic ring (2-NZH) did not alter the selectivity, but it did decrease the IC_{50} for the inactivation of both HRP and PGHS-2. On the basis of these findings, 3-NH_2-2-NZH is expected to have properties of a lead compound for the development of an HRP-selective POX inhibitor. The introduction of ring substituents, indicated by the X group in Figure 8.1 may result in increased selectivity. Similarly, the results of this study demonstrate that 3-OH-2-NZH is a good lead compound for a PGHS-2-selective POX inhibitor, and selectivity may be increased by the introduction of ring substituents (indicated by the X group in Figure 8.2).

The effects of NSAID binding on the structure and conformational flexibility of PGHS-2 also suggest a number of future experiments. The FTIR-monitored thermal denaturation study presented here could be complemented by an investigation of the

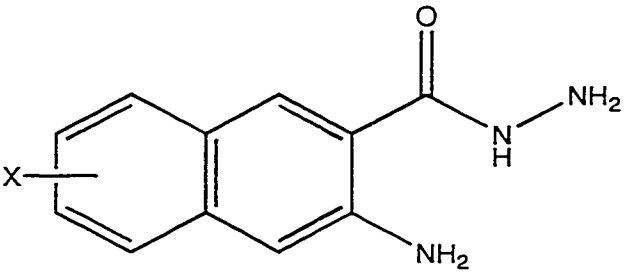

Figure 8.1. Lead compound for the development of an HRP-selective hydrazide.

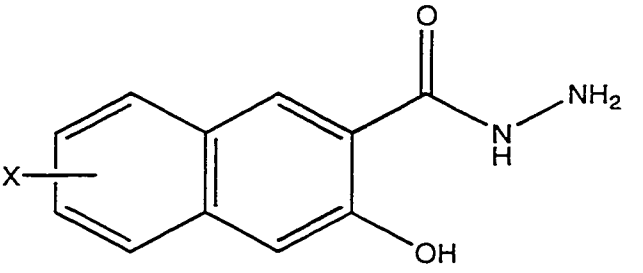

Figure 8.2. Lead compound for the development of an PGHS-2-selective hydrazide.

effect of NSAID binding on the chemical denaturation (*e.g.*, guanidinium hydrochloride) of PGHS-2. Gel filtration chromatography and analytical ultracentrifugation could be used to determine whether the NSAID-induced reduction in conformational stability and solvent accessibility of the protein indicated by FTIR is due to stabilization of the dimeric form of PGHS-2.

Comparison of the thermodynamics of binding of the four fenamates investigated here suggests that the highly enthalpically favorable and entropically unfavorable binding of diclofenac is due to two factors: (1) the perpendicular arrangement of the aromatic rings and (2) the additional methylene group which extends the reach of the carboxylate group. Investigation of the thermodynamics of binding of the series of diclofenac analogues shown in Figure 8.3 to PGHS-2 would assist in the interpretation of the factors determining the binding of diclofenac and the other fenamates (*i.e.*, role of the salt bridge and chlorine atoms in diclofenac binding).

Preliminary data are provided here on the inactivation of the COX and POX activities of PGHS-2. The results indicate that a number of mechanisms may be involved in the inactivation of the POX and COX activities of PGHS-2. Additionally, the relative importance of the different mechanism(s) may be dependent on the experimental conditions. Potential mechanisms include: intramolecular crosslinking, conformational changes, oxidation of active site residues and incorporation of activated intermediates or products (*e.g.*, levuglandins). The investigation of sites of peptide modification will require peptide mapping to isolate crosslinked peptides, oxidized residues and sites of adduct formation. The protocol for PGHS-2 digestion developed in here will be useful in these studies.

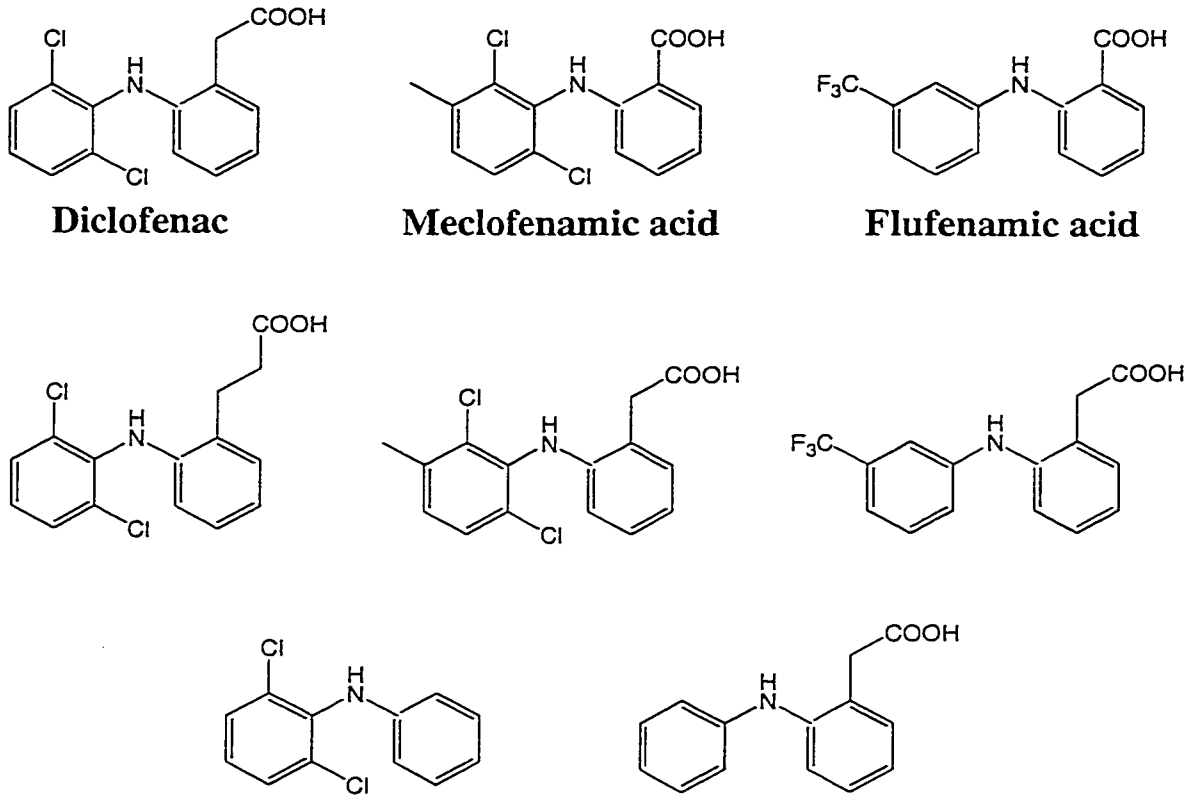

Figure 8.3. Structure of fenamates which could assist in the interpretation of the thermodynamics of diclofenac binding to PGHS-2.

9. REFERENCES

1. Everse, J., and Everse, K. E. E. (1991) *Peroxidases in Chemistry and Biology*, Vol. 1 and 2, CRC Press, Boca Raton.
2. Ortiz de Montellano, P. R. (1992) *Annu Rev Pharmacol Toxicol 32*, 89-107.
3. Smulevich, G. (1998) *Biospectroscopy 4*, S3-17.
4. Welinder, K. G., and Gajhede, M. (1993) in *Plant Peroxidases: Biochemistry and Physiology* (Greppin, H., Rasmussen, S. K., Welinder, K. G., and Penel, C., Eds.) pp 35-42, University of Copenhagen and University of Geneva, Geneva.
5. Welinder, K. G., Mauro, J. M., and Norskov-Lauritsen, L. (1992) *Biochem Soc Trans 20*, 337-40.
6. Welinder, K. G. (1991) in *Biochemical, Molecular, and Physiological Aspects of Plant Peroxidases* (Lobarzewski, J., Greppin, H., Penel, C., and Greppin, T., Eds.) pp 1-13, University of Geneva, Geneva.
7. Welinder, K. G. (1992) *Curr. Op. Struct. Biol. 2*, 388-393.
8. Li, H., and Poulos, T. L. (1994) *Structure 2*, 461-4.
9. Poulos, T. L., Patterson, W. R., and Sundaramoorthy, M. (1995) *Biochem Soc Trans 23*, 228-32.
10. Schuller, D. J., Ban, N., Huystee, R. B., McPherson, A., and Poulos, T. L. (1996) *Structure 4*, 311-21.
11. Gajhede, M., Schuller, D. J., Henriksen, A., Smith, A. T., and Poulos, T. L. (1997) *Nat Struct Biol 4*, 1032-8.
12. Henriksen, A., Welinder, K. G., and Gajhede, M. (1998) *J Biol Chem 273*, 2241-8.
13. Banci, L. (1997) *J Biotechnol 53*, 253-63.
14. Zeng, J., and Fenna, R. E. (1992) *J Mol Biol 226*, 185-207.
15. Picot, D., Loll, P. J., and Garavito, R. M. (1994) *Nature 367*, 243-9.
16. Dunford, H. B. (1991) in *Peroxidases in Chemistry and Biology* (Everse, J., Everse, K. E., and Grisham, M. B., Eds.) pp 1-24, CRC, Boca Raton.
17. Finzel, B. C., Poulos, T. L., and Kraut, J. (1984) *J Biol Chem 259*, 13027-36.
18. Bosshard, H. R., Anni, H., and Yonetani, T. (1991) in *Peroxidases in Chemistry and Biology* (Everse, J., Everse, K. E., and Grisham, M. B., Eds.) pp 51-84, CRC Press, Boca Raton.
19. Poulos, T. L., and Kraut, J. (1980) *J Biol Chem 255*, 8199-205.
20. Thomas, E. L., Bozeman, P. M., and Learn, D. B. (1991) in *Peroxidases in Chemistry and Biology* (Everse, J., Everse, K. E., and Grisham, M. B., Eds.) pp 123-142, CRC, Boca Raton.

21. Paul, K.-G., and Ohlsson, P. (1985) in *The Lactoperoxidase System: Chemistry and Biological Significance* (Pruitt, K. M., and Tenovuo, J. O., Eds.) pp 15-29, Marcel Dekker, New York.

22. Kohler, H., and Jenzer, H. (1989) *Free Radic Biol Med 6*, 323-39.

23. Magnussen, R. P. (1991) in *Peroxidases in Chemistry and Biology* (Everse, J., Everse, K. E., and Grisham, M. B., Eds.) pp 199-219, CRC, Boca Raton.

24. Hurst, J. K. (1991) in *Peroxidases in Chemistry and Biology* (Everse, J., Everse, K. E., and Grisham, M. B., Eds.) pp 37-62, CRC, Boca Raton.

25. Marnett, L. J., and Maddipati, K. R. (1991) in *Peroxidases in Chemistry and Biology* (Everse, J., Everse, K. E., and Grisham, M. B., Eds.) pp 293-334, CRC Press, Boca Raton.

26. Henderson, W. R. (1991) in *Peroxidases in Chemistry and Biology* (Everse, J., Everse, K. E., and Grisham, M. B., Eds.) pp 105-121, CRC, Boca Raton.

27. Vitello, L. B., Erman, J. E., Miller, M. A., Wang, J., and Kraut, J. (1993) *Biochemistry 32*, 9807-18.

28. Erman, J. E., Vitello, L. B., Miller, M. A., Shaw, A., Brown, K. A., and Kraut, J. (1993) *Biochemistry 32*, 9798-806.

29. Miller, M. A., Shaw, A., and Kraut, J. (1994) *Nat Struct Biol 1*, 524-31.

30. Adediran, S. A., and Dunford, H. B. (1983) *Eur J Biochem 132*, 147-50.

31. Moss, T. H., Ehrenberg, A., and Bearden, A. J. (1969) *Biochemistry 8*, 4159-62.

32. Schulz, C. E., Rutter, R., Sage, J. T., Debrunner, P. G., and Hager, L. P. (1984) *Biochemistry 23*, 4743-54.

33. Lang, G., Spartalian, K., and Yonetani, T. (1976) *Biochim Biophys Acta 451*.

34. Penner-Hahn, J. E., Eble, K. S., McMurry, T. J., Renner, M., and Balch, A. L. (1986) *J. Am. Chem. Soc. 108*, 7819-7825.

35. Browett, W. R., Gasyna, Z., and Stillman, M. J. (1988) *J. Am. Chem. Soc. 110*, 3633-3640.

36. Myers, D., and Palmer, G. (1985) *J Biol Chem 260*, 3887-90.

37. Edwards, S. L., Nguyen, H. X., Hamlin, R. C., and Kraut, J. (1987) *Biochemistry 26*, 1503-11.

38. Dolphin, D., Forman, A., Borg, D. C., Fajer, J., and Felton, R. H. (1971) *Proc Natl Acad Sci U S A 68*, 614-8.

39. Andrawis, A., Johnson, K. A., and Tien, M. (1988) *J Biol Chem 263*, 1195-8.

40. Wariishi, H., Akileswaran, L., and Gold, M. H. (1988) *Biochemistry 27*, 5365-70.

41. Andersen, M. B., Hsuanyu, Y., Welinder, K. G., Schneider, P., and Dunford, H. B. (1991) *Acta Chem. Scand. 45*, 1080-1086.

42. Farhangrazi, Z. S., Copeland, B. R., Nakayama, T., Amachi, T., Yamazaki, I., and Powers, L. S. (1994) *Biochemistry 33*, 5647-52.

43. Patterson, W. R., Poulos, T. L., and Goodin, D. B. (1995) *Biochemistry 34*, 4342-5.

44. Sivaraja, M., Goodin, D. B., Smith, M., and Hoffman, B. M. (1989) *Science 245*, 738-40.

45. Courtin, F., Deme, D., Virion, A., Michot, J. L., Pommier, J., and Nunez, J. (1982) *Eur J Biochem 124*, 603-9.

46. Courtin, F., Michot, J. L., Virion, A., Pommier, J., and Deme, D. (1984) *Biochem Biophys Res Commun 121*, 463-70.

47. Virion, A., Courtin, F., Deme, D., Michot, J. L., Kaniewski, J., and Pommier, J. (1985) *Arch Biochem Biophys 242*, 41-7.

48. Deme, D., Virion, A., Michot, J. L., and Pommier, J. (1985) *Arch Biochem Biophys 236*, 559-66.

49. Nakamura, M., Yamazaki, I., Kotani, T., and Ohtaki, S. (1985) *J Biol Chem 260*, 13546-52.

50. Lardinois, O. M., Medzihradszky, K. F., and Ortiz de Montellano, P. R. (1999) *J Biol Chem 274*, 35441-8.

51. Tsaprailis, G. (1997) in *Chemistry and Biochemistry* pp 219, Concordia University, Montreal.

52. Shephard, T. (1999) in *Chemistry and Biochemistry* pp 100, Concordia University, Montreal.

53. Karthein, R., Dietz, R., Nastainczyk, W., and Ruf, H. H. (1988) *Eur J Biochem 171*, 313-20.

54. Shimokawa, T., Kulmacz, R. J., DeWitt, D. L., and Smith, W. L. (1990) *J Biol Chem 265*, 20073-6.

55. Gunther, M. R., Hsi, L. C., Curtis, J. F., Gierse, J. K., Marnett, L. J., Eling, T. E., and Mason, R. P. (1997) *J Biol Chem 272*, 17086-90.

56. Goodwin, D. C., Gunther, M. R., Hsi, L. C., Crews, B. C., Eling, T. E., Mason, R. P., and Marnett, L. J. (1998) *J Biol Chem 273*, 8903-9.

57. Smith, W. L., and Marnett, L. J. (1991) *Biochim Biophys Acta 1083*, 1-17.

58. Wu, G., Wei, C., Kulmacz, R. J., Osawa, Y., and Tsai, A. L. (1999) *J Biol Chem 274*, 9231-7.

59. Veitch, N. C., Gao, Y., Smith, A. T., and White, C. G. (1997) *Biochemistry 36*, 14751-61.

60. English, A. M., and Tsaprailis, G. (1995) *Adv Inorg Chem 43*, 79-124.

61. Henriksen, A., Schuller, D. J., Meno, K., Welinder, K. G., Smith, A. T., and Gajhede, M. (1998) *Biochemistry 37*, 8054-60.

62. Veitch, N. C. (1995) *Biochem Soc Trans 23*, 232-40.

63. Schonbaum, G. R. (1973) *J Biol Chem 248*, 502-11.

64. La Mar, G. N., Hernandez, G., and de Ropp, J. S. (1992) *Biochemistry 31*, 9158-68.

65. Sakurada, J., Takahashi, S., and Hosoya, T. (1986) *J Biol Chem 261*, 9657-62.

66. Veitch, N. C., and Williams, R. J. (1990) *Eur J Biochem 189*, 351-62.

67. Veitch, N. C. (1993) in *Plant Peroxidases: Biochemistry and Physiology* (Welinder, K. G., Rasmussen, S. K., Penel, G., and Greppin, H., Eds.) pp 57-64, University of Geneva, Geneva.

68. Saxena, A., Modi, S., Behere, D. V., and Mitra, S. (1990) *Biochim Biophys Acta 1041*, 83-93.

69. Thanabal, V., La Mar, G. N., and de Ropp, J. S. (1988) *Biochemistry 27*, 5400-7.

70. Smith, A. T., Sanders, S. A., Sampson, C., Bray, R. C., Burke, J. F., and Thorneley, R. N. F. (1993) in *Plant Peroxidases: Biochemistry and Physiology* (Welinder, K. G., Rasmussen, S. K., Penel, C. T., and Greppin, H., Eds.) pp 159-168, University of Geneva, Geneva.

71. Smulevich, G., Paoli, M., Burke, J. F., Sanders, S. A., Thorneley, R. N., and Smith, A. T. (1994) *Biochemistry 33*, 7398-407.

72. Holzbaur, I. E., English, A. M., and Ismail, A. A. (1996) *J Am Chem Soc 118*, 6266-79.

73. Howes, B. D., Rodriguez-Lopez, J. N., Smith, A. T., and Smulevich, G. (1997) *Biochemistry 36*, 1532-43.

74. Itakura, H., Oda, Y., and Fukuyama, K. (1997) *FEBS Lett 412*, 107-10.

75. Tsukamoto, K., Itakura, H., Sato, K., Fukuyama, K., Miura, S., Takahashi, S., Ikezawa, H., and Hosoya, T. (1999) *Biochemistry 38*, 12558-68.

76. Davey, C. A., and Fenna, R. E. (1996) *Biochemistry 35*, 10967-73.

77. Wallace, A. C., Laskowski, R. A., and Thornton, J. M. (1995) *Protein Eng 8*, 127-34.

78. McDonald, I. K., and Thornton, J. M. (1994) *J Mol Biol 238*, 777-93.

79. Davis, A. M., and Teague, S. J. (1999) *Angew. Chem. Int. Ed. 38*, 736-749.

80. Paul, K. G., and Ohlsson, P. I. (1978) *Acta Chem Scand [B] 32*, 395-404.

81. Hosoya, T., Sakurada, J., Kurokawa, C., Toyoda, R., and Nakamura, S. (1989) *Biochemistry 28*, 2639-44.

82. Nakatani, H., and Takahashi, K. (1986) *Biochem 25*, 3515-3518.

83. Wiseman, T., Williston, S., Brandts, J. F., and Lin, L. N. (1989) *Anal Biochem 179*, 131-7.

84. Dray, A., and Urban, L. (1996) *Annu Rev Pharmacol Toxicol 36*, 253-80.

85. Dubois, R. N., Abramson, S. B., Crofford, L., Gupta, R. A., Simon, L. S., Van De Putte, L. B., and Lipsky, P. E. (1998) *Faseb J 12*, 1063-73.

86. Hemler, M., and Lands, W. E. (1976) *J Biol Chem 251*, 5575-9.

87. Miyamoto, T., Ogino, N., Yamamoto, S., and Hayaishi, O. (1976) *J Biol Chem 251*, 2629-36.

88. DeWitt, D. L., and Smith, W. L. (1988) *Proc Natl Acad Sci U S A 85*, 1412-6.

89. Merlie, J. P., Fagan, D., Mudd, J., and Needleman, P. (1988) *J Biol Chem 263*, 3550-3.

90. Yokoyama, C., Takai, T., and Tanabe, T. (1988) *FEBS Lett 231*, 347-51.

91. Xie, W. L., Chipman, J. G., Robertson, D. L., Erikson, R. L., and Simmons, D. L. (1991) *Proc Natl Acad Sci U S A 88*, 2692-6.

92. Kujubu, D. A., Fletcher, B. S., Varnum, B. C., Lim, R. W., and Herschman, H. R. (1991) *J Biol Chem 266*, 12866-72.

93. Hla, T., and Neilson, K. (1992) *Proc Natl Acad Sci U S A 89*, 7384-8.

94. O'Banion, M. K., Winn, V. D., and Young, D. A. (1992) *Proc Natl Acad Sci U S A 89*, 4888-92.

95. Hla, T., Bishop-Bailey, D., Liu, C. H., Schaefers, H. J., and Trifan, O. C. (1999) *Int J Biochem Cell Biol 31*, 551-7.

96. Reed, D. W., Bradshaw, W. S., Xie, W., and Simmons, D. L. (1996) *Prostaglandins 52*, 269-84.

97. Luong, C., Miller, A., Barnett, J., Chow, J., Ramesha, C., and Browner, M. F. (1996) *Nat Struct Biol 3*, 927-33.

98. Kurumbail, R. G., Stevens, A. M., Gierse, J. K., McDonald, J. J., Stegeman, R. A., Pak, J. Y., Gildehaus, D., Miyashiro, J. M., Penning, T. D., Seibert, K., Isakson, P. C., and Stallings, W. C. (1996) *Nature 384*, 644-8.

99. McKeever, B. M., Pandya, S., Percival, M. D., Ouellet, M., Bayly, C., O'Neill, G. P., Bastien, L., Kennedy, B., Adam, M., Cromlish, W., Roy, P., Black, C., Guay, D., and LeBlanc, Y. (1996) in *International Conference on Prostaglandins '96*, Vienna, Austria.

100. Kulmacz, R. J., Pendleton, R. B., and Lands, W. E. (1994) *J Biol Chem 269*, 5527-36.

101. Barnett, J., Chow, J., Ives, D., Chiou, M., Mackenzie, R., Osen, E., Nguyen, B., Tsing, S., Bach, C., Freire, J., and et al. (1994) *Biochim Biophys Acta 1209*, 130-9.

102. Laneuville, O., Breuer, D. K., Dewitt, D. L., Hla, T., Funk, C. D., and Smith, W. L. (1994) *J Pharmacol Exp Ther 271*, 927-34.

103. Lands, W. E., Sauter, J., and Stone, G. W. (1978) *Prostaglandins Med 1*, 117-20.

104. Smith, W. L., Garavito, R. M., and DeWitt, D. L. (1996) *J Biol Chem 271*, 33157-60.

105. Smith, W. L., and DeWitt, D. L. (1996) in *Advances in Immunology* (Dixon, F. J., Ed.) pp 167-215, Academic Press, Orlando.

106. Crofford, L. J. (1997) *J Rheumatol 24 Suppl 49*, 15-9.

107. DeWitt, D. L., and Meade, E. A. (1993) *Arch Biochem Biophys 306*, 94-102.

108. Evett, G. E., Xie, W., Chipman, J. G., Robertson, D. L., and Simmons, D. L. (1993) *Arch Biochem Biophys 306*, 169-77.

109. Kujubu, D. A., Reddy, S. T., Fletcher, B. S., and Herschman, H. R. (1993) *J Biol Chem 268*, 5425-30.

110. Han, J. W., Sadowski, H., Young, D. A., and Macara, I. G. (1990) *Proc Natl Acad Sci U S A 87*, 3373-7.

111. Jones, D. A., Carlton, D. P., McIntyre, T. M., Zimmerman, G. A., and Prescott, S. M. (1993) *J Biol Chem 268*, 9049-54.

112. O'Sullivan, M. G., Chilton, F. H., Huggins, E. M., Jr., and McCall, C. E. (1992) *J Biol Chem 267*, 14547-50.

113. Amin, A. R., Attur, M., Patel, R. N., Thakker, G. D., Marshall, P. J., Rediske, J., Stuchin, S. A., Patel, I. R., and Abramson, S. B. (1997) *J Clin Invest 99*, 1231-7.

114. Kang, R. Y., Freire-Moar, J., Sigal, E., and Chu, C. Q. (1996) *Br J Rheumatol 35*, 711-8.

115. Anderson, G. D., Hauser, S. D., McGarity, K. L., Bremer, M. E., Isakson, P. C., and Gregory, S. A. (1996) *J Clin Invest 97*, 2672-9.

116. Bjarnason, I. (1999) *Ital J Gastroenterol Hepatol 31*, S27-36.

117. Golden, B. D., and Abramson, S. B. (1999) *Rheum Dis Clin North Am 25*, 359-78.

118. Shimokawa, T., and Smith, W. L. (1991) *J Biol Chem 266*, 6168-73.

119. Landino, L. M., Crews, B. C., Gierse, J. K., Hauser, S. D., and Marnett, L. J. (1997) *J Biol Chem 272*, 21565-74.

120. Ohki, S., Ogino, N., Yamamoto, S., and Hayaishi, O. (1979) *J Biol Chem 254*, 829-36.

121. Lambeir, A. M., Markey, C. M., Dunford, H. B., and Marnett, L. J. (1985) *J Biol Chem 260*, 14894-6.

122. Dietz, R., Nastainczyk, W., and Ruf, H. H. (1988) *Eur J Biochem 171*, 321-8.

123. Dunford, H. B., and Stillman, J. S. (1976) *Coord. Chem. Rev. 19*, 187-251.

124. Nastainczyk, W., Schuhn, D., and Ullrich, V. (1984) *Eur J Biochem 144*, 381-5.

125. Yonetani, T. (1976) in *The Enzymes* (Boyer, P., Ed.) pp 345-362, Academic Press, New York.

126. Markey, C. M., Alward, A., Weller, P. E., and Marnett, L. J. (1987) *J Biol Chem 262*, 6266-79.

127. Ple, P., and Marnett, L. J. (1989) *J Biol Chem 264*, 13983-93.

128. Ogino, N., Yamamoto, S., Hayaishi, O., and Tokuyama, T. (1979) *Biochem Biophys Res Commun 87*, 184-91.

129. Ohkuchi, M., Tsukamoto, M., Yokoyama, T., Shiratsuchi, M., and Uchida, Y. (1988) *Prostaglandins 36*, 787-95.

130. Proctor, P. (1970) *Nature 228*, 868.

131. Ames, B. N., Cathcart, R., Schwiers, E., and Hochstein, P. (1981) *Proc Natl Acad Sci U S A 78*, 6858-62.

132. Marnett, L. J., Rowlinson, S. W., Goodwin, D. C., Kalgutkar, A. S., and Lanzo, C. A. (1999) *J Biol Chem 274*, 22903-6.

133. Bhattacharyya, D. K., Lecomte, M., Rieke, C. J., Garavito, M., and Smith, W. L. (1996) *J Biol Chem 271*, 2179-84.

134. Hamberg, M., and Samuelsson, B. (1967) *J Biol Chem 242*, 5336-43.

135. Mason, R. P., Kalyanaraman, B., Tainer, B. E., and Eling, T. E. (1980) *J Biol Chem 255*, 5019-22.

136. Sameulsson, B. (1965) *J. Am. Chem. Soc. 87*, 3011.

137. Nugteren, D. H., and Dorp, D. A. v. (1965) *Biochim Biophys Acta 98*, 654-6.

138. Nugteren, D. H., and Hazelhof, E. (1973) *Biochim Biophys Acta 326*, 448-61.

139. Hamberg, M., Svensson, J., Wakabayashi, T., and Samuelsson, B. (1974) *Proc. Natl. Acad. Sci. U.S.A. 71*, 345-353.

140. Stubbe, J., and van der Donk, W. A. (1998) *Chem. Rev. 98*, 705-762.

141. Kulmacz, R. J., Ren, Y., Tsai, A. L., and Palmer, G. (1990) *Biochemistry 29*, 8760-71.

142. Tsai, A. L., Palmer, G., and Kulmacz, R. J. (1992) *J Biol Chem 267*, 17753-9.

143. Kulmacz, R. J., Palmer, G., and Tsai, A. L. (1993) *J Lipid Mediat 6*, 145-54.

144. Tsai, A., Wu, G., Palmer, G., Bambai, B., Koehn, J. A., Marshall, P. J., and Kulmacz, R. J. (1999) *J Biol Chem 274*, 21695-700.

145. Wei, C., Kulmacz, R. J., and Tsai, A. L. (1995) *Biochemistry 34*, 8499-512.

146. Eling, T. E., and Curtis, J. F. (1992) *Pharmacol Ther 53*, 261-73.

147. Smith, B. J., Curtis, J. F., and Eling, T. E. (1991) *Chem Biol Interact 79*, 245-64.

148. Eling, T. E., Thompson, D. C., Foureman, G. L., Curtis, J. F., and Hughes, M. F. (1990) *Annu Rev Pharmacol Toxicol 30*, 1-45.

149. Albrich, J. M., McCarthy, C. A., and Hurst, J. K. (1981) *Proc Natl Acad Sci U S A 78*, 210-4.

150. Winterbourn, C. C. (1985) *Biochim Biophys Acta 840*, 204-10.

151. Davies, B., and Edwards, S. W. (1989) *Biochem J 258*, 801-6.

152. Rich, P. R., Wiegand, N. K., Blum, H., Moore, A. L., and Bonner, W. D., Jr. (1978) *Biochim Biophys Acta 525*, 325-37.

153. Ikeda-Saito, M., Shelley, D. A., Lu, L., Booth, K. S., Caughey, W. S., and Kimura, S. (1991) *J Biol Chem 266*, 3611-6.

154. Silverman, R. B. (1988) *Mechanism-based enzyme inactivation: chemistry and enzymology*, Vol. 1, CRC Press, Boca Raton.

155. Orgiazzi, J., and Millot, L. (1994) *Ann Endocrinol 55*, 1-5.

156. Cooper, D. S. (1984) *N Engl J Med 311*, 1353-62.

157. Kettle, A. J., Gedye, C. A., Hampton, M. B., and Winterbourn, C. C. (1995) *Biochem J 308*, 559-63.

158. Kettle, A. J., Gedye, C. A., and Winterbourn, C. C. (1997) *Biochem J 321*, 503-8.

159. Mandell, G. L., and Petri, W. A. (1996) in *Pharmacological Basis of Therapeutics* (Goodman, L. S., and Gilman, A., Eds.) pp 1155-1174, McGraw Hill, Health Professions Division, New York.

160. Lei, B., Wei, C. J., and Tu, S. C. (2000) *J Biol Chem 275*, 2520-6.

161. Mizuno, K., Yamamoto, S., and Lands, W. E. (1982) *Prostaglandins 23*, 743-57.

162. Ouellet, M., and Percival, M. D. (1995) *Biochem J 306*, 247-51.

163. Vane, J. R. (1971) *Nat New Biol 231*, 232-5.

164. Andersen, K., Launer, L. J., Ott, A., Hoes, A. W., Breteler, M. M., and Hofman, A. (1995) *Neurology 45*, 1441-5.

165. McGeer, P. L., Schulzer, M., and McGeer, E. G. (1996) *Neurology 47*, 425-32.

166. Stewart, W. F., Kawas, C., Corrada, M., and Metter, E. J. (1997) *Neurology 48*, 626-32.

167. Rome, L. H., and Lands, W. E. (1975) *Proc Natl Acad Sci U S A 72*, 4863-5.

168. Smith, W. L., and DeWitt, D. L. (1995) *Semin Nephrol 15*, 179-94.

169. Kulmacz, R. J., and Lands, W. E. (1985) *J Biol Chem 260*, 12572-8.

170. Copeland, R. A., Williams, J. M., Giannaras, J., Nurnberg, S., Covington, M., Pinto, D., Pick, S., and Trzaskos, J. M. (1994) *Proc Natl Acad Sci U S A 91*, 11202-6.

171. Callan, O. H., So, O. Y., and Swinney, D. C. (1996) *J Biol Chem 271*, 3548-54.

172. Houtzager, V., Ouellet, M., Falgueyret, J. P., Passmore, L. A., Bayly, C., and Percival, M. D. (1996) *Biochemistry 35*, 10974-84.

173. Kulmacz, R. J. (1989) *J Biol Chem 264*, 14136-44.

174. Hemler, M. E., and Lands, W. E. (1980) *Arch Biochem Biophys 201*, 586-93.

175. Lands, W. E. M., Kulmacz, R. J., and Marshall, P. J. (1984) in *Free Radicals in Biology* (Pryor, W. A., Ed.) pp 39-, Academic Press, New York.

176. Kulmacz, R. J. (1986) *Arch Biochem Biophys 249*, 273-85.

177. Chen, Y. N., Bienkowski, M. J., and Marnett, L. J. (1987) *J Biol Chem 262*, 16892-9.

178. Smith, W. L., and Lands, W. E. (1972) *Biochemistry 11*, 3276-85.

179. Hemler, M. E., and Lands, W. E. (1980) *J Biol Chem 255*, 6253-61.

180. Marshall, P. J., Kulmacz, R. J., and Lands, W. E. (1987) *J Biol Chem 262*, 3510-7.

181. Kulmacz, R. J. (1987) *Biochem Biophys Res Commun 148*, 539-45.

182. MacDonald, I. D., Graff, G., Anderson, L. A., and Dunford, H. B. (1989) *Arch Biochem Biophys 272*, 194-202.

183. Hsuanyu, Y., and Dunford, H. B. (1990) *Biochem Cell Biol 68*, 965-72.

184. Hsuanyu, Y., and Dunford, H. B. (1992) *J Biol Chem 267*, 17649-57.

185. Hsuanyu, Y. C., and Dunford, H. B. (1992) *Arch Biochem Biophys 292*, 213-20.

186. Percival, M. D., Ouellet, M., Vincent, C. J., Yergey, J. A., Kennedy, B. P., and O'Neill, G. P. (1994) *Arch Biochem Biophys 315*, 111-8.

187. Kyte, J. (1995) *Mechanism in Protein Chemistry*, Garland Publishing, Inc., New York.

188. Ator, M. A., and Ortiz de Montellano, P. R. (1987) *J Biol Chem 262*, 1542-51.

189. kauppinen, J. K., Moffat, D. J., Mantsch, H. H., and Camerson, D. G. (1981) *Appl Spectrosc 35*, 271-276.

190. Hadden, J. M., Bloemendal, M., Haris, P. I., Srai, S. K., and Chapman, D. (1994) *Biochim Biophys Acta 1205*, 59-67.

191. Dong, A., Huang, P., and Caughey, W. S. (1990) *Biochemistry 29*, 3303-8.

192. Dong, A. C., Huang, P., and Caughey, W. S. (1992) *Biochemistry 31*, 182-9.

193. Doyle, M. L. (1997) *Curr Opin Biotechnol 8*, 31-5.

194. Ladbury, J. E., and Chowdhry, B. Z. (1996) *Chem Biol 3*, 791-801.

195. Klebe, G., and Bohm, H. J. (1997) *J Recept Signal Transduct Res 17*, 459-73.

196. Weber, P. C., Pantoliano, M. W., Simons, D. M., and Salemme, F. R. (1994) *J. Am. Chem. Soc. 116*, 2717-1724.

197. Adar, F. (1978) in *The porphyrins, Physical Chemistry* (Dolphin, D., Ed.) pp 167-209, Academic Press, New York.

198. Scheidt, W. R., and Gouterman, M. (1983) in *Iron Porphyrins* (Lever, A. B. P., and Gray, H. B., Eds.) pp 89-139, Addison-Wesley, Reading, MA.

199. Smulevich, G., Neri, F., Marzocchi, M. P., and Welinder, K. G. (1996) *Biochemistry 35*, 10576-85.

200. Smulevich, G., Feis, A., Indiani, C., Becucci, M., and Marzocchi, M. P. (1999) *J Biol Inorg Chem 4*, 39-47.

201. Veitch, N. C., Williams, R. J., Bray, R. C., Burke, J. F., Sanders, S. A., Thorneley, R. N., and Smith, A. T. (1992) *Eur J Biochem 207*, 521-31.

202. Tanaka, M., Nagano, S., Ishimori, K., and Morishima, I. (1997) *Biochemistry 36*, 9791-8.

203. Smulevich, G., English, A. M., Mantini, A. R., and Marzocchi, M. P. (1991) *Biochemistry 30*, 772-9.

204. Smith, A. T., Sanders, S. A., Thorneley, R. N., Burke, J. F., and Bray, R. R. (1992) *Eur J Biochem 207*, 507-19.

205. Uno, T., Nishimura, Y., Tsuboi, M., Makino, R., Iizuka, T., and Ishimura, Y. (1987) *J Biol Chem 262*, 4549-56.

206. Aviram, I. (1981) *Arch Biochem Biophys 212*, 483-90.

207. Fasman, G. D. (1975) *CRC Handbook of Biochemistry and Molecular Biology*, CRC Press, Cleveland.

208. Christensen, J. J., Hansen, L. D., and Izatt, R. M. (1976) *Handbook of proton ionization heats and related thermodynamic quantities*, Wiley, New York.

209. Harbury, H. A. (1956) *J Biol Chem 225*, 1009-19.

210. Sitter, A. J., Shifflett, J. R., and Terner, J. (1988) *J Biol Chem 263*, 13032-8.

211. Feis, A., Marzocchi, M. P., Paoli, M., and Smulevich, G. (1994) *Biochemistry 33*, 4577-83.

212. Tam, S. S., Lee, D. H., Wang, E. Y., Munroe, D. G., and Lau, C. Y. (1995) *J Biol Chem 270*, 13948-55.

213. Reddy, S. G., Scapin, G., and Blanchard, J. S. (1996) *Biochemistry 35*, 13294-302.

214. Morgan, B. P., Scholtz, J. M., Ballinger, M. D., Zipkin, I. D., and Bartlett, P. A. (1991) *J. Am. Chem. Soc. 113*, 297-307.

215. Fersht, A. R., Shi, J. P., Knill-Jones, J., Lowe, D. M., Wilkinson, A. J., Blow, D. M., Brick, P., Carter, P., Waye, M. M., and Winter, G. (1985) *Nature 314*, 235-8.

216. Kato, Y., Conn, M. M., and Rebek, J., Jr. (1995) *Proc Natl Acad Sci U S A 92*, 1208-12.

217. Habermann, S. M., and Murphy, K. P. (1996) *Protein Sci 5*, 1229-39.

218. Frisch, C., Schreiber, G., Johnson, C. M., and Fersht, A. R. (1997) *J Mol Biol 267*, 696-706.

219. Larsen, I. K. (1978) *Acta Crystallogr B34*, 962-4.

220. Levitt, M., and Perutz, M. F. (1988) *J Mol Biol 201*, 751-4.

221. Lumry, R., and Rajender, S. (1970) *Biopolymers 9*, 1125-227.

222. Dunitz, J. D. (1995) *Chem Biol 2*, 709-12.

223. Ator, M. A., David, S. K., and Ortiz de Montellano, P. R. (1989) *J Biol Chem 264*, 9250-7.

224. DePillis, G. D., and Ortiz de Montellano, P. R. (1989) *Biochemistry 28*, 7947-52.

225. DePillis, G. D., Wariishi, H., Gold, M. H., and Ortiz de Montellano, P. R. (1990) *Arch Biochem Biophys 280*, 217-23.

226. Harris, R. Z., Wariishi, H., Gold, M. H., and Ortiz de Montellano, P. R. (1991) *J Biol Chem 266*, 8751-8.

227. Samokyszyn, V. M., and Ortiz de Montellano, P. R. (1991) *Biochemistry 30*, 11646-53.

228. Ortiz de Montellano, P. R. (1995) *Biochimie 77*, 581-93.

229. Shoeb, H. A., Bowman, B. U., Jr., Ottolenghi, A. C., and Merola, A. J. (1985) *Antimicrob Agents Chemother 27*, 408-12.

230. Shoeb, H. A., Bowman, B. U., Jr., Ottolenghi, A. C., and Merola, A. J. (1985) *Antimicrob Agents Chemother 27*, 399-403.

231. Timbrell, J. A. (1979) *Drug Metab Rev 10*, 125-47.

232. Brambilla, G., Cavanna, M., Faggin, P., Pino, A., Robbiano, L., Bennicelli, C., Zanacchi, P., Camoirano, A., and De Flora, S. (1982) *J Toxicol Environ Health 9*, 287-303.

233. Jiang, X., Khursigara, G., and Rubin, R. L. (1994) *Science 266*, 810-3.

234. Torffvit, O., Thysell, H., and Nassberger, L. (1994) *Hum Exp Toxicol 13*, 563-7.

235. Reilly, C. A., and Aust, S. D. (1997) *Chem Res Toxicol 10*, 328-34.

236. Goldberg, B., Stern, A., and Peisach, J. (1976) *J Biol Chem 251*, 3045-51.

237. Christman, L. (1984) (Klusek-Hamilton, H., Ed.) pp 878, Springhouse Corporation, Springhouse, PA.

238. Berkow, R., Beers, M. H., and Fletcher, A. J. (1997) pp 1509, Merck Research Laboratories, Whitehouse Station, N.J.

239. Jaffe, H. H. (1953) *J Am Chem Soc*, 191-261.

240. Rodriguez-Lopez, J. N., Smith, A. T., and Thorneley, R. N. (1997) *J Biol Chem 272*, 389-95.

241. Hayashi, Y., and Yamazaki, I. (1979) *J Biol Chem 254*, 9101-6.

242. Nakajima, R., and Yamazaki, I. (1987) *J Biol Chem 262*, 2576-81.

243. Adediran, S. A. (1996) *Arch Biochem Biophys 327*, 279-84.

244. Weast, R. C., Astle, M. J., and Beyer, W. H. (1988) , CRC Press, Inc, Boca Raton.

245. Sinha, B. K. (1983) *J Biol Chem 258*, 796-801.

246. Rapaport, E., Cass, M. W., and White, E. H. (1972) *J. Am. Chem. Soc. 94*, 3153-3159.

247. Elias, A. N., Goodman, M. M., Liem, W. H., and Barr, R. J. (1993) *J Am Acad Dermatol 29*, 78-81.

248. Meyer, U. A. (1996) *J Pharmacokinet Biopharm 24*, 449-59.

249. Argentieri, D. C., Ritchie, D. M., Ferro, M. P., Kirchner, T., Wachter, M. P., Anderson, D. W., Rosenthale, M. E., and Capetola, R. J. (1994) *J Pharmacol Exp Ther 271*, 1399-408.

250. Burner, U., Obinger, C., Paumann, M., Furtmuller, P. G., and Kettle, A. J. (1999) *J Biol Chem 274*, 9494-502.

251. Modi, S., Behere, D. V., and Mitra, S. (1990) *J Inorg Biochem 38*, 17-25.

252. Kimura, S., and Yamazaki, I. (1979) *Arch Biochem Biophys 198*, 580-8.

253. Tsai, A. L., Kulmacz, R. J., Wang, J. S., Wang, Y., Van Wart, H. E., and Palmer, G. (1993) *J Biol Chem 268*, 8554-63.

254. Gaspard, S., Chottard, G., Mahy, J. P., and Mansuy, D. (1996) *Eur J Biochem 238*, 529-37.

255. Lindner, H. J., and Gottlicher, S. (1969) *Acta Crystallogr B25*, 832-42.

256. Betz, M., Huxley, P., Davies, S. J., Mushtaq, Y., Pieper, M., Tschesche, H., Bode, W., and Gomis-Ruth, F. X. (1997) *Eur J Biochem 247*, 356-63.

257. Gearing, A. J., Beckett, P., Christodoulou, M., Churchill, M., Clements, J., Davidson, A. H., Drummond, A. H., Galloway, W. A., Gilbert, R., Gordon, J. L., and et al. (1994) *Nature 370*, 555-7.

258. McGeehan, G. M., Becherer, J. D., Bast, R. C., Jr., Boyer, C. M., Champion, B., Connolly, K. M., Conway, J. G., Furdon, P., Karp, S., Kidao, S., and et al. (1994) *Nature 370*, 558-61.

259. Mohler, K. M., Sleath, P. R., Fitzner, J. N., Cerretti, D. P., Alderson, M., Kerwar, S. S., Torrance, D. S., Otten-Evans, C., Greenstreet, T., Weerawarna, K., and et al. (1994) *Nature 370*, 218-20.

260. Moore, W. M., and Spilburg, C. A. (1986) *Biochem Biophys Res Commun 136*, 390-5.

261. Wilkes, S. H., and Prescott, J. M. (1983) *J Biol Chem 258*, 13517-21.

262. Laufer, R., Ewenson, A., Gilon, C., Chorev, M., and Selinger, Z. (1985) *Eur J Biochem 150*, 135-40.

263. Summers, J. B., Mazdiyasni, H., Holms, J. H., Ratajczyk, J. D., Dyer, R. D., and Carter, G. W. (1987) *J Med Chem 30*, 574-80.

264. Summers, J. B., Kim, K. H., Mazdiyasni, H., Holms, J. H., Ratajczyk, J. D., Stewart, A. O., Dyer, R. D., and Carter, G. W. (1990) *J Med Chem 33*, 992-8.

265. Ohemeng, K. A., Nguyen, V. N., Schwender, C. F., Singer, M., Steber, M., Ansell, J., and Hageman, W. (1994) *Bioorg Med Chem 2*, 187-93.

266. Rich, P. R., and Bonner, W. D., Jr. (1978) *Biochim Biophys Acta 501*, 381-95.

267. Kobashi, K., Takebe, S., Terashima, N., and Hase, J. (1975) *J Biochem (Tokyo) 77*, 837-43.

268. Munakata, K., Kobashi, K., and Hase, J. (1980) *J Pharmacobiodyn 3*, 457-62.

269. Akers, H. A. (1981) *Experientia 37*, 229-30.

270. van't Riet, B., Kier, L. B., and Elford, H. L. (1980) *J Pharm Sci 69*, 856-7.

271. Malejka-Giganti, D., and Ritter, C. L. (1994) *Environ Health Perspect 102 Suppl 6*, 75-81.

272. Surewicz, W. K., and Mantsch, H. H. (1988) *Biochim Biophys Acta 952*, 115-30.

273. Branden, C. (Tooze, J.) *Introduction to Protein Structure*, 1 ed., Garland Publishing, Inc., New York.

274. Eliot, A., and Ambrose, E. J. (1950) *Nature 165*, 921-922.

275. Susi, H. (1972) *Methods Enzymol 26*, 455-72.

276. Susi, H., and Byler, D. M. (1983) *Biochem Biophys Res Commun 115*, 391-7.

277. Haris, P. I., and Chapman, D. (1996) *Infrared spectroscopy of biomolecules*, John Wiley and Sons, Toronto.

278. Byler, D. M., and Susi, H. (1986) *Biopolymers 25*, 469-87.

279. Arrondo, J. L., Muga, A., Castresana, J., and Goni, F. M. (1993) *Prog Biophys Mol Biol 59*, 23-56.

280. Filosa, A., Ismail, A. A., and English, A. M. (1999) *J Biol Inorg Chem 4*, 717-26.

281. Olinger, J. M., Hill, D. M., Jakobsen, R. J., and Brody, R. S. (1986) *Biochim Biophys Acta 869*, 89-98.

282. Holloway, P. W., and Mantsch, H. H. (1989) *Biochemistry 28*, 931-5.

283. Englander, S. W., and Kallenbach, N. R. (1994) *Q. Rev. Biophys. 16*, 521-655.

284. Fernandez-Ballester, G., Castresana, J., Arrondo, J. L., Ferragut, J. A., and Gonzalez-Ros, J. M. (1992) *Biochem J 288*, 421-6.

285. Greenfield, N. J. (1996) *Anal Biochem 235*, 1-10.

286. Kelly, S. M., and Price, N. C. (1997) *Biochim Biophys Acta 1338*, 161-85.

287. Ladbury, J. E., and Chowdhry, B. Z. (1998) pp 345, John Wiley and Sons, Toronto.

288. Vane, J. R., and Botting, R. M. (1995) *Inflamm Res 44*, 1-10.

289. Kulmacz, R. J., and Wu, K. K. (1989) *Arch Biochem Biophys 268*, 502-15.

290. So, O. Y., Scarafia, L. E., Mak, A. Y., Callan, O. H., and Swinney, D. C. (1998) *J Biol Chem 273*, 5801-7.

291. Guo, Q., Chang, S., Diekman, L., Xiao, G., and Kulmacz, R. J. (1997) *Arch Biochem Biophys 344*, 150-8.

292. Hinz, H. J. (1983) *Annu Rev Biophys Bioeng 12*, 285-317.

293. Brandts, J. F., and Lin, L. N. (1990) *Biochemistry 29*, 6927-40.

294. Mancini, J. A., Vickers, P. J., O'Neill, G. P., Boily, C., Falgueyret, J. P., and Riendeau, D. (1997) *Mol Pharmacol 51*, 52-60.

295. Fabian, H., Schultz, C., Naumann, D., Landt, O., Hahn, U., and Saenger, W. (1993) *J Mol Biol 232*, 967-81.

296. Krimm, S., and Bandekar, J. (1980) *Biopolymers 19*, 1-29.

297. Bandekar, J., and Krimm, S. (1980) *Biopolymers 19*, 31-6.

298. van Stokkum, I. H., Linsdell, H., Hadden, J. M., Haris, P. I., Chapman, D., and Bloemendal, M. (1995) *Biochemistry 34*, 10508-18.

299. Parrish, J. R., Jr., and Blout, E. R. (1972) *Biopolymers 11*, 1001-20.

300. Trewhella, J., Liddle, W. K., Heidorn, D. B., and Strynadka, N. (1989) *Biochemistry 28*, 1294-301.

301. Reisdorf, W. C., Jr., and Krimm, S. (1996) *Biochemistry 35*, 1383-6.

302. Rothschild, K. J., and Clark, N. A. (1979) *Science 204*, 311-2.

303. Krimm, S., and Dwivedi, A. M. (1982) *Science 216*, 407-8.

304. Xiao, G., Chen, W., and Kulmacz, R. J. (1998) *J Biol Chem 273*, 6801-11.

305. Mancini, J. A., O'Neill, G. P., Bayly, C., and Vickers, P. J. (1994) *FEBS Lett 342*, 33-7.

306. Mancini, J. A., Riendeau, D., Falgueyret, J. P., Vickers, P. J., and O'Neill, G. P. (1995) *J Biol Chem 270*, 29372-7.

307. Greig, G. M., Francis, D. A., Falgueyret, J. P., Ouellet, M., Percival, M. D., Roy, P., Bayly, C., Mancini, J. A., and O'Neill, G. P. (1997) *Mol Pharmacol 52*, 829-38.

308. Grossmann, J. G., Neu, M., Pantos, E., Schwab, F. J., Evans, R. W., Townes-Andrews, E., Lindley, P. F., Appel, H., Thies, W. G., and Hasnain, S. S. (1992) *J Mol Biol 225*, 811-9.

309. Kilar, F., and Simon, I. (1985) *Biophys J 48*, 799-802.

310. Holzbaur, I. E., English, A. M., and Ismail, A. A. (1996) *Biochemistry 35*, 5488-94.

311. Cladera, J., Villaverde, J., Hartog, A. F., Padros, E., Berden, J. A., Rigaud, J. L., and Dunach, M. (1995) *FEBS Lett 371*, 115-8.

312. Kalgutkar, A. S., Crews, B. C., and Marnett, L. J. (1996) *Biochemistry 35*, 9076-82.

313. Pouplana, R., Perez, C., Sanchez, J., Lozano, J. J., and Puig-Parellada, P. (1999) *J Comput Aided Mol Des 13*, 297-313.

314. Kothekar, V., Sahi, S., and Srinivasan, M. (1999) *J Biomol Struct Dyn 16*, 901-15.

315. Hsi, L. C., Hoganson, C. W., Babcock, G. T., Garavito, R. M., and Smith, W. L. (1995) *Biochem Biophys Res Commun 207*, 652-60.

316. Tsai, A., Hsi, L. C., Kulmacz, R. J., Palmer, G., and Smith, W. L. (1994) *J Biol Chem 269*, 5085-91.

317. Iyer, R. S., Ghosh, S., and Salomon, R. G. (1989) *Prostaglandins 37*, 471-80.

318. Boutaud, O., Brame, C. J., Salomon, R. G., Roberts, L. J., 2nd, and Oates, J. A. (1999) *Biochemistry 38*, 9389-96.

319. Salomon, R. G., Miller, D. B., Zagorski, M. G., and Coughlin, D. J. (1984) *J. Am. Chem. Soc. 106*, 6049-6060.

320. Murthi, K. K., Friedman, L. R., Oleinick, N. L., and Salomon, R. G. (1993) *Biochemistry 32*, 4090-7.

321. Salomon, R. G., and Miller, D. B. (1985) *Adv Prostaglandin Thromboxane Leukot Res 15*, 323-6.

322. Percival, M. D., Bastien, L., Griffin, P. R., Kargman, S., Ouellet, M., and O'Neill, G. P. (1997) *Protein Expr Purif 9*, 388-98.

323. Mevkh, A. T., Miroshnikov, K. A., Igumnova, N. D., and Varfolomeev, S. D. (1993) *FEBS Lett 321*, 205-8.